

Copyright
by
Mireya Loreley McKee
2007

**The Dissertation Committee for Mireya Loreley McKee certifies that this is
the approved version of the following dissertation:**

**Synthesis and biological evaluation of
2-(2'-hydroxyphenyl) benzoxazole analogs of UK-1
and
G-Quadruplex selectivity of perylene diimide compounds**

Committee:

Sean M. Kerwin, Supervisor

David Hoffman

Rick Russell

Jennifer Brodbelt

Walter Fast

**Synthesis and biological evaluation of
2-(2'-hydroxyphenyl) benzoxazole analogs of UK-1
and
G-Quadruplex selectivity of perylene diimide compounds**

by

Mireya Loreley McKee, B. S.

Dissertation

Presented to the Faculty of the Graduate School of

The University of Texas at Austin

in Partial Fulfillment

of the Requirements

for the Degree of

Doctor of Philosophy

The University of Texas at Austin

December, 2007

Dedication

To my family, in particular to my parents, and especially, to my loving husband

Chad

Acknowledgements

I am here today because of all the people who have inspired and motivated me throughout my life both academically and personally. I would like to thank Dr. Sean Kerwin for his great mentorship throughout my doctoral degree, and for his constant support and patience. His knowledge in the chemical and biological fields is truly inspiring. I would also like to thank the members of my committee, Dr. Hoffmann, Dr. Brodbelt, Dr. Fast, and Dr. Russell, for their assistance and advice in this endeavor. I would like to acknowledge our collaborators in the Brodbelt Research group, particularly Carolyn Mazzitelli, and Dr. David at Texas State University. I also need to thank all of the research groups who facilitated this work by providing helpful discussions, or sharing equipment or supplies such as the Georgiou Lab, the Fast Lab, and the Richburg Lab, with special thanks to Chad McKee. I want to acknowledge my coworkers in the Kerwin Research Group for sharing numerous experiences, both in experimental successes as well as troubleshooting problems, and for their friendship.

Most of all however, I need to thank my family, for their constant encouragement and love. My parents, brothers and grandmother, with their own personal successes and confidence in me have motivated me to complete this graduate degree. In particular, I need to thank my husband Chad McKee. He has

been my pillar of support all these years, with words of encouragement and strength at every step. He inspires me with his great passion for research, and strong will to carry it out. He has helped me in numerous ways, both in my research endeavors and making me grow as a person. He has picked me up when I have been down, and pushed when I needed to move forward, and most importantly has been my best friend. Thank you for your unlimited patience and love.

**Synthesis and biological evaluation of
2-(2'-hydroxyphenyl) benzoxazole analogs of UK-1
and
G-Quadruplex selectivity of perylene diimide compounds**

Publication No. _____

Mireya Loreley McKee, Ph. D.
The University of Texas at Austin, 2007

Supervisor: Sean M. Kerwin

A great number of pharmaceutical drugs target nucleic acids. However, drug-DNA interactions can be region non-specific and lead to undesired side effects. Understanding the mechanisms that regulate drug-DNA binding can help in the design of potent and selective therapeutic agents with fewer deleterious side effects. The present investigation explores the metal-mediated DNA binding of a group of 2-(2-hydroxyphenyl)benzoxazole (HPB) ligands and the aggregation dependant G-quadruplex selectivity of a series of perylene tetracarboxylic acid diimides (PTCDI) compounds.

HPB ligands are simplified analogs of the bis-benzoxazole natural product UK-1. This compound is able to inhibit cell growth of various tumor cell lines, bind divalent cations, and interact with DNA in a metal dependant fashion. The HPB moiety present in UK-1 was identified as relevant for its metal ion binding and

biological properties. For this work, novel HPB ligands were synthesized with different substitutions at the C4 or C7 position. Their ability to bind metal ions and DNA was evaluated and their cytotoxicity was assessed in multiple cancer cell lines. The ligands bound to Cu^{2+} with the highest affinity among metals studied. Consequently, Cu^{2+} promoted the most dramatic increase in DNA binding and affected the ligand's cellular cytotoxicity.

The second project focused on targeting four-stranded structures called G-quadruplexes, which can form in G-rich nucleic acid sequences. Compounds that stabilize these structures may inhibit nucleic acid-processing enzymes such as telomerase and potentially act as anti-cancer agents. PIPER is a PTCDI that is particularly selective for G-quadruplex DNA versus duplex DNA under conditions in which it forms aggregates. This work investigated ligand aggregation in a series of PIPER analogs with different structural features under high and low salt buffers, changes in pH, metal binding and temperature changes. A negatively charged analog was determined to form metal-mediated aggregates while novel thermophilic mediated aggregation was discovered for an analog with methoxyethoxymethyl groups. The ability of these ligands to bind different DNA structures was evaluated under aggregating and non-aggregating conditions. This study supports the idea that ligand aggregation increases their quadruplex selectivity and decreases double-stranded DNA binding.

TABLE OF CONTENTS

LIST OF FIGURES	xvi
LIST OF TABLES	xx
LIST OF SCHEMES	xxi

PART I: SYNTHESIS AND BIOLOGICAL EVALUATION OF BENZOXAZOLE ANALOGS OF UK-1 1

CHAPTER 1. INTRODUCTION	1
1.1. DNA as a good biological target	1
1.2. Small molecules that bind to DNA	5
1.2.1. Covalent Interactions	6
1.2.2. Non-covalent Interactions	7
1.3. Factors that affect DNA binding	10
1.4. Metallo-DNA binders	11
1.4.1. Aureolic acid group of antitumor antibiotics	12
1.4.2. Quinolones	13
1.4.3. Benzoxazole, Benzothiazole, and Benzimidazole Ligands	15
1.5. The Bis-benzoxazole natural product UK-1	15
1.5.1. Discovery	15
1.5.2. Biological properties	17
1.5.3. Structure activity relationships of UK-1 analogs	18

CHAPTER 2. DESIGN AND SYNTHESIS OF NOVEL SIMPLIFIED BENZOXAZOLE ANALOGS OF UK-1 AND METAL COMPLEXES	22
2.1 Rationale for the Design of New Analogs	22
2.1.1. Disposition of N and O in the benzoxazole moiety	22
2.1.2. Effect of modification of the methyl ester position	23
2.2. Synthesis of Novel Benzoxazole ligands	25
CHAPTER 3. AFFINITY OF ANALOGS FOR METAL IONS	29
3.1. Methyl ester at the C4 or C7 position of the HPB ring affects metal binding ability	29
3.2. Ester and amide substitutions at the C4-position of the HPB ring affect metal binding abilities	33
3.3. Apparent association constants to divalent cations	37
3.4. Synthesis of a UK-1-Cu ²⁺ chelate.....	41
3.5. General trends observed for metal affinity.....	44
CHAPTER 4. METAL MEDIATED DNA BINDING AND CYTOTOXICITY	46
4.1. Analog affinity for DNA in the presence and absence of metals.....	46
4.1.1. Results obtained from SPR.....	47
4.1.2. Results obtained from mass spectroscopy	52
4.2. Cytotoxicity of 2-(2'-hydroxyphenyl)benzoxazole analogs	53
4.2.1. Cytotoxicity of HPB analogs with a carbomethoxy group at the C4 or C7 position.....	53
4.2.2. Cytotoxicity of HPB analogs with different C4 substituents	54
4.2.3. Cytotoxicity of UK-1 and its copper complex.....	56
4.3. Apoptosis induced by UK-1 and its copper complex	57
4.4. Conclusions.....	58

CHAPTER 5. SUMMARY AND FUTURE DIRECTIONS	61
5.1. Summary.....	61
5.2. Future Directions.....	63
CHAPTER 6. EXPERIMENTALS FOR PART I	65
6.1. General Information.....	65
6.2. Metal Binding Assays.....	66
6.3. Surface Plasmon Resonance.....	67
6.4. Electrospray ionization mass spectrometry.....	69
6.5. Cytotoxicity Assays.....	69
6.6. Western blot analysis.....	71
6.7. Synthetic Procedures.....	72
6.7.1. Compound 8	72
6.7.2. Compound 9	72
6.7.3. Compound 10	74
6.7.4. Compound 11	75
6.7.5. Compound 12	76
6.7.6. Compound 13	77
6.7.7. Compound 14	78
6.7.8. Compound 15	79
6.7.9. Compound 16	79
6.7.10. Compound 17	80
6.7.11. Compound 18	81
6.7.12. Compound 19	82
6.7.13. Compound 20	82
6.7.14. Compound 21	83
6.7.15. Cu ²⁺ -UK-1 Complex.....	84
REFERENCES FOR PART I	85

**PART II: G-QUADRUPLEX SELECTIVITY OF PERYLENE DIIMIDE
COMPOUNDS 95**

CHAPTER 7. INTRODUCTION 95

7.1. DNA Structures	95
7.1.1 B-DNA and other Helical Structures	95
7.1.2 Alternative DNA Structures	96
7.2. G-Quadruplex DNA topology and polymorphism.....	104
7.3. G-rich sequences and G-quadruplexes	106
7.3.1 Telomeric DNA.....	106
7.3.2 Other regions in the Genome	111
7.3.3 Evidence of G-Quadruplex formation in vivo	113
7.4. G-Quadruplex as a good biological target	115
7.5. G-Quadruplex interactive ligands	116
7.5.1 Telomestatin.....	117
7.5.2 Porphyrins	118
7.5.3 TOTA ⁺	119
7.5.4 Disubstituted Anthraquinone Derivatives.....	119
7.5.5. Carbocyanine dyes.....	120
7.5.6 Perylene Diimides	120

**CHAPTER 8. PERYLENE DIIMIDES LIGAND AGGREGATION AND G-
QUADRUPLEX DNA SELECTIVITY UNDER LOW SALT CONDITIONS 122**

8.1. Properties of Perylene Diimides	122
8.2. Modified Perylene Diimide Analogs.....	126
8.3. Results and Discussion	128
8.3.1. Visible Absorbance Spectroscopy experiments	128
8.3.2. Fluorescence and Resonance Light Scattering experiments	133
8.3.3. Fluorescence quenching experiments	135

8.4. Conclusions.....	140
-----------------------	-----

CHAPTER 9. PERYLENE DIIMIDES METAL AND THERMAL MEDIATED AGGREGATION AND G-QUADRUPLEX SELECTIVITY 142

9.1. Temperature and metal ion dependant-aggregation of perylene diimide compounds in the presence of metal ions and temperature changes.....	142
9.1.1. Absorbance Spectroscopy.....	143
9.1.2. Resonance Light Scattering and fluorescence spectroscopy	149
9.2. G-Quadruplex DNA Selectivity	152
9.2.1. Visible Absorbance Spectroscopy Experiment	152
9.2.2. Surface Plasmon Resonance Experiments	159
9.3. Cell entry and cytotoxicity.....	161
9.4. Conclusions.....	166

CHAPTER 10. SUMMARY AND FUTURE DIRECTIONS..... 168

10.1. Summary.....	168
10.2. Future Directions.....	169

CHAPTER 11. EXPERIMENTALS FOR PART II..... 171

11.1. General Information	171
11.2. DNA Synthesis	171
11.3. Fluorescence and RLS Spectroscopy	172
11.4. Visible and absorbance Spectroscopy	173
11.5. Circular Dichroism.....	173
11.6. Surface Plasmon Resonance Experiments.....	174
11.7. Cytotoxicity Assays	175
11.8. Fluorescent detection of PTCDI cellular entry.....	175

REFERENCES FOR PART II 176

LIST OF APPENDICES 191

APENDIX A. SELECTED SPECTRA FOR UK-1 ANALOGS 191

A.1. ¹ H and ¹³ C NMR of compound 8 in CDCl ₃ /MeOD 1:1.....	191
A.2. gHSQC of compound 8 in CDCl ₃	192
A.3. gHMBC Compound 8 in CDCl ₃ /MeOD 1:1	193
A.4. Compound 8 COSY in CDCl ₃	194
A.5. ¹ H and ¹³ C NMR of Compound 9 (CDCl ₃ /MeOD 1:1)	195
A.6. gHSQC compound 9 in CDCl ₃ /MeOD 1:1	196
A.7. gHMBC of compound 9 in CDCl ₃ /MeOD 1:1	197
A.8. Compound 9 COSY in CDCl ₃	198
A.9. ¹ H and ¹³ C NMR of compound 10	199
A.10. ¹ H and ¹³ C NMR of compound 11	200
A.11. ¹ H and ¹³ C NMR of compound 12	201
A.12. ¹ H and ¹³ C NMR of compound 13	202
A.13. ¹ H and ¹³ C NMR of compound 14	203
A.14. ¹ H and ¹³ C NMR NMR of compound 15	204
A.15. ¹ H and ¹³ C NMR NMR of compound 16	205
A.16. ¹ H and ¹³ C NMR NMR of compound 17	206
A.17. ¹ H and ¹³ C NMR NMR of compound 18	207
A.18. ¹ H and ¹³ C NMR NMR of compound 19	208
A.19. ¹ H and ¹³ C NMR NMR of compound 20	209
A.20. ¹ H and ¹³ C NMR NMR of compound 21	210

APENDIX B. NMR CHEMICAL SHIFTS OF COMPOUNDS 8 AND 9 IN THE PRESENCE OF MG(NO₃)₂.....211

B.1. ¹ H NMR shifts of compound 8	211
B.2. ¹³ C NMR shifts of compound 8	212
B.3. ¹ H NMR shifts of compound 9	213
B.4. ¹³ C NMR shifts of compound 9	214

APENDIX C. METAL-MEDIATED DNA BINDING OBSERVED BY ESI-MS ...215
C.1. Fraction of HPB bound to DNA in the presence of metal ions215

APENDIX D. CD SPECTRA OF DNA SEQUENCES USED IN PTCDI STUDIES
.....216
D.1. CD spectra of DNA sequences in 70 mM potassium phosphate, 100 mM potassium chloride, 1 mM EDTA buffer, pH 7216
D.2. CD spectra of DNA sequences in 8 mM sodium phosphate, 185 mM NaCl, pH 7 (BPS buffer).....217
D.3. CD Spectra of DNA sequences in 8 mM sodium phosphate, 185 mM NaCl, pH 7 (BPS buffer), supplemented with 25 μM $\text{Zn}(\text{NO}_3)_2$218

VITA 219

LIST OF FIGURES

Figure 1.1. DNA nucleotides and base-pairing.	2
Figure 1.2. Major and minor grooves in DNA.	3
Figure 1.3. DNA binding molecules may interfere with DNA processing enzymes	4
Figure 1.4. Examples of covalent DNA-binding drugs.....	7
Figure 1.5. Non-covalent small molecule-DNA interactions.....	7
Figure 1.6. Examples of external electrostatic DNA binders.	8
Figure 1.7. Examples of groove binders	9
Figure 1.8. Examples of intercalators.....	10
Figure 1.9. Members of the aureolic acid group of antitumor antibiotics.	13
Figure 1.10. Members of the quinolone family of drugs	14
Figure 1.11. Structure of UK-1 and bis-benzoxazole derivatives	16
Figure 1.12. Structures of UK-1 analogs 1-8	19
Figure 2.1. Disposition of the Nitrogen and Oxygen atoms in the benzoxazole moiety of compounds 8 and 9	22
Figure 2.2. Structural motif in UK-1 analogs important for activity	24
Figure 3.1. ¹ HNMR Spectrum of Compound 8 in the presence of Mg ²⁺	30
Figure 3.2. ¹ HNMR Spectrum of Compound 9 in the presence of Mg ²⁺	31
Figure 3.3. UV-Vis spectral changes of Compounds 8 and 9 upon addition of Mg ²⁺ and Cu ²⁺ ions	33
Figure 3.4. Structures of benzoxazoles 16-21 modified at the C4 position.	34
Figure 3.5. UV-Vis spectral changes of compound 17 upon addition of divalent cations.	35
Figure 3.6. UV-Vis spectral changes of UK-1 upon addition of divalent cations .	36
Figure 3.7. Binding isotherms of compound 17 with metal cations.	38
Figure 3.8. UV-Vis spectral changes of compound of 1 μM compound 17 and UK-1 upon addition of Cu ²⁺	40

Figure 3.9. Fraction Cu^{2+} bound to compound 8 at various ligand concentrations..	41
Figure 3.10. IR Spectra of UK-1 and its copper chelate.....	43
Figure 3.11. UV-Vis Spectrum of the UK-1- Cu^{2+} Complex in MeOH.....	43
Figure 4.1. Sensograms of the UK-1-DNA interactions in the presence of 20 mM MgCl_2 or 20 μM CuCl_2	49
Figure 4.2. Sensograms of Chromomycin -DNA interactions in the presence of 20 mM MgCl_2	50
Figure 4.3. SPR response of benzoxazole ligands in the presence of 20 μM CuCl_2	59
Figure 4.4. Caspase-8 levels in the presence of UK-1 and the UK-1- Cu^{2+} complex.....	58
Figure 5.1. Future HPB analogs with substitutions at the C2', C3' or C4' position..	64
Figure 7.1. Helical DNA structure and base-pairing.....	96
Figure 7.2. Hairpin Loops and DNA cruciforms.....	97
Figure 7.3. Holliday Junctions.....	98
Figure 7.4. Triplex DNA.....	99
Figure 7.5. Examples of Triplex-DNA binding ligands.....	100
Figure 7.6. G-tetrads and G-Quadruplexes.....	101
Figure 7.7. Strand Stoichiometries in G-Quadruplexes.....	102
Figure 7.8. Possible strand orientations in G-Quadruplexes.....	103
Figure 7.9. The i-motif.....	104
Figure 7.10. Topological forms of G4' and G'2-DNA generated by alternatives in loop connectivity.....	105
Figure 7.11. The end replication problem.....	108
Figure 7.12. Putative roles of G-Quadruplexes in the telomeres.....	110

Figure 7.13. Transcriptional regulation by quadruplex forming sequences in promoter regions.....	112
Figure 7.14. Examples of G-Quadruplex interactive compounds.....	117
Figure 8.1. End-stacking ligand interactions.	122
Figure 8.2. Structures of PIPER and Tel01 and their pH-dependant aggregation.	124
Figure 8.3. Modifications in the PTCDI structure.....	127
Figure 8.5. CD spectra of G5-DNA. 100 μ M of $[d(T_2G_5T)]_4$ in 3:1 water/methanol 25 mM ammonium acetate buffer, pH 7.....	129
Figure 8.6. Absorption spectra of PIPER and Tel01 with different DNA structures.	130
Figure 8.7. Absorption spectra of charged perylenes with different DNA structures.....	131
Figure 8.8. Absorption spectra of bay-substituted and benzannulated perylenes with different DNA structures.	133
Figure 8.9. Relative fluorescence and RLS signal of PTCDI.....	134
Figure 8.10. Normalized fluorescence titration data for different perylene diimides at 1 μ M concentration	137
Figure 8.11. Fluorescence quenching of Tel12 in low and high salt buffers.....	138
Figure 9.1. Terpyridine and EDTA functionalized perylene derivatives.....	144
Figure 9.2. Absorbance spectra of perylene diimides in the presence of metal cations.	145
Figure 9.3. Structure of Tel45.	146
Figure 9.4. Absorbance spectra of Tel45 with metal cations in aqueous and organic solvents.....	146
Figure 9.5. Absorbance Spectra of Tel45 with increasing temperature.....	147
Figure 9.6. H- and J-aggregates.	149

Figure 9.7. Fluorescence and Resonance Light scattering of Tel12 in the presence of Zn ²⁺ ions.....	150
Figure 9.8. Fluorescence and Resonance light scattering of Tel45 with increasing temperature.	151
Figure 9.9. UV-Vis Spectra of Tel11 and Tel12 in the presence of Zn ²⁺ with quadruplex and duplex DNA.	154
Figure 9.10. UV-Vis Spectra of Tel11 and Tel45 at different temperatures in the presence of quadruplex and duplex DNA.	157
Figure 9.11. SPR sensorgrams TMPyP4 and Tel11 binding to G4' human telomeric DNA.....	160
Figure 9.12. Cellular localization of A549 cells treated with Tel11, Tel12 and Tel45.	162
Figure 9.13. Fluorescence micrographs of MCF-7cells.....	163
Figure 9.14. Fluorescence micrographs of A549 cells.	164
Figure 9.15. Fluorescence and RLS of Tel45 in cell culture media.....	165
Figure 10.1. Future PTCDI analogs.	170

LIST OF TABLES

Table 1.1. Anticancer activity of UK-1 and analogs 1-8	19
Table 3.1. Apparent association constants of HPB analogs for Mg^{2+} , Zn^{2+} , Ni^{2+} , and Cu^{2+} in MeOH (M^{-1})	37
Table 3.2. Lower limit of the association constants for Cu^{2+} binding in MeOH (M^{-1}) at 1 μM ligand	40
Table 4.1. Apparent binding constants of HPB ligands for GC-Hairpin DNA in the presence of 20 mM $MgCl_2$ or 20 μM $CuCl_2$	51
Table 4.2. Cytotoxicity of PC-3 or HT-29 cells after 72h incubation with UK-1, compound 8 or compound 9	54
Table 4.3. Cytotoxicity of MCF-7 or A549 cells treated with HPB analogs during 72h.	55
Table 4.4. Cytotoxicity of Cells treated for 24 or 72 h in the presence of UK-1 and copper analogs.	56
Table 8.1. Fluorescence quenching of PTCDIs by quadruplex, duplex, and single-stranded DNA.	140
Table 9.1. Relationship between metal-mediated PTCDI aggregation and G-Quadruplex Selectivity	155
Table 9.2. Relationship between temperature dependant PTCDI aggregation and G-Quadruplex Selectivity	158
Table 9.3. Cytotoxicity of MCF-7 or A549 cells treated with PTCDI analogs during 72h.	166

LIST OF SCHEMES

Scheme 2.1. Synthesis of compound 9	26
Scheme 2.2. Synthesis of Compound 10	26
Scheme 2.3. Synthesis of compound 11	27
Scheme 2.4. Synthesis of compounds 12-15	27
Scheme 2.5. Synthesis of compounds 16-21	28
Scheme 3.1. Synthesis of UK-1 Cu ²⁺ Complex.....	42

PART I: SYNTHESIS AND BIOLOGICAL EVALUATION OF BENZOXAZOLE ANALOGS OF UK-1

CHAPTER 1. INTRODUCTION

1.1. DNA as a good biological target

DNA is the basis of heredity in all higher organisms, and its regulation determines the expression of gene products that promote homeostasis within the cell. Any variation of normal DNA regulation, whether by mutation or physical damage, can lead to changes in cellular balance potentially resulting in cell death. Therefore, the study of DNA is important for understanding physiological applications and to elucidate functions of human health.

The structure of DNA was elucidated by Watson and Crick in 1953 (1). Since then, scientists have strived to understand the factors and structural features that encompass this unique biomolecule. DNA strands are composed of repeating nucleotide units, which consist of a 2'-deoxyribose sugar, a phosphate, and a heterocyclic base (2, 3). There are two types of bases, purines and pyrimidines. The first contains a fused five and six membered ring that are comprised of adenine and guanine, while the latter possess a six-membered heterocycle, and include the bases thymine and cytosine. The 2'-deoxyribose sugar is connected to the N9 of the purine bases and the N1 of the pyrimidine bases. The DNA chain is made through phosphodiester bonds between the 3' and 5' carbons of adjacent sugar rings (Figure 1.1A). Due to the asymmetry in the sugar phosphate backbone, DNA strands have direction, and their ends are referred to as 3' or 5' according to the position of hydroxyl groups in the first and last sugar rings.

Erwin Chargaff investigated the base composition of different sources of DNA and his studies revealed that the fraction of purines was always proportional

to the amount of pyrimidines. (4). Watson and Crick incorporated Chargaff's observations in their DNA model establishing that adenine could base pair with thymine through two hydrogen bonds and guanine could base pair with cytosine through three hydrogen bonds (1). Two opposing complementary DNA strands can then interact through a hydrogen bonding network formed by their nucleobases. The base pairing between two DNA strands is known as the Watson-Crick base pairing and can give rise to a helical DNA structure such as that shown in Figure 1.1B.

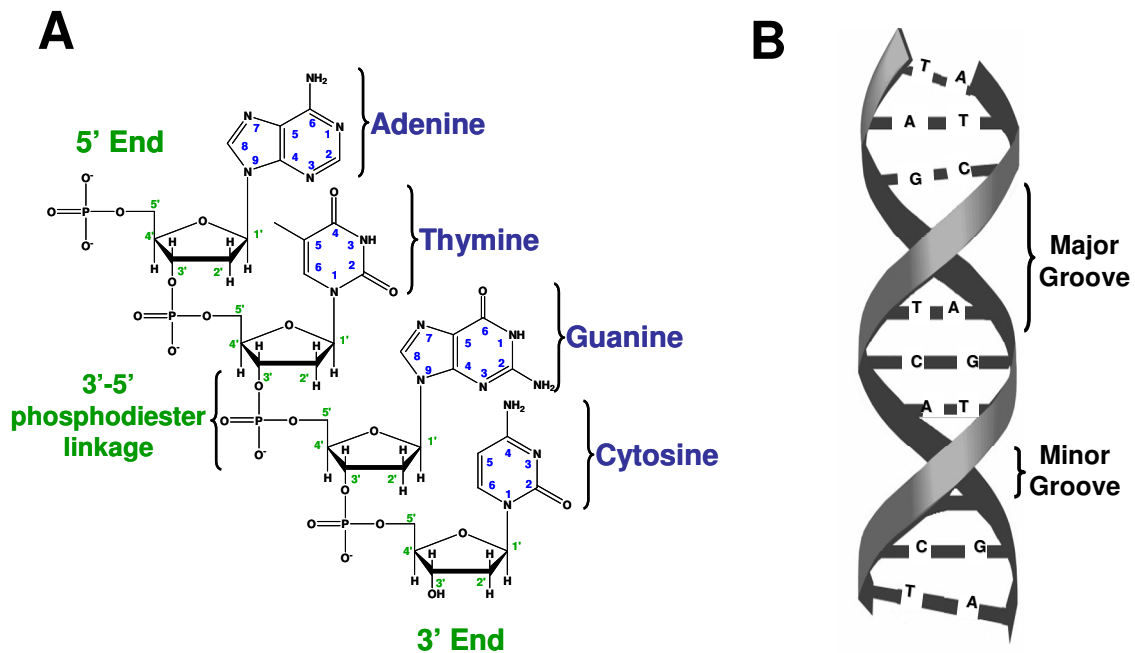


Figure 1.1. DNA nucleotides and base-pairing. (A) Nucleotides consist of a 2'-deoxyribose sugar, a phosphate, and a heterocyclic base. DNA strands are formed through phosphodiester linkages in the 3' and 5' of adjacent sugars. (B) Double stranded DNA is formed from the base-pairing of Adenine with Thymine and Guanine with Cytosine

There are many structural traits in DNA that make this biopolymer distinctive. Its stacked nucleobases form a hydrophobic interior, while its negatively charged sugar-phosphate backbone is hydrophilic. The majority of genomic double stranded DNA is found as a right-handed helical structure

termed “B-DNA”, which has 10.5 base pairs per helical turn, an average of 24 Å in diameter and 3.3 Å in length per base-pair (5, 6). Under certain conditions DNA can adopt other helical conformations that vary in width, and size of the grooves such as “A” or “Z” DNA (7). These and other, non-canonical DNA structures will be elaborated upon in chapter 7.

The phosphate backbones of two DNA strands in the B conformation form different sized grooves as they twist around each other: a major groove, 22 Å wide, and a minor groove, 12 Å wide (8). As seen in Figure 1.2, the minor groove contains the pyrimidine O2 and the purine N3 of the base pair, while the major groove is located on the opposite side. Many of the structural features of DNA play crucial biological roles. For instance, groove recognition is essential for many protein-DNA interactions (9).

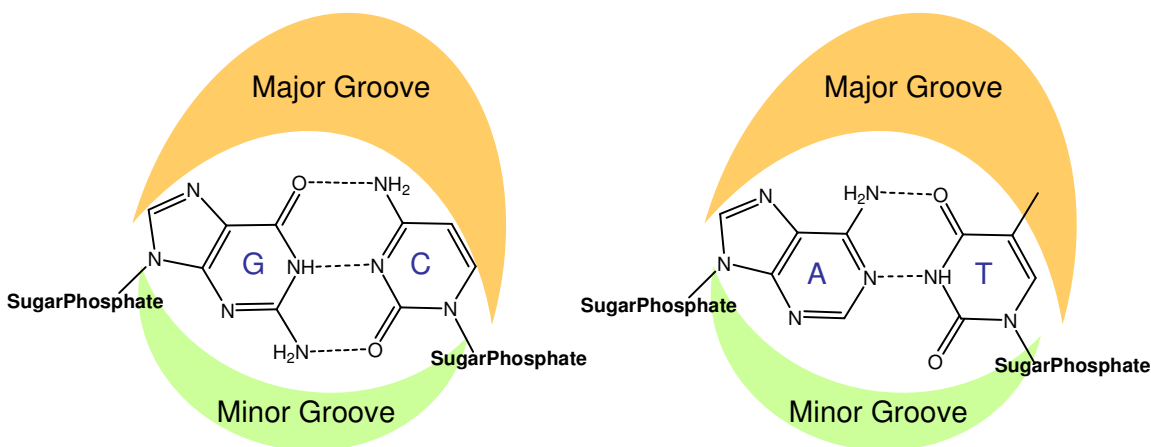


Figure 1.2. Major and minor grooves in DNA. The glycosidic bonds in a base pair are not located in opposite positions in the helix. This defines two sides of different size, a larger defined as major groove, and a smaller side, or minor groove.

DNA is the carrier of genetic information and has critical cellular functions such as cell division. Therefore, it is not surprising that many drugs that are currently in clinical use or in advanced clinical trials are directed at nucleic acids (10). As illustrated in the simple schematic in Figure 1.3, small molecules that

bind to nucleic acids can alter gene expression or induce apoptotic cell death by interfering with the cell's replication, transcription, or translation machinery. Therefore, targeting DNA to inhibit or alter the expression of a particular gene or to selectively influence infected or diseased cell populations presents very attractive possibilities for drug design. Therapeutic applications of DNA-interactive drugs include antiviral, antifungal, antibacterial and antineoplastic potential.

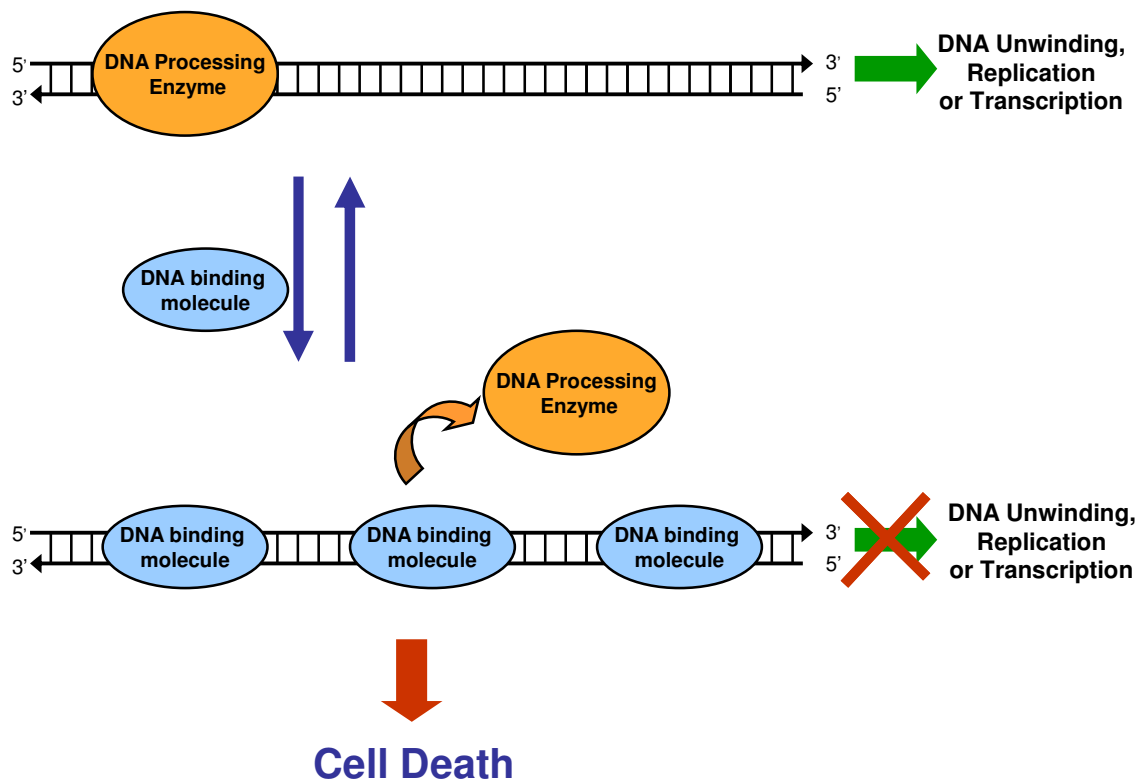


Figure 1.3. DNA binding molecules may interfere with DNA processing enzymes. When small molecules bind to nucleic acids they can alter the processes carried out by DNA processing such as unwinding, replication and transcription, eventually causing cell death

DNA binding molecules are particularly important as anticancer agents because of the differential growth rate of healthy tissues and cancerous cells. Cancer cells divide and replicate uncontrollably and thus can be predominantly targeted for cell death. Early data suggesting that small molecules could act as

chemotherapeutic agents was indirectly discovered from chemical warfare used in World Wars I and II (11). It was noted that survivors of mustard gas exposure had lower white blood cell counts. Researchers eventually recognized that cell division was affected in these cells and realized that other fast-dividing cells such as cancer could be potentially targeted (12). Consequently, in the 1940s, nitrogen mustard was used successfully to treat several patients with advanced lymphomas (13). It is now known that mustard gas, or 1,1-thiobis(2-chloroethane), acts by forming cross-links to DNA (14-16). These discoveries led to a rapidly expanding field that investigates DNA-binding drugs to treat diseases such as cancer.

However, as evidenced with the toxic mustard gas, DNA-binding drugs can have negative side effects that include increased mutagenic and carcinogenic properties (14-17). Many have poor tissue specificity and may non-specifically target other fast-dividing cells such as bone marrow or germ cells (18). In order to design potent and selective DNA-interactive anticancer agents, it is necessary to identify important structural elements involved in DNA binding and understand the factors that regulate their interactions with DNA. Some of these factors will be elaborated on in the following sections of this chapter. However, a brief summary of classical DNA interactive molecules and their binding modes to DNA will be discussed next.

1.2. Small molecules that bind to DNA

Small molecules can bind to DNA either covalently or non-covalently through electrostatic, hydrogen bonding, or hydrophobic interactions. In contrast to non-covalent agents, most covalent interactions are irreversible. Robust, irreversible interactions are useful in treatment of tumors or foreign bodies such as viruses and bacteria (19). These drugs ultimately generate cell death in targeted cells by inducing DNA lesions. Therefore covalent drugs can be toxic

and have long-lasting effects which make them less desirable from a clinical standpoint. (10). The challenge in drug design is to develop agents that can effectively bind to their targets and have fewer deleterious side effects by selectively targeting the cancerous over regular cells (20).

1.2.1. Covalent Interactions

Compounds that form covalent bonds with nucleic acids can interfere with the normal function of DNA by irreversibly modifying nucleotides, either by causing base-pairing mismatches during DNA replication, or by cross-linking the strands of the DNA helix. Some examples of such covalent drugs are Cisplatin, Mitomycin C, and Alkeran, shown in Figure 1.4. Cisplatin, or cis-diamine-dichloro-platinum, is the most widely used anticancer drug. Studies have shown that cisplatin can platininate the N-7 of guanine bases, causing intra-strand crosslinks, potentially interfering with the mobility of DNA polymerases. Mitomycin-C is an anti-tumor antibiotic which can form cross-links between guanine bases on adjacent strands of DNA. This inhibits the formation of single stranded DNA and affects the cells' replication and transcription machinery. Alkeran is an alkylating agent that can react with nucleophilic sites on the DNA. It attacks the N7 position of guanine bases causing a conformational change in the base. Although covalent DNA binding drugs represent vast opportunities for drug design, this chapter will focus on non-covalent DNA binders, as they represent the interactions that concern the compounds used in this study.

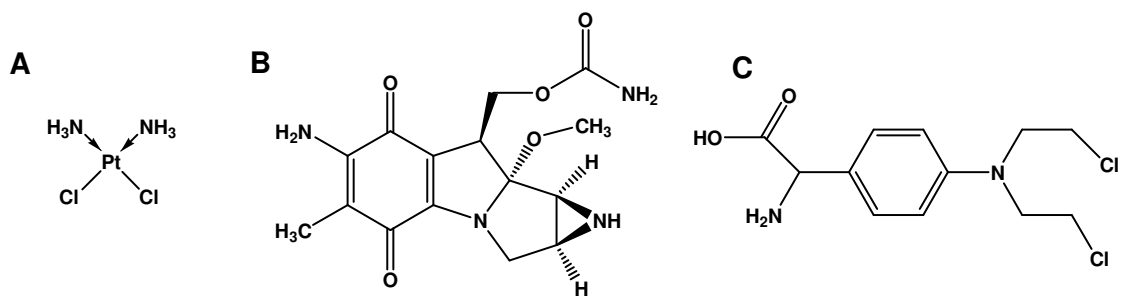


Figure 1.4. Examples of covalent DNA-binding drugs. (A) Cisplatin. (B) Mitomycin-C. (C) Alkeran.

1.2.2. Non-covalent Interactions

Non-covalent DNA binding interactions include external electrostatic binding, groove binding, and intercalation. The schematic in Figure 1.5 illustrates these reversible drug-DNA interactions.

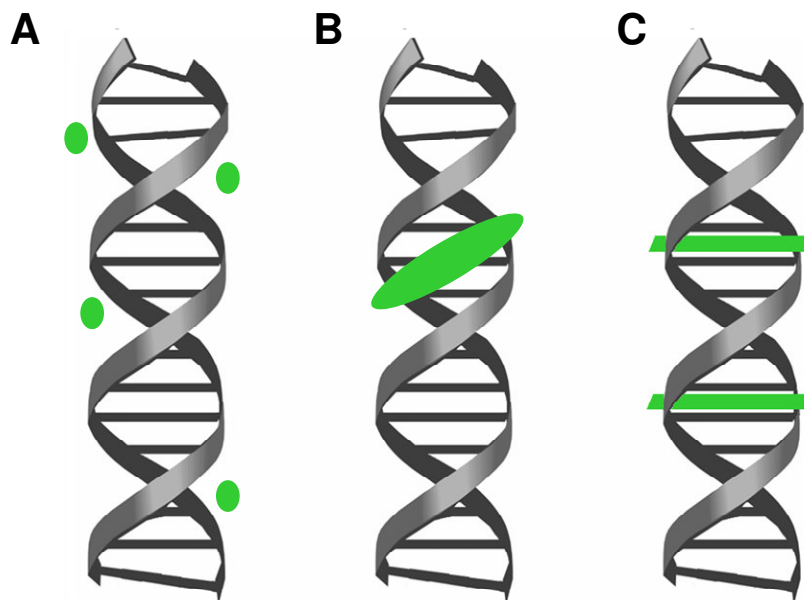


Figure 1.5. Non-covalent Small molecule-DNA interactions. (A) External electrostatic. (B) Groove binding. (C) Intercalation

The first type of reversible association occurs through non-specific electrostatic interactions. DNA is a highly charged polyanion with two negative

charges per base pair. Positively charged counter-ions surround the DNA and affect its stability, structure and interactions. Cationic ligands can interact with the negatively charged phosphates in the DNA backbone (21). These associations can be favored entropically by the release of counterions upon binding and are generally not sequence or location specific. An example of a group of drugs that binds through this mode are the cationic polyamines such as spermine and spermidine, shown in Figure 1.6 Polyamine drugs are currently being studied to induce apoptosis in cancer cells as these have a higher requirement of natural polyamines for their cell growth (22).

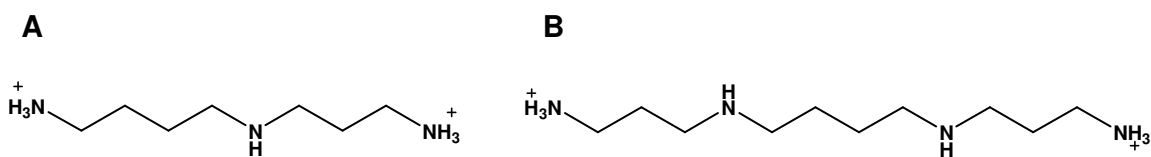


Figure 1.6. Examples of external electrostatic DNA binders. (A) Spermine. (B) Spermidine

Groove-binding molecules interact with the major or minor groove of DNA. They are generally composed of simple aromatic rings that are connected by bonds with torsional freedom (2, 23, 24). There are many groove binding molecules that are currently in clinical or preclinical trials; for a review see reference (24). Figure 1.7 shows some of the classical groove binders, DAPI (4',6'-diamidino-2-phenylindole), Hoechst 33238, and distamycin. Groove binders can displace cations and water molecules from the grooves and can extend over many base-pairs, which can allow for high sequence specific recognition (23). They tend to bind preferentially to AT rich sequences since they can form hydrogen bonds with the C2 carbonyl oxygen of thymine bases and the N3 nitrogen of adenine bases (2). In contrast, the amino group of guanine hydrogen bonds with the carbonyl oxygen of cytosine, sterically blocking other molecules from binding in the minor group at GC base pairs (2).

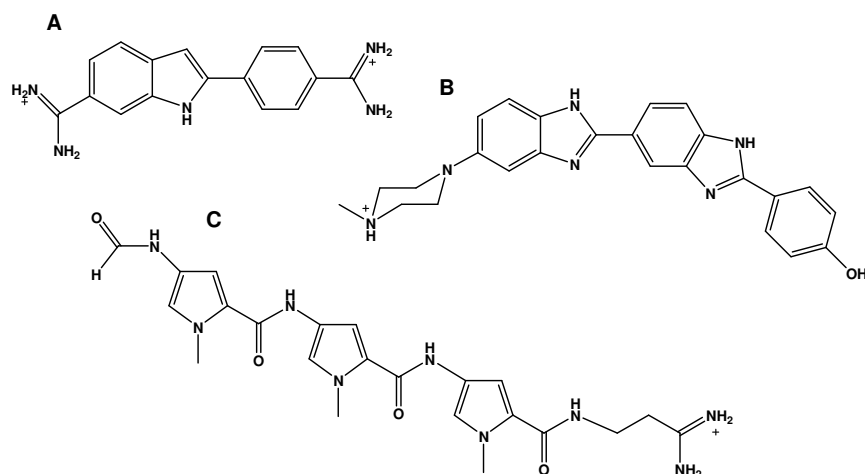


Figure 1.7. *Examples of Groove Binders.* (A) DAPI. (B) Hoechst 33258. (C) Distamycin

Intercalation occurs when molecules fit themselves in between base pairs of DNA (25). Intercalators are mostly polycyclic, aromatic, and planar compounds, such as ethidium, proflavine, daunomycin, or the naphthalene bisimides (Figure 1.8). Unlike the first two types of non-covalent binding modes, intercalation requires a degree of unwinding of the DNA helix to open up a space between the base pairs to fit the intercalating ring system (26). This mode of binding is generally slower than groove binding and is stabilized by hydrophobic contacts between the drugs and the DNA bases. Most intercalators display either no binding preference or a slight GC base pair preference (25). This is probably due to the larger dipole moment of the GC relative to AT base pairs (2). Many intercalating drugs are presently used to treat a variety of cancers and others are in different phases of clinical trials (26).

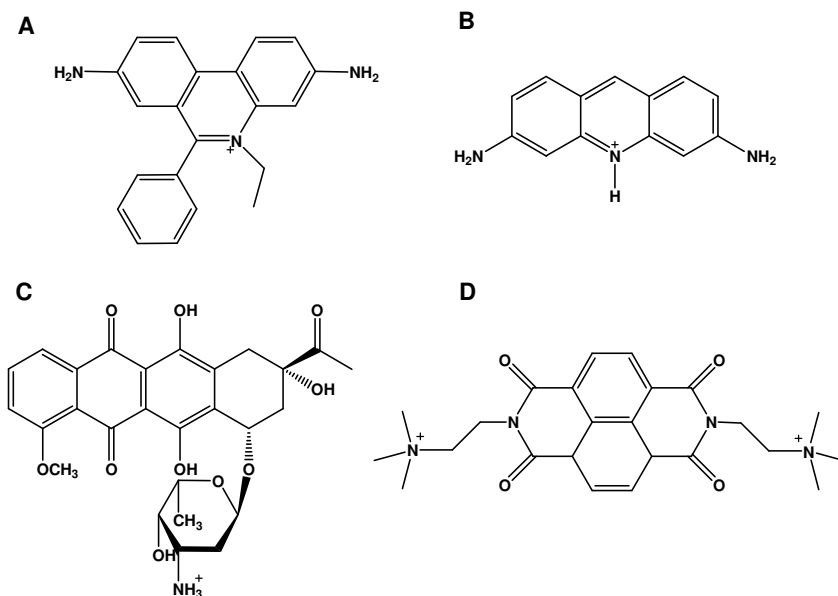


Figure 1.8. *Examples of Intercalators.* (A) Ethidium. (B) Proflavin. (C) Daunomycin. (D) Naphthalene-bisimide

1.3. Factors that affect DNA binding

There are many factors that affect small molecule-DNA interactions. As discussed in the previous section, a drug's structure can influence its mode of binding, for instance by facilitating hydrogen bonding with the grooves or π - π stacking interactions with the DNA bases. Modifying structural elements of a drug can alter its mode of action and selectivity. Hence, structure-activity relationship studies are useful to determine key structural elements in a drug's mechanism of action. A molecule's chirality and spatial characteristics can also determine whether it will fit and interact with its desired target. The physicochemical properties of a drug are central for its interactions. For instance, solubility and partition coefficient are critical for its transport between lipophilic and hydrophilic compartments in the cell. Other conditions such as ionic strength, temperature or pH affect drug-DNA interactions as well.

Because DNA is a charged polyion, metal cations also play a vital role in the mechanism of action of DNA-targeting pharmaceuticals. They can change a ligand's geometry and physico-chemical properties, help direct a drug to specific targets, change their oxidation state, or affect their bioavailability (27-29). Furthermore, metal ions can affect the structures and interactions of nucleic acids and proteins, and can regulate cellular processes such as DNA-packaging, repair, recombination, replication, transcription and translation (30, 31). The metal ions involved are generally the ubiquitous divalent cations Mg^{2+} or Ca^{2+} , but transition metals can substitute them in some cases.

Due to the intrinsic relationship between metal ions and nucleic acid structure and function, innovative metal-containing compounds may serve as useful probes in the fight of diseases and cancer. The metal-related interactions of a family of novel ligands will be the focus of the body of work in this study. Examples of these and other metallo-DNA binders are given in the following section.

1.4. Metallo-DNA binders

Pharmaceutical agents having metal ions as components are becoming increasingly prevalent in treating a wide variety of diseases and metabolic disorders (27, 28, 32-36). Cancerous cells experience unchecked growth, requiring tumor cells to have an elevated level of nutrients, membrane permeability and blood flow with a consequent accumulation of transition metals (32, 37-40). The result can be a greater uptake of metallo-pharmaceuticals within the cancerous cells (38-41). Metal complexes also have higher tendency for hydrolysis, redox and photoreactions that may be exploited as a mechanism of action (42). In addition, having a positive metal ion facilitates the interaction of drugs to the negatively charged nucleic acids, which makes many metal complexes promising therapeutic agents (30, 31, 43, 44).

There are many metallodrugs that are currently in clinical trials, including cisplatin, carboplatin, auranofin, sodium nitroprusside, and cardiolyte (36). Cisplatin (section 1.2.1) is perhaps the most commonly used chemotherapeutic agent, and is administered to treat various types of cancer, particularly testicular cancer (45). In spite of the wide usage of cisplatin, this drug presents high general toxicity that result in undesired side effects, and many tumor cell types are resistance to this drug (46). Studies of cisplatin have stimulated research of other transition-metal based compounds. Metallodrugs have emerged that show promising antibacterial or antineoplastic activity, including complexes with palladium, ruthenium, gold, rhodium, copper, and lanthanum (43, 47). A few representative examples will be discussed in the next section.

1.4.1. Aureolic acid group of antitumor antibiotics

The aureolic acid antitumor antibiotics, such as chromomycin or mithramycin (Figure 1.9), were originally isolated from *Streptomyces* species and consist of tricyclic polyketides attached to oligosaccharide chains of variable length such as (48). Mithramycin has been studied since the 1950s and is currently used as a chemotherapeutic agent for the treatment of several types of cancer (49, 50).

Chromomycin and mithramycin are known to interact with the DNA minor groove of GC rich sequences in the presence of divalent cations (51). The metal-mediated DNA binding in the presence of Mg^{2+} is well documented, but other metal complexes have also been recently investigated (51-57). Besides magnesium ions, mithramycin has also been shown to bind to Cu^{2+} , Fe^{3+} , and Tb^{3+} ions (58). A recent study showed that mithramycin formed stable complexes with Fe^{3+} ions with higher cytotoxicity in several cancer cell lines and higher affinity for DNA than its magnesium counterpart (52).

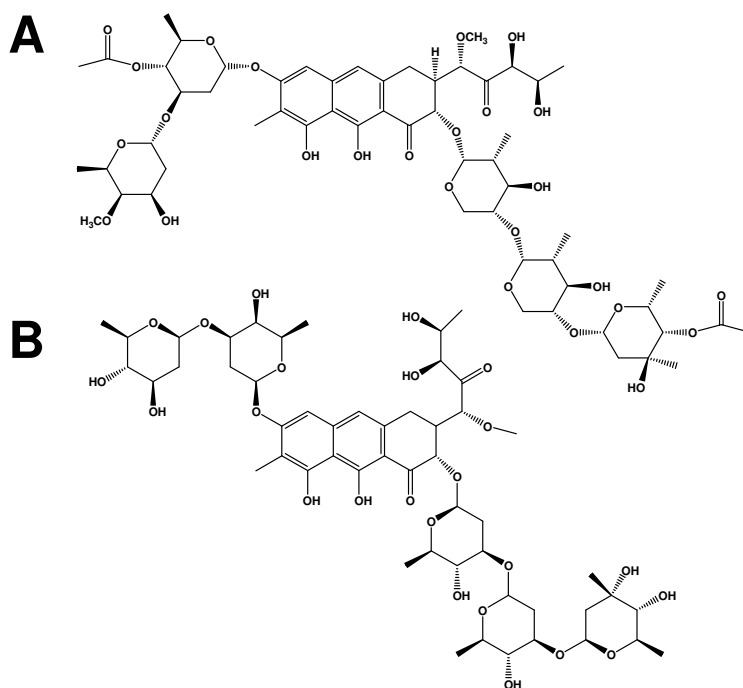


Figure 1.9. Members of the aureolic acid group of antitumor antibiotics. (A) Chromomycin. (B) Mithramycin.

1.4.2. Quinolones

Quinolones and fluoroquinolones were first investigated as bactericidal drugs. The first generation of compounds were originally synthesized in the 1960's and included compounds such as nalidixic acid (Figure 1.10A), which was used for urinary tract infections (59). However, because of its poor efficacy and side-effects, it was dropped from clinical use several years later. By 1980's a series of improved quinolones such as Ciprofloxacin (Figure 1.10B) were developed with a fluorine addition at the C-6 position; these compounds showed enhancement of potency against Gram negative and positive bacteria (60, 61). To date, Ciprofloxacin is the most active and broad range oral antibacterial in clinical use. Third generation quinolones include compounds such as Levofloxacin with increased efficacy against resistant strains of bacteria (Figure 1.10C) (62).

Studies have shown that some of the main targets of these compounds are DNA gyrase and topoisomerase IV-DNA complexes which are essential in all bacteria (63). Quinolones interact at or near site of DNA scission of these enzymes; they perturb the local DNA structure and increase levels of enzyme-DNA cleavage complexes eventually leading to cell death.

Later studies showed that some quinolones did not display antibacterial activity but were cytotoxic against several cancer cell lines (64). The cytotoxicity has been correlated with Topoisomerase II inhibition, which is the eukaryotic counterpart of DNA Gyrase. These properties are being exploited and new quinolones are now being investigated as antineoplastic agents (65, 66).

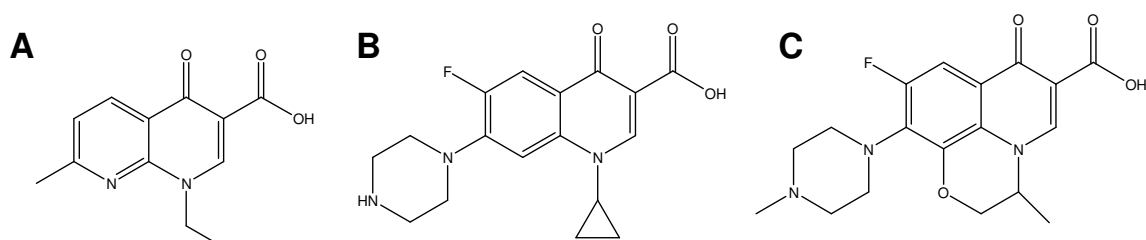


Figure 1.10. Members of the quinolone family of drugs. (A) Nalidixic acid (B) Ciprofloxacin (C) Levofloxacin

A key determinant in the mechanism of action of these drugs is their ability to bind to single-stranded DNA. These interactions are closely related to their interactions with metal ions. As with the aureolic acids, Mg^{2+} -quinolone complexes have been extensively studied and coordination with this metal has proven to be fundamental with the DNA-enzyme complexes (67). Recent studies have also investigated complexes of quinolones with other transition metals such as Co^{2+} , Cu^{2+} , Ni^{2+} , and Zn^{2+} ; in vitro tests indicate that the complexes display stronger activity than that of uncomplexed drugs (68). Some compounds described in the following section of exhibit similar binding characteristics to this family of compounds and will be discussed further in later chapters.

1.4.3. Benzoxazole, Benzothiazole, and Benzimidazole Ligands

Benzoxazole, benzothiazole and benzimidazole compounds have been studied for decades for their wide array of biological properties (69-71). They possess a degree of structural similarity with purine nucleic bases such as guanine or adenine that can facilitate their interactions with biopolymers such as DNA. Not surprisingly, as in other groups of DNA-interactive molecules, these moieties are often encountered in compounds that present a variety of therapeutic activities, including antimutagen, antiallergic, analgesic, anti-inflammatory, antipyretic, antioxidant, antiaggregant, antiparasitic, antibacterial, antiviral, or antitumor properties (69-84). In many cases these compounds can coordinate metal ions through the nitrogen or oxygen atoms of the ring system (85-95). UK-1 is an example of a bis-benzoxazole ligand that can form metal complexes and presents very interesting biological properties. The first part of this dissertation encompasses the synthesis and biological evaluation of simplified benzoxazole analogs of UK-1. Further discussion of this natural product and some of its analogs are given in the following sections.

1.5. The Bis-benzoxazole natural product UK-1

1.5.1. Discovery

UK-1 was originally isolated from *Streptomyces* sp. 517-02 by Akei and coworkers while screening for new antibiotics (96). Although UK-1 did not present any growth inhibitory activity against Gram-negative and Gram-positive bacteria, yeasts or fungi up to 100 µg/ml, it did show cytotoxicity against the cancer cell lines B16, HeLa and P388 (IC_{50} = 3.0, 3.2, and 0.3 µM respectively). The same research group also carried out the structural elucidation of this novel metabolite (97), uncovering a unique bis-benzoxazole in which the 2-position of

one benzoxazole was joined to the 4-position of the second ring as shown in Figure 1.11A.

As part of the structural characterization of UK-1 two new derivatives were prepared, the mono-methyl ether MUK-1 produced by methylation with methyl iodide and anhydrous potassium carbonate, and the corresponding carboxylic acid, DMUK-1, generated by alkaline hydrolysis (97). Later biological studies of DMUK-1 and MUK-1 revealed that these non-cytotoxic compounds possessed antibacterial and antifungal activity against certain strains (98, 99). Sato *et al.* also isolated a related bis-benzoxazole product from *Streptomyces* sp AJ9561 (100). This compound, AJI9561, like UK-1, presented cytotoxicity against Jurkat and P388 cells (0.88 μM and 1.63 μM respectively). The structures of MUK-1, DMUK-1, and AJI9561 are shown in Figure 1.11, panels B-D.

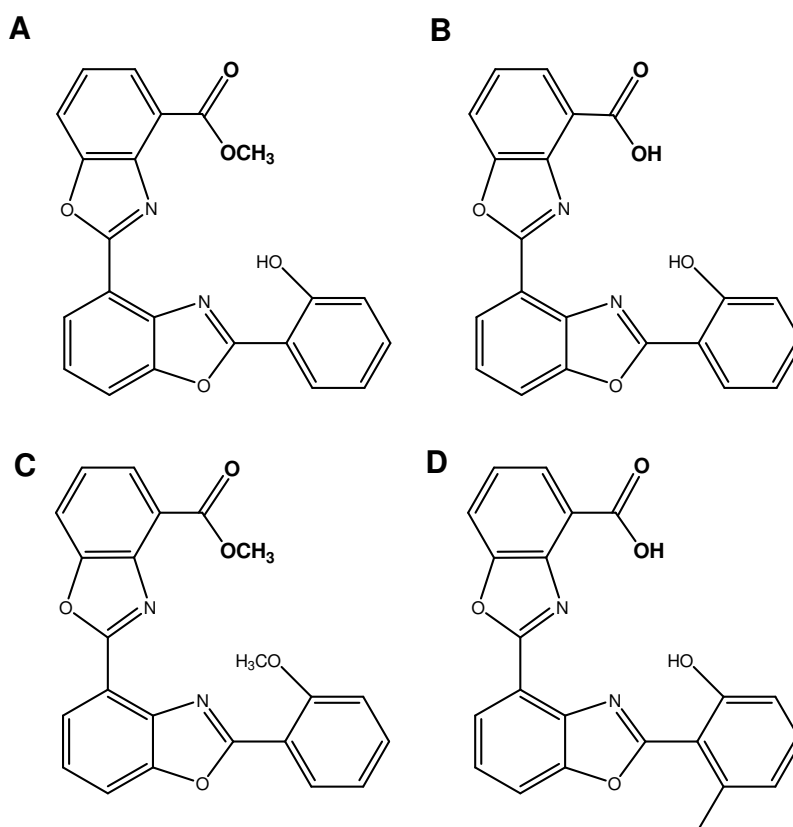


Figure 1.11. Structure of UK-1 and bisbenzoxazole derivatives. (A) UK-1. (B) DMUK-1. (C) MUK-1. (D) AJI9561

1.5.2. Biological properties

The Kerwin research group became interested in the unusual biological properties of these bis-benzoxazoles compounds as potential anticancer agents. Previous studies by DeLuca and Kerwin achieved the total synthesis of UK-1 and DMUK-1, confirming the assigned structures (101). Further biological studies were conducted to obtain insight into the possible mechanism of action of UK-1 (102).

One of the aspects explored was the possibility that the interactions of UK-1 could involve metal ions. The rationale was initiated by the structural comparison to known synthetic metal complexes that contain the 2-(2'-hydroxyphenyl) benzoxazole moiety present in UK-1 (85, 93, 95). Furthermore, the related 2-(2'-hydroxyphenyl)oxazoline moiety is present in several microbial siderophore natural products that can bind iron or copper, such as Nocobactin NA, Asteroidic acid, Mycobactin M, Brasilibactin A, Parabactin or Exochelin 772SM (103-107). Experiments by Reynolds *et al.* showed that in fact UK-1 did exhibit spectral changes upon addition of several divalent cations (102). It was determined that this compound could form stable complexes with Mg^{2+} and Zn^{2+} with an overall stoichiometry of 1:1. Weaker binding to other ions like Fe^{3+} and Ca^{2+} was observed, while no variations in the spectra occurred in the presence of monovalent cations like K^+ . Addition of excess NaOH caused similar changes as those examined upon metal ion binding, suggesting that the phenolate species is involved in metal coordination.

Unlike the unbound ligand, the 1:1 complexes of UK-1 with divalent and trivalent metal ions are cationic, which could lead to favorable interactions with DNA. This led Kumar *et al.* to investigate the affinity of UK-1 for calf thymus DNA in the presence and absence of Mg^{2+} ions. A ten-fold tighter association was observed when magnesium was present, as well as an increase in the melting

temperature of the DNA (102). This study also showed that UK-1 could inhibit the activity of human Topoisomerase II in decatenation assays, indicating that it can interfere with DNA-processing enzymes. The metal-mediated DNA binding of UK-1 was corroborated by mass spectrometry studies, where complexes of UK-1 with oligonucleotide sequences were only observed in the presence of divalent cations like Zn^{2+} , Co^{2+} , and Ni^{2+} (108). To further understand the structural basis of the biological properties of UK-1 structure-activity relationship studies were previously carried out as described below.

1.5.3. Structure activity relationships of UK-1 analogs

A number of analogs of UK-1 were synthesized by Kumar and co-workers in which the carbomethoxy-substituted benzoxazole ring was either modified or deleted, as shown in Figure 1.12 (109). To evaluate their anticancer activity, cytotoxicity studies were performed in various cancer cells lines, including the breast cancer (MCF-7), leukemia (HL-60), colon carcinoma (HT-29), and prostate cancer (PC-3) cells. Table 1.1 shows the IC_{50} values obtained which represent the concentration of the compound required for 50% growth inhibition compared to untreated cells.

Modification to a benzimidazole ring as in **1** abolished the cytotoxicity in 3 of the 4 cell lines studied. The benzyl adduct **2** was isolated as a side product during the synthesis of UK-1. This compound presented a diminished degree of activity compared to UK-1 except in HT-29 cells. Most of the other analogs studied did not exhibit anticancer activity against the cancer cell lines, except for the 2-(2-hydroxy-phenyl)-benzoxazole-4-carboxylic acid methyl ester **8**, which displayed a similar toxicity profile to UK-1.

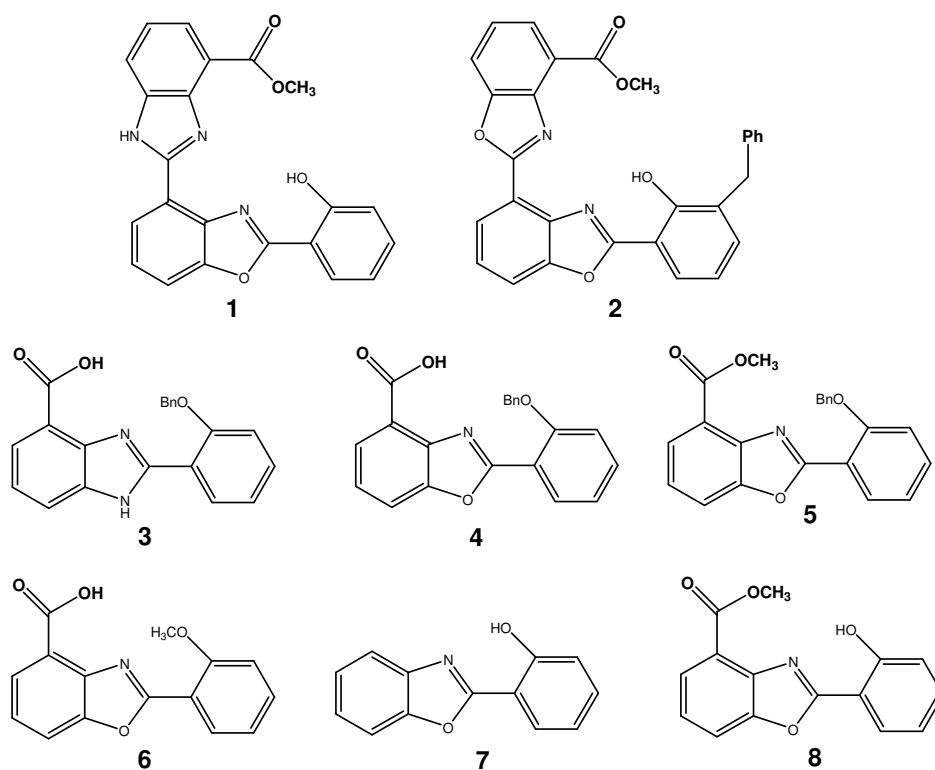


Figure 1.12. Structures of UK-1 analogs 1-8. Analogs synthesized by Kumar *et al* (109).

Table 1.1. Anticancer activity of UK-1 and analogs 1-8. Table adapted from reference (109). Cytotoxicity against MCF-7, HL-60, HT-29, and PC-3 cells was determined after 72 h incubation with compound at 37 °C using the AlamarBlue Assay.

Compound	IC ₅₀ (μM)			
	MCF-7	HL-60	HT-29	PC-3
UK-1	1.6	0.32	65	0.4
1	>100	70	>100	>100
2	13	27	5.2	4.5
3	>100	>100	>100	>100
4	>100	>100	>100	>100
5	>100	>100	>100	>100
6	>100	>100	>100	>100
7	>100	>100	>100	>100
8	1.5	5.7	9.1	0.88

The antibacterial activity of these series against was also examined in two strains of *S.aureus*. The benzimidazole acid **3** and the benzoxazole acid **4** presented very modest activity against the two bacterial strains. Like UK-1, the rest of the compounds did not show any antibacterial activity up to a concentration of 50 µg/ml.

It was also established that within this series of compounds there was a correlation between metal binding affinity and cytotoxicity. The spectra of methanolic solutions of these compounds were monitored in the presence of varying concentrations of Mg²⁺, Zn²⁺, Ca²⁺, or Fe³⁺ ions. Analogs that have a benzyl or methyl protected phenyl group (compounds **3-6**) did not form complexes with any of the metal ions studied and were not active against cancer cells. The inactive 4-unsubstituted 2-(2'-hydroxyphenyl)-benzoxazole **7** could form complexes with some of the metals, but not magnesium. Likewise, the benzimidazole analog **1** showed lower affinity for Mg²⁺ compared to UK-1. Conversely, the cancer cell cytotoxic analog **8** presented similar Mg²⁺ and other metal ions binding with respect to the natural product. These results indicate that substituting the 4-(benzoxazo-2-yl) moiety in UK-1 for a 4-carbomethoxy substituent, as in **8**, retain Mg²⁺ ion binding ability and cytotoxicity, while the 4-(benzimidazo-2-yl) substituent (as in **1**) does not. Removing the 4-carboxymethoxy group altogether, as in **7** greatly reduces metal ion affinity and abolishes activity. The data taken together indicated that compound **8** represents a minimum pharmacophore of the selective anticancer activity and metal ion chelation of UK-1.

As noted earlier, UK-1 has been shown to form metal ion complexes that can bind to DNA and can inhibit DNA processing enzymes (102, 108). While it is unlikely that metal ion binding per se is the origin of the selective cytotoxicity of UK-1 or compound **8**, this study pointed out that metal ion affinity, in particular Mg²⁺, might be key to retain activity. An appropriately substituted 2-(2'-hydroxyphenyl) benzoxazole moiety, such as the simplified analog **8**, is crucial to preserve the biological properties of UK-1. However, the structural basis for

metal ion recognition and anticancer activity for this structure requires further investigation.

Compound **8** represents an important lead to design more potent anticancer drugs, and has been used as a starting point encompassed in the following work. An experimental plan was developed with the following aims: 1) To design and synthesize novel benzoxazole analogs of compound **8**, 2) to examine key structural elements for metal binding, and 3) to investigate the effects of metal binding on DNA affinity and biological activity.

The synthesis and design of DNA interacting compounds is a potentially important strategy in the treatment of cancer cells. Determining the binding conditions of novel metal chelated ligands and their DNA targets provide a powerful mechanism to inhibit unchecked cell growth. Furthermore, the study of these small molecules may offer insight into how metal ion complexes can be harnessed in the design of selective cytotoxins.

CHAPTER 2. DESIGN AND SYNTHESIS OF NOVEL SIMPLIFIED BENZOXAZOLE ANALOGS OF UK-1 AND METAL COMPLEXES

2.1. Rationale for the Design of New Analogs

2.1.1. Disposition of N and O in the benzoxazole moiety

As discussed in section 1.5.3, structure-activity-relationship comparisons by Kumar and co-workers determined that the simplified compound **8** was the minimum pharmacophore structure that retained the selective cytotoxicity of the natural product UK-1 (*109*). It was also noted that affinity for metal ions was correlated with their activity. In order to further investigate the relationship between biological activity and metal coordination it is important to examine the structural elements that are important for metal binding. Compound **8** consists of a 2-(2'-hydroxyphenyl)-benzoxazole with a methyl ester at position 4 of the benzoxazole ring (Figure 2.1A).

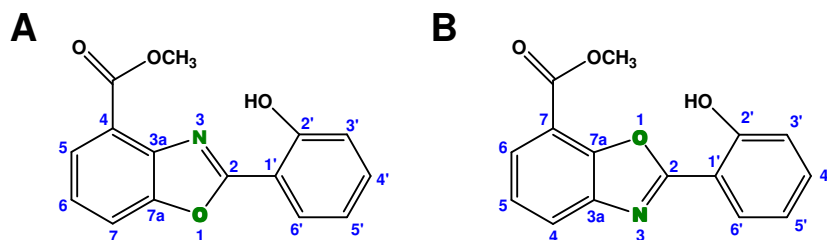


Figure 2.1. Disposition of the Nitrogen and Oxygen atoms in the benzoxazole moiety of compounds **8** and **9**. (A). The methyl ester is positioned in the same side as the N in the benzoxazole ring in compound **9**. (B) The methyl ester is positioned in the opposite side of the ring as the N heteroatom.

Studies on benzoxazole itself have revealed that this compound is able to form metal complexes with Co²⁺, Cu²⁺, Ni²⁺ and Zn²⁺ through coordination with

the nitrogen heteroatom of the cycle (86, 88). Improved coordination is found in the compound 2-(2'-hydroxyphenyl)-benzoxazole (compound **7**) which has been reported to chelate with Co^{2+} , Cd^{2+} , Cu^{2+} , Ni^{2+} and Zn^{2+} , stabilized through interactions with both the phenolate O and its benzoxazole ring N (87, 93, 95, 110). However, this compound is unable to bind Mg^{2+} ions and did not present any cytotoxicity in the cancer cell lines studied by Kumar *et al.* (109). Introduction of 4-carbomethoxy substituent to the benzoxazole core, as in **8**, appeared to impart Mg^{2+} ion binding ability as well as activity against cancer cell lines to the 2-(2'-hydroxyphenyl)-benzoxazole core.

To expand on this idea, the isomeric benzoxazole analog (**9**), 2-(2'-hydroxy-phenyl)-benzoxazole-7-carboxylic acid methyl ester, was synthesized as described in the following section. Compound **9** differs with **8** solely in the disposition of the benzoxazole N and O atoms within the cycle; unlike compound **8**, the methyl ester is located on the opposite face of the ring to the N heteroatom (see Figure 2.1). If the methyl ester is not involved in metal coordination, no differences between metal affinities would be expected between the two compounds. Discrepancies between within their binding modes and biological activities would aid in the understanding of the structural significance of a substitution at the 4 position of benzoxazole ligands.

2.1.2. Effect of modification of the methyl ester position

To design more potent analogs with improved physicochemical properties it is imperative to modify structural elements that will not lessen their biological activity. Modifications of the 4-carbomethoxy position of compound **8** could serve as a starting point for new structure activity relationships. Because it is likely that metal coordination occurs between the N in the benzoxazole ring, the phenolate O and is further stabilized through interactions with an O in the methyl ester, it is important to design analogs that retain these characteristics.

Further evidence for this idea came from the studies of Wang and coworkers (111). The authors synthesized three new UK-1 analogs and studied their inhibition of the enzyme Topoisomerase II. They observed that deletion of the methyl ester or the 2'-hydroxyl group in UK-1 (Compounds Wang-1 and Wang-2 in Figure 2.2) did not affect enzymatic inhibition significantly. On the other hand, the removal of both functional groups abolished the compound's activity (Compound Wang-3). Their research suggested that the analogs required a structural motif comprised of an isosceles triangular arrangement between the oxygen atom of carbonyl group, the heterocyclic nitrogen atoms, and/or the phenolic hydroxyl for enzyme inhibition (Figure 2.2). They also noted that the simplified compound **8** possesses a similar arrangement of basic sites; they proposed that this structural motif could be involved with metal ion chelation and activity.

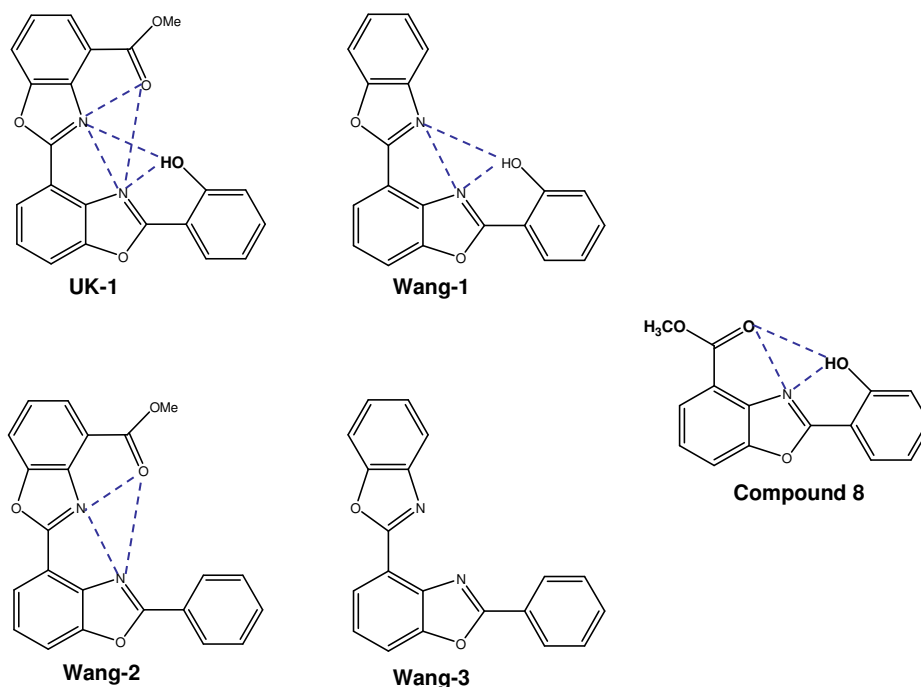
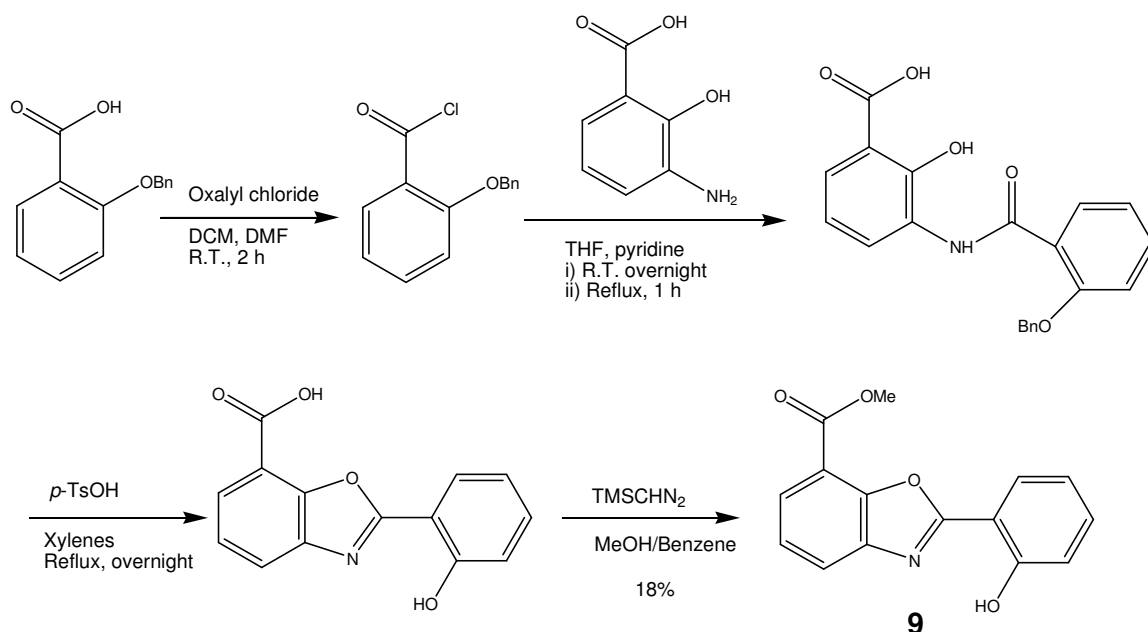


Figure 2.2. Structural motif in UK-1 analogs important for activity. UK-1 analogs prepared by Wang *et al.* suggest that an isosceles triangular arrangement between the nitrogen atom in the benzoxazole core and at least two other heteroatoms, as in compound **8**, UK-1, and Wang compounds **1** and **2**, is necessary to retain activity. The calculated distances between the highlighted groups are 2.9–3.0 Å on two sides and 4.5–4.7 Å on the remaining side (111).

Keeping these considerations in mind, a new series of compounds that explore effects of different 4-substituents of compound **8** while retaining the benzoxazole core and the 2-(2'-hydroxyphenyl) substituent were prepared. In particular, the effect of homologation of the 4-methyl ester and its replacement with an amide were addressed. Given the evidence that metal ion complexation is important for cytotoxicity in previous UK-1 derivatives, additional potential metal ion coordination sites were introduced in some analogs. As previously observed, UK-1 and compound **8** have low aqueous solubility, so polar groups at this position were also included (102, 109).

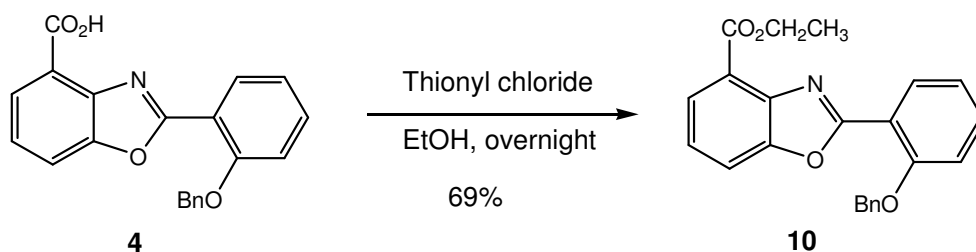
2.2. Synthesis of Novel Benzoxazole ligands

The synthesis of these analogs was accomplished through adaptation of the previously reported procedures for UK-1 and compound **8** (101, 109). The synthesis of methyl 2-(2'-hydroxyphenyl)-benzoxazole-7-carboxylate (**9**) was carried out as a one-pot procedure depicted in Scheme 2.1. The condensation of 2-benzyloxybenzoic acid chloride with 3-amino-2-hydroxybenzoic acid yielded the intermediate 3-(2-benzyloxy-benzoylamino)-2-hydroxy-benzoic acid which was cyclized and de-protected with *p*-TsOH. Methylation using TMS-CHN₂ afforded compound **9** with 18% overall yield.



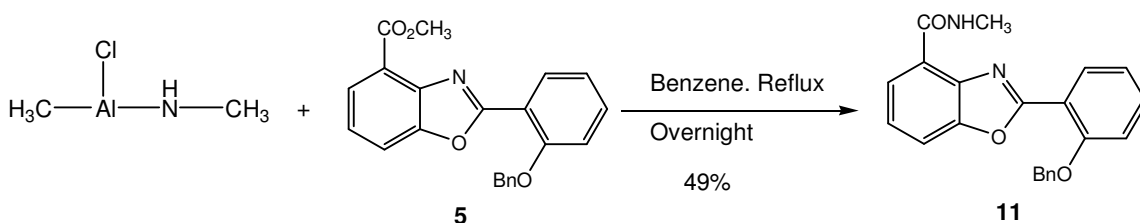
Scheme 2.1. *Synthesis of compound 9*

Modification at the C4 position of compound **8** were carried out using a key intermediate, the benzyl-protected carboxylic acid **4** (Figure 1.12) through esterification (compounds **10,15**) or coupling with a primary amine (compounds **11-14**). Analog **10** possesses an ethoxy group instead of the methoxy group, and was synthesized as described in Scheme 2.2; esterification of compound **4** in EtOH using thionyl chloride produced the ethyl ester in a 69 % yield.

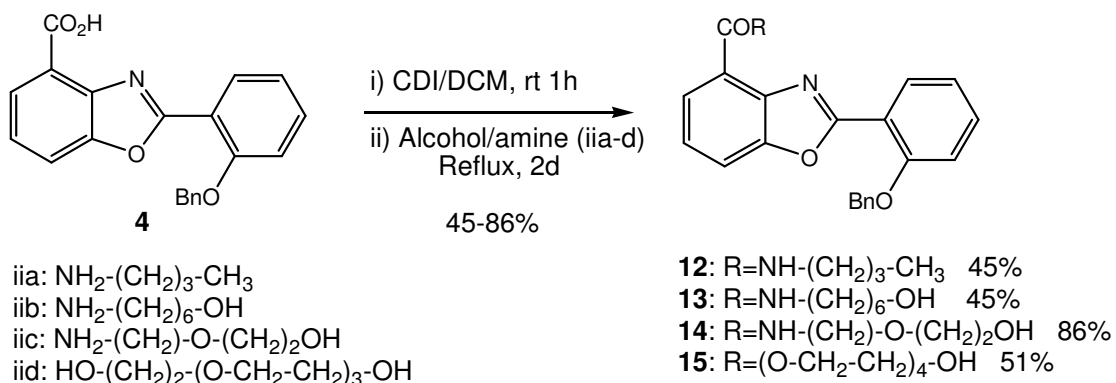


Scheme 2.2. *Synthesis of Compound 10. Coupling of EtOH to compound 4 was achieved through a simple esterification with thionyl chloride.*

The methylamide **11** was prepared with a 49% yield from the methyl ester **5** through coupling with a methylaluminumchloride-methylamide reagent (Scheme 2.3). Other analogs with extended esters and amides were also synthesized via CDI coupling of compound **4** with butylamine, aminohexanol, 2-(2-aminoethoxy)ethanol, or tetraethylene glycol to give compounds **12-15** respectively with yields ranging from 45-86 % (Scheme 2.4).

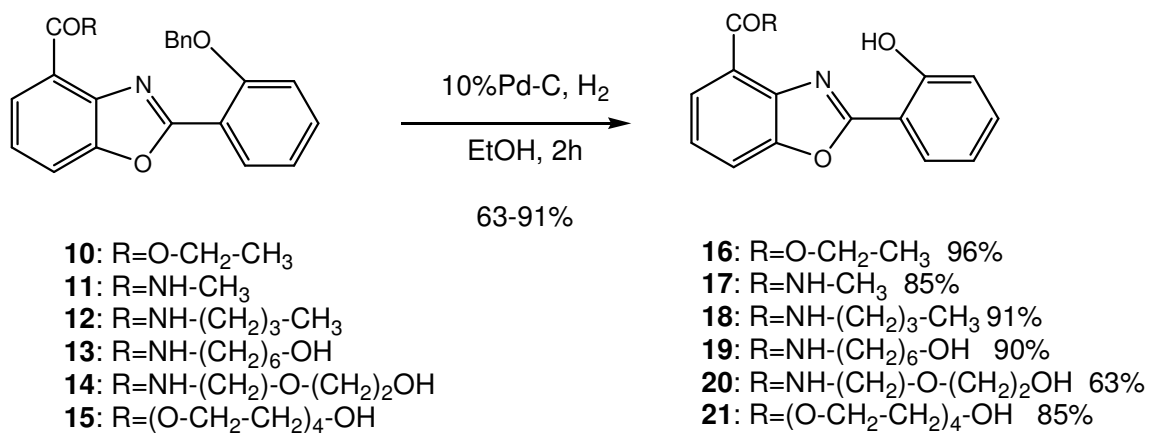


Scheme 2.3. Synthesis of compound **11**. The benzyl protected ester **5** was reacted with a methylaluminum-methylamide reagent to give compound **11**.



Scheme 2.4. Synthesis of compounds **12-15**. Compound **4** was coupled using CDI to various esters and amines yielding analogs **12-15**.

The resulting esters and amides were subjected to hydrogenolysis to remove the benzyl phenol protecting group to afford the 2-(2'-hydroxyphenyl) benzoxazoles (compounds **16-21**) in 63-91% yield as depicted in Scheme 2.5.



Scheme 2.5. Synthesis of compounds **16-21**. The esters and amides **10-15** were deprotected through hydrogenolysis

CHAPTER 3. AFFINITY OF ANALOGS FOR METAL IONS

The majority of DNA binding agents do not require metal ions to exert their biological activity, but some, such as members of the aureolic acid group of antitumor antibiotics and quinolone derivatives (see section 1.4) require metal coordination for proper function and structure. Similarly, the bis-benzoxazole natural product UK-1 is able to form complexes with divalent and trivalent cations and can bind to DNA in the presence of metal ions (102, 112). The new simplified benzoxazoles discussed in the previous chapter contain a 2-(2'-hydroxyphenyl)benzoxazole (HPB) moiety present in UK-1 which has been associated with its ability to bind to transition metals and with its biological properties (102, 109). It is therefore important to investigate if substitutions to the C4 or C7 position in the HPB core affect metal coordination of these ligands.

3.1. Methyl ester at the C4 or C7 position of the HPB ring affects metal binding ability

As discussed in section 2.1.1, compounds **8** and **9** differ in the disposition of the nitrogen and oxygen atoms with respect to their carbomethoxy substituent; the methyl ester is located on position C4 in compound **8** whereas it is located on position C7 in compound **9**. NMR studies were carried out to compare the metal ion binding affinity of compound **8** and **9**. Solutions of **8** in 1:1 CD₃OD/CDCl₃ (100 mM) were prepared and all ¹H and ¹³C NMR resonances were assigned by a combination of COSY, HMBC, and HMQC NMR spectra (see Appendix A). Compound **8** was then titrated with Mg(NO₃)₂·(H₂O)₆ in CD₃OD (2.5 M) and the NMR spectra was recorded after each addition (¹H NMR spectra is shown in Figure 3.1). The initial addition of Mg²⁺ (0.25 eq.) caused a marked broadening of all the ¹H NMR resonances and shifts in specific peaks. Notably, certain

resonances, such as that due to the benzoxazole C7 hydrogen (ca. 7.5 ppm), shifted downfield while other resonances, such as those due to the 4-carbomethoxy group (ca. 3.7 ppm) shifted upfield (a complete list of ^1H and ^{13}C NMR shifts is shown in Appendix B). Further additions of Mg^{2+} resulted in upfield shifts of all resonances, but in particular those due to the 4-carbomethoxy group and the ortho-hydroxyphenyl moiety (ca. 6.7 and 6.8 ppm), indicating that these residues are most affected upon metal coordination.

These solution studies support the role of the 4-carbomethoxy group in metal binding by **8** and also implicate the benzoxazole moiety and the ortho-hydroxyphenyl substituent in metal ion coordination. The complex relationship between ^1H NMR resonance shifts and Mg^{2+} concentration may be due to the formation of different metal ion complexes of different stoichiometries during the titration experiment.

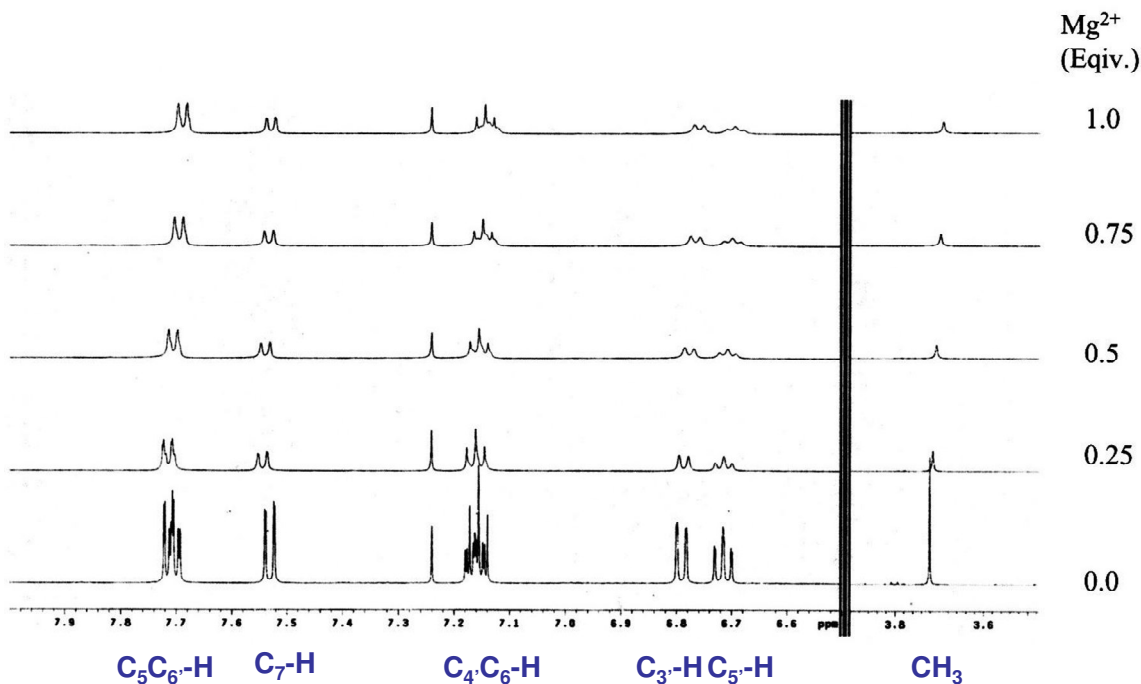


Figure 3.1. ^1H NMR Spectrum of Compound **8** in the presence of Mg^{2+} . Line broadening of all peak resonances occurred after the first addition of 0.25 eq. Mg^{2+} , and continued until 1 eq. Peak resonances corresponding to hydrogens in the structure of compound **8** are indicated beneath the spectrum; for structure, see Figure 2.1

Further evidence for the role of the benzoxazole moiety in metal ion coordination can be achieved by comparing the results obtained from metal binding with compound **9**. As discussed in the previous chapter, this analog is the reverse isomer of **8** in which the position of the benzoxazole N and O atoms are interchanged with respect to the carbomethoxy substituent. The ^1H NMR spectral changes observed upon addition of Mg^{2+} to the isomeric benzoxazole analog **9** (Figure 3.2, Appendix B) are quite distinct from those observed for **8**. The ^1H NMR resonances for this analog are uniformly shifted upfield in the presence of increasing concentrations of Mg^{2+} , with no evidence of the line broadening emblematic of metal binding until an excess of Mg^{2+} is added. The apparent difference in the metal ion complexation between the **8** and **9** must be due to the difference in the disposition of the benzoxazole N and O atoms, further supporting a role for Mg^{2+} coordination between the phenol oxygen and the nitrogen atom in the benzoxazole moiety aided by the carbonyl oxygen of the methyl ester group.

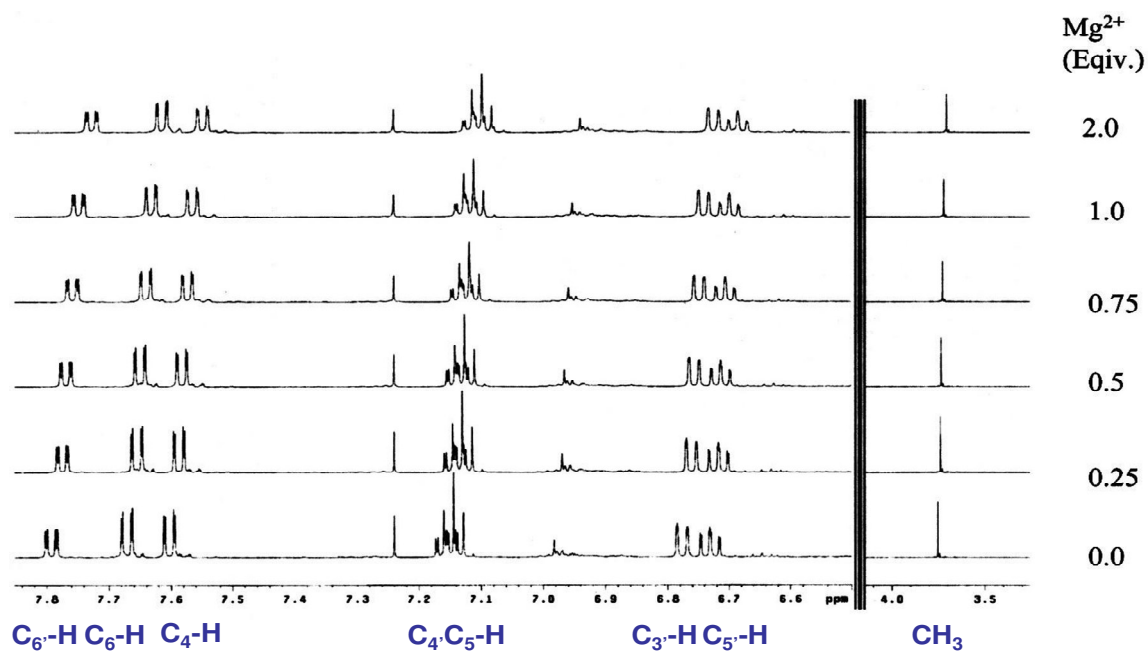


Figure 3.2. ^1H NMR Spectrum of Compound **9** in the presence of Mg^{2+} . Peak resonances are uniformly shifted upfield upon addition of increasing concentrations of Mg^{2+} , but are not

significantly broadened. Peak resonances corresponding to hydrogens in the structure of compound **9** are indicated beneath the spectrum; for structure, see Figure 2.1.

Unfortunately, attempts to shed light on potential differences in structure between the complexes formed with **8** and **9** Mg^{2+} or Ni^{2+} by NMR titrations are precluded by the paramagnetic properties of the latter. NMR titrations of **8** with various Cu^{2+} salts also resulted in severe line broadening, presumably due to formation of paramagnetic Cu^+ species. To circumvent this issue, the spectral changes of these analogs in the presence of varying concentrations of metal ions were monitored by UV-Vis (Figure 3.3). These measurements were carried out in methanolic solutions due to the low solubility of compounds **8** and **9** in aqueous buffers.

As with NMR experiments, the spectral changes of compounds **8** and **9** were distinct. Addition of Mg^{2+} to a 10 μM solution of **8** in methanol resulted in a marked hyperchromicity in the 350-450 nm region, even at low Mg^{2+} /ligand ratios (Figure 3.3A). In contrast, compound **9** displayed no significant shifts even at 1 mM concentration of Mg^{2+} (Figure 3.3B). Both compounds displayed spectral shifts upon addition of Cu^{2+} metal ion salts, but compound **9** required much higher concentrations to reach saturation (Figure 3.3C and D respectively). The data indicates that an appropriate substituent at the C4 position, represented by compound **8**, aids in tighter copper coordination and grants the ability to bind magnesium cations. The triangular arrangement between the phenolic hydroxyl group, the benzoxazole nitrogen atom, and the ester in this ligand could have a favorable geometry for metal coordination. Analogs with different modifications at the C4 position, such as those covered in the following section, can help understand the role of the C4 substituent on metal coordination and biological properties.

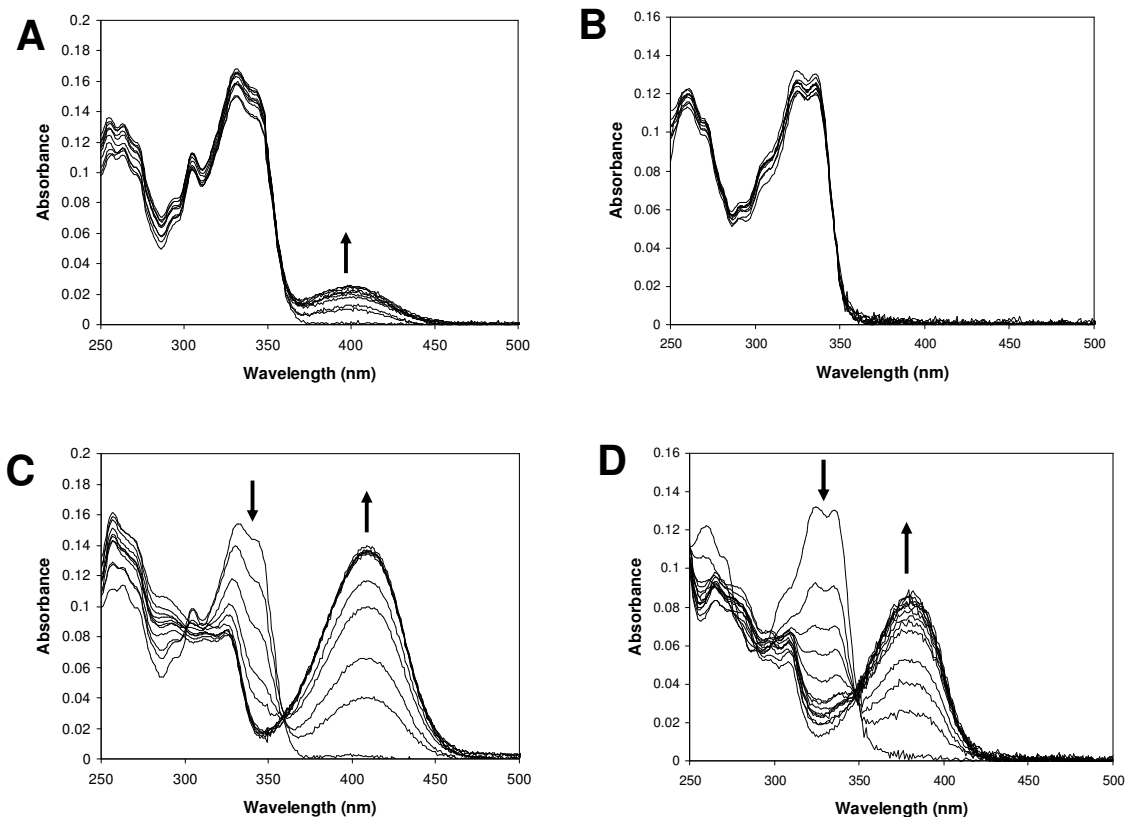


Figure 3.3. UV-Vis spectral changes of Compounds **8** and **9** upon addition of Mg^{2+} and Cu^{2+} ions. Absorbance spectra of 10 μM compounds **8** (A and C) and **9** (B and D) in methanol in the presence of increasing concentrations of Mg^{2+} (A) and (B) or Cu^{2+} (C) and (D) respectively. Metal concentrations ranged from 0-90 μM in the case of compound **8**, and were varied from 0-1 mM in the case of compound **9**. Arrows denote the changes in absorbance with increasing metal ion concentrations.

3.2. Ester and amide substitutions at the C4-position of the HPB ring affect metal binding abilities

Because metal binding has been correlated with cytotoxicity in other benzoxazole compounds, the affinity of new benzoxazole analogs of **8**, compounds **16-21** (which contain a substitution at the C4 position, Figure 3.4) for various metal ions was studied. All of these analogs possess a carbonyl group, whether an amide or an ester, that can potentially aid in metal coordination.

Solutions of these compounds in methanol change from colorless to yellow upon addition of divalent cation such as Mg^{2+} , Zn^{2+} , Ni^{2+} , and Cu^{2+} , indicating complexation between the analogs and the metal ions. Although compounds **19-21** displayed increased water solubility relative to UK-1 and compound **8**, metal coordination was assayed in methanol due to the low aqueous solubility of some of the ligands. Compound **21** with a tetraethyleneglycol side chain was the most soluble in the series, and the only one which remained in solution in aqueous buffers at concentrations up to 100 μM .

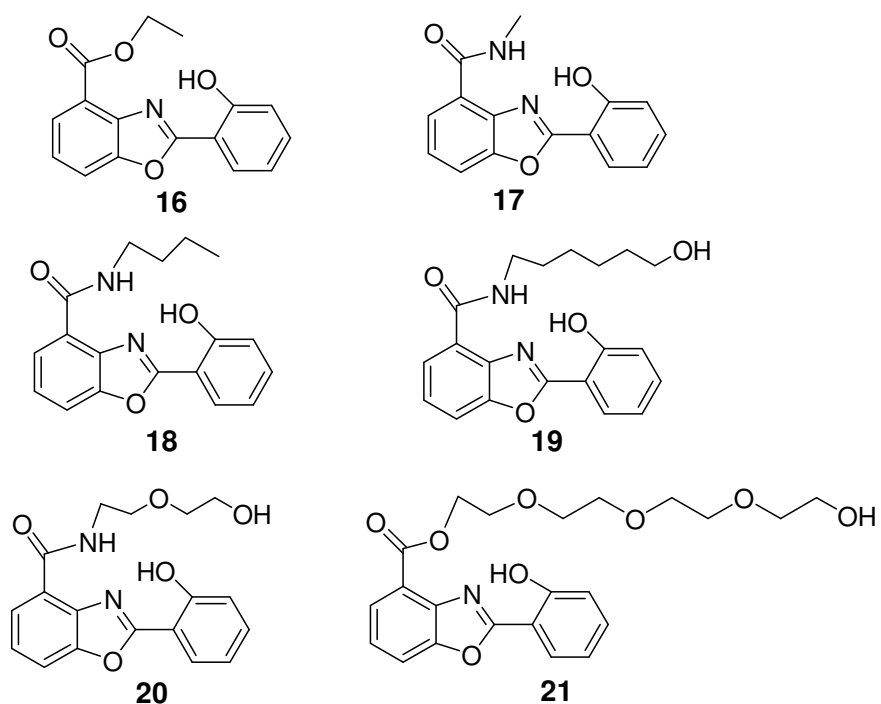


Figure 3.4. Structures of benzoxazoles **16-21** modified at the C4 position.

The most pronounced change occurs in the presence of copper ions. The metal complex formation with these divalent ions was monitored by UV/Vis spectral changes upon addition of increasing concentrations of the metal ion nitrate salts in methanol. A marked hyperchromicity in the 350-450 nm region was observed upon addition of the metal ion, concomitant with a hypochromicity in the 315-350 region. A

clear isosbestic point was present at approximately 350 nm, with slight variation of the wavelength of maximum absorbance depending on the analog studied. The observation of an isosbestic point indicates that the two species, bound and unbound ligand have the same molar absorptivity at this particular wavelength. A representative data set for compound **17** for binding to the four divalent cations is shown in Figure 3.5. The methyl phenyl ether **6** (Figure 1.12) was used as a negative control, and no significant spectral changes were observed upon addition of any of the metal ion salts used in this study.

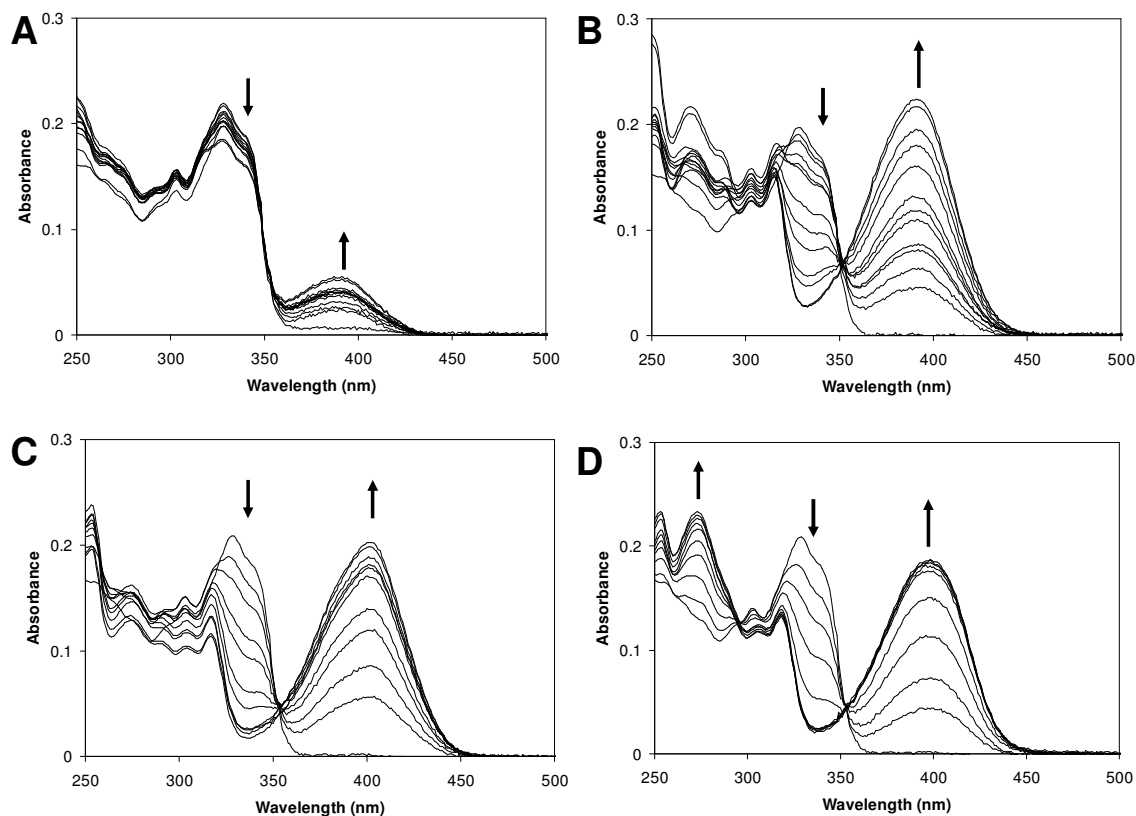


Figure 3.5. UV-Vis spectral changes of compound **17** upon addition of divalent cations. Absorbance spectra of 10 μM compound **17** in methanol was recorded in the presence of increasing concentrations of Mg^{2+} , 0-500 μM (A); Zn^{2+} , 0-500 μM (B); Ni^{2+} , 0-500 μM (C); or Cu^{2+} , 0-90 μM (D). Arrows denote the changes in absorbance with increasing metal ion concentrations.

To compare the binding affinity of the new modified benzoxazole ligands with that of the bis-benzoxazole UK-1, metal ion binding was also examined using the natural compound. As seen in Figure 3.6, UK-1 readily forms complexes with the four metal cations and, as with the other benzoxazole ligands, the spectral changes were most prominent with Cu^{2+} . There is an evident hyperchromicity in the 375-500 and 260-290 nm regions, with an associated hypochromicity in the 355-375 nm wavelengths. Several isosbestic points are observed, around 260, 290, 335, 355, and 375 nm.

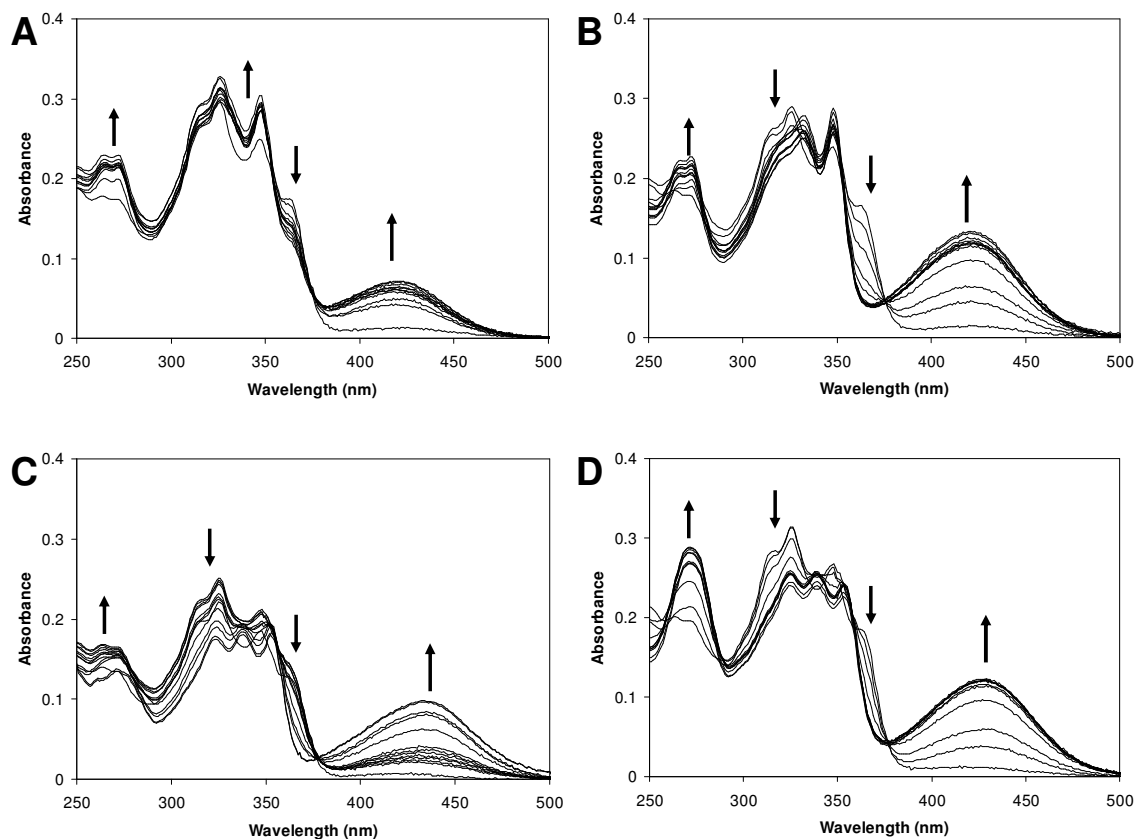


Figure 3.6. UV-Vis spectral changes of UK-1 upon addition of divalent cations. Absorbance spectra of 10 μM UK-1 in methanol was recorded in the presence of increasing concentrations of Mg^{2+} , 0-500 μM (A); Zn^{2+} , 0-500 μM (B); Ni^{2+} , 0-500 μM (C); or Cu^{2+} , 0-90 μM (D). Arrows denote the changes in absorbance with increasing metal ion concentrations.

3.3. Apparent association constants to divalent cations

The change in absorbance of the peak in the 350-500 nm region was plotted against metal ion concentration to obtain binding isotherms, from which the association constants of all the analogs were determined and are summarized in Table 3.1. Data fitting was accomplished using nonlinear regression of the quadratic equation [2] (section 6.2), with assumption of formation of a 1:1 complex (1:1 complexes resulted in higher correlation factors than using alternate stoichiometries). A representative data set for the binding isotherms of compound **17** with the four divalent cations is shown in Figure 3.7.

Table 3.1. Apparent association constants for Mg^{2+} , Zn^{2+} , Ni^{2+} , and Cu^{2+} in MeOH (M^1). Constants were calculated based on the formation of a 1:1 ligand:metal complex.

Compound	K_a (M^{-1})			
	Mg^{2+}	Zn^{2+}	Ni^{2+}	Cu^{2+}
UK-1	$5 \pm 1 * 10^5$	$1.0 \pm 0.5 * 10^6$	$5 \pm 2 * 10^4$	$^a 8 \pm 3 * 10^6$
6	^c No binding	^b n.d.	^b n.d.	^c No binding
7	^c No binding	^b n.d.	^b n.d.	$4 \pm 1 * 10^5$
8	$7 \pm 3 * 10^5$	$4 \pm 2 * 10^6$	$6 \pm 2 * 10^4$	$^a 3 \pm 2 * 10^7$
9	No binding	^b n.d.	^b n.d.	$3.8 \pm 0.4 * 10^4$
16	$1.5 \pm 0.4 * 10^5$	$2.5 \pm 0.5 * 10^5$	$2.6 \pm 0.5 * 10^4$	$^a 3 \pm 2 * 10^6$
17	$6 \pm 2 * 10^4$	$4.5 \pm 0.5 * 10^4$	$4 \pm 1 * 10^5$	$^a 6 \pm 2 * 10^6$
18	$1.1 \pm 0.2 * 10^4$	$3 \pm 1 * 10^4$	$5.6 \pm 0.6 * 10^5$	$^a 6 \pm 4 * 10^7$
19	$2.4 \pm 0.4 * 10^4$	$5.5 \pm 0.8 * 10^4$	$1.1 \pm 0.2 * 10^6$	$^a 2 \pm 1 * 10^7$
20	$2.8 \pm 0.7 * 10^5$	$8 \pm 2 * 10^5$	$8 \pm 4 * 10^6$	$^a 7 \pm 6 * 10^7$
21	$8 \pm 3 * 10^5$	$1.3 \pm 0.4 * 10^4$	$2.0 \pm 0.7 * 10^4$	$^a 7 \pm 6 * 10^7$

^a Values represent lower limit for the association constant

^b Not determined

^c No spectral changes observed up to 1 mM metal ion concentration

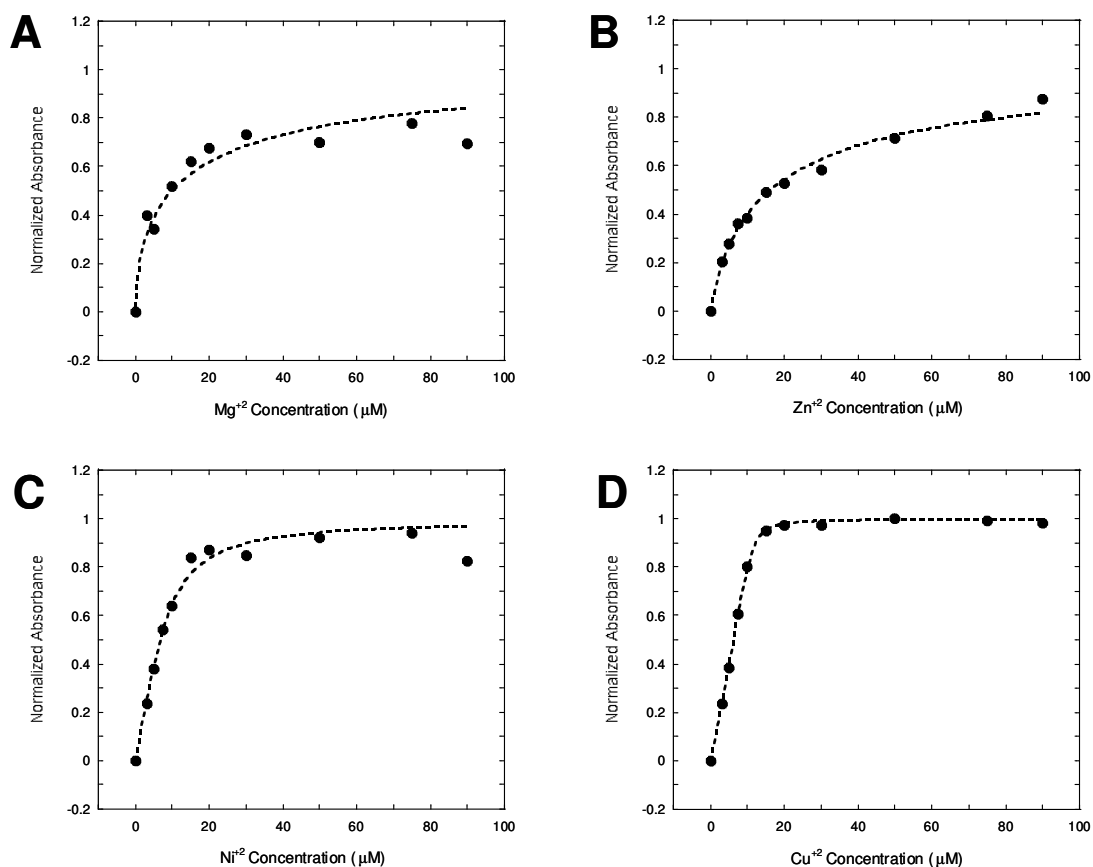


Figure 3.7. Binding isotherms of Compound 17 with metal cations. The normalized increase in absorbance ($\Delta A/\Delta A_{\text{max}}$) was monitored with respect to the free metal ion concentration at 387 nm for Mg²⁺ (A), 391 nm for Zn²⁺ (B), and 400 nM for Ni²⁺ and Cu²⁺ (C and D respectively). The connecting curves were generated by nonlinear fitting of experimental points as described in the experimental section.

As seen in Table 3.1, the C4-substituted HPB analogs **16-21** bind copper with relatively high affinity as 1:1 complexes; after addition of 1 equivalent Cu²⁺ ions there are no further changes in the absorbance spectra. In contrast, the C7-substituted benzoxazole analog **9** is a relatively poor ligand for Cu²⁺ compared to the rest of the analogs, and is the only HPB that does not bind Mg²⁺. In addition, the methyl phenyl ether **6** did not form complexes with any of the salts studied. In general, the Cu²⁺ binding ability of the C4-substituted benzoxazoles, UK-1, **8** and **16-21**, is relatively insensitive to changes in the 4-substituent. In contrast, the

binding affinity towards the other metals is dependant on the nature of the groups at this position. The analogs with amide substituents do not bind Mg^{2+} as well as those with ester groups. As a result, the amides particularly, are more selective ligands for Cu^{2+} versus Mg^{2+} . On the other hand, the amides bind Ni^{2+} with stronger affinity than the esters, with longer side chains such as in compound **19** and **20** binding better than those with smaller groups, like **17** and **18**. The ability to bind Zn^{2+} decreased in the order of compound **8**>**16**>**21**, indicating that the length of the side chains could also play a role in Zn^{2+} coordination.

The critical role played by the benzoxazole C4-substituent in metal ion recognition is also demonstrated by comparison of these substituted benzoxazoles with 2-(2'-hydroxyphenyl)benzoxazole (compound **7**, Figure 1.12). Under these conditions this compound does not bind Mg^{2+} , and although it does complex Cu^{2+} , its apparent association constant for is significantly lower than any of the C4-substituted benzoxazoles.

Because all of the C4-substituted HPB appear to have very tight binding to copper ions (close to or higher than $1 \cdot 10^7 M^{-1}$), attempts were made to determine the association constants of these analogs with greater accuracy at lower ligand concentrations. As seen in Figure 3.8 and Table 3.2, tight copper binding is still observed at 1 μM ligand (compare with the results obtained for **17** and UK-1 in Figure 3.5 and Figure 3.6). Figure 3.9 shows an example of the fraction metal bound as a factor of ligand concentration using compound **8** at 10, 5, 2.5 and 1 μM . All of the graphs overlap and yield association constants in the same range ($10^7 M^{-1}$). Unfortunately, the signal to noise ratio precluded lower compound concentrations to be examined. Therefore, the copper binding constants shown in Table 3.1 and 3.2 can only be regarded as lower binding limits.

The strong binding to copper ions is very interesting because previous studies suggested that Mg^{2+} was the primary cation involved in coordination with UK-1 and **8** (109). However, Cu^{2+} could be a significant player in the interaction of both UK-1 and the C4 substituted HPB ligands The binding preference of the natural product for Cu^{2+} relative to other cations studied previously is also

exciting in light of the many copper chelates possessing anticancer activity (27, 28, 32, 34, 36, 41, 113). Furthermore, as discussed in the introductory chapter, UK-1 was originally thought to be similar to bacterial siderophores. However, its affinity for iron was relatively low (102). This study has shown that UK-1 prefers to chelate copper ions with higher affinity than any other metals studied so far, which raises the possibility of its involvement in the biological role for the natural product. Transition metal coordination can greatly affect the properties of DNA-binding molecules and therefore the DNA-binding properties of UK-1 and the HPB series should be studied in the presence of Cu^{2+} and the more abundant Mg^{2+} ions.

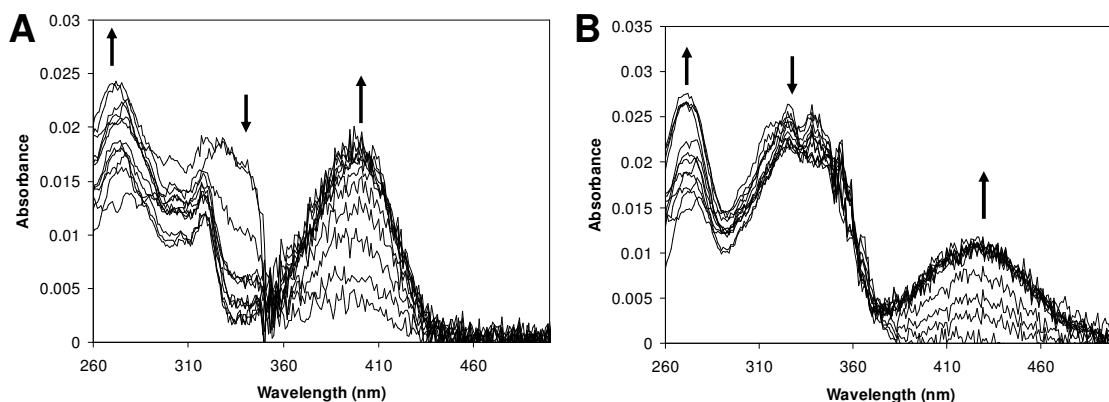


Figure 3.8. UV-Vis spectral changes of compound of 1 μM Compound 17 and UK-1 upon addition of Cu^{2+} . Absorbance spectra of 1 μM compound 17 (A) or UK-1 (B) in methanol were recorded in the presence of increasing concentrations of Cu^{2+} , ranging from 0-9 μM . Arrows denote the changes in absorbance with increasing metal ion concentrations.

Table 3.2. Lower limit of the association constants for Cu^{2+} binding in MeOH (M^{-1}) at 1 μM ligand

Compound	Cu^{2+}
UK-1	$5 \pm 5 \times 10^7$
8	$4 \pm 2 \times 10^7$
16	$3 \pm 1 \times 10^7$
17	$3 \pm 2 \times 10^7$

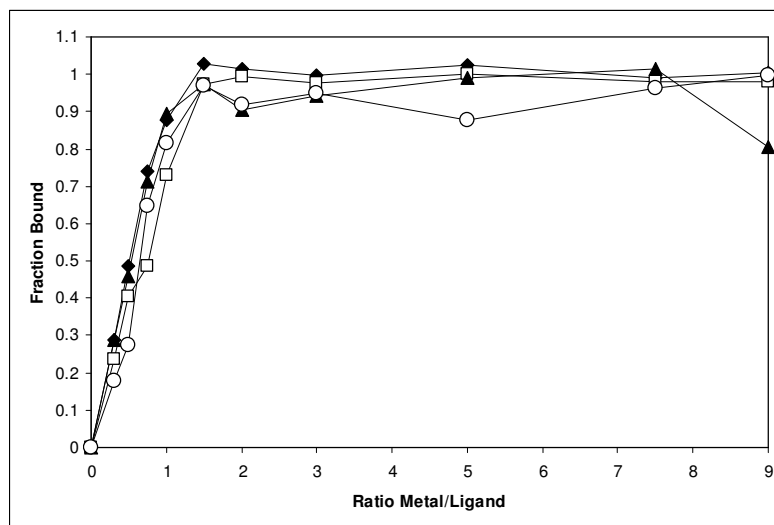


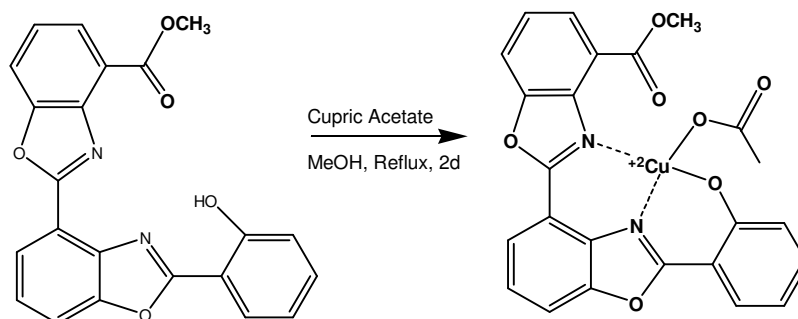
Figure 3.9. Fraction Cu^{2+} bound to Compound **8** at various ligand concentrations. The absorbance at 410 nm was monitored by increasing the ratios of metal/ligand using 10 μM (filled diamonds), 5 μM (empty squares), 2.5 μM (filled triangles), or 1 μM (empty circles) compound **8**.

3.4. Synthesis of a UK-1- Cu^{2+} chelate

To further study the copper chelation of UK-1, its copper complex was prepared by refluxing the ligand with cupric acetate as shown in Scheme 3.1. Elemental analysis and mass spectroscopy confirmed the formation of a 1:1 complex which was isolated as green needle-like crystals. It is anticipated the copper atom is coordinated between the two nitrogen atoms of the benzoxazole rings, and the oxygen from the phenol group of UK-1. There may also be an additional coordination site with the carbonyl oxygen of the methyl ester. Similar coordination sites could occur between the benzoxazole nitrogen, the phenol oxygen and the carbonyl oxygen in the C4-substituted HPB analogs, and could explain the lower metal affinities observed for the C7 or unsubstituted analogs.

Attempts to generate a 2:1 ligand:metal neutral complex were unsuccessful, even at excess concentration of UK-1. Further evidence of the stoichiometry of the UK-1 copper complex arises by comparison to the chelates of compound **7**, hydroxyphenyl 2-(2'-hydroxyphenyl)benzoxazole. It has been

reported that metal complexes from this compound with different stoichiometries differ in their fluorescence quantum yields; transition metal 1:1 metal chelates, unlike the neutral molecular complexes do not display fluorescence (95). Similarly, the isolated UK-1 copper complex does not exhibit any fluorescence.



Scheme 3.1. Synthesis of UK-1 Cu Complex.

The IR spectra of the UK-1-copper chelate was compared to the unbound ligand. As seen in Figure 3.10, the IR resonances change significantly upon metal chelation. In particular, the phenol group around 3000 cm^{-1} becomes very pronounced. The peak corresponding to the ester, at approximately 1712 cm^{-1} also shifts to 1750 cm^{-1} . The IR bands assigned to the $\nu(\text{C}=\text{N})$ 1592 and 1548 , are shifted to 1562 and 1529 upon coordination to the copper ions. Most of the peaks between the 600 - 1600 area were also broaden upon metal chelation and an intense peak above 3000 cm^{-1} appeared. These results support a possible coordination of copper with the nitrogen atoms of the benzoxazole rings, the phenol oxygen and possibly the carbonyl oxygen.

The UV spectrum of the copper complex was also recorded in MeOH, and is shown in Figure 3.11. The complex displays peaks at 418 , 348 , 333 , 317 , 275 , 267 , and 236 nm , similar to those observed from the Cu^{2+} titration experiments with the natural compound (see Figure 3.6D). This could indicate that similar

species are formed by simple addition of copper to the solvent and the isolated copper complex.

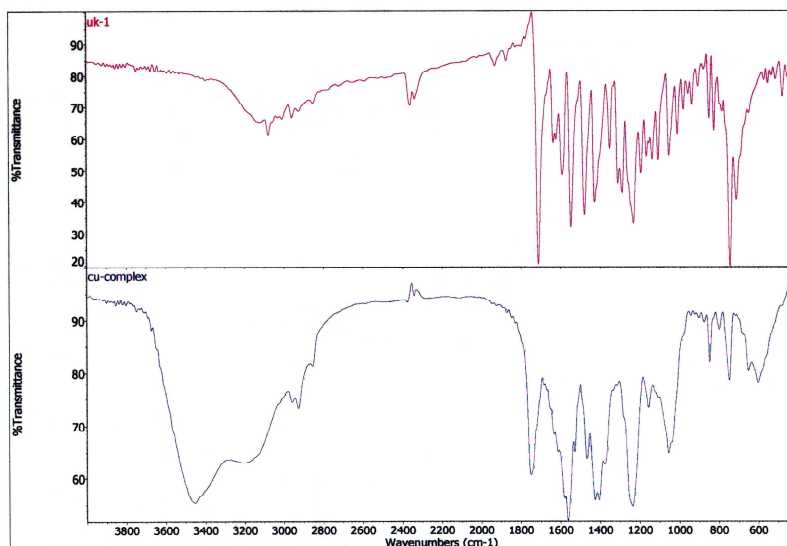


Figure 3.10. IR Spectra of UK-1 and its copper chelate. Top panel, UK-1, bottom panel, UK-1-copper complex

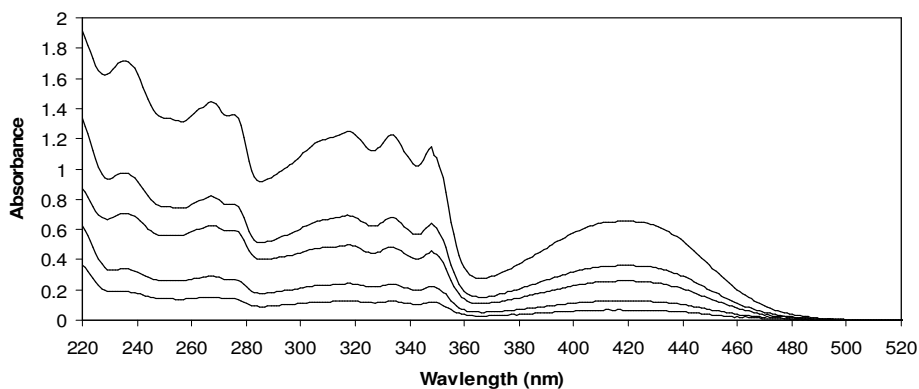


Figure 3.11. UV-Vis Spectrum of the UK-1-Cu²⁺ Complex in MeOH. The spectra were recorded at 5, 10, 20, 30 and 50 μM complex concentrations.

The isolation of the UK-1 copper complex will allow for direct comparison of the biological properties of the chelate and those of the uncomplexed ligand. Future X-Ray crystallography studies could aid in the structural elucidation of the

complex. It is possible that Cu^{2+} coordination could facilitate DNA interactions by charge attraction to the negatively charged phosphates in nucleic acids. The metal could also assist in cellular entry or alter reactivity and thus lower cytotoxicity values could be obtained when the ligand is complexed. Some of these properties will be investigated in the following chapter.

3.5. General trends observed for metal affinity

The metal ion binding ability of a series of novel benzoxazole ligands was determined spectrophotometrically in methanol. The spectral differences observed between the C4 and C7 substituted compounds **8** and **9**, have made evident that the disposition of the N and O with respect to the carbomethoxy substituent plays an important role in metal ion coordination. The geometry in compound **8** with a C4-ester facilitates Mg^{2+} and Cu^{2+} ion binding ability whereas metal affinity is greatly diminished in the C7-substituted benzoxazole. This suggests that metal coordination occurs between the nitrogen atom in the benzoxazole ring, the oxygen phenol group and is assisted by coordination with the carbonyl oxygen at the C4 position.

This study has also shown that it is possible to modify the C4 position with esters and amides of varying length and retain metal binding capability. While the Cu^{2+} ion binding of the C4-substituted HPB analogs is relatively unaffected by the nature of the groups at this position, metal ion binding affinities for the other metals vary with the nature of this substituent. The effect that these structural modifications have on DNA binding and cytotoxicity in cancer cell lines will be addressed in the following chapter. It should also be noted that UK-1 and all of the 2-(2'-hydroxyphenyl) benzoxazoles bind copper with greater affinity than the rest of the metal ions studied. This is relevant because it was previously thought that Mg^{2+} was the cation of preference for UK-1 and compound **8** (102). In addition, many copper chelates have the ability to inhibit cancer cell growth,

which raises the possibility that these compounds could also be useful as therapeutic drugs (114-118). A 1:1 UK1-copper complex was also synthesized and isolated. The biological properties of this chelate will also be investigated in the next section.

CHAPTER 4. METAL MEDIATED DNA BINDING AND CYTOTOXICITY

4.1. Analog affinity for DNA in the presence and absence of metals

Metal ions can facilitate the interaction of drugs with negatively charged nucleic acids, and thus many metal complexes are promising DNA-targeting therapeutic agents. Because all of the new 2-(2'-hydroxyphenyl)-benzoxazoles (HPBs) form complexes with divalent cations it is important to investigate if metal binding affects their affinity for DNA. It is also essential to examine if the substitutions at the C4 and C7 position affect the biological properties of the HPB ligands. The chapter will discuss the metal-mediated DNA binding and cytotoxicity of the new benzoxazole compounds. Structure-activity relationships derived from this study may aid in the design of future metallo-drugs.

As mentioned in the introductory chapter, one of the unique properties of the natural compound UK-1 is its ability to bind to DNA in the presence of metal cations (102, 108). UK-1 was originally studied as a possible siderophore for the producing *Streptomyces* organism because the 2-(2'-hydroxyphenyl) moiety in UK-1 is actually present in a class of microbial siderophores that bind Fe^{3+} (106, 119). However, its affinity to bind Fe^{3+} was not found to be particularly strong (102). Nevertheless, there are examples of Cu^{2+} binding siderophores, and as discussed in the previous chapter, both UK-1 and the 2-(2'-hydroxyphenyl)benzoxazoles bind to copper with high affinities. It is possible that copper or another transition metal plays a role in the mechanism of action of UK-1. Therefore, the cytotoxicity and biological properties of a UK-1- Cu^{2+} complex will also be examined.

4.1.1. Results obtained from SPR

Spectroscopy methods commonly used to monitor the interactions of small molecules with DNA could not be used to investigate the metal-mediated benzoxazole-duplex DNA interactions due to the complex spectral properties of the metal complexes. In addition, UV/Vis spectral changes of UK-1 and HPB ligands upon DNA binding were subtle compared to those due to metal ion complexation. Fluorescence spectroscopy was precluded because the metals of interest such as Cu^{2+} and Ni^{2+} completely quenched the intrinsic fluorescence of UK-1 and the HPB analogs upon metal ion binding. Metal ions of interest also quenched the fluorescence of dyes like ethidium bromide, preventing the use of displacement assays to study the metal-mediated DNA binding of these ligands (120).

Surface-plasmon resonance (SPR) monitors the change in refractive index of flow cells on a sensor chip surface upon complex formation and is a very useful and sensitive technique to study small molecule-DNA interactions (121-123). SPR can provide equilibrium and kinetic constants of complex formation by comparing response units (RU) between control and DNA-immobilized flow cells. This method is particularly useful to investigate the interactions of the benzoxazole ligands covered in this work because metal ions do not interfere with the measurement of resonance units observed upon compound binding to DNA on the surface of the chip. Furthermore, SPR metal-mediated DNA binding studies have been reported for the aureolic antibiotics Mithramycin and Chromomycin as well as for a series of quinolone derivatives (52, 124, 125).

The interactions of UK-1 and selected HPB ligands were investigated using a biotin labeled short GC-DNA hairpin with limited number of binding sites which was immobilized on a streptavidin-coated sensor chip. Binding studies were carried out in 30 mM Tris-HCl, 50 mM NaCl, pH 7.3 with or without addition of 20 mM MgCl_2 . Compounds were tested between 650 nM to 20 μM and included 20 μM CuCl_2 for the Cu^{2+} -DNA mediated binding studies. Chromomycin

was used as positive control for Mg^{2+} -mediated binding. Samples were supplemented with 0.5% or 5% DMSO due to the limited aqueous solubility of some of the analogs. Although sensograms were corrected by double reference subtraction for differences between flow cells caused by the high refractive index from DMSO, there were large spikes at the beginning and end of each sample injection, as seen in Figure 4.1. This precluded analysis of kinetic k_{on} and k_{off} constants. Nevertheless, equilibrium binding data could be obtained from plateau steady-state regions in the sensograms.

It is important to note that under the experimental conditions employed none of the analogs studied exhibited changes in RU signal in buffer alone or buffer containing 20 mM $MgCl_2$. Figure 4.1A shows a representative series of sensograms obtained in 20 mM $MgCl_2$ buffer after injection of UK-1 samples ranging between 650 nM and 20 μM ; no changes in RU signal were observed indicating that no discernable complex between the ligands and the DNA hairpin were formed. In contrast, supplementing the samples with 20 μM $CuCl_2$ (1000-fold lower concentration than Mg^{2+}) resulted in a marked increase in signal dependent on ligand concentration (Figure 4.1B). Steady state equilibrium was achieved even at low compound concentrations, with fast association and dissociation rates. Chromomycin-A was used as a positive control for magnesium-mediated binding and positive RU signals were obtained using this compound. In contrast to UK-1 and the HPB analogs, Chromomycin exhibited slow association and dissociation rates in the presence of 20 mM $MgCl_2$ (Figure 4.2), in accordance to the described behavior in the literature; it also required injections of 50 mM NaOH, 1 M NaCl to regenerate the surface (124).

Higher concentrations than 20 μM were not tested for the HPB ligands due to potential precipitation and clogging of the fluidics system. Because a maximum binding response was not achieved at this concentration, RU_{max} values were estimated in the data fitting parameters as described in section 6.3. The observed RU values were plotted as a function of ligand concentration (Figure 4.3) and were fitted to a 1:1 binding model to obtain apparent binding constants

in the presence of Mg^{2+} or Cu^{2+} ; 2:1 models resulted in lower correlation factor than those obtained assuming 1:1 DNA ligand stoichiometry. The results are summarized in Table 4.1.

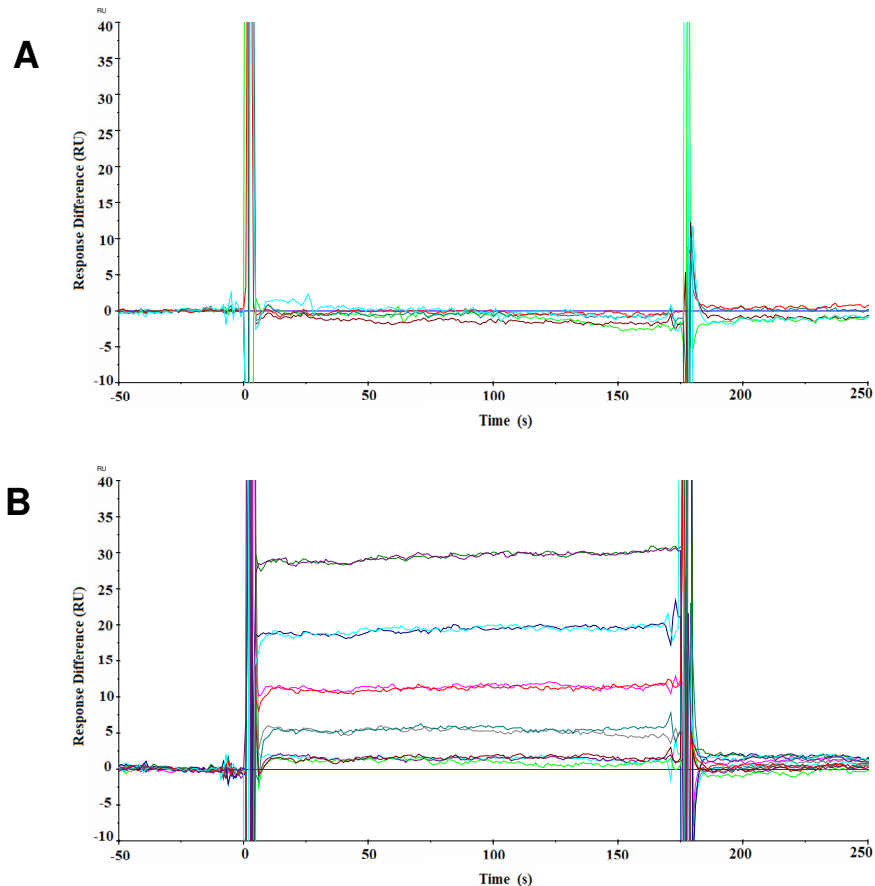


Figure 4.1. Sensograms of the UK-1-DNA interactions in the presence of 20 mM $MgCl_2$ or 20 μM $CuCl_2$. UK-1 samples (30 μl) were injected at a flow rate of 10 $\mu l/min$ at 0.650 μM , 1.25 μM , 2.5 μM , 5 μM , 10 μM , and 20 μM in the presence of 20 mM $MgCl_2$ (A) or 20 μM $CuCl_2$ (B)

Although the DNA binding isotherms had not reached saturation under the experimental conditions employed and therefore the calculated binding constants carry significant error, it is still possible to examine the major differences in affinities observed between analogs. The fact that neither UK-1 nor the rest of the HPB ligands exhibited magnesium dependant DNA binding suggests that this metal does not promote significant binding to nucleic acids or that binding is not strong enough to be observed at the concentration ranges employed.

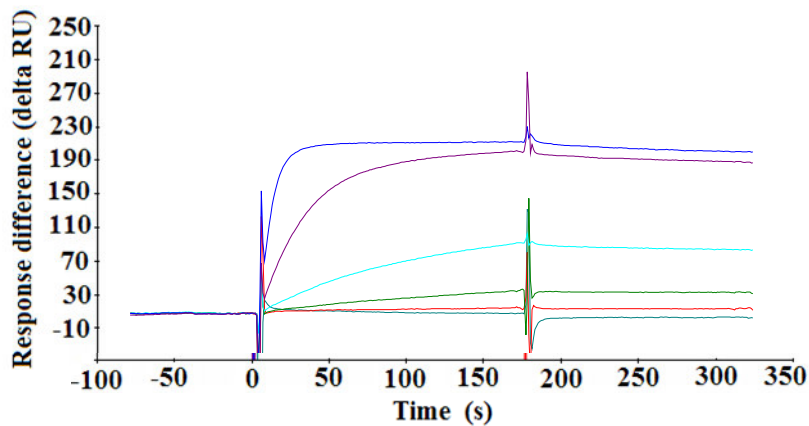


Figure 4.2. Sensograms of Chromomycin -DNA interactions in the presence of 20 mM $MgCl_2$. Chromomycin samples (30 μ l) were injected at a flow rate of 10 μ l/min at 0.650 μ M, 1.25 μ M, 2.5 μ M, 5 μ M, 10 μ M, and 20 μ M in the presence of 20 mM $MgCl_2$ or 20 μ M $CuCl_2$

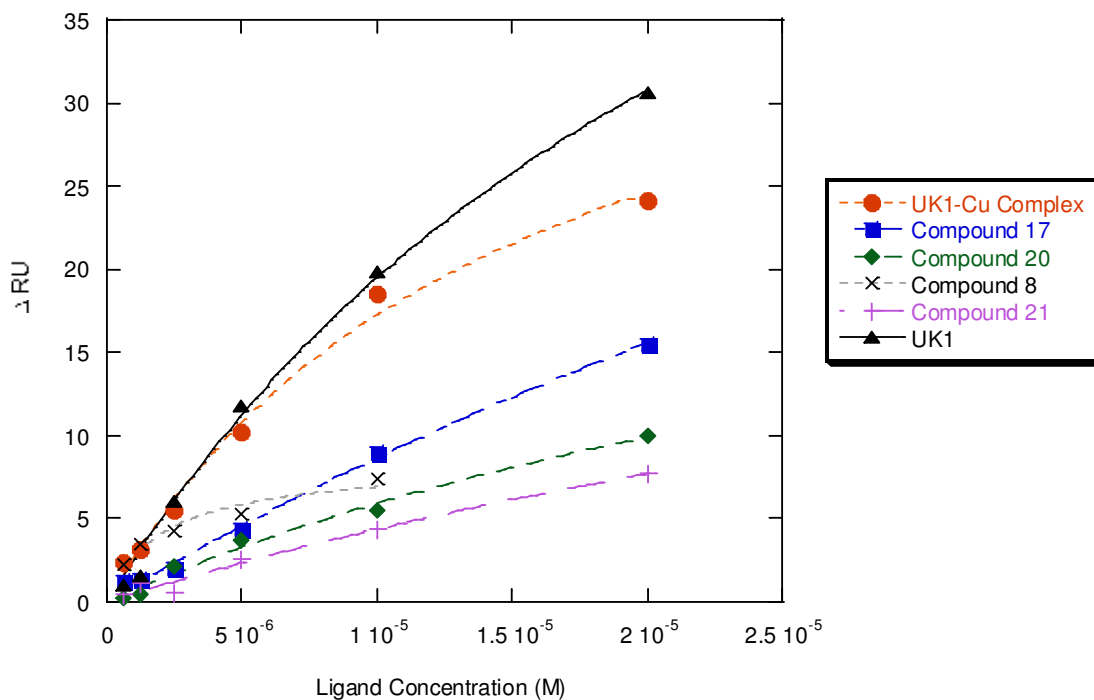


Figure 4.3. SPR response of benzoxazole ligands in the presence of 20 μ M $CuCl_2$. Differential RU units obtained between GC-Hairpin immobilized and reference flow cells with increasing ligand concentration were fitted to a 1:1 binding model as described in section 6.3. Only analogs that displayed differences between flow cells are shown.

Comparison between copper mediated DNA binding (Table 4.1) indicates that the substitutions at the C4 or C7 position of the 2-(2'-hydroxyphenyl benzoxazoles) greatly influence the interactions with the DNA-hairpin substrate. All of the C4 substituted ligands tested, compounds **8**, **17**, **20** and **21**, exhibited copper mediated binding to the DNA hairpin with affinities ranging from $2 \cdot 10^3$ to $5 \cdot 10^5 \text{ M}^{-1}$. As expected, the methyl ether **6**, used as a negative control, was the only analog not capable of binding Cu^{2+} ions, did not present any binding to the DNA substrate in the presence of $20 \text{ }\mu\text{M}$ CuCl_2 . Similarly, the unsubstituted HPB analog compound **7**, and the C7 substituted analog **9**, which displayed copper affinities several orders of magnitude lower than the C4 analogs (section 3.3), did not present any observable copper-mediated DNA binding. The affinity calculated for Chromomycin here, $2.7 \pm 0.9 \cdot 10^5 \text{ M}^{-1}$, was within the range reported in the literature (54).

Table 4.1. Apparent binding constants of HPB ligands for GC-Hairpin DNA in the presence of 20 mM MgCl_2 or 20 μM CuCl_2

Compound	20 μM CuCl_2		20 mM MgCl_2	
	K_A (1/M)	RU_{max}	K_A (1/M)	RU_{max}
UK-1	$3.7 \pm 0.8 \cdot 10^4$	73 ± 11	n.b. ^a	n.b. ^a
UK-1 Cu-Complex	$7 \pm 1 \cdot 10^4$	43 ± 5	n.b. ^a	n.b. ^a
Compound 6	n.b. ^a	n.b. ^a	n.b. ^a	n.b. ^a
Compound 7	n.b. ^a	n.b. ^a	n.b. ^a	n.b. ^a
Compound 8	$5 \pm 2 \cdot 10^5$	8 ± 1	n.b. ^a	n.b. ^a
Compound 9	n.b. ^a	n.b. ^a	n.b. ^a	n.b. ^a
Compound 17	$1.3 \pm 0.5 \cdot 10^4$	75 ± 25	n.b. ^a	n.b. ^a
Compound 20	$2.5 \pm 1.0 \cdot 10^4$	30 ± 9	n.b. ^a	n.b. ^a
Compound 21	$2 \pm 1 \cdot 10^3$	32 ± 21	n.b. ^a	n.b. ^a
Chromomycin	n.d. ^b	n.d. ^b	$2.7 \pm 0.9 \cdot 10^5$	245 ± 28

^a No binding was observed
^b Not determined

4.1.2. Results obtained from mass spectroscopy

The metal-mediated DNA binding behavior of the modified 2-(2'-hydroxyphenyl) benzoxazoles was also investigated by Electrospray Ionization Mass Spectrometry (ESI-MS) in a collaborative work with the Jennifer Brodbelt research group. Studies were carried out by Carolyn Mazzitelli in ammonium acetate buffer containing 10 μM Mg^{2+} , Ca^{2+} , Ni^{2+} , Cu^{2+} , or Zn^{2+} and 10 μM benzoxazole ligand to screen for metal complex formation. No complexes were observed with Mg^{2+} or Ca^{2+} ions, even with a 10-fold increase in metal concentration. However, experiments carried out in 100% methanol did present abundant Mg^{2+} complexes, in agreement with the observed UV-Vis experiments (see Chapter 3). The lack of detectable magnesium complexes in aqueous buffers by ESI-MS may be due to the differences in metal ion solvation in different solvents, and highlights the importance of solvent for metal ion binding of the benzoxazole ligands, and may explain the lack of Mg^{2+} -mediated binding seen in SPR experiments. Binding to Mg^{2+} was previously thought to be important for the mechanism of action of UK-1 and the HPB analogs, but the absence of Mg^{2+} complexes in aqueous buffers suggests binding to this cation does not have as much biological significance as does coordination to other transition metals.

In aqueous buffers, all of the C4-substituted HPB ligands formed 1:1 complexes with the divalent transition metals Ni^{2+} , Cu^{2+} , and to a lesser extent Zn^{2+} . Ligands with shorter side chains, such as compound **8** and **16-18**, displayed water adducts in their 1:1 complexes and were also able to form 2:1 ligand/metal ion complexes. Longer side chains like those in **19-21** mainly formed 1:1 complexes without solvent adducts, possibly because of coordination of the metal ion with atoms within the ligand's side chain. As expected, the

methyl ether **6**, which lacks a phenyl moiety, did not form complexes with any of the metal ions studied.

Ligand binding to duplex DNA in the presence and absence of metal ions was also evaluated at equimolar concentrations of ligand, metal and DNA (10 μ M) in ammonium acetate buffer using oligonucleotides of varying G/C and A/T base pair composition. No apparent sequence selectivity was evident. Long chained benzoxazoles **19-21** formed low abundance complexes with duplex DNA in the absence of metal ions, while the short chain compounds **8**, and **16-18** did not, suggesting that longer side chains at the C4 position can promote non-metal mediated DNA binding.

DNA-ligand interactions were also examined in the presence of the metals that formed complexes with the 2'-(2-hydroxybenzoxazoles) by ESI-MS, Ni²⁺, Cu²⁺, and Zn²⁺ (see supplementary table in Appendix C). The most significant increase in DNA binding occurred in the presence of Cu²⁺ ions for all of the analogs studied except compound **6**, which did not display any interactions with the oligonucleotides studied. Although long chain analogs **19-21** exhibited slight binding in the absence of metal ions, DNA complexes increased upon Cu²⁺ addition, particularly for compounds **19** and **21**. Overall, the benzoxazoles that demonstrated highest enhancement in DNA binding upon addition of metal ions were compounds **16** and **17** for the shorter side chain compounds and compound **21** for those with longer side chains.

4.2. Cytotoxicity of 2-(2-hydroxyphenyl)benzoxazole analogs

4.2.1. Cytotoxicity of HPB analogs with a carbomethoxy group at the C4 or C7 position

The effect of having a HPB with a carbomethoxy substituent either at the C4 or C7 position was addressed by evaluating the cytotoxicity of compound **8** (C4) and its isomeric 2-(2'-hydroxyphenyl) benzoxazole **9** (C7) in the prostate

cancer cell line PC-3, and the colon cancer cell line HT-29 (Table 4.2). As previously reported, the C4 methoxy substituted HPB analog **8** displayed toxicity to both PC-3 and HT-29 cancer cells ($IC_{50} = 0.4$ and $9.1 \mu\text{M}$, respectively) (109). In contrast, compound **9** displayed only weak cytotoxicity against PC-3 prostate cancer cells ($IC_{50} = 47 \mu\text{M}$), over 50-fold less than that of the isomeric benzoxazole **8**, and over 100-fold weaker than the natural product UK-1 (109). The C7 substituted analog was also only weakly active against HT-29 cells ($IC_{50} = 36 \mu\text{M}$), as compared to the isomeric benzoxazole **8** ($IC_{50} = 9.1 \mu\text{M}$). Thus, the cancer cell cytotoxicity of these benzoxazole analogs of UK-1 is strongly sensitive to their structural features, and mirrors their relative ability to form DNA-drug-metal complexes.

Table 4.2. Cytotoxicity of PC-3 or HT-29 cells after 72h incubation with UK-1, compound **8** or compound **9**. Cellular proliferation was assayed using the AlamarBlue assay. IC_{50} values represent 50% growth inhibition relative to cell treated with vehicle alone

Compound	IC_{50} for PC-3 (μM)	IC_{50} for HT-29 (μM)
Compound 8	0.91	9.1
Compound 9	47	36

4.2.2. Cytotoxicity of HPB analogs with different C7 substituents

The effects of having different substituents at the C7 position was also assayed by measuring the cytotoxicity of the new 2-(2'-hydroxyphenyl) benzoxazole analogs **16-21** using the AlamarBlue assay in the breast cancer cell line MCF-7 and the lung cancer cell line A549. For comparison, UK-1, and the benzoxazole carboxylic acid phenyl ether **6**, an isomer of **8**, were also tested. As expected based on previous reports, the anticancer activity of compound **8** was somewhat less than that of UK-1, whereas the phenyl ether **6** was not cytotoxic at the highest concentration tested ($50 \mu\text{M}$). Therefore, losing the phenol moiety

completely abolishes activity, which points out the importance of having a phenolate group not only for metal coordination but also for cytotoxicity.

Table 4.3. Cytotoxicity of MCF-7 or A549 cells treated with HPB analogs during 72h. Cellular proliferation was assayed using the AlamarBlue assay. IC₅₀ values represent 50% growth inhibition relative to cell treated with vehicle alone

Compound	IC ₅₀ for MCF7 (μM)	IC ₅₀ for A549 (μM)
UK-1	1.4 ± 0.9	2.0 ± 0.5
Compound 6	>50	>50
Compound 8	4±2	12±3
Compound 9	7±1	35±4
Compound 16	15 ± 5	40 ± 10
Compound 17	10 ± 8	11 ± 1
Compound 18	30 ± 10	14 ± 4
Compound 19	31 ± 7	39 ± 17
Compound 20	> 50	41 ± 17
Compound 21	13 ± 2	11 ± 1
MMC	0.20 ± 0.07	0.4 ± 0.1

Structure activity relationships can be drawn by comparing the activity of the HPBs with different groups at the C4 position. Changing the methoxy group to a methyl amide retains the anticancer properties, as observed for compound **17** (IC₅₀ = 10 and 11 μM). However, as the side chain length of the amide group increases it appears that the cytotoxicity decreases as observed for the butylamide analog **18** (IC₅₀ = 30 and 14 μM), and more so for compounds **19** (IC₅₀ = 31 and 39 μM) and **20** (IC₅₀ = 41 and > 50 μM). The ethyl ester **16** is less active than **8** in the A549 cells (IC₅₀ = 40 μM), but has similar cytotoxicity in the MCF-7 cell line (IC₅₀ = 15 μM). The tetraethyleneglycol ester **21** has a similar cytotoxic profile to **8**, retaining activity against both cell lines. This compound has the advantage of having increased solubility in aqueous solutions, and therefore

is of particular interest as a drug candidate. Overall, compounds **17** and **21** are the most promising HPB analogs investigated in this study in terms of metal-mediated DNA binding and cytotoxicity.

4.2.3. Cytotoxicity of UK-1 and its copper complex

To test for the effect of copper chelation on the cytotoxicity of the natural product UK-1, cell viability of A549 and MCF-7 cell lines treated with either vehicle alone, UK-1, UK-1-Cu²⁺ complex, UK-1 + 10 μM CuCl₂, or vehicle + 10 μM CuCl₂, was measured at two time points, 24 and 72 h. Cellular growth of UK-1 treated cells was compared to those treated with vehicle alone, whereas the cytotoxicity of the copper complex and UK-1 samples in the presence of 10 μM Cu²⁺ were compared to copper only treated cells. The IC₅₀ values obtained are summarized in Table 4.4. Treatment of both cell lines with 10 μM CuCl₂ for 72 h did not affect cellular viability. On the other hand, there was marked difference between the cell death observed for both cell lines (> 3 fold) when treated with UK-1, the copper complex, or UK-1 with 10 μM CuCl₂ at the 24 h time point, indicating a synergistic effect between UK-1 and copper treatments. At 72 h, the IC₅₀ values for UK-1 treatment alone resulted in less marked differences compared to cells treated in the presence of copper. This results that copper binding may aid in the anticancer activity of UK-1, perhaps by facilitating access to its target.

Table 4.4. Cytotoxicity of Cells treated for 24 or 72 h in the presence of UK-1 and copper analogs. IC₅₀ values are expressed in μM concentration.

Compound	MCF-7 Cells		A549 Cells	
	24h	72h	24h	72h
UK-1	31 ± 5	1.7 ± 0.2	17 ± 2	1 ± 0.1
[UK-1]Cu ²⁺ Complex	6.8 ± 1.2	1.2 ± 0.2	7.5 ± 1.5	0.4 ± 0.06
UK-1 + 10 μM CuCl ₂	4.6 ± 0.6	1.2 ± 0.2	4.5 ± 0.7	0.20 ± 0.04
Mitomycin-C	5 ± 2	0.29 ± 0.08	5 ± 2	0.24 ± 0.03

4.3. Apoptosis induced by UK-1 and its copper complex

Apoptosis is the process of programmed cell death (PCD). PCD is a normal physiological process used by the body to combat unchecked cell growth (126). Improper apoptosis has been connected to many diseases and forms of cancer (127, 128). Because various organic copper complexes have been used to induce apoptosis in human cancers, it is important to evaluate if coordination of UK-1 to copper affects cellular apoptosis (118, 129, 130). To do so, caspase-8 levels in A549 cells were measured by Chad McKee using western blot analysis.

Caspase-8 is an integral protein in driving the death-receptor mediated apoptotic pathway (131). Therefore, its expression and activation is commonly used as an indicator of apoptosis (132, 133). Cells were evaluated after 24 h treatment with UK-1 in the presence and absence of copper. Figure 4.4 shows the protein levels observed at 55 kDa, corresponding to caspase-8 levels, after treatment with vehicle, 10 μM CuCl_2 , 5 μM UK-1, 5 μM UK-1 + 10 μM CuCl_2 , or 5 μM UK-1- Cu^{2+} -complex. As expected, the control lane displayed no discernable amounts of the protein whereas treatment with 10 μM CuCl_2 resulted in only a modest increase in caspase-8 expression. Similar protein levels were detected after incubation with 5 μM UK-1 alone. In contrast, combined treatments of 5 μM UK-1 with 10 μM CuCl_2 resulted in a marked increase in caspase-8 levels, indicating that the apoptotic pathway is significantly increased when both UK-1 and copper are added to the cells. Higher caspase-8 levels were observed for the copper complex compared to treatment with either UK-1 or copper alone, but the effect was somewhat lower than that observed for the combined treatment.

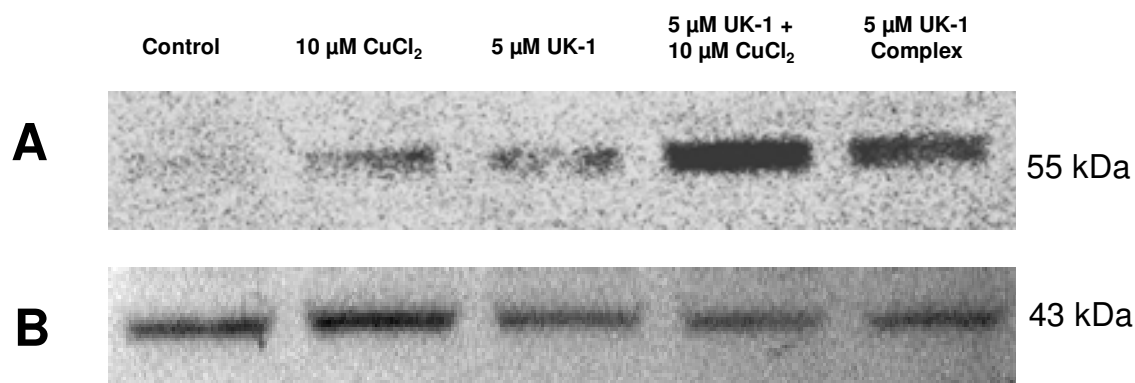


Figure 4.4. Caspase-8 levels in the presence of UK-1 and the UK-1- Cu^{2+} complex. (A) Caspase-8 expression was measured via western blot analysis after 24 h treatment with vehicle, 10 μM CuCl_2 , 5 μM UK-1, 5 μM UK-1 + 10 μM CuCl_2 , or 5 μM UK-1- Cu^{2+} -complex (B) β -actin loading control.

4.4. Conclusions

The results obtained from SPR and mass spectrometry experiments have shown that UK-1 and the C4 substituted HPB ligands form complexes with DNA in the presence of transition metals such as copper, but not the more abundant Mg^{2+} ions under the conditions studied; possible magnesium-ligand interactions were too weak in aqueous buffers to be observed even at 20 mM Mg^{2+} concentration. In contrast, significant binding was observed to a DNA substrate at 20 μM Cu^{2+} , which is within the range reported of serum copper blood levels and thus has physiological relevance (134, 135). This study has also shown that substitutions at the C4 or C7 position can affect metal-mediated DNA binding and cytotoxicity of the 2-(2'-hydroxyphenyl) benzoxazole compounds. Although compound **7**, an HPB analog without substituents, and compound **9**, with a carbomethoxy group at position C7, had the ability to bind to Cu^{2+} ions, they did not exhibit copper mediated DNA binding. This is likely due to their lower affinity for Cu^{2+} ions in comparison to the C4 substituted compounds. Compound **9** also exhibited less cytotoxicity than its isomeric C4-substituted analog compound **8**, in the entire cell lines studied. Compound **6** was the only analog that did not display

any metal binding, and consequently, no metal-mediated DNA binding or cytotoxicity.

In contrast, C4 substituted HPB analogs displayed Cu²⁺-mediated DNA binding by SPR and ESI-MS studies. Slight non-specific binding was observed in the absence of metal ions for the analogs with longer side chains, **19-21**, in ESI-MS but these interactions were not strong enough to be observed in SPR experiments. The lack of sequence selectivity in DNA binding suggests that the HPB analogs could interact via an intercalation mechanism. The longer side chains at the C4 position were also correlated to lower cytotoxicity for amide substituents. In particular, changing the methyl ester to a small amide group such as **17** retains anticancer activity, but as the length of the chain increases so do the IC₅₀ values, as seen for amides **19** and **20**. Conversely, the longer ester **21** was active against the cancer cell lines with the advantage of being more soluble in aqueous buffers. In general, there is a correlation between the HPBs that demonstrated highest enhancement in DNA binding upon addition of metal ions by ESI-MS and those that exhibited low IC₅₀ values (*i. e.* compounds **17** and **21**). This could indicate that the ability of these ligands to interact with DNA by coordination of transition metals may be related to their mechanism of action.

The ability of UK-1 and its copper chelate to induce cytotoxicity in cancer cells was also surveyed. It appears that coordination of UK-1 with copper ions enhances the activity of the natural compound, particularly during shorter incubation periods. Additionally, caspase-8 levels were monitored after treatment with UK-1 in the presence and absence of Cu²⁺, and the UK-1-Cu²⁺ chelate. Higher caspase-8 levels were observed in the presence of both the copper complex and with treatment of UK-1 in the presence of Cu²⁺, indicating higher apoptotic levels under these conditions. This is important in light of the large number of copper complexes have been recently screened for anti cancer activity (114-117). Studies have shown that copper can accumulate in tumors due to the selective permeability of cancer cell membranes to copper compounds (37, 39-41, 114). Furthermore, many anticancer DNA-binding drugs such as Mitomycin-

C, Doxorubicin, and Mithramycin have been tested in the presence of metal ions such as Fe^{3+} , Pt^{2+} , and Cu^{2+} to amplify their potential in tumor cells (52, 136, 137). Similarly, the enhancement of activity of UK-1 upon copper chelation could be a promising strategy for anticancer therapy.

CHAPTER 5. SUMMARY AND FUTURE DIRECTIONS

5.1. Summary

DNA-binding molecules are widely used as therapeutic agents because they can interfere with DNA processing enzymes or cause DNA damage that may lead to cellular death. Because DNA binding drugs target primarily fast-dividing cells, they are commonly used for anti-cancer treatment. However, poor tissue specificity and non-specific binding can result in negative side effects. Understanding the mechanisms that influence the interactions of small molecules with nucleic acids can assist in drug design for more effective agents that preferentially enter the cell populations of interest.

Amongst the many factors that affect drug-DNA interactions, metal cations play a very important role in the mechanism of action of ligands; coordination to a metal can change a drug's physical and chemical properties, geometry, reactivity, and bioavailability. Furthermore, tumor cells require an elevated level of nutrients, membrane permeability and blood flow, which allows for accumulation of various transition metals. The result is a potentially greater uptake of metallopharmaceuticals and drugs that bind to DNA in a metal mediated fashion. Compounds with these characteristics can be potent antineoplastic agents. Examples of drugs that bind to DNA in the presence of divalent cations include compounds from aureolic group of antitumor antibiotics, such as Mithramycin and Chromomycin, as well as members of the quinolone family. Studies have shown that the nucleotide specific binding of these agents is dependent on the presence of divalent ions, and that metal complexes appear to have higher cell cytotoxicity than the drugs alone.

In order to design new potent metallopharmaceuticals that can target specific biomolecules such as DNA, it is important to find a suitable ligand that can form complexes with the metal of interest. Many oxazole and benzoxazole structures present a wide variety of biological activities and in many cases can also form metal complexes. UK-1 is an example of a bis-benzoxazole compound that presents very interesting biological properties. It is a natural product that was originally isolated from *Streptomyces*, can bind various metal ions, bind to DNA in a metal mediated fashion, and possesses growth inhibitory activity against a variety of human cancer cell lines. The simplified analog of UK-1, 2-(2'-hydroxyphenyl)-benzoxazole-4-carboxylic acid methyl ester, compound **8**, was previously identified as having similar metal chelating and biological properties as the natural compound.

This work investigated the effects of modifications to the 2-(2'-hydroxyphenyl)-benzoxazole (HPB) core on metal binding, metal-mediated DNA binding and cytotoxicity. Novel HPB analogs were synthesized with modifications at the C4 or C7 position. The isomeric analog of **8**, compound **9** contains a methyl ester at position 7 instead of position 4. This analog showed diminished metal binding properties, did not display metal-mediated DNA binding, and exhibited lower cytotoxicity than compound **8**. This highlighted the importance of the arrangement between the nitrogen and oxygen atoms in benzoxazole core with respect to the carboxymethyl substituent for metal coordination and biological properties.

Modifications at the C4 position to extended amides and esters resulted in compounds that retained metal binding capability. The affinity for Mg^{2+} , Zn^{2+} and Ni^{2+} was affected according to the type of side chain. In contrast, Cu^{2+} binding was largely unaffected with respect to the substituent; in general all the new analogs displayed strong binding to Cu^{2+} ions, with binding affinities several orders of magnitude stronger than analogs with no substituents in the HPB core, or groups at the C7 position. While the C4 analogs showed Mg^{2+} binding in methanolic solutions, no magnesium binding was observed in aqueous buffers.

Consequently, no magnesium-mediated DNA binding was apparent for these analogs. In contrast, abundant complexes with DNA were observed in the presence of Cu^{2+} ions. Compounds that exhibited the most pronounced enhancement in DNA binding in the presence of metal ions, the methyl amide **17**, and the tetraethyleneglycol ester **21**, were also the compounds with lowest cytotoxicity values in two cancer cell lines. The latter is of particular interest because of its increased water-solubility.

Due to the preferential binding of all of the HPB analogs to Cu^{2+} , the copper binding properties of UK-1 were also investigated. The bis-benzoxazole showed preference for this metal and presented increased DNA binding in the presence of Cu^{2+} ions. A UK-1 copper complex was synthesized to compare its biological properties with the natural compound. Copper complexation increases overall cytotoxicity in the cancer cells A549 and MCF-7. In addition, the reduction in cell viability is correlative with increases in caspase-8, and indicator of apoptosis. This study has shown that transition metal coordination could be involved in the mechanism of action of UK-1 and that copper complexes of UK-1 and the HPB ligands could be promising anticancer agents.

5.2. Future Directions

This study suggests that UK-1 and the HPB ligands can bind to divalent metals through coordination with nitrogen atoms of the benzoxazole ring, the phenol oxygen, and the carbonyl oxygen at the C4 position. Further insights into the exact metal coordination geometry of the natural product can arise from X-Ray crystallography studies of the synthesized UK-1 copper complex.

This study also showed that substitutions at the C4 position can retain some of the key biological properties of the natural compound UK-1. In particular, compounds **17** and **21** have shown promising metal-mediated DNA binding and cytotoxicity in cancer cells. These compounds should be studied with respect to

non-cancerous cell lines as well as with DNA-processing enzymes such as Topoisomerase II in the presence and absence of transition metals to investigate if this could be relevant to their mechanism of action. The tetraethyleneglycol side chain of compound **21** allows for greater water solubility, making it suitable for cellular assays.

This study can also serve as a starting point for the design of more potent ligands. The compounds with hydrophilic groups at the C4 position can be further modified to increase cytotoxicity and retain water solubility. New analogs with modifications in the hydroxyphenyl ring are also currently being investigated (Figure 5.1). It is now known that changing the C2' hydroxyl group on the phenolate ring to a methyl ether abolishes activity (i. e. as observed for compound **6**). However, changing the OH group to other polar groups such as amides could actually increase copper binding affinity and potentially increase metal-mediated DNA binding and cytotoxicity. Design of novel HPB analogs includes ligands with NH₂ or F at the C2' position. The effect of the OH group at positions C2', C3' or C4' is also presently being studied. In addition, having more than one hydroxyl group could potentially increase activity or serve as an anchor for surface immobilization.

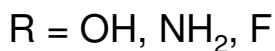
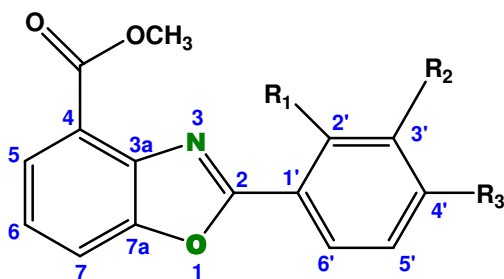


Figure 5.1. Future HPB analogs with substitutions at the C2', C3' or C4' position

CHAPTER 6. EXPERIMENTALS FOR PART I

6.1. General Information

All reagents were purchased from commercial suppliers and used without further purification unless noted. Cell viability assays were carried out in sterile black polystyrene 96-well plates from Nalgene Nunc International (Rochester, NY, part no. 137101). The MCF-7 and A549 cell lines were kind gifts from Profs. Shawn Bratton and Bob Krug (The University of Texas at Austin) respectively. The media for the MCF-7 cell line was the improved MEM (Richter's Modification, part no. 10-026-CV) and F-12 K (Kaighn's Modification, part no. 10-025-CV) for the A549 cell line (from MediaTech Inc., Manassas, VA); both contain *L*-glutamine and were supplemented with 10% fetal bovine serum and 1% penicillin/streptomycin. Cytotoxicity experiments with PC-3 and HT-29 cell lines were carried out by MDS Pharma Services (King of Prussia, PA).

Unless otherwise noted, ^1H and ^{13}C NMR spectra were determined in CDCl_3 on a Varian INOVA 500, or a Varian UNITY 300s spectrometer operating at 300 and 500 MHz respectively. Two dimensional NMR experiments were run on a 500 MHz instrument; selected spectra are shown in Appendix A. All mass spectra were obtained by chemical ionization using methane as the ionizing gas. Chromatography refers to flash chromatography on silica gel, and R_f values were determined using silica gel-GF TLC plates using the solvent system indicated. Melting points were determined using a Büchi B-540 melting point apparatus (New Castle, DE), and IR spectra were recorded in a Nicolet IR100 instrument from Thermo Electron (Waltham, MA). Elemental Analysis was performed by Quantitative Technologies, Incorporated of Whitehouse, NJ. Compounds **4**, **5**, and **8** were synthesized as described previously (*101*, *109*).

6.2. Metal Binding Assays

Stock solutions of UK-1 and analogs as well as $\text{Mg}(\text{NO}_3)_2$, $\text{Zn}(\text{NO}_3)_2$, $\text{Ni}(\text{NO}_3)_3$, and $\text{Cu}(\text{NO}_3)_2$, were prepared fresh on the day of the spectrophotometric titrations. The fraction of complex formed was measured by using solutions of increasing mole fraction of metal ion, keeping the concentration of ligand constant, at 10, 5, 2.5 or 1 μM , using as a reference the absorbance of a solution containing the same concentration of metal ion without the ligand. The change in absorbance was monitored from 600 to 200 nm for each sample, as a function of the concentration of metal ion. The maximum absorbance change for the ligand-metal complex was recorded at each metal-ion concentration.

Spectrophotometric data was analyzed by equations [1] and [2]. The apparent binding constants were calculated by non-linear regression of the experimental points using the program Kaleidagraph based on the equilibrium:

$$K_d = [C_0 - (\Delta A/\Delta A_{\max})C_0][C_m - (\Delta A/\Delta A_{\max})C_0]/[(\Delta A/\Delta A_{\max})C_0] \quad [1]$$

$$C_0(\Delta A/\Delta A_{\max})^2 - (C_0 + C_m + K_d)(\Delta A/\Delta A_{\max}) + C_m = 0 \quad [2]$$

Where:

K_d is the dissociation constant, C_0 is the initial concentration of the UK-1 analog, C_m is the concentration of the metal ion, ΔA is the increase in absorption at the wavelength of maximum absorbance for the ligand-metal ion complex (~400 nm) upon addition of each metal ion concentration, and ΔA_{\max} is the same parameter when the ligand is totally bound to the metal ion, determined in excess metal ion until no further spectral changes were observed. The apparent binding constants (K_a) were calculated as the inverse value of K_d s.

6.3. Surface Plasmon Resonance

Binding measurements were performed with BIAcore 1000 or BIAcore 3000 instruments using pre-coated streptavidin SA5 chips (part no. BR-1000-32, from BIAcore, Piscataway, NJ). With this technique, the change in resonance angle is monitored and is reported as resonance units (RU). The increase in RU is proportional to the amount of compound bound to an immobilized target, in this case a biotinylated oligonucleotide (138).

To prepare the SA5 sensor chip, it was docked, primed and the buffer, HBS-EP (10 mM HEPES, 150 mM NaCl, 3 mM EDTA, 0.005% v/v polysorbate 20, pH 7.4), was set at a flow rate of 20 μ l/min. The surface was pre-conditioned with multiple 1-min injections of 50 mM NaOH, 1 M NaCl until there was a difference of less than 10 RUs of the baseline before and after the injections; this procedure was repeated for all 4 flow-cells. Biotin-labeled GGCC DNA hairpin, Bio-5'-CGGCCTCCTCCCCAGGCCG-3', (Integrated DNA Technologies, Coralville, IA) at 25 nM concentration was injected at a flow rate of 5 μ l/min using the INJECT command and immobilized on the flow cell's 2 and 3 surface by noncovalent capture. Buffer was injected until a stable baseline increase of 457 and 461 RU units respectively were observed. Flow cell 1 was left blank as a control reference cell, while flow cell 3 was only used to compare relative responses between flow cells over time.

Data was obtained from sensograms utilizing 30 mM Tris-HCl, 50 mM NaCl, and 0.0005% P20, pH 7.3 with or without addition of 20 mM MgCl₂, as a running buffer. UK-1 and analogs samples, along with Chromomycin-A as a positive control (part no. 150686, from MP biomedical, Solon, OH), were prepared in the running buffer and supplemented with 20 μ M CuCl₂ where indicated. DMSO was added to each sample to give a total of 0.5% or 5% final concentration as specified in the text. The sample concentrations ranged from 650 nM to 20 μ M. All sensograms included a double reference subtraction (subtraction of the signal from each injection in the underivatized reference flow

cell 1, in addition to the subtraction of an injection containing only the buffer with the appropriate amount of cations and DMSO). The first subtraction corrects for any change in refractive index due to unbound ligand that flows through solution as well as non-specific interactions with the blank flow cell surfaces, while the second adjusts for any small differences between the reference and DNA flow cells (139).

Samples were injected using an auto-sampler at a flow rate of 10 $\mu\text{l}/\text{min}$ using the KINJECT command for a total of 180 s (30 μl) with a delayed wash after 120 s. Surfaces were regenerated by sequential injections of injections of 50 mM EDTA (20 μl), 50 mM NaOH, 1 M NaCl (10 μl), and running buffer (20 μl). During each ligand injection, a steady-state plateau can be reached when there is no change in signal with time; this is the RU_{eq} at a particular drug concentration and represents that the rate of binding of the small molecule equals the rate of dissociation of the complex (121). To obtain equilibrium binding constants, the steady state RU_{eq} signals obtained from each injection were plotted against ligand concentration considering a single binding site for each nucleic acid sample, and fitted with the program Kaleidagraph by nonlinear least-squares to equation 3 (121):

$$R_{\text{eq}} = \text{RU}_{\text{max}}(K_{\text{eq}}[\text{Ligand}_{\text{free}}]) / (1 + K_{\text{eq}}[\text{Ligand}_{\text{free}}]) \quad [3]$$

Where:

R_{eq} is the observed steady state response in refractive index units at each ligand concentration, and L_{free} is the unbound concentration of the ligand. When saturation of the immobilized nucleic acid is approached, the RU_{eq} approaches the maximum value, RU_{max} . This parameter is included as a fit parameter in equation 3.

6.4. Electrospray ionization mass spectrometry

ESI-MS studies were carried out by Carolyn Mazzitelli using the benzoxazole ligands and oligonucleotides from IDT Technologies (Coralville, IA). Duplex DNA was annealed by preparing equimolar (1 mM) concentrations of the non-self complementary oligonucleotides d(GCGGGATGGGGCG) and d(CGCCCCATCCCCGC); d(GCGGGAATTGGGCG) and d(CGCCCAATTCCCCGC); d(GCGGAAATTTGGGCG) and d(CGCCTTTAAACCGC). Analytical solutions containing a ligand and metal salt, a ligand and DNA duplex, or a ligand, metal salt, and DNA duplex were prepared at equimolar (10 μ M) concentrations in 50 mM ammonium acetate solutions with 50% methanol. The samples were directly infused at 3 μ L/min into a Thermo Electron (San Jose, CA) LCQ mass spectrometer. For the DNA binding experiments, the instrument was operated in the negative ion mode with an electrospray voltage of 3.5 kV and a heated capillary temperature of 90 to 110 $^{\circ}$ C with sheath and auxiliary gas flows of 40 and 10 arbitrary units, respectively. Ligand/metal ion solutions were examined in the positive ion mode using an electrospray voltage of 4.5 kV and the same heated capillary and gas flow rates used for the solutions containing DNA.

6.5. Cytotoxicity Assays

Cell viability was determined using the AlamarBlue reagent (part no. BUF012B, from AbD Serotec, Kidlington, Oxford, UK). This reagent can be used to easily detect changes in cell proliferation based on the ability of viable cells to cause AlamarBlue to change from its oxidized (non-fluorescent) to a reduced (fluorescent) form (140). Cell culture cytotoxicity assays were carried out as described by Kumar *et al* (109). Aliquots of 100 μ L cell suspension ($1-3 \times 10^3$ cells) were placed in microtiter plates in an atmosphere of 5% CO₂ at 37 $^{\circ}$ C. After 24 h, 100 μ L of culture media and 2 μ L of the compound in DMSO were added to each

well in duplicate, and the plates incubated an additional 24 or 72 h at 37 °C. There was no effect on the growth of cells compared to that of cells in culture media alone at this DMSO concentration. Compounds, along with Mitomycin-C (part no. 100498, from MP Biomedicals, Solon, OH) as a positive control were evaluated at final concentrations ranging from 0.001 to 50 µM.

After the 24 or 72 h incubation, the culture media was removed from each well, and 200 µL of fresh media and 20 µL of AlamarBlue reagent were added, followed by additional 6 h incubation. Cell viability was detected by fluorescence intensity using a Beckman Coulter DTX880 plate reader (Fullerton, CA) with excitation at 530 nm and emission at 590 nm.

The fluorescence data obtained from the cytotoxicity studies was used to calculate the percent growth according to the following equation:

$$\% \text{ Growth} = 100 * (\text{Mean} F_{\text{test}} - \text{Mean} F_{\text{time0}}) / (\text{Mean} F_{\text{ctrl}} - \text{Mean} F_{\text{time0}}) \quad [4]$$

Where:

Mean F_{time0} = the averaged measured fluorescence intensities of AlamarBlue reagent at the time just before the exposure of the cells to the test substance.

Mean F_{test} = the averaged measured fluorescence intensities of AlamarBlue reagent after 24 or 72 h exposure of the cells to the test substance at a particular concentration.

Mean F_{ctrl} = the averaged measured fluorescence intensities of AlamarBlue reagent after 24 or 72 h exposure of the cells to the vehicle without the test substance.

The IC_{50} (50% Inhibition Concentration) is defined as the test compound concentration where the increase from time_0 in the number of mass of treated cells was only 50% as much as the corresponding increase in the vehicle-control at the end of the experiment. The IC_{50} values of UK-1 analogs were determined by non-linear regression using the program Kaleidagraph and fitting the data to the following equation:

$$y = \text{Min} + (\text{Max}-\text{Min})/(1+10^{((x-\log I C_{50}) * \text{Hillslope}))} \quad [5]$$

Where:

Min= the minimum response plateau (0%Growth)

Max= the maximum response plateau (100% Growth)

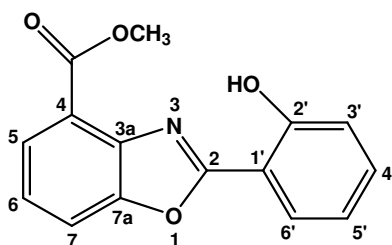
y= % Growth at each test compound concentration

6.6. Western blot analysis

Western blot analyses were performed by Chad McKee (The University of Texas at Austin). All proteins of interest were evaluated in A549 cell lines for total cellular protein levels via western blot analysis. Cells were treated for 24 h with vehicle, 10 μM CuCl_2 , 5 μM UK-1, 5 μM UK-1 + 10 μM CuCl_2 or 5 μM UK-1- Cu^{2+} -complex prior to sample collection. Western blots were performed using the primary antibodies caspase-8 (R&S Systems, Minneapolis, MN, part no. AF1650) and β -actin (Santa Cruz Biotechnology, Santa Cruz, Ca, part no. SC-1616) against the relevant protein in the appropriate dilution (usually 0.5 $\mu\text{g}/\text{ml}$). Horseradish peroxidase-conjugated secondary antibodies (SantaCruz Biotechnology, part no. SC-2031) were used to detect primary antibodies. Signals were detected by the use of an ECL kit (Amersham Pharmacia Biosciences, Piscataway, NJ). Images were collected by a Kodak DC-290 digital camera. Equal loading (20 μg) was verified by comparing expression levels of β -actin.

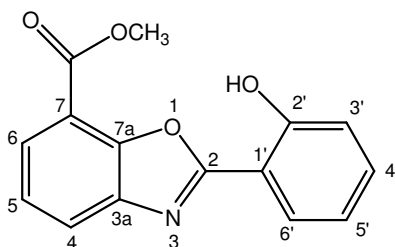
6.7. Synthetic Procedures

6.7.1. Compound 8. 2-(2-Hydroxy-phenyl)-benzoxazole-4-carboxylic acid methyl ester



This compound was synthesized as described previously, COSY and NOSY relations were used to determine peak assignments (109). M.p. 134–135 °C; Rf 0.578 (30% EtOAc in hexanes); ¹H NMR d 4.05 (s, 3H, CH₃), 6.99 (t, 1H, J=, 7.8 Hz, C₅-H), 7.13 (dd, 1H, J= 8.5, 0.5 Hz, C₃-H), 7.45-7.41, (m, 2H, C₄-H, C₆-H), 7.80, (dd, 1H, J= 8.5, 1.0 Hz, C₇-H), 7.99-7.96 (m, 2H, C₅-H, C₆-H); ¹³C NMR (CDCl₃/MeOD 1:1) d 52.66 (CH₃), 110.42 (C₂), 115.69 (C₇), 117.92 (C₃), 120.28 (C₄), 121.50 (C₄), 125.51 (C₆), 127.79 (C₅), 127.80 (C₆'), 134.78 (C₅'), 140.04 (C_{3a}), 150.42 (C_{7a}), 159.56 (C₂), 164.90 (C₁'), 166.39 (CO₂); CIMS m/z 270 (MH⁺); HRMS m/z calcd. for C₁₅H₁₂NO₄: 270.0766, found 270.0766.

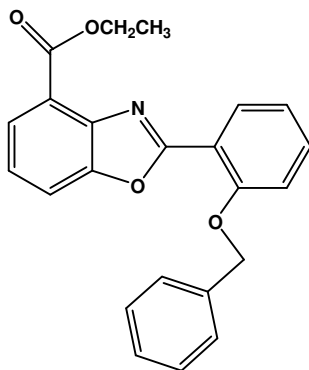
6.7.2. Compound 9. Methyl 2-(2'-hydroxyphenyl)-benzoxazole-7-carboxylate



Oxalyl chloride (1.75 mL) was added to a solution of 2-benzyloxybenzoic acid (2 mmol, 456 mg) in 12 mL of dry dichloromethane, and the solution was stirred for 10 min. Dimethylformamide (0.3 mL) was then added drop-wise, and the mixture

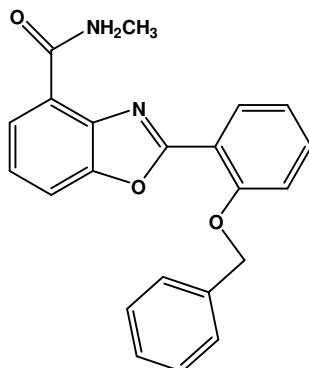
was allowed to stir for 2 h, after which the solvents were removed in vacuo. To the residue was added a solution of 3-amino-2-hydroxybenzoic acid (2 mmol, 306 mg) in 30 mL THF, and 5 mL pyridine. The reaction mixture was stirred at room temperature overnight then heated under reflux for 1 h. The solvent was evaporated and the resulting brown mass was dissolved in xylenes (50 mL). *p*-Toluenesulfonic acid monohydrate (3.8 g, 20mmol) was added, and the mixture was heated under reflux overnight and then quenched with NaOH (20 mL, 1N). The layers were separated, and the aqueous phase was acidified with conc. HCl to pH 2 and extracted with ethyl acetate. The organic phases were combined, dried, and evaporated. The residue was dissolved in a mixture of MeOH/benzene (1:4, 20 mL) and TMSCHN₂ (2M solution in ether, 2 mL, 4mmol) was added. The reaction mixture was then concentrated in vacuo and subjected to flash chromatography (SiO₂, EtOAc/Hex gradient) to afford **3** as light pink crystals (95 mg, 18%): mp 112–113 °C; ¹H NMR (CDCl₃/MeOD 1:1) δ 3.75 (s, 3H, CH₃), 6.73, (t, 1H, J=, 7.56 Hz, C₅-H), 6.78, (dd, 1H, J= 8.70, 0.81 Hz, C₃'-H), 7.17-7.13, (m, 2H, C₄'-H, C₅-H), 7.60, (dd, 1H, J= 7.91, 1.13 Hz, C₄-H), 7.67 (dd, 1H, J= 7.7, 1.13 Hz, C₆-H), 7.79 (dd, 1H, J=7.91, 1.7 Hz, C₆'-H); ¹³C NMR (CDCl₃/MeOD 1:1) δ 51.804 (CH₃), 109.494 (C₁'), 114.386 (C₇), 116.64 (C₃'), 119.327 (C₅'), 123.458 (C₄), 124.311 (C₅), 126.776 (C₆), 127.047 (C₆'), 133.525 (C₄'), 140.966 (C_{3a}), 147.581 (C_{7a}), 157.976 (C₃'), 163.24(C₂), 164.195 (CO₂); MS (CI) *m/z* 270 (MH⁺); HRMS *m/z* 270.077127 (Calc. 270.076633, C₁₅H₁₂NO₄).

6.7.3. Compound **10**. 2-(2-Benzyloxy-phenyl)-benzooxazole-4-carboxylic acid ethyl ester



Compound **4**, 2-(2-Benzyloxy-phenyl)-benzooxazole-4-carboxylic acid, (142 mg, 0.41 mmol) was dissolved in absolute ethanol (1.25 ml) in a flask fitted with a drying tube. Thionyl chloride (45 μ l, 0.62 mmol) was then added drop-wise while stirring, and the reaction was left stirring overnight at room temperature. Afterwards, the reaction mixture was poured over ice, extracted with DCM, washed with sodium bicarbonate, 1% HCl, water, dried over anhydrous sodium sulfate, and filtered. The product was then concentrated by roto-evaporation, and purified by column chromatography (20% EtOAc in hexanes) to give a white solid (103 mg, 69 % yield). m.p. 112-114 $^{\circ}$ C; R_f 0.30 (20% EtOAc in hexanes); ^1H NMR δ 1.44 (t, 3H, $J=7.2$ Hz), 4.49 (dd, 2H, $J=14, 7.2$ Hz), 5.27 (s, 2H), 7.07-7.12 (m, 2H), 7.27-7.49 (m, 5H), 7.63 (d, 2H, $J=7.8$ Hz), 7.71 (d, 1H, $J=8.1$ Hz), 8.00 (d, 1H, $J=7.5$ Hz), 8.28 (dd, 1H, $J=8, 2$ Hz); ^{13}C NMR δ 14.32, 61.09, 70.50, 113.65, 114.41, 116.31, 120.97, 122.34, 123.97, 126.43, 126.72, 127.59, 128.40, 131.94, 133.07, 136.62, 141.50, 151.24, 157.62, 163.64, 165.14 CIMS m/z 374(MH $^+$); HRMS m/z calc for $\text{C}_{23}\text{H}_{20}\text{NO}_4$: 374.1392, found 374.1389

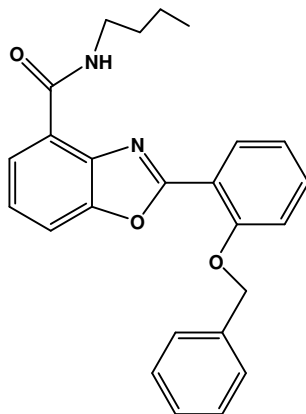
6.7.4. Compound **11**. 2-(2-Benzyloxy-phenyl)-benzoxazole-4-carboxylic acid methylamide



Methylaluminumchloride-methylamide was prepared as described by Levin *et al* (141). Briefly, methylaminehydrochloride (675 mg, 10 mmol) was suspended in 10 ml dry benzene, and placed in an ice bath. Trimethyl aluminum (2 M solution in hexanes, 5 ml) was carefully added portion-wise with evolution of methane. After the addition, the mixture was allowed to warm to room temperature and stirred for 2 hours. Compound **5**, methyl 2-[2-(benzyloxy)phenyl]-1,3-benzoxazole-4-carboxylate (100 mg, 0.28mmol) was dissolved in 2.8 ml dry benzene. To this reaction mixture, 830 μ l of the aluminum amide solution (0.67 M, 0.56 mmol) was added, and placed under reflux overnight. The reaction mixture was then cooled to room temperature and quenched with 5% HCl. The organic layer was separated and the aqueous layer was extracted 3 times with EtOAc. The organic layers were combined, dried over magnesium sulfate, and concentrated in vacuo. The compound was recrystallized from EtOAc/hexanes to give light pink needle-like crystals (49 mg, 49 % yield). mp. 158.5-160°C; Rf 0.74(10% MeOH in DCM); ^1H NMR δ 2.82 (d, 3H, J= 4.8Hz), 5.24 (s, 2H), 7.11-7.17 (m, 2H), 7.32-7.44 (m, 4H), 7.50-7.55 (m, 3H), 7.65 (dd, 1H, J= 8, 0.8Hz), 8.16-8.19 (m, 2H), 8.90(s, 1H); ^{13}C NMR δ 26.20, 70.64, 113.15, 113.56, 115.50, 121.03, 123.89, 124.69, 125.29, 127.03, 128.00,

128.56, 131.29, 133.40, 136.29, 139.47, 150.01, 157.77, 161.84, 164.92; CIMS m/z 359 (MH⁺); HRMS m/z calc for C₂₂H₁₉N₂O₃: 359.1396, found 359.1398

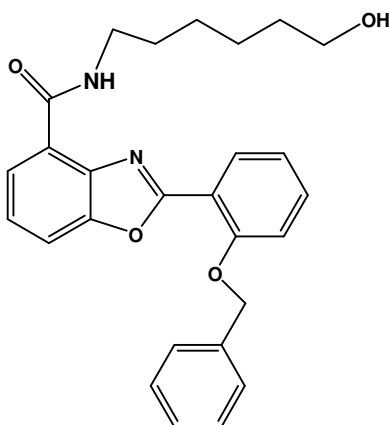
6.7.5. Compound **12**. General Procedure for CDI Coupling. 2-(2-Benzyloxy-phenyl)-benzoxazole-4-carboxylic acid butylamide.



The benzoxazole acid imidazolide was prepared by dissolving **4**, (2-(2-Benzyloxy-phenyl)-benzoxazole-4-carboxylic acid, in dry dichloromethane (DCM), approximately 6 ml/g, and adding portion-wise 1.3 equivalents of CDI with stirring for 1 hour at room temperature, until the evolution of CO₂ ceased. Butylamine (215 mg, 3 mmol) was added to the reaction mixture, which was heated under reflux for 2 days. The reaction mixture was diluted with dichloromethane, and washed with 0.1 N HCl (x2), H₂O (x2), 0.1 N NaOH (x2), and H₂O (x2). The organic layer was dried over anhydrous Na₂SO₄, and the solvent was evaporated. Compound **12** was obtained after column chromatography as white needle-like crystals (157 mg, 45 % yield). mp. 122-123°C; R_f 0.22 (20% EtOAc in hexanes); ¹H NMR δ 0.89 (t, 3H, J= 7.2 Hz), 1.34-1.42 (m, 2H), 1.49-1.57 (m, 2H), 3.42, (q, 2H, 6.4 Hz), 5.29 (s, 2H), 7.11-7.15 (m, 2H), 7.29-7.52 (m, 7H), 7.66 (dd, 1H, J=8, 0.8 Hz), 8.16-8.20 (m, 2H), 9.16 (m, 1H); ¹³C NMR δ 13.68, 20.16, 31.53, 39.31, 70.50, 113.11, 113.76, 115.72, 121.03, 124.08, 124.64, 125.35, 126.67, 127.86, 128.48, 131.36, 133.33, 136.38,

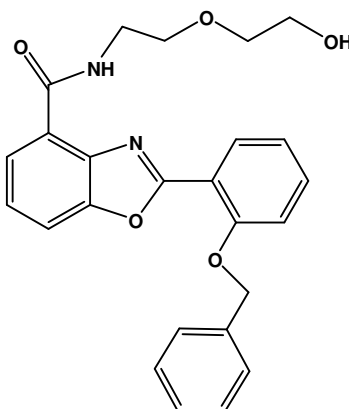
139.35, 150.21, 157.67, 162.11, 164.16; CIMS m/z 401 (MH⁺); HRMS m/z calc for C₂₅H₂₄N₂O₃: 401.1865, found 401.1870

6.7.6. Compound **13**. 2-(2-Benzyloxy-phenyl)-benzoxazole-4-carboxylic acid (6-hydroxy-hexyl)-amide



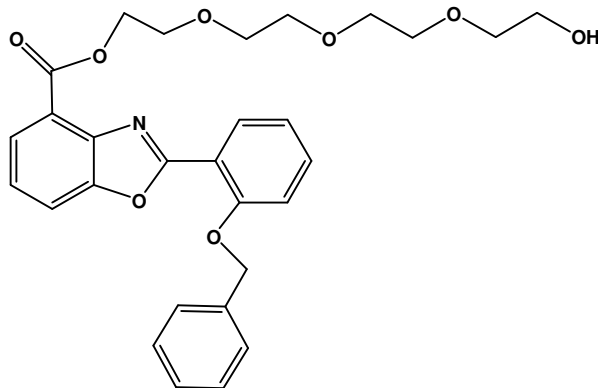
Following the general procedure described above, compound **4** (232 mg, 0.67 mmol) was coupled with 262 mg of aminohexanol (2.24 mmol). Compound **13** was obtained after column chromatography as white crystals (135 mg, 45 % yield). mp. 139-141°C; R_f 0.54 (10%MeOH in DCM) ¹H NMR δ 1.35-.1.52 (m, 8H), 2.47 (s, 1H), 3.38, (dd, 2H, J=13.2, 6.6 Hz), 3.57, (t, 2H, J= 6.6 Hz), 5.22 (s, 2H), 7.09 (t, 2H, J= 7.2 Hz), 7.26-7.50 (m, 7H), 7.60 (d, 1H, J=7.5Hz), 8.14 (t, 2H, J=7.4Hz), 9.16 (m, 1H); ¹³C NMR δ 25.19, 26.58, 29.37, 32.47, 39.34, 62.37, 70.45, 113.17, 113.70, 115.56, 120.99, 123.82, 124.62, 125.29, 126.64, 127.80, 128.44, 131.29, 133.35, 136.33, 139.28, 150.14, 157.60, 162.12, 164.27; CIMS m/z 445 (MH⁺); HRMS m/z calc for C₂₇H₂₈N₂O₄: 445.2127, found:445.2126

6.7.7. Compound **14**. 2-(2-Benzyloxy-phenyl)-benzoxazole-4-carboxylic acid [2-(2-hydroxy-ethoxy)-ethyl]-amide



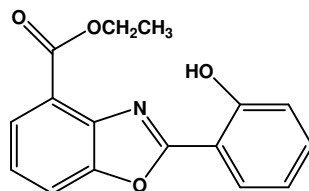
Following the general procedure described above, compound **4** (112 mg, 0.32 mmol) was coupled with 113mg of 2-(2-aminoethoxy)ethanol (1.08 mmol) Compound **14** was obtained after the aqueous workup as a white solid (120 mg, 86 % yield). mp. 91-94 °C Rf 0.68 (10% MeOH in DCM); ¹H NMR δ 2.2 (s(br), 1H), 3.54-3.67 (m, 8H), 5.28 (s, 2H), 7.12-7.15 (m, 2H), 7.29-7.53 (m, 7H), 7.65-7.68 (dd, 1H, J=8, 0.8Hz), 8.16-8.20 (m, 2H), 9.42 (m, 1H); ¹³C NMR δ 39.22, 61.69, 69.86, 70.77, 72.08, 113.47, 114.01, 115.80, 121.21, 123.80, 124.76, 125.53, 126.92, 127.96, 128.55, 131.56, 133.54, 136.45, 139.42, 150.38, 157.72, 162.49, 164.56; CIMS *m/z* 433 (MH⁺); HRMS *m/z* calc for C₂₅H₂₄N₂O₅: 433.1763, found: 433.1747

6.7.8. Compound **15**. 2-(2-Benzyloxy-phenyl)-benzoxazole-4-carboxylic acid 2-(2-[2-(2-hydroxy-ethoxy)-ethoxy]-ethoxy)-ethyl ester



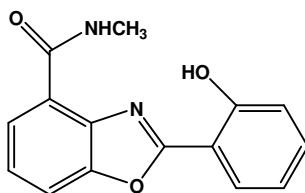
Following the general procedure described above, compound **4** (112 mg, 0.32 mmol) was coupled with 210 mg of tetraethyleneglycol (1.08 mmol). Compound **15** was obtained after column chromatography as a transparent oil (86 mg, 51% yield). Rf 0.76 (10% MeOH in DCM); ^1H NMR δ 2.6 (s(br), 1H), 3.52-3.54 (m, 2H), 3.58-3.70 (m, 8H), 3.72-3.74(m, 2H), 3.87 (t, 2H, J= 4.8 Hz), 4.58, (t, 2H, J= 4.8 Hz), 5.27 (s, 2H), 7.06-7.11 (m, 2H), 7.28-7.48 (m, 5H), 7.61 (d, 2H, J= 7.2Hz), 7.71 (dd, 1H, J= 8, 0.8 Hz), 8.01 (dd, 1H, J= 7.6, 0.8 Hz), 8.27 (dd, 1H, J= 8.2, 1.8 Hz); ^{13}C NMR δ 61.54, 64.18, 69.08, 70.16, 70.44, 70.48, 70.58, 72.37, 113.60, 114.61, 116.23, 120.95, 121.80, 123.96, 126.57, 126.68, 127.59, 128.40, 131.97, 133.12, 136.57, 141.57, 151.27, 157.59, 163.78, 164.86; CIMS m/z 522 (MH⁺); HRMS m/z calc for C₂₉H₃₁NO₈: 521.2050, found: 521.2036

6.7.9. Compound **16**. General procedure for hydrogenolysis. 2-(2-Hydroxy-phenyl)-benzoxazole-4-carboxylic acid ethyl ester



The benzyl ether compound **10** (103 mg, 0.28 mmol) was dissolved in absolute EtOH (4 ml/mmol), and an equal weight of 10% palladium on activated carbon was added. The reaction mixture was placed under a balloon of hydrogen for approximately 2 hours. After verifying by TLC that the reaction had gone to completion, the solution was filtered through celite and washed with EtOAc and CH₂Cl₂. The solution was then evaporated under reduced pressure conditions, and the compound was purified by column chromatography (10% EtOAc in hexanes), recovering **16** as white crystals (75 mg, 96% yield). mp. 122-123.5 °C; R_f 0.56 (20% EtOAc in hexanes); ¹H NMR δ 1.49 (t, 3H, J= 6.9 Hz), 4.46 (dd, 2H, J= 14.4, 7.2Hz), 6.95 (t, 1H, J= 7.4Hz), 7.08 (d, 1H, J= 8.7Hz), 7.34-7.43 (m, 2H), 7.70 (d, 1H, J= 8.4 Hz), 7.92 (d, 1H, J= 7.5 Hz), 8.00 (dd, 1H, J= 7.8Hz), 11.80 (s, 1H); ¹³C NMR δ 14.23, 61.34, 109.82, 114.66, 117.51, 119.43, 121.39, 124.59, 127.02, 127.24, 134.05, 139.20, 149.57, 159.30, 164.06, 165.03; CIMS *m/z* 284 (MH⁺); HRMS *m/z* calc for C₁₆H₁₄NO₄: 284.0923, found: 284.0926; EA calc for C₁₆H₁₃NO₄: C, 67.84; H, 4.63; N, 4.94; found: C, 67.63; H, 4.52; N, 4.91

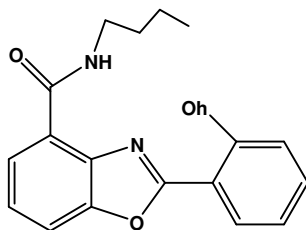
6.7.10. Compound **17**. 2-(2-Hydroxy-phenyl)-benzoxazole-4-carboxylic acid methylamide



Following the general procedure for hydrogenolysis, compound **11** (44 mg, 0.12 mmol) was de-protected to give compound **17**, which was purified by column chromatography (10% MeOH in DCM), and re-crystallized from MeOH in DCM to recover white crystals (27.87 mg, 85% yield) mp. 225.5-226.5°C; R_f

0.74(10% MeOH in hexanes); ^1H NMR δ 3.14 (d, 3H, $J= 7.2$ Hz), 7.06 (t, 1H, $J=7.2\text{Hz}$), 7.13 (dd, 1H, $J= 8.7, 0.9$ Hz), 7.46-7.53 (m, 2H), 7.73 (dd, 1H, $J= 7.8, 0.9\text{Hz}$), 8.06 (dd, 1H, $J=8.1, 1.5$), 8.20 (dd, 1H, $J= 0.9, 7.5$); ^{13}C NMR δ 26.69, 109.89, 113.55, 117.45, 120.25, 123.96, 125.48, 126.48, 127.75, 134.57, 137.18, 148.95, 158.27, 163.39, 164.54 CIMS m/z 269 (MH^+); HRMS m/z calc for $\text{C}_{15}\text{H}_{13}\text{N}_2\text{O}_3$: 269.0926, found 269.0926; EA calc for $\text{C}_{15}\text{H}_{12}\text{N}_2\text{O}_3$: C, 67.16; H, 4.51; N, 10.44; found: C, 67.06, H, 4.54, N, 9.85

6.7.11. Compound **18**. 2-(2-Hydroxy-phenyl)-benzooxazole-4-carboxylic acid butylamide .



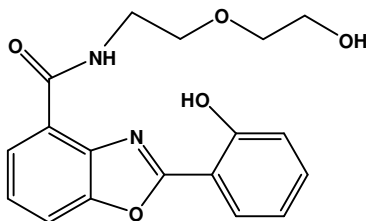
Following the general procedure for hydrogenolysis, compound **12** (150 mg, 0.37 mmol) was de-protected to give compound **18**, which was recrystallized from EtOAc/hexanes to give white-flake like crystals (105.94 mg, 91% yield) mp. 181-183°C; Rf 0.22 (20% EtOAc in hexanes); ^1H NMR δ 0.99 (t, 3H, $J= 7.2$ Hz), 1.45-1.52 (m, 2H), 1.66-1.72 (m, 2H), 3.56 (dd, 2H, $J= 12.8, 6$ Hz), 7.00 (t, 1H, $J= 8.4$ Hz), 7.08 (d, 1H, $J= 8$ Hz), 7.42-7.46 (m, 2H), 7.68 (d, 1H, $J= 8.4$ Hz), 7.80 (s(br), 1H), 7.99 (dd, 1H, $J= 8.2, 1.4$ Hz), 8.15 (d, 1H, $J= 8.1$ Hz), 10.37 (s, 1H); ^{13}C NMR δ 13.72, 20.23, 31.53, 39.60, 109.81, 113.41, 117.43, 120.14, 124.08, 125.42, 126.40, 127.65, 134.50, 137.15, 148.88, 158.33, 163.31, 163,70; CIMS m/z 311 (MH^+); HRMS m/z calc for $\text{C}_{18}\text{H}_{19}\text{N}_2\text{O}_3$: 311.1396, found: 311.1397; EA calc for $\text{C}_{18}\text{H}_{18}\text{N}_2\text{O}_3+1/4\text{H}_2\text{O}$: C, 68.69; H, 5.92; N, 8.90; found: C, 68.68; H, 5.73; N, 8.69

6.7.12. Compound **19**. 2-(2-Hydroxy-phenyl)-benzooxazole-4-carboxylic acid (6-hydroxy-hexyl)-amide

Error! Objects cannot be created from editing field codes.

Following the general procedure for hydrogenolysis, compound **13** (120 mg, 0.27 mmol) was de-protected to give compound **19**, which was purified by column chromatography (10% MeOH in DCM), to afford an off-white solid (87 mg, 90% yield). mp. 145.5-147°C; Rf 0.54(10% MeOH in DCM); ¹H NMR δ 1.47-1.49 (m, 4H), 1.59-1.62 (m, 2H), 1.70-1.74 (m, 2H), 1.82 (s(br), 1H), 3.58 (dd, 2H, J=12.8, 6.8 Hz), 3.64 (t, 2H, J= 6.4Hz), 7.03 (t, 1H, J= 7.4 Hz), 7.10(d, 1H, J= 8.4 Hz), 7.44-7.48 (m, 2H), 7.70 (d, 1H, J= 8 Hz), 7.83(m, 1H), 8.03 (dd, 1H, J= 8, 1.2Hz), 8.16 (d, 1H, J= 7.6 Hz), 10.44 (s, 1H); ¹³C NMR δ 25.30, 26.72, 29.55, 32.54, 39.71, 62.62, 109.89, 113.53, 117.46, 120.27, 124.04, 125.51, 126.48, 127.74, 134.60, 137.20, 148.95, 158.30, 163.40, 163.84; CIMS *m/z* 355 (MH⁺); HRMS *m/z* calc for C₂₀H₂₃N₂O₄: 355.1658, found: 355.1660; EA calc for C₂₀H₂₂N₂O₄: C, 67.78; H, 6.26; N, 7.90; found: C, 67.64; H, 6.33; N, 7.48

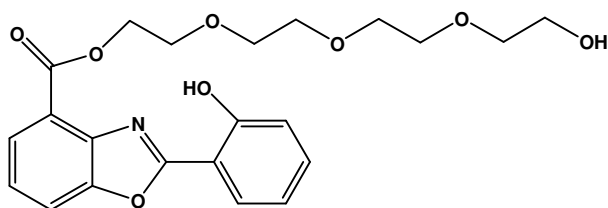
6.7.13. Compound **20**. 2-(2-Hydroxy-phenyl)-benzooxazole-4-carboxylic acid [2-(2-hydroxy-ethoxy)-ethyl]-amide



Following the general procedure for hydrogenolysis, compound **14** (111 mg, 0.27 mmol) was de-protected to give compound **20**, which was purified by column chromatography (10% MeOH in DCM), recovering white crystals (56 mg, 63 % yield). mp. 157-159°C; Rf 0.68 (10% MeOH in DCM); ¹H NMR δ 2.65 (s(br), 1H), 3.67 (t, 2H, J= 4.4 Hz), 3.74(t, 2H, J= 4.6), 3.80-3.84 (m, 4H), 7.05 (t, 1H, J= 7.8 Hz), 7.12 (dd, 1H, J= 8.4, 0.8 Hz), 7.45-7.50 (m, 2H), 7.72 (dd, 1H, J=

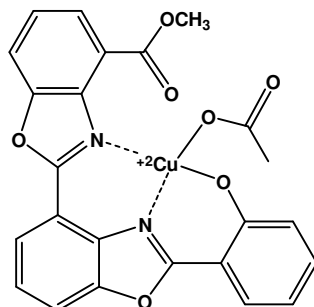
8, 0.8 Hz), 8.04 (dd, 1H, J= 8.2, 1.4 Hz), 8.19 (dd, 1H, J= 7.4, 1 Hz), 8.38 (m, 1H), 10.80 (s, 1H); ^{13}C NMR δ 39.41, 61.93, 70.08, 73.24, 109.93, 113.70, 117.59, 120.62, 123.87, 125.56, 126.54, 127.71, 134.69, 137.29, 149.01, 157.72, 163.35, 163.64; CIMS m/z 343 (MH⁺); HRMS m/z calc for C₁₈H₁₉N₂O₅: 343.1294, found: 343.1285; EA calc for C₁₈H₁₈N₂O₅+1/3H₂O: C, 62.06; H, 5.40; N, 8.04; found: C, 62.24; H, 5.19; N, 7.69

6.7.14. Compound **21**. 2-(2-Hydroxy-phenyl)-benzooxazole-4-carboxylic acid 2-(2-[2-(2-hydroxy-ethoxy)-ethoxy]-ethoxy)-ethyl ester



Following the general procedure for hydrogenolysis, compound **15** (65 mg, 0.12 mmol) was de-protected to give compound **21**, which was purified by column chromatography (10% MeOH in DCM), recovering a yellow oil (46 mg, 85% yield). R_f 0.76 (10% MeOH in DCM); ^1H NMR δ 2.60 (s(br), 1H), 3.52-3.54 (m, 2H), 3.59-3.71 (m, 8H), 3.74-3.77 (m, 2H), 3.91 (t, 2H, J= 4.8 Hz), 4.58, (t, 2H, J=4.8 Hz), 6.98 (t, 1H, J= 7.6 Hz), 7.09 (d, 1H, J= 8 Hz), 7.39-7.46 (m, 2H), 7.76 (dd, 1H, J= 8, 0.8 Hz), 7.98 (dd, 1H, J= 8, 1.6 Hz), 8.05 (dd, 1H, J= 8, 0.8 Hz), 11.82 (s, 1H); ^{13}C NMR δ 61.64, 64.50, 69.10, 70.24, 70.53, 70.61, 72.44, 109.88, 114.90, 117.59, 119.49, 121.16, 124.68, 127.13, 127.46, 134.12, 139.42, 149.67, 159.34, 164.19, 165.04; CIMS m/z 432 (MH⁺); HRMS m/z calc for C₂₂H₂₆NO₈: 432.1675, found 432.1658; EA calc for C₂₂H₂₅NO₈+1/3H₂O: C, 60.40; H, 5.91; N, 3.26; found: C, 60.53; H, 5.92; N, 3.10

6.7.15. UK-1-Cu²⁺-Complex



UK-1 (19.81 mg, 0.051mmoles) was dissolved in MeOH. A concentrated solution of copper acetate in MeOH (2.94 ml of a 8.74mM solution, 0.026 mmoles) was added portion-wise. The solution was left under reflux for 2 days, after which solvent was slowly evaporated. The metal chelate was recovered after filtration and re-crystallization in MeOH; m.p. > 300 °C; UV $\lambda_{\text{max}}^{\text{MeOH}}$ nm (ϵ) 236 (33814), 267 (28423), 275 (26787), 317 (24749), 333 (24232), 348 (22749), 418 (12974); ; Rf 0.27 (10% MeOH in DCM); IR $\nu_{\text{max}}(\text{KCl}_{\text{pellet}})$ 1750 cm^{-1} ; CIMS m/z 432 (MH⁺); HRMS m/z calc for C₂₂H₁₃N₂O₅Cu⁺: 448.0114, found 448.0115; EA calc for C₂₄H₁₈N₂O₈Cu: C, 54.81; H, 3.45; N, 5.33; found: C, 54.85; H, 2.81; N, 5.33

REFERENCES FOR PART I

1. Watson, J. D., and Crick, F. H. (1953) Molecular structure of nucleic acids; a structure for deoxyribose nucleic acid, *Nature* 171, 737-738.
2. Blackburn, G. M., and Royal Society of Chemistry (Great Britain) (2006) *Nucleic acids in chemistry and biology*, 3rd ed., RSC Pub., Cambridge.
3. Bates, A. D., and Maxwell, A. (2005) *DNA topology*, 2nd ed., Oxford University Press, Oxford ; New York.
4. Chargaff, E. (1950) Chemical specificity of nucleic acids and mechanism of their enzymatic degradation, *Experientia* 6, 201-209.
5. Wang, J. C. (1979) Helical repeat of DNA in solution, *Proc Natl Acad Sci U S A* 76, 200-203.
6. Mandelkern, M., Elias, J. G., Eden, D., and Crothers, D. M. (1981) The dimensions of DNA in solution, *J Mol Biol* 152, 153-161.
7. Ghosh, A., and Bansal, M. (2003) A glossary of DNA structures from A to Z, *Acta Crystallogr D Biol Crystallogr* 59, 620-626.
8. Wing, R., Drew, H., Takano, T., Broka, C., Tanaka, S., Itakura, K., and Dickerson, R. E. (1980) Crystal structure analysis of a complete turn of B-DNA, *Nature* 287, 755-758.
9. Pabo, C. O., and Sauer, R. T. (1984) Protein-DNA recognition, *Annu Rev Biochem* 53, 293-321.
10. Bischoff, G., and Hoffmann, S. (2002) DNA-Binding of Drugs Used in Medicinal Therapies, *Curr. Med. Chem.* 9, 321-348.
11. Hirsch, J. (2006) An anniversary for cancer chemotherapy., *JAMA* 296, 1518-1520.
12. Krumbhaar, E. B. (1919) Role of the blood and the bone marrow in certain forms of gaspoisoning., *JAMA* 72, 39-41.
13. Goodman, L. S., Wintrobe, M. M., Dameshek, W., Goodman, M. J., Gilman, A., and McLennan, M. T. (1946) Nitrogen mustard therapy: use of methyl-bis(beta-chloroethyl)amine hydrochloride and tris(beta-chloroethyl)amine hydrochloride for Hodgkin's disease, lymphosarcoma, leukemia, and certain allied and miscellaneous disorders, *JAMA* 132, 126-132.
14. Borresen, H. C. (1969) [Structure and mode of action of alkylating agents used in the therapy of neoplastic diseases], *Nord Med* 81, 65-72.
15. Danneberg, P., Druckrey, H., Kaiser, K., Lo, H. W., Mecke, R., Jr., Nieper, H. A., and Schmahl, D. (1956) [Comparative investigation of the chemotherapeutic action of N-oxide-mustard gas and other alkylating compounds in rat tumors.], *Arzneimittelforschung* 6, 539-550.

16. Bignold, L. P. (2006) Alkylating agents and DNA polymerases, *Anticancer Res* 26, 1327-1336.
17. Weiss, A., and Weiss, B. (1975) [Carcinogenesis due to mustard gas exposure in man, important sign for therapy with alkylating agents], *Dtsch Med Wochenschr* 100, 919-923.
18. Kamb, A., Wee, S., and Lengauer, C. (2007) Why is cancer drug discovery so difficult?, *Nat Rev Drug Discov* 6, 115-120.
19. Strekowski, L., and Wilson, B. (2007) Noncovalent interactions with DNA: an overview, *Mutat Res* 623, 3-13.
20. Nelson, S. M., Ferguson, L. R., and Denny, W. A. (2004) DNA and the chromosome - varied targets for chemotherapy, *Cell Chromosome* 3, 2.
21. Subirana, J. A., and Soler-Lopez, M. (2003) Cations as hydrogen bond donors: a view of electrostatic interactions in DNA, *Annu Rev Biophys Biomol Struct* 32, 27-45.
22. Thomas, T., Balabhadrapathruni, S., Gallo, M. A., and Thomas, T. J. (2002) Development of polyamine analogs as cancer therapeutic agents, *Oncol Res* 13, 123-135.
23. Waring, M. J., and Royal Society of Chemistry (Great Britain) (2006) *Sequence-specific DNA binding agents*, RSC Publishing, Cambridge.
24. Baraldi, P. G., Bovero, A., Fruttarolo, F., Preti, D., Tabrizi, M. A., Pavani, M. G., and Romagnoli, R. (2004) DNA minor groove binders as potential antitumor and antimicrobial agents, *Med Res Rev* 24, 475-528.
25. Wheate, N. J., Brodie, C. R., Collins, J. G., Kemp, S., and Aldrich-Wright, J. R. (2007) DNA intercalators in cancer therapy: organic and inorganic drugs and their spectroscopic tools of analysis, *Mini Rev Med Chem* 7, 627-648.
26. Brana, M. F., Cacho, M., Gradillas, A., de Pascual-Teresa, B., and Ramos, A. (2001) Intercalators as anticancer drugs, *Curr Pharm Des* 7, 1745-1780.
27. Thompson, K. H., and Orvig, C. (2003) Boon and bane of metal ions in medicine, *Science* 300, 936-939.
28. Thompson, K. H., and Orvig, C. (2006) Metal complexes in medicinal chemistry: new vistas and challenges in drug design, *Dalton Trans*, 761-764.
29. Meggers, E. (2007) Exploring biologically relevant chemical space with metal complexes, *Curr Opin Chem Biol* 11, 287-292.
30. Sigel, A., and Sigel, H. (1996) *Interactions of metal ions with nucleotides, nucleic acids, and their constituents*, M. Dekker, New York.
31. Sigel, A., and Sigel, H. (1996) *Probing of nucleic acids by metal ion complexes of small molecules*, Marcel Dekker, New York.
32. Farrell, N. (1989) *Transition metal complexes as drugs and chemotherapeutic agents*, Kluwer Academic Publishers, Dordrecht ; Boston.

33. Kraatz, H.-B., and Metzler-Nolte, N. (2006) *Concepts and models in bioinorganic chemistry*, Wiley-VCH, Weinheim.
34. Nash, R. A. (2005) Metals in medicine, *Altern Ther Health Med* 11, 18-25.
35. Sigel, R. K. (2007) Intimate Relationships between Metal Ions and Nucleic Acids, *Angew Chem Int Ed Engl* 46, 654-656.
36. Zhang, C. X., and Lippard, S. J. (2003) New metal complexes as potential therapeutics, *Curr Opin Chem Biol* 7, 481-489.
37. Apelgot, S., Coppey, J., Fromentin, A., Guille, E., Poupon, M. F., and Roussel, A. (1986) Altered distribution of copper (⁶⁴Cu) in tumor-bearing mice and rats, *Anticancer Res* 6, 159-164.
38. Ranade, S. S., and Panday, V. K. (1983) Transition metals in human cancer. I. Oesophagus and bone marrow, *Sci Total Environ* 29, 177-181.
39. Ranade, S. S., and Panday, V. K. (1984) Transition metals in human cancer II, *Sci Total Environ* 40, 245-257.
40. Sigel, H. (1980) *Carcinogenicity and metal ions*, M. Dekker, New York.
41. Sigel, A., and Sigel, H. (2004) *Metal complexes in tumor diagnosis and as anticancer agents*, Marcel Dekker, New York.
42. Boerner, L. J., and Zaleski, J. M. (2005) Metal complex-DNA interactions: from transcription inhibition to photoactivated cleavage, *Curr Opin Chem Biol* 9, 135-144.
43. Richards, A. D., and Rodger, A. (2007) Synthetic metallomolecules as agents for the control of DNA structure, *Chem Soc Rev* 36, 471-483.
44. Sigel, H. (1975) Nucleic base-metal ion interactions. Acidity of the N(1) or N(3) proton in binary and ternary complexes of Mn-2+, Ni-2+, and Zn-2+ with the 5'-triphosphates of inosine, guanosine, uridine, and thymidine, *J Am Chem Soc* 97, 3209-3214.
45. Wong, E., and Giandomenico, C. M. (1999) Current status of platinum-based antitumor drugs, *Chem Rev* 99, 2451-2466.
46. Wang, D., and Lippard, S. J. (2005) Cellular processing of platinum anticancer drugs, *Nat Rev Drug Discov* 4, 307-320.
47. Bergamo, A., and Sava, G. (2007) Ruthenium complexes can target determinants of tumour malignancy, *Dalton Trans*, 1267-1272.
48. Lombo, F., Menendez, N., Salas, J. A., and Mendez, C. (2006) The aureolic acid family of antitumor compounds: structure, mode of action, biosynthesis, and novel derivatives, *Appl Microbiol Biotechnol* 73, 1-14.
49. Grundy, W. E., Goldstein, A. W., Rickher, J. C., Hanes, M. E., Warren, H. B., and Sylvester, J. C. (1953) Aureolic acid, a new antibiotic. I. Microbiological studies., *Antimicrob Chemother* 3, 1215-1221.
50. Du Priest, R. W., and Fletcher, W. S. (1973) Chemotherapy of testicular germinal tumors., *Oncology* 28, 147-113.
51. Chakrabarti, S., Bhattacharyya, D., and Dasgupta, D. (2000) Structural basis of DNA recognition by anticancer antibiotics, chromomycin A(3), and mithramycin: roles of minor groove width and ligand flexibility, *Biopolymers* 56, 85-95.

52. Hou, M. H., and Wang, A. H. (2005) Mithramycin forms a stable dimeric complex by chelating with Fe(II): DNA-interacting characteristics, cellular permeation and cytotoxicity, *Nucleic Acids Res* 33, 1352-1361.
53. Majee, S., Dasgupta, D., and Chakrabarti, A. (1999) Interaction of the DNA-binding antitumor antibiotics, chromomycin and mithramycin with erythroid spectrin, *Eur J Biochem* 260, 619-626.
54. Aich, P., and Dasgupta, D. (1995) Role of magnesium ion in mithramycin-DNA interaction: binding of mithramycin-Mg²⁺ complexes with DNA, *Biochemistry* 34, 1376-1385.
55. Sastry, M., and Patel, D. J. (1993) Solution structure of the mithramycin dimer-DNA complex, *Biochemistry* 32, 6588-6604.
56. Aich, P., and Dasgupta, D. (1990) Role of Mg⁺⁺ in the mithramycin-DNA interaction: evidence for two types of mithramycin-Mg⁺⁺ complex, *Biochem Biophys Res Commun* 173, 689-696.
57. Cons, B. M., and Fox, K. R. (1989) Interaction of mithramycin with metal ions and DNA, *Biochem Biophys Res Commun* 160, 517-524.
58. Pereira, M. A., Figueiredo, T. L., and Demicheli, C. (1997) Spectrophotometric Study of Mithramycin Complexes with Cu(II), Fe(III), and Tb(III), *Anal Lett* 30, 2555-2563.
59. Goss, W. A., Deitz, W. H., and Cook, T. M. (1965) Mechanism of Action of Nalidixic Acid on Escherichia Coli.li. Inhibition of Deoxyribonucleic Acid Synthesis, *J Bacteriol* 89, 1068-1074.
60. Giamarellou, H., Efstratiou, A., Tsagarakis, J., Petrikkos, G., and Daikos, G. K. (1984) Experience with ciprofloxacin in vitro and in vivo, *Arzneimittelforschung* 34, 1775-1778.
61. Koga, H., Itoh, A., Murayama, S., Suzue, S., and Irikura, T. (1980) Structure-activity relationships of antibacterial 6,7- and 7,8-disubstituted 1-alkyl-1,4-dihydro-4-oxoquinoline-3-carboxylic acids, *J Med Chem* 23, 1358-1363.
62. Blondeau, J. M. (1999) Expanded activity and utility of the new fluoroquinolones: a review, *Clin Ther* 21, 3-40; discussion 41-42.
63. Hooper, D. C. (1993) Quinolone mode of action--new aspects, *Drugs* 45 Suppl 3, 8-14.
64. Tabarrini, O., Cecchetti, V., Fravolini, A., Nocentini, G., Barzi, A., Sabatini, S., Miao, H., and Sissi, C. (1999) Design and synthesis of modified quinolones as antitumoral acridones, *J Med Chem* 42, 2136-2144.
65. Sissi, C., and Palumbo, M. (2003) The quinolone family: from antibacterial to anticancer agents, *Curr Med Chem Anticancer Agents* 3, 439-450.
66. Anderson, V. E., and Osheroff, N. (2001) Type II topoisomerases as targets for quinolone antibacterials: turning Dr. Jekyll into Mr. Hyde, *Curr Pharm Des* 7, 337-353.
67. Sissi, C., Andreolli, M., Cecchetti, V., Fravolini, A., Gatto, B., and Palumbo, M. (1998) Mg(2+)-mediated binding of 6-substituted quinolones to DNA: relevance to biological activity, *Bioorg Med Chem* 6, 1555-1561.

68. Chohan, Z. H., Supuran, C. T., and Scozzafava, A. (2005) Metal binding and antibacterial activity of ciprofloxacin complexes, *J Enzyme Inhib Med Chem* 20, 303-307.
69. Elnima, E. I., Zubair, M. U., and Al-Badr, A. A. (1981) Antibacterial and antifungal activities of benzimidazole and benzoxazole derivatives, *Antimicrob Agents Chemother* 19, 29-32.
70. Boiani, M., and Gonzalez, M. (2005) Imidazole and benzimidazole derivatives as chemotherapeutic agents, *Mini Rev Med Chem* 5, 409-424.
71. Spasov, A. A., Yozhitsa, I. N., Bugaeva, L. I., and Anisimova, V. A. (1999) Benzimidazole Derivatives: Spectrum of Pharmacological Activity and Toxicological Properties (A Review), *Pharmac Chem J* 33, 6-17.
72. Akbay, A., Oren, I., Temiz-Arpaci, O., Aki-Sener, E., and Yalcin, I. (2003) Synthesis and HIV-1 reverse transcriptase inhibitor activity of some 2,5,6-substituted benzoxazole, benzimidazole, benzothiazole and oxazolo(4,5-b)pyridine derivatives, *Arzneimittelforschung* 53, 266-271.
73. Arakawa, K., Inamasu, M., Matsumoto, M., Okumura, K., Yasuda, K., Akatsuka, H., Kawanami, S., Watanabe, A., Homma, K., Saiga, Y., Ozeki, M., and Iijima, I. (1997) Novel benzoxazole 2,4-thiazolidinediones as potent hypoglycemic agents. Synthesis and structure-activity relationships, *Chem Pharm Bull (Tokyo)* 45, 1984-1993.
74. Gualtiere, F., Brody, G., Fieldsteel, A. H., and Skinner, W. A. (1971) Antiviral agents. 1. Benzothiazole and benzoxazole analogs of 2-(alpha-hydroxybenzyl)benzimidazole, *J Med Chem* 14, 546-549.
75. Kaplancikli, Z. A., Turan-Zitouni, G., Revial, G., and Guven, K. (2004) Synthesis and study of antibacterial and antifungal activities of novel 2-[[[(benzoxazole/benzimidazole-2-yl)sulfanyl] acetylamino]thiazoles, *Arch Pharm Res* 27, 1081-1085.
76. Oren, I., Temiz, O., Yalcin, I., Sener, E., and Altanlar, N. (1999) Synthesis and antimicrobial activity of some novel 2,5- and/or 6-substituted benzoxazole and benzimidazole derivatives, *Eur J Pharm Sci* 7, 153-160.
77. Paramashivappa, R., Phani Kumar, P., Subba Rao, P. V., and Srinivasa Rao, A. (2003) Design, synthesis and biological evaluation of benzimidazole/benzothiazole and benzoxazole derivatives as cyclooxygenase inhibitors, *Bioorg Med Chem Lett* 13, 657-660.
78. Rida, S. M., Ashour, F. A., El-Hawash, S. A., ElSemary, M. M., Badr, M. H., and Shalaby, M. A. (2005) Synthesis of some novel benzoxazole derivatives as anticancer, anti-HIV-1 and antimicrobial agents, *Eur J Med Chem* 40, 949-959.
79. Sondhi, S. M., Singh, N., Kumar, A., Lozach, O., and Meijer, L. (2006) Synthesis, anti-inflammatory, analgesic and kinase (CDK-1, CDK-5 and GSK-3) inhibition activity evaluation of benzimidazole/benzoxazole derivatives and some Schiff's bases, *Bioorg Med Chem* 14, 3758-3765.
80. Sun, L. Q., Chen, J., Bruce, M., Deskus, J. A., Epperson, J. R., Takaki, K., Johnson, G., Iben, L., Mahle, C. D., Ryan, E., and Xu, C. (2004) Synthesis

- and structure-activity relationship of novel benzoxazole derivatives as melatonin receptor agonists, *Bioorg Med Chem Lett* **14**, 3799-3802.
81. Unlu, S., Baytas, S. N., Kupeli, E., and Yesilada, E. (2003) Studies on novel 7-acyl-5-chloro-2-oxo-3H-benzoxazole derivatives as potential analgesic and anti-inflammatory agents, *Arch Pharm (Weinheim)* **336**, 310-321.
 82. von Geldern, T. W., Lai, C., Gum, R. J., Daly, M., Sun, C., Fry, E. H., and Abad-Zapatero, C. (2006) Benzoxazole benzenesulfonamides are novel allosteric inhibitors of fructose-1,6-bisphosphatase with a distinct binding mode, *Bioorg Med Chem Lett* **16**, 1811-1815.
 83. Velik, J., Baliharova, V., Fink-Gremmels, J., Bull, S., Lamka, J., and Skalova, L. (2004) Benzimidazole drugs and modulation of biotransformation enzymes, *Res Vet Sci* **76**, 95-108.
 84. Barreca, M. L., Chimirri, A., De Clercq, E., De Luca, L., Monforte, A. M., Monforte, P., Rao, A., and Zappala, M. (2003) Anti-HIV agents: design and discovery of new potent RT inhibitors, *Farmaco* **58**, 259-263.
 85. Claustro, I., Abate, G., Sanchez, J., and Acquaye, H. (2003) Synthesis, spectroscopic and electrochemical properties of ruthenium-2-(2'-hydroxyphenyl)-benzoxazole complexes. Crystal structure of [Ru(terpy)(HPB)Cl], *Inorg Chim Acta* **342**, 29-36.
 86. Duff, E. J., Hughes, M. N., and Rutt, K. J. (1969) Structure and Infrared Spectra of Some Nitrate-complexes of Cobalt (II), Nickel(II), Copper(II), and Zinc(II) with Heterocyclic Ligands *J Chem Soc (A)*, 2126-2128.
 87. Nikolova, A., Ivanov, D., Buyukliev, R., Konstantinov, S., and Karaivanova, M. (2001) Preparation, physicochemical characterization and pharmacological study of novel ruthenium(III) complexes with imidazole and benzimidazole derivatives, *Arzneimittelforschung* **51**, 758-762.
 88. Duff, E. J., and Hughes, M. N. (1968) Oxazole Complexes. Part I. N-Bonded Complexes of Benzoxazole with Cobalt (II), Copper (II), and Zinc (II), *J Chem Soc (A)*, 2144-2146.
 89. Abbotto, A., Bradamante, S., Facchetti, A., and Pagani, G. A. (2002) Metal chelation aptitudes of bis(o-azaheteroaryl)methanes as tuned by heterocycle charge demands, *J Org Chem* **67**, 5753-5772.
 90. Lane, T. J., Nakagwa, I., Walter, J. L., and Kandathil, A. J. (1962) Infrared Investigation of Certain Imidazole Derivatives and their Metal Chelates, *Inorg Chem* **1**, 267-276.
 91. Gomez-Segura, J., Prieto, M. J., Font-Bardia, M., Solans, X., and Moreno, V. (2006) Crystal structure and DNA interaction of the facial-type rac-tris[2-(aminomethyl)benzimidazole]cobalt(III) complex, *Inorg Chem* **45**, 10031-10033.
 92. Zhou, Q., and Yang, P. (2006) Crystal structure and DNA-binding studies of a new Cu(II) complex involving benzimidazole, *Inorg Chim Acta* **359**, 1200-1206.

93. Lorenz, D. R., Barbara, T. M., and Wasson, J. R. (1976) Copper(II) and zinc(II) complexes of 2-(o-hydroxyphenyl)benzoxazole and -benzothiazole, *Inorg Nucl Chem Lett* 12, 65-71.
94. Tellez, F., Pena-Hueso, A., Barba-Behrens, N., Contreras, R., and Flores-Parra, A. (2006) Coordination compounds in a pentacyclic aromatic system from 2-aminobenzothiazole derivatives and transition metal ions, *Polyhedron* 25, 2363-2374.
95. Kuznetsova, L. I., Gilyanovskii, P. V., Derevyanko, L. I., Knyazhanskii, M. I., Garanovskii, A. D., and Osipov, O. A. (1976) Complexes of metals with some nitrogen-containing ligands. XXXIII. Spectral properties of complexes of bivalent metals with 2-(hydroxyphenyl)benzoxazole, *Zhurnal Obshchei Khimii* 46, 670-675.
96. Ueki, M., Ueno, K., Miyadoh, S., Abe, K., Shibata, K., Taniguchi, M., and Oi, S. (1993) UK-1, a novel cytotoxic metabolite from *Streptomyces* sp. 517-02. I. Taxonomy, fermentation, isolation, physico-chemical and biological properties, *J Antibiot (Tokyo)* 46, 1089-1094.
97. Shibata, K., Kashiwada, M., Ueki, M., and Taniguchi, M. (1993) UK-1, a novel cytotoxic metabolite from *Streptomyces* sp. 517-02. II. Structural elucidation, *J Antibiot (Tokyo)* 46, 1095-1100.
98. Ueki, M., Shibata, K., and Taniguchi, M. (1998) UK-1, a novel cytotoxic metabolite from *Streptomyces* sp. 517-02. IV. Antifungal action of methyl UK-1, *J Antibiot (Tokyo)* 51, 883-885.
99. Ueki, M., and Taniguchi, M. (1997) UK-1, a novel cytotoxic metabolite from *Streptomyces* sp. 517-02. III. Antibacterial action of demethyl UK-1, *J Antibiot (Tokyo)* 50, 788-790.
100. Sato, S., Kajiura, T., Noguchi, M., Takehana, K., Kobayashi, T., and Tsuji, T. (2001) AJ19561, a new cytotoxic benzoxazole derivative produced by *Streptomyces* sp, *J Antibiot (Tokyo)* 54, 102-104.
101. DeLuca, M. R., and Kerwin, S. M. (1997) The Total Synthesis of UK-1, *Tetrahedron Lett* 38, 199-202.
102. Reynolds, M. B., DeLuca, M. R., and Kerwin, S. M. (1999) The Novel Bis(Benzoxazole) Cytotoxic Natural Product UK-1 is a Magnesium Ion-Dependent DNA Binding Agent and Inhibitor of Human Topoisomerase II, *Bioorg Chem* 27, 326-337.
103. Ratledge, C., and Snow, G. A. (1974) Isolation and structure of nocobactin NA, a lipid-soluble iron-binding compound from *Nocardia asteroides*, *Biochem J* 139, 407-413.
104. Kalinowski, D. S., and Richardson, D. R. (2005) The evolution of iron chelators for the treatment of iron overload disease and cancer, *Pharmacol Rev* 57, 547-583.
105. Hodges, Y. K., Weinberger, H. D., Stephens, J., Horwitz, M. A., and Horwitz, L. D. (2006) Desferri-Exochelin, a lipid-soluble, hexadentate iron chelator, effectively removes tissue iron, *Transl Res* 148, 63-71.

106. Mitchell, J. M., and Shaw, J. T. (2007) Synthesis and stereochemical assignment of brasilibactin A, *Org Lett* **9**, 1679-1681.
107. Cavanaugh, P. F., Jr., Porter, C. W., Tukalo, D., Frankfurt, O. S., Pavelic, Z. P., and Bergeron, R. J. (1985) Characterization of L1210 cell growth inhibition by the bacterial iron chelators parabactin and compound II, *Cancer Res* **45**, 4754-4759.
108. Reyzer, M. L., Brodbelt, J. S., Kerwin, S. M., and Kumar, D. (2001) Evaluation of complexation of metal-mediated DNA-binding drugs to oligonucleotides via electrospray ionization mass spectrometry, *Nucleic Acids Res* **29**, E103-103.
109. Kumar, D., Jacob, M. R., Reynolds, M. B., and Kerwin, S. M. (2002) Synthesis and evaluation of anticancer benzoxazoles and benzimidazoles related to UK-1, *Bioorg Med Chem* **10**, 3997-4004.
110. Rodembusch, F. S., Brand, F. R., Correa, D. S., Pocos, J. C., Martinelli, M., and Stefani, V. (2005) Transition metal complexes from 2-(2'-hydroxyphenyl)benzoxazole: A spectroscopic and thermogravimetric stability study *Mat Chem and Phys* **92**, 389-393.
111. Wang, B. B., Maghami, N., Goodlin, V. L., and Smith, P. J. (2004) Critical structural motif for the catalytic inhibition of human topoisomerase II by UK-1 and analogs, *Bioorg Med Chem Lett* **14**, 3221-3226.
112. Oehlers, L., Mazzitelli, C. L., Brodbelt, J. S., Rodriguez, M., and Kerwin, S. (2004) Evaluation of complexes of DNA duplexes and novel benzoxazoles or benzimidazoles by electrospray ionization mass spectrometry, *J Am Soc Mass Spectrom* **15**, 1593-1603.
113. Chohan, Z. H., Supuran, C. T., and Scozzafava, A. (2004) Metalloantibiotics: synthesis and antibacterial activity of cobalt(II), copper(II), nickel(II) and zinc(II) complexes of kefzol, *J Enzyme Inhib Med Chem* **19**, 79-84.
114. Brewer, G. J. (2001) Copper control as an antiangiogenic anticancer therapy: lessons from treating Wilson's disease, *Exp Biol Med (Maywood)* **226**, 665-673.
115. Nitiss, J. L. (2002) A copper connection to the uptake of platinum anticancer drugs, *Proc Natl Acad Sci U S A* **99**, 13963-13965.
116. Rajendiran, V., Karthik, R., Palaniandavar, M., Stoeckli-Evans, H., Periasamy, V. S., Akbarsha, M. A., Srinag, B. S., and Krishnamurthy, H. (2007) Mixed-ligand copper(II)-phenolate complexes: effect of coligand on enhanced DNA and protein binding, DNA cleavage, and anticancer activity, *Inorg Chem* **46**, 8208-8221.
117. Sorenson, J. R., and Wangila, G. W. (2007) Co-treatment with copper compounds dramatically decreases toxicities observed with cisplatin cancer therapy and the anticancer efficacy of some copper chelates supports the conclusion that copper chelate therapy may be markedly more effective and less toxic than cisplatin therapy, *Curr Med Chem* **14**, 1499-1503.

118. Daniel, K. G., Gupta, P., Harbach, R. H., Guida, W. C., and Dou, Q. P. (2004) Organic copper complexes as a new class of proteasome inhibitors and apoptosis inducers in human cancer cells, *Biochem Pharmacol* 67, 1139-1151.
119. Pahl, P. M., Reese, S. M., and Horwitz, L. D. (2007) A lipid-soluble iron chelator alters cell cycle regulatory protein binding in breast cancer cells compared to normal breast cells, *J Exp Ther Oncol* 6, 193-200.
120. Atherton, S. J., and Beaumont, P. C. (1986) Quenching of the Fluorescence of DNA-Intercalated Ethidium Bromide by some Transition-Metal Ions, *J Phys Chem* 90, 2252-2259.
121. Nguyen, B., Tanious, F. A., and Wilson, W. D. (2007) Biosensor-surface plasmon resonance: quantitative analysis of small molecule-nucleic acid interactions, *Methods* 42, 150-161.
122. Ciolkowski, M. L., Fang, M. M., and Lund, M. E. (2000) A surface plasmon resonance method for detecting multiple modes of DNA-ligand interactions, *J Pharm Biomed Anal* 22, 1037-1045.
123. Tombelli, S., Minunni, M., and Mascini, M. (2002) A Surface Plasmon Resonance Biosensor for the Determination of the Affinity of Drugs for Nucleic Acids, *Anal Lett* 35, 599-613.
124. Gambari, R., Feriotto, G., Rutigliano, C., Bianchi, N., and Mischiati, C. (2000) Biospecific interaction analysis (BIA) of low-molecular weight DNA-binding drugs, *J Pharmacol Exp Ther* 294, 370-377.
125. Noble, C. G., Barnard, F. M., and Maxwell, A. (2003) Quinolone-DNA interaction: sequence-dependent binding to single-stranded DNA reflects the interaction within the gyrase-DNA complex, *Antimicrob Agents Chemother* 47, 854-862.
126. Cohen, J. J., Duke, R. C., Fadok, V. A., and Sellins, K. S. (1992) Apoptosis and programmed cell death in immunity, *Annu Rev Immunol* 10, 267-293.
127. Thompson, C. B. (1995) Apoptosis in the pathogenesis and treatment of disease, *Science* 267, 1456-1462.
128. Nicholson, D. W. (1996) ICE/CED3-like proteases as therapeutic targets for the control of inappropriate apoptosis, *Nat Biotechnol* 14, 297-301.
129. Chen, D., Peng, F., Cui, Q. C., Daniel, K. G., Orlu, S., Liu, J., and Dou, Q. P. (2005) Inhibition of prostate cancer cellular proteasome activity by a pyrrolidine dithiocarbamate-copper complex is associated with suppression of proliferation and induction of apoptosis, *Front Biosci* 10, 2932-2939.
130. Cai, X., Pan, N., and Zou, G. (2007) Copper-1,10-phenanthroline-induced apoptosis in liver carcinoma Bel-7402 cells associates with copper overload, reactive oxygen species production, glutathione depletion and oxidative DNA damage, *Biometals* 20, 1-11.
131. Cohen, G. M. (1997) Caspases: the executioners of apoptosis, *Biochem J* 326 (Pt 1), 1-16.

132. Lamkanfi, M., Festjens, N., Declercq, W., Vanden Berghe, T., and Vandenaabeele, P. (2007) Caspases in cell survival, proliferation and differentiation, *Cell Death Differ* 14, 44-55.
133. Kumar, S. (2007) Caspase function in programmed cell death, *Cell Death Differ* 14, 32-43.
134. Leone, N., Courbon, D., Ducimetiere, P., and Zureik, M. (2006) Zinc, copper, and magnesium and risks for all-cause, cancer, and cardiovascular mortality, *Epidemiology* 17, 308-314.
135. Ford, E. S. (2000) Serum copper concentration and coronary heart disease among US adults, *Am J Epidemiol* 151, 1182-1188.
136. Fiallo, M. M., Deydier, E., Bracci, M., Garnier-Suillerot, A., and Halvorsen, K. (2003) Mitomycin antitumor compounds. 2. Interaction of transition metal ions with mitomycin C. Solution structure and biological activity of a Pd(2+)-MMC complex, *J Med Chem* 46, 1683-1689.
137. Fiallo, M. M., Drechsel, H., Garnier-Suillerot, A., Matzanke, B. F., and Kozlowski, H. (1999) Solution structure of iron(III)-anthracycline complexes, *J Med Chem* 42, 2844-2851.
138. Malmqvist, M., and Granzow, R. (1994) Biomolecular Interaction Analysis, *Methods* 6, 95-98.
139. Myszka, D. G. (1999) Improving biosensor analysis, *J Mol Recognit* 12, 279-284.
140. O'Brien, J., Wilson, I., Orton, T., and Pognan, F. (2000) Investigation of the Alamar Blue (resazurin) fluorescent dye for the assessment of mammalian cell cytotoxicity, *Eur J Biochem* 267, 5421-5426.
141. Levin, J. I., Turos, E., and Weinreb, S. M. (1982) An alternative procedure for the aluminum-mediated conversion of esters to amides", *Syn Comm* 12, 989-993.

PART II: G-QUADRUPLEX SELECTIVITY OF PERYLENE DIIMIDE COMPOUNDS

CHAPTER 7. INTRODUCTION

7.1. DNA Structures

7.1.1. B-DNA and other Helical Structures

As discussed in chapter 1, the majority of genomic DNA exists as a double-stranded, antiparallel structure that is held together by a specific network of hydrogen bonds of its heterocyclic bases (Figure 7.1). The purine bases adenine and guanine are able to base-pair with the pyrimidine bases thymine and cytosine through two and three hydrogen bonds respectively giving rise to the classical “Watson-Crick” model of DNA. This arrangement leads to a structure that consists of a helix with a hydrophobic interior where the nucleic acid bases are stacked on top of each other and a hydrophilic exterior with the sugar phosphate backbone of the bases (1).

The most common conformation of DNA is the B form, which is right-handed helix with the bases oriented perpendicularly to the axis. It has approximately 10.5 base pairs for every turn of the helix, 20 Å in diameter and distinct major and minor grooves; the former is wide and deep while the latter is a narrow and deep (2, 3). Other helical forms of DNA such as A and Z DNA have also been observed in *in vitro* studies, and have been proposed to occur *in vivo* under certain circumstances such as in promoter regions or during transcription (4).

The A-form of DNA is broader (26 Å in diameter) and less twisted (11 base pairs/turn) compared to the B-form. Other differences include the position of the bases, which lay off the helix axis, as well as the size of the grooves, with a

narrow and deep major groove and a wide a shallow minor groove (5, 6). Z-DNA is left-handed and has zigzag pattern in the sugar-phosphate backbone. It has approximately 12 bases per turn, and 18 Å in diameter (5, 7). While it does not have pronounced major groove, it does have a deep and narrow minor groove. Its formation is favored by high salt concentrations and alternating GC sequences (8, 9).

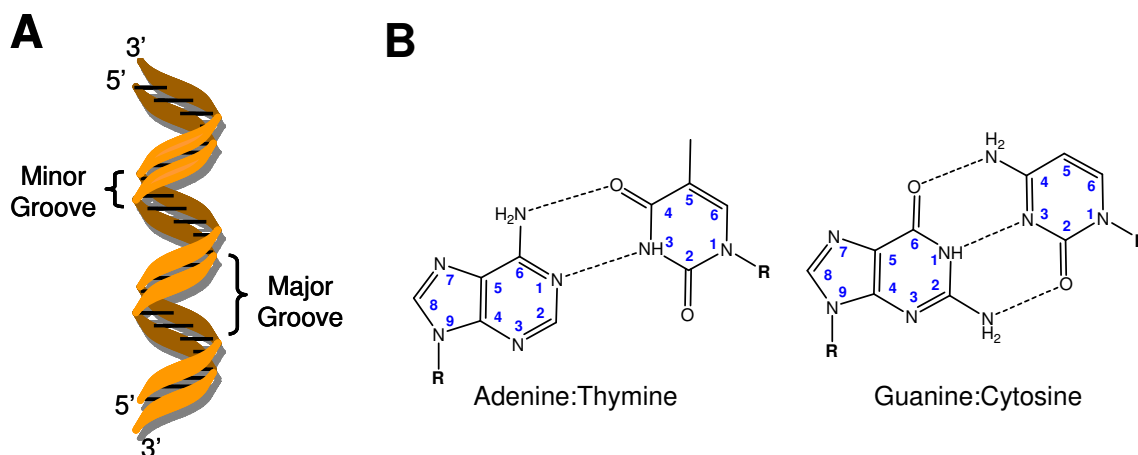


Figure 7.1. *Helical DNA structure and base-pairing.* (A) Schematic representation of the double Helix; the major and a minor groove are highlighted. (B) DNA base pairing; adenine forms two hydrogen bonds with thymine, and guanine forms three hydrogen bonds with cytosine

7.1.2. Alternative DNA Structures

In contrast to proteins that favor a particular structure based on its sequence, DNA molecules can be considered as an array of structural states. Over the past decades it has become evident that some of the structures that DNA can also adopt vary from the classical helical forms. Such structures include cruciforms, Holliday junctions, triplexes and quadruplexes. Initially studied as oddities, many of these structures are currently being studied for their possible biological roles within the cell and as potential targets for drug design (4, 10-12) .

7.1.2.1. Hairpin loops, Cruciforms and Holliday Junctions

Hairpin Loops (Figure 7.2A) can form when an oligonucleotide that contains a segment of inverted complementarity folds and base pairs with itself. Longer palindromic duplex DNA sequences have the potential to form similar structures with two stems and two hairpin loops (Figure 7.2B). These branched structures are called cruciforms and occur when intra-strand base pairs replace the inter-strand base pairs of the duplex within the inverted complementary sequences (13, 14). Negative DNA supercoiling under conditions of torsion stress can favor the formation of these structures. There is evidence they can form *in vivo* and may be involved in transcription and DNA replication (14-17).

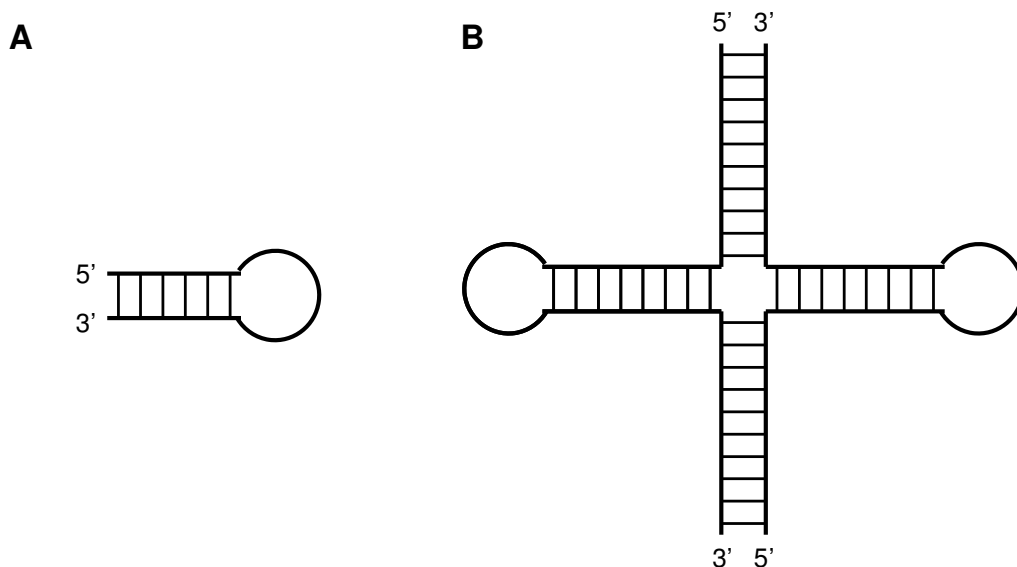


Figure 7.2. *Hairpin Loops and DNA cruciforms.* (A) Hairpin loop formed by an oligonucleotide with an inverted complementary sequence. (B) DNA cruciform from an inverted sequence repeat in double stranded DNA.

A structure related to the cruciform is the Holliday junction. These structures were originally proposed in the 60's by Robin Holliday, and consist of a

four-armed transitory structures formed by two DNA duplexes during homologous recombination (15, 16).

In this model, nicks are introduced at the same position in two DNA molecules which are located in different alleles. The single strands can then anneal to the complementary sequences in the other allele, as shown in Figure 7.3. The crossover of the strands forms the four-stranded Holliday Junction. The two DNA helices can then separate by breaks in the junction that result in heteroduplex DNA.

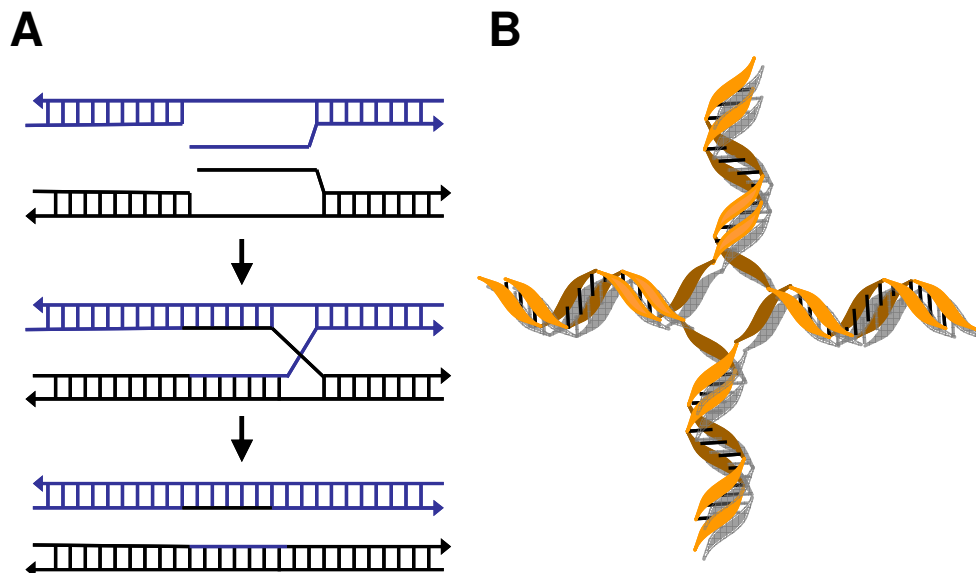


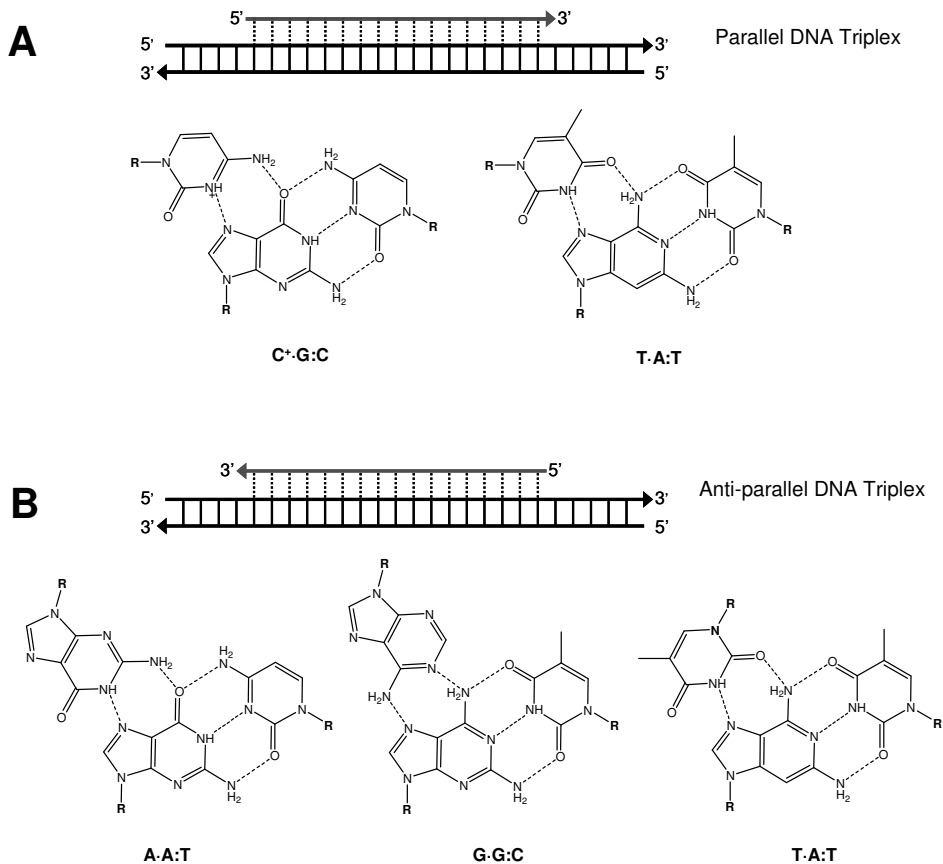
Figure 7.3. *Holliday Junctions.* (A) After DNA replication nicks are introduced on two homologous chromosomes. Strand exchange can occur giving rise to a Holliday junction which can result in crossover sequences. (B) Schematic model of an antiparallel open planar Holliday Junction.

7.1.2.2. Triplex DNA

Gel electrophoresis supercoiled DNAs carrying a homopurine-homopyrimidine inverted repeats revealed that an unusual structure formed. This structure was named “H-DNA” because it was stabilized in the presence of hydrogen ions. The main element of the H-DNA is an intramolecular triple helix

formed by the entire pyrimidine strand and half of the purine strand; the other half of the purine strand remains single stranded (17, 18). Later studies showed that H-DNA is abundant in eukaryotic genomes.

The triple helix is stabilized by base pairs that involve alternative donor and acceptor partners to the standard Watson-Crick base pairs called Hoogsten base pairs. In this manner, two nucleobases on each strand can be held together by hydrogen bonds in the major groove. A parallel triple helical DNA can result from the interaction of two homo-pyrimidine and one homo-purine strand Figure 7.4A. Protonated C can form hydrogen bonds to the N7 and O6 of G, and T can hydrogen bond with the N7 and the C6 amino group of A. Anti-parallel triplexes may also form through base pairing as in Figure 7.4B.



Triplex binders generally include extended planar aromatic rings that can allow stacking interactions with the base triplets. They also tend to have at least one cationic charge on the chromophore that can stabilize the larger negative charge density of the triplex. Some examples of common triplex-DNA selective binders include benzo[e]pyridoinole, BePI, and fused heterocycles such as Naphthylquinoline and Coralyne (Figure 7.5) (7).

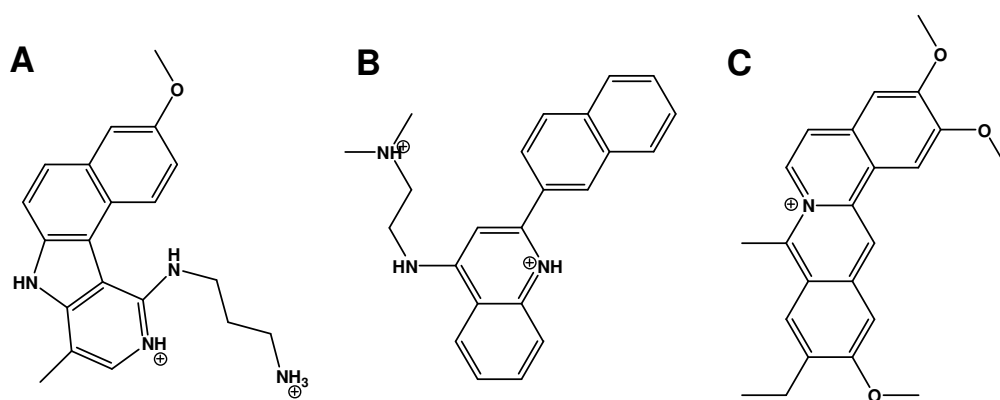


Figure 7.5. Examples of Triplex-DNA binding ligands. (A) BePI, benzo[e]pyridoinole. (B) Naphthylquinoline. (C) Coralyne

7.1.2.3. Four stranded structures: G-Quadruplex and i-motifs

Certain DNA sequences can form four stranded helices by the folding of a single strand or through the association of two, or four strands of DNA (19). In particular, sequences with consecutive runs of Gs are prone to higher ordered structures. As early as 1962 it was observed by fiber diffraction studies that guanylic acid could form a four-stranded helix (20). Other studies noted that G-rich sequences presented unusual gel electrophoresis mobility (21, 22). Sen and Gilbert also showed that the unusual mobility bands were protected from the

characteristic methylation at the N7 position of guanines by dimethyl sulfate, which suggested their involvement in Hoogsten base pairing (22).

In fact guanine nucleobases are capable of forming Hoogsten hydrogen-bonds through the N7 and N2 amino groups, and the N1 amino and O6 carbonyl forming structures called G-tetrads, as seen in Figure 7.6A; the result is an almost coplanar arrangement, with each guanine both accepting and donating two hydrogen bonds, and directing its O6 carbonyl group into the core of the tetrad (23). The cavity in the center of the tetrad allows for metal binding, which also stabilizes the arrangement. The specific hydrogen bond network in the G-tetrads causes the imino protons resonances in the ^1H NMR spectrum to shift and are characteristic of these structures (24, 25). When two or more tetrads are stacked on top of each other they can form structures known as G-Quadruplexes or DNA tetraplexes (Figure 7.6B).

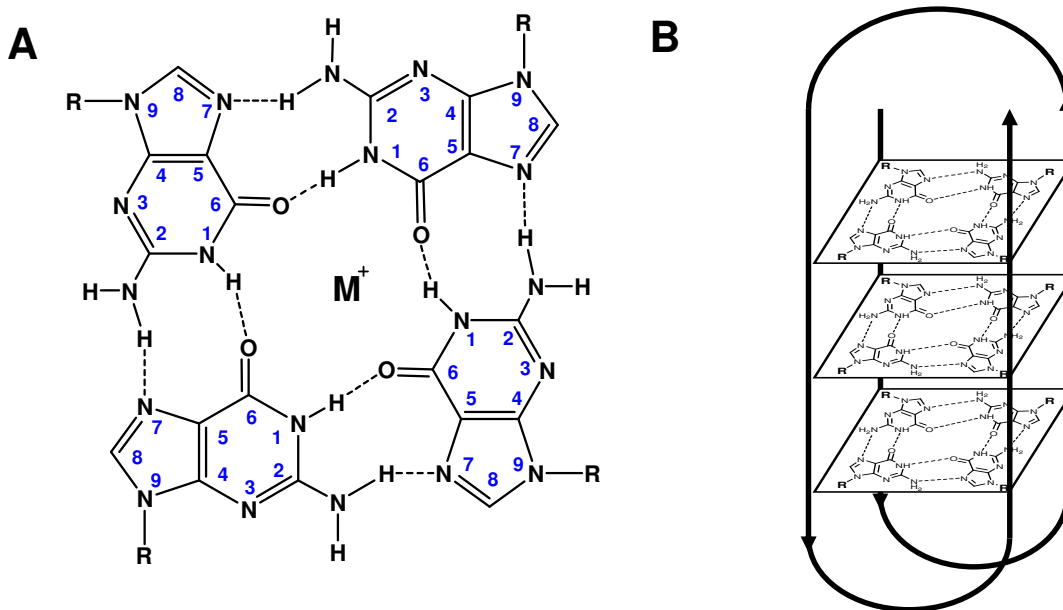


Figure 7.6. *G-tetrads and G-Quadruplexes.* (A) Guanine bases can hydrogen bond through Hoogsten-base pairs in a planar configuration to give rise to a G-tetrad. (B) Schematic of an intramolecular G-quadruplex structure

The quadruplexes can be formed with various strand stoichiometries. A G-rich single stranded sequence can fold on itself and give rise to an intramolecular quadruplex (Figure 7.7A). A sequence with two separate runs of Gs can also fold into a hairpin and associate with another hairpin to generate an intermolecular dimeric quadruplex (Figure 7.7B). Four separate strands can also combine and create a tetramolecular quadruplex (Figure 7.7C). In theory, quadruplexes could also be formed from the association of three strands, but this arrangement has yet to be observed. There is a wide array of nomenclature used throughout the literature to refer to these structures. For this work, conventional nomenclature will be employed; intramolecular quadruplexes will be referred to as G4'-DNA, while the dimeric quadruplexes will be described as G'2-DNA and tetrameric quadruplexes as G4-DNA (22, 26, 27).

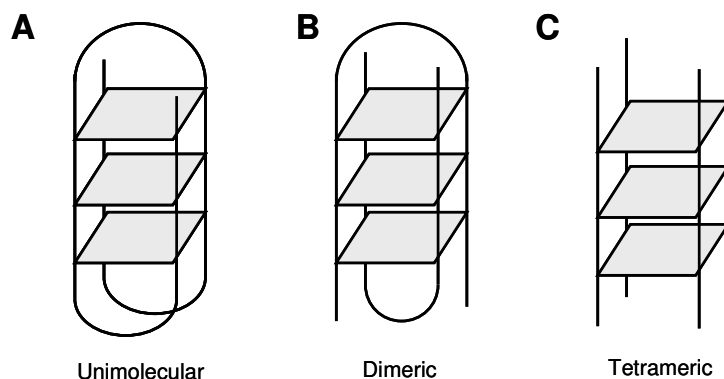


Figure 7.7. *Strand Stoichiometries in G-Quadruplexes.* (A) Unimolecular quadruplexes, or G4'-DNA, formed by the folding of a single strand. (B) Dimeric quadruplexes (G'2-DNA) formed from two strands. (C) Association of four strands generates tetrameric quadruplexes, (G4-DNA)

The four participating strands can have their phosphodiester backbones in a parallel, antiparallel, or mixed orientation regardless of the number of strands participating in the quadruplex (28). Figure 7.8A shows a schematic of all the strands arranged in a parallel configuration, while figures Figure 7.8B, Figure

7.8C, and Figure 7.8D present the possible arrangements when 1 or 2 strands are positioned in opposite directions.

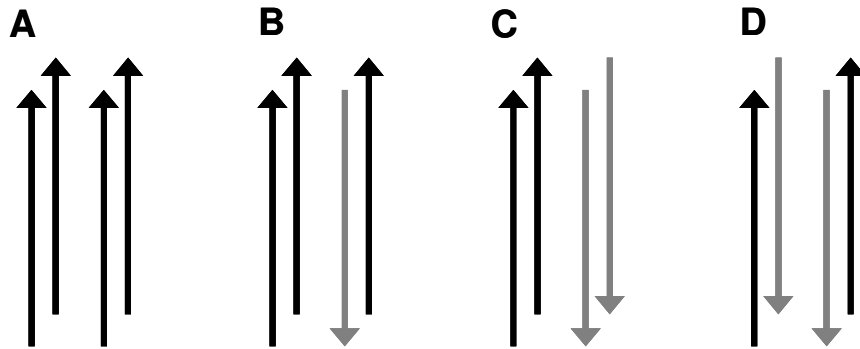


Figure 7.8. Possible strand orientations in G-Quadruplexes. (A). All strands parallel. (B). Three strands parallel and one strand antiparallel. (C) Two adjacent parallel and two adjacent antiparallel strands. (D). Alternating antiparallel stands

C-rich sequences are also able to form four-stranded structures, termed i-motifs. These structures were discovered in 1993 by Gehring and coworkers, revealing that two parallel duplexes of protonated cytosine–cytosine base pairs could intercalate with each other in an antiparallel orientation as seen in Figure 7.9 (29). One of the main differences between G-quadruplexes and i-motifs is that the first are stable at neutral pH, whereas the i-motifs require protonation of half the cytosine residues, and therefore are only stable under slightly acidic conditions (30, 31).

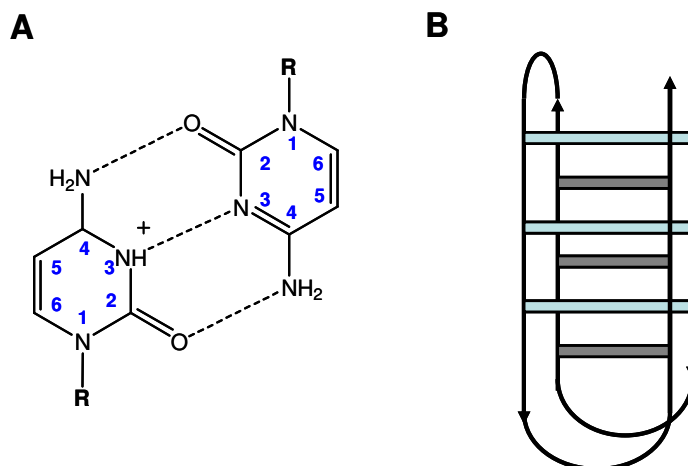


Figure 7.9. *The i-motif.* (A) The C-C⁺ base pair. (B) An intercalated intramolecular i-motif

7.2. G-Quadruplex DNA topology and polymorphism

G-rich sequences can assemble into an extensive number of quadruplex structures. The loops that connect the guanine tracts of G'2-DNA and G4'-DNA can be connected to the tetrads through various orientations (26, 28). Figure 7.10A presents some of the known conformations for G4' loop connectivity; strands can be connected in an adjacent-diagonal-adjacent (basket), adjacent-adjacent-adjacent (chair), diagonal-diagonal-diagonal (parallel), or a diagonal-adjacent-adjacent (dog-eared) fashion. Bimolecular quadruplexes have been proposed or shown to have loops that connect the tetrads diagonally or edge-wise, as shown in Figure 7.10B. Crossover G'2-DNA have loops that connect the opposite ends of the outer tetrads diagonally. Each strand in the edge quadruplex connects adjacent sides on opposing sides of the tetrad and can be in a parallel or in an alternating antiparallel (shown) configuration; the loops formed by the strands face opposite sides of the quadruplex. Syn-edge quadruplexes are similar to the edge, except the two strands face the same side of the quadruplex.

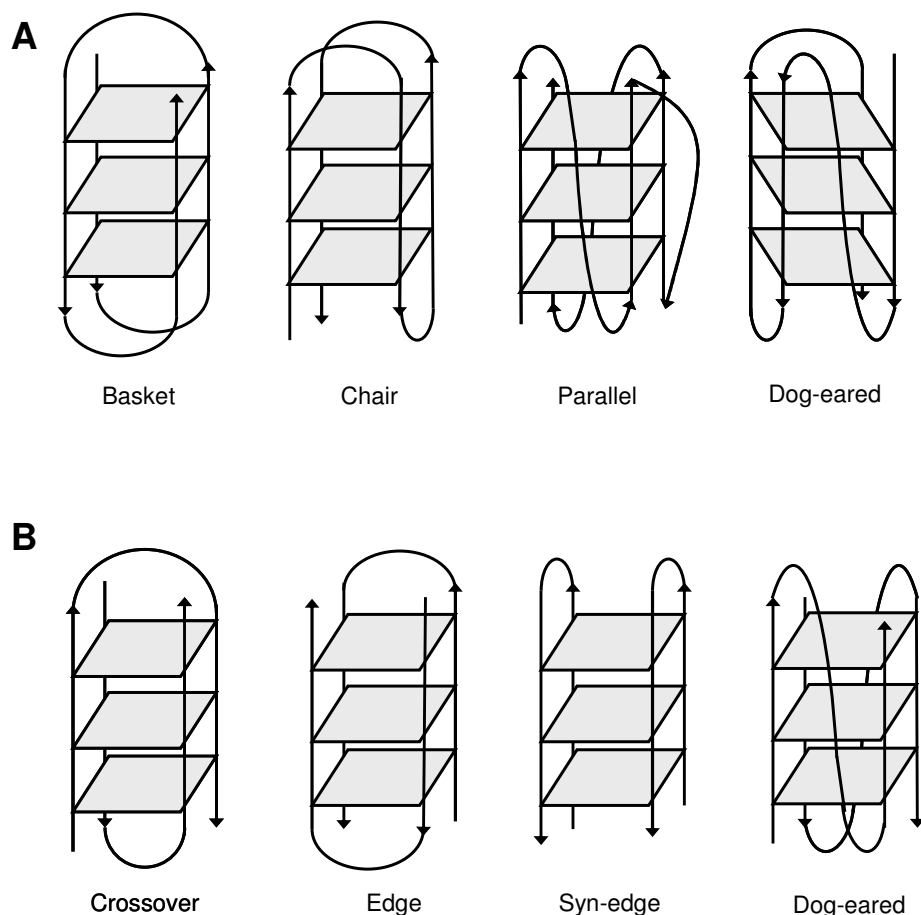


Figure 7.10. Topological forms of $G4'$ and $G2$ -DNA generated by alternatives in loop connectivity. (A) $G4'$ Intramolecular quadruplexes where the strands adopt a basket, chair, parallel, or dog-eared configuration. (D) $G2$ dimeric quadruplexes can adopt edge, crossover, syn-edge, or dog-eared type intermolecular quadruplexes.

Many sequences are capable of forming more than one quadruplex structure (32-35). For instance, different intramolecular structures were uncovered for the oligonucleotide $AG_3(T_2AG_3)_3$ via NMR and X-Ray crystallography. The NMR solution (in sodium ions) presented a basket-like intramolecular quadruplex, while the crystal structure (in potassium ions) displayed a parallel-type $G4'$ conformation (34, 36-38). Later studies showed that both structures can be present at the same time under near-physiological conditions and can interconvert on a minute time scale (32, 39). Still another

intramolecular quadruplex structure for this sequence was discovered recently, finding a dog-eared structure in potassium solution (40, 41). It is clear that there is a wide array of polymorphism on the structures that G-rich sequences can adopt, and future studies are likely to unravel novel quadruplex structures.

The stability of a particular structure depends on many factors, including the concentration, the number of strands, the number of tetrads, the sequence of the loops that connect the tetrads, and the solution conditions (19, 23, 42-49). The type and concentration of counterions is one of the most influential factors in the stabilization of a particular structure. The general stabilization of quadruplexes by counterions follows the order: $\text{Sr}^{2+} > \text{K}^+ > \text{Rb}^+ \sim \text{Ba}^{2+} > \text{NH}_4^+ > \text{Ca}^{2+} > \text{Na}^+ > \text{Mg}^{2+} \sim \text{Cs}^+ >> \text{Li}^+$ (23, 25). Cations of ionic radii close to 1.3 Å, such as potassium and strontium can fit well in the cavities formed between the planes of two tetrads, coordinate with the eight O6 carbonyls of the guanines, and stabilize the quadruplex structures thermodynamically and kinetically (24, 25, 38, 50-53). Cations can affect the polymorphism of quadruplex. For example, the formation of G4-DNA is favored under high K^+ ion concentrations, while lower K^+ or lower K^+/Na^+ ratios lead preferentially to G4' structures (25, 54-56). Cations can also affect the geometry of the loops in quadruplex structures and can favor the conversion from duplex DNA to quadruplex structures (53, 54, 57).

7.3. G-rich sequences and G-quadruplexes

7.3.1. Telomeric DNA

Telomeres are located at the end of eukaryotic chromosomes and contain non-coding tandem repeats of G-rich sequences. The human telomeric repeat is between 2 and 10 kb long, and consists of repeats of the sequence d(TTAGGG); other known telomeric sequences include those of *Tetrahymena* (protozoa) and *Oxytricha nova* (protozoa), d(TTTTGGGG), and *S. cerevisiae* (yeast), d(TG₁₋₃)

(49, 58). In humans, most of the telomeric repeats are contained within the duplex regions, but there is also a nucleotide single stranded overhang of approximately 200 nucleotides long at the 3' end of the telomeres (59, 60). Griffith and co-authors have observed the chromosome ends of HeLa nuclear extracts through electron micrographs (61). They noted that telomere overhangs are able to form loop-back structures (T-loops) that are incorporated into the double stranded telomeric region (D-loops); these structures are stabilized by the telomeric repeat-binding factors, TRF1 and TRF2, and could aid in preventing chromosome end-to-end fusions and degradation (61).

Telomeres shorten after every round of replication because of the end-replication problem (62, 63). DNA polymerases move in a 5' to 3' direction and can replicate DNA on the leading strand uninterrupted. In contrast, the lagging strand is oriented 3' to 5' can only be replicated in a discontinuous fashion, as described in Figure 7.11. Short RNA primers attach to the complementary strand close to the initiation site, allowing DNA polymerase to replicate the lagging strand in stretches called Okazaki fragments. DNA ligase then converts the RNA primers to their respective DNA sequences and seals the gaps in between the Okazaki fragments. DNA polymerase cannot add new nucleotides to the 5' end of the lagging strand because of the lack of a new RNA primer in 3' end of the complementary DNA sequence. This ultimately causes a section of the telomeres to be lost after every round of replication (64).

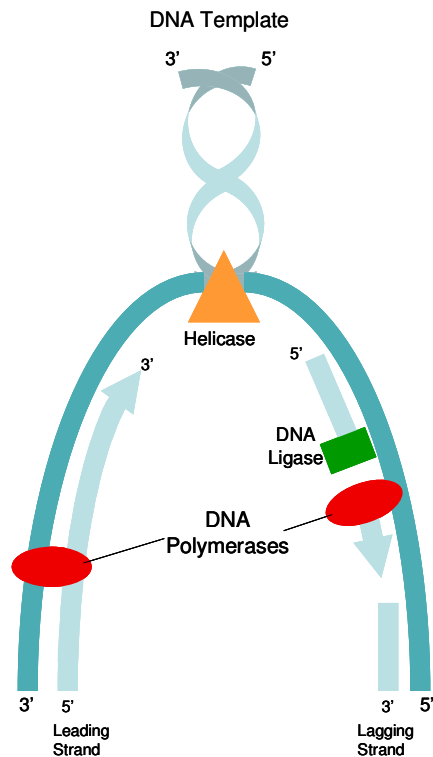


Figure 7.11. *The end replication problem.* DNA polymerase can replicate the leading strand uninterrupted, while the lagging strand gets replicated in short discontinuous fragments. The lagging strand gets shortened after every round of replication because DNA polymerase cannot add nucleotides to the last fragment at the 5' end

In humans, approximately 50-200 base pairs in the telomeres are lost after every replication cycle (65, 66). Because of their shortening, telomeres play an important role in the regulation of cellular longevity and apoptosis. Programmed cell death can be signaled when telomeric sequences are reduced to a particular length (58, 67, 68). Somatic cells have a finite number of cell divisions until they become senescent (69). However, certain types of cells such as stem, endometrial, skin or germ cells have high proliferation rates, and require longer life spans (70-72). These cells are able to overcome the replication problem by expressing a ribonucleoprotein with reverse transcriptase activity called telomerase (70, 72). This enzyme is able to bind to a region of DNA on the 3' end of the complementary strand and insert additional telomeric repeats (73, 74). An

RNA primer can then to bind to the end of the complementary strand and be extended through normal lagging strand synthesis.

Williamson and coworkers were able to see that the G-rich telomeric sequences could form quadruplexes *in vitro* (52). Since then, the formation of quadruplex structures from telomeric sequences *in vitro* has been well characterized by NMR, X-ray crystallography and FRET methods (24, 36, 38, 39, 50, 75, 76). While the biological role of quadruplexes at the telomeres has not been elucidated, several speculative roles for these structures have been proposed and are depicted in Figure 7.12 (77, 78). Intramolecular G-quadruplexes could form in the single-stranded overhang region to cap the telomeres and protect them from inappropriate recombination or nucleolytic attack as alternative or part of the T-loop structures (Figure 7.12 A and B) (78). In support of this idea, Tsai *et al.* have shown that the human telomeric 3' single-stranded overhangs sequence can protect the telomeres from being recognized as double strand breaks when G-quadruplex structures are present (79). G4' quadruplexes could also facilitate packing of the telomeres by condensing the single strand overhang (Figure 7.12C) (77). Dimeric quadruplexes could also assist in telomere alignment and capping through interchromosomal associations, and tetrameric structures could appear during meiosis (Figure 7.12 D and E respectively) (22, 80).

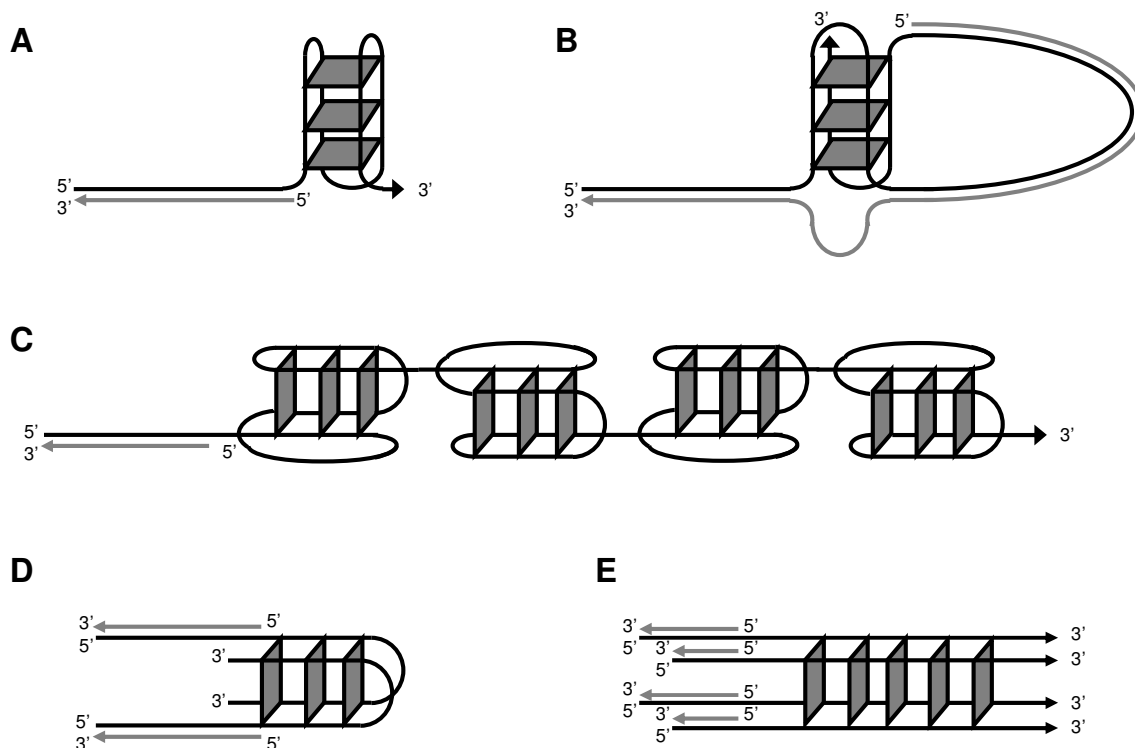


Figure 7.12. Putative roles of G-Quadruplexes in the telomeres. (A) Intramolecular G-quadruplex formed from the single-stranded overhang in the telomeres could help telomere capping. (B) Quadruplex could form part of the T-loop structure. (C) G-Quadruplex structures may facilitate packing of telomeric DNA. (D) Dimeric quadruplexes could form during interchromosomal associations and serve as protective caps (D) Tetrameric quadruplex could be involved in chromosome alignment

The formation of quadruplex structures in the telomeres has been correlated with decreased telomerase activity. (81). Studies have also shown that telomerase is active in over 85% of all cancers promoting their immortalization (82, 83). Thus, telomerase inhibition is an active target of anticancer drug design. Ligands that can stabilize telomeric quadruplex structures can serve as potential telomerase inhibitors and are currently being studied by numerous groups. Further discussion of G-quadruplex as a target for drug design will be covered later in this chapter.

7.3.2. Other regions in the Genome

Telomeric DNA is not the only G-rich sequence capable of forming quadruplex structures. In fact, there has been considerable interest in locating putative quadruplex sequences in non-telomeric genomic DNA. Part of the interest was heightened by the discovery that *c-myc*, which is one of the most commonly malfunctioning genes in human cancer, could form a biologically relevant quadruplex in a nuclease hypersensitive region upstream of the promoter known to control its activity (84, 85). Furthermore, it was established that *c-myc* transcription could be regulated by G-quadruplex stabilization through ligand binding (84, 86). Since then, it has been discovered that G-quadruplex forming sequences are present in the promoter regions of other proto-oncogenes such as RET, c-kit, bcl-2, VEGF, K-ras, N-ras, and RFP2 (87-97). These studies have set forward the idea that quadruplex motifs could be directly involved in gene regulation, either by suppressing or modifying their transcription when quadruplex sequences are formed (Figure 7.13). Furthermore, studies have demonstrated that the levels of certain ions such as potassium and sodium can affect gene expression and apoptosis, and are altered in certain tumor cells. The modified ratios of these cations in cancer cells could result in conformational changes in quadruplex structures and potentially in altered telomere function or gene transcription (98-101).

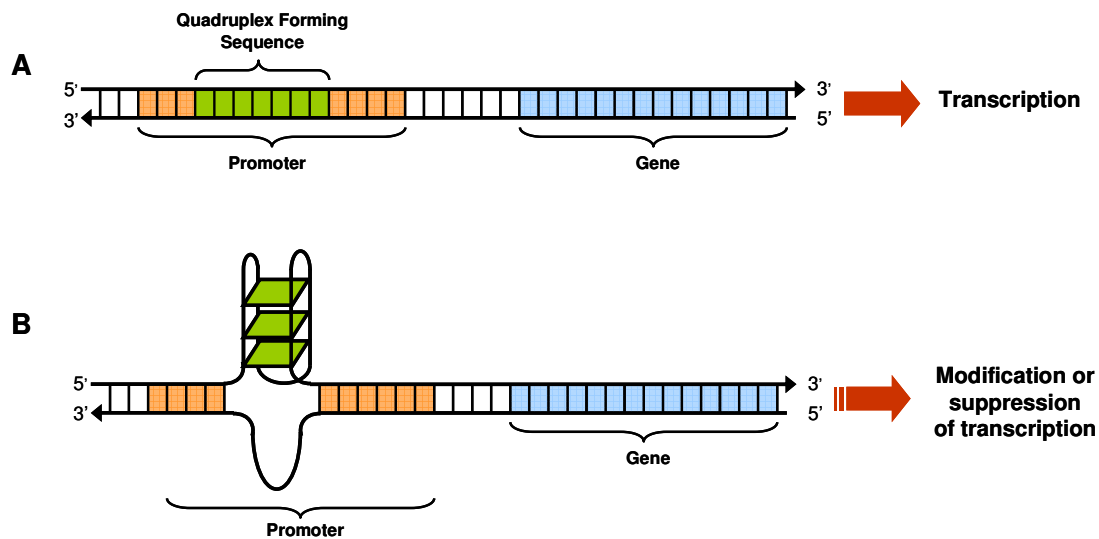


Figure 7.13. Transcriptional regulation by quadruplex forming sequences in promoter regions. A. When quadruplex forming sequences are in a double stranded conformation, regular transcription occurs. B. Quadruplex formation can suppress or alter the transcription of a gene

Recently several computational and web server tools have been created to predict quadruplex forming structures within genomic sequences (102-106). The putative quadruplex sequences, or PQS, are defined as four equal length sets of guanines separated by arbitrary nucleotide sequences forming at least three tetrads (in some programs the user can include searches with only two tetrads and modify the length of the loops); sequences that follow the folding pattern $d(G_{3+}N_{1-7}G_{3+}N_{1-7}G_{3+}N_{1-7}G_{3+})$, where N is any base, are tagged as having the potential to form quadruplex structures. Using this algorithm over 370,000 PQS have been identified in the human genome (105, 106).

Several noteworthy observations were made in these studies regarding the location and frequency of the PQS. Huppert and Balasubramanian noticed that promoter regions of genes are significantly enriched in quadruplex motifs relative to the rest of the genome, finding that over 40% of human gene promoters have at least one PQS (103). Elevated tendency to form quadruplex motifs in promoter regions was uncovered in proto-oncogenes, as well as in genes with transcription factor activity, development, neurogenesis and kinase

activity, while those less likely to have promoter PQS included olfaction, G-protein signaling, immune response, nucleic acid binding and protein biosynthesis (103). Another important discovery is PQS are over 200-fold more likely to be found in regions of the genome that have both nuclease hypersensitivity and are found within promoter regions, compared to the rest of the genome. Regions that have sensitivity to nucleases (such as DNase I) in regulatory sequences like promoters and enhancers occurs when relevant elements are active; the sensitivity is thought to be due to a perturbation in the nucleosome that renders the adjacent sequences available for nuclease attack, such as by interaction with specific DNA binding proteins or because of altered DNA structures (107). All these observations substantiate a possible role of G-quadruplexes in the regulation of gene expression.

7.3.3. Evidence of G-Quadruplex formation *in vivo*

Many G-rich sequences have the ability to form quadruplex structures and have been structurally characterized *in vitro* by NMR or X-ray crystallography as discussed in section 7.2. On the other hand, the existence of G-quadruplexes in intracellular environments is still controversial (108). However, there is some recent compelling evidence that quadruplex structures can form *in vivo* (77). Some of the initial proof came from Schaffitzel and coworkers, who generated high-affinity antibodies specific for the guanine-quadruplex formed by the *Stylonychia lemnae* (ciliate) telomeric repeat; they were able to observe macronuclei staining by immunofluorescence using these antibodies (109). Staining was not detected in the replication band, which suggested that the quadruplex structures detected by the antibodies are resolved during DNA replication. Other groups are currently working on antibodies that target other quadruplex forming sequences (110, 111).

Further evidence for the existence of DNA *in vivo* comes from the expanding list of viral and cellular proteins that can recognize and interact with quadruplex DNA (77, 112). For instance, studies have demonstrated that helicases in the RecQ family, such as RecQ, Sgs1p, BLM, and WRN exhibit G-quadruplex unwinding capability (113-116). Non-RecQ helicases such as SV40 large T-antigen have been investigated by the Kerwin group and others, and can also unwind G-quadruplex structures, even with a greater affinity than double stranded DNA (117-119). Furthermore, known G-quadruplex interactive agents can in some cases inhibit the unwinding capability of these helicases (117, 120-124). It has been suggested that G-quadruplex unwinding of these helicases could be necessary during DNA replication and recombination, validating a biological existence of quadruplex structures (116).

Other quadruplex interacting proteins can bind selectively and tightly to tetraplex DNA, and in some cases also promote their formation (77). A recent study investigated the telomeric binding proteins α TBP and β TBP and demonstrated using RNA_i that both proteins regulate G-quadruplex formation *in vivo* (80). In addition, their data also indicated that β TBP is under the control of a cell-cycle phosphorylation event, possibly allowing for resolution of the quadruplexes during telomere synthesis. Additional quadruplex binding proteins include the repressor-activator protein 1 (Rap1), the G-Binding proteins TGP1 and TGP3, the mammalian nucleolar protein Nucleolin, the Human Topoisomerase I enzyme (Topo I), the human replication protein (RPA), and the meiotic synaptonemal complex in yeast Hop1 (125-131). Nucleases that can cleave G-quadruplexes have also been found; for example, the KEM1 gene in *S. cerevisiae*, and GQN1 in humans; both cleave single stranded DNA when it is 5' of a quadruplex structure, and release intact quartets after the cleavage (132, 133). The wide range proteins that can recognize and interact with G-quadruplexes discovered thus far corroborates the idea that quadruplex are biologically relevant species.

Some of the most convincing proof of the existence of G-quadruplex DNA in cells comes from a study by Duquette and co-authors (134). They inserted a plasmid with the TTAGGG human telomeric repeat in *E. coli* cells and monitored their intracellular transcription using electron microscopy. They were able to visualize novel structures termed “G-loops” in the non-template G-rich strand, and a RNA-DNA hybrid in the C-rich strand. The authors also corroborated that the G-loops contained quadruplex DNA by examining their interaction with proteins with high affinity towards quadruplex structures, such as GQN1 and Nucleolin, and through DMS footprinting. The formation of quadruplex DNA only occurred during the transitory denaturation of double stranded DNA that arises during the transcription of the G-rich region in their substrates. This suggests that quadruplex formation could occur in G-rich sequences during other events where there is a momentary denaturation of double stranded DNA, such as recombination or replication.

7.4. G-Quadruplex as a good biological target

As discussed earlier, telomerase is a ribonucleoprotein enzyme that elongates the G-rich strand of telomeres by reverse transcription. The majority of normal somatic cells has very low levels of this enzyme and ceases to proliferate after their telomeres reach a critically short length. In contrast, over 85% of cancer cells express high levels of this enzyme (82, 83). Telomerase expression *per se* does not cause tumorigenesis, but expression of the enzyme in cancerous cells can unintentionally assist them in immortalization by allowing a selective advantage to growth arrest and senescence (135-137). Inhibition of telomerase therefore presents an attractive target for drug design. One strategy to design inhibitors of this enzyme is to target its DNA substrate, in particular the quadruplex structures that telomeric sequences can form. In fact, Zahler and co-authors showed that stabilization of telomeric DNA into quadruplex structures

inhibited telomere elongation by telomerase (81). One way to stabilize quadruplex structures is through the interaction with ligands; not surprisingly, many small molecules that can bind to quadruplexes are being designed and researched by many laboratories.

As reviewed earlier, quadruplexes are not only found at the telomeres but are also located throughout the genome, in particular in the promoter regions of many oncogenes (section 7.3.2). It has been postulated that quadruplex stabilization could be involved in the transcriptional regulation of these genes (84, 103, 138). Consequently, targeting G-quadruplex structures in promoters of oncogenes has also become an emerging field in anticancer drug design (84, 91). Moreover, because of the apparent ubiquitous nature of quadruplexes in the genome, much research is needed to understand their biological significance and the factors that influence their formation. G-quadruplex interactive molecules may not only be used as anticancer treatment agents but can also be used as biophysical probes to investigate the biological role of quadruplexes in cells.

7.5. G-Quadruplex interactive ligands

Over the past years several worthy review papers have been published about G-quadruplex interacting ligands. (26, 78, 139-142). Because of the planar structure of the G-tetrads (section 7.1.2.3), compounds that can bind to quadruplex structures are generally polycyclic aromatic ligands substituted at multiple positions. Some of the most widely studied compounds will be described below and are depicted in Figure 7.14.

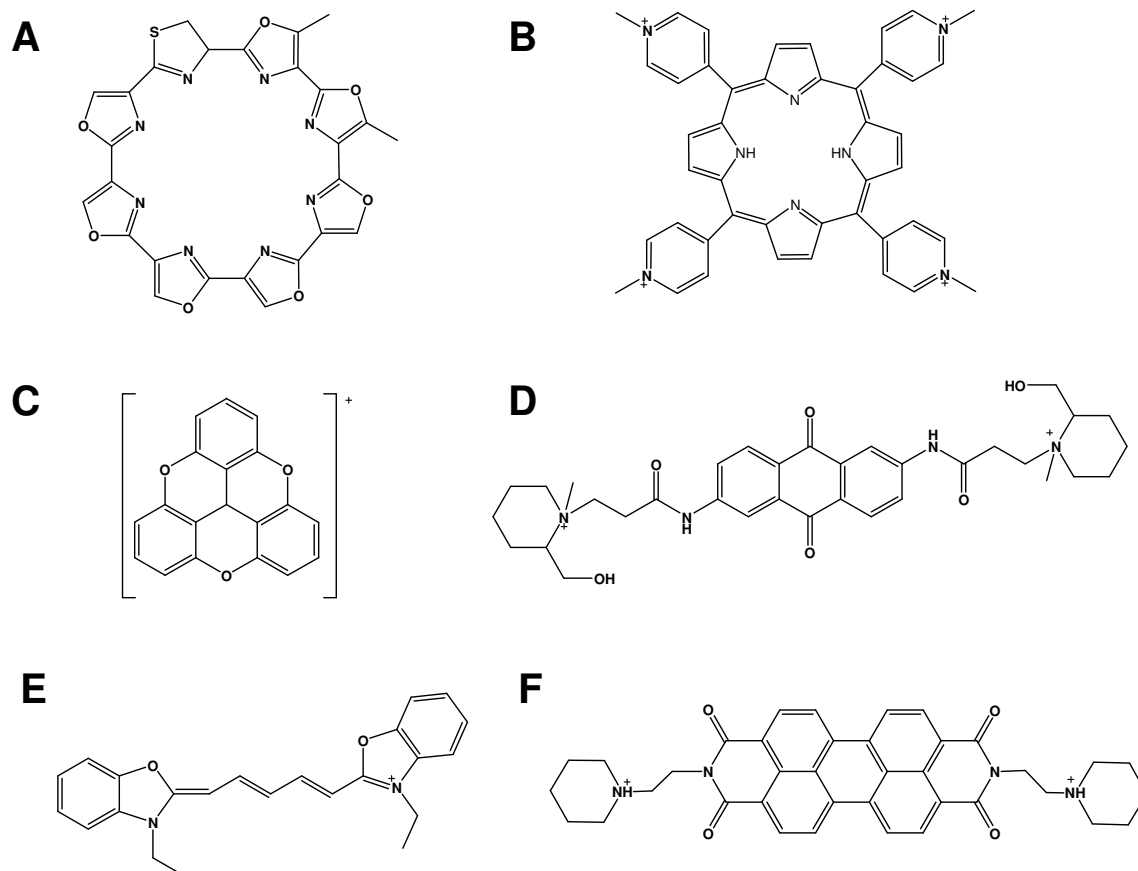


Figure 7.14. Examples of G-Quadruplex interactive compounds. (A) Telomestatin. (B) [tetra-(N-methyl-4-pyridyl)-porphine] (TMPyP4). (C) 4,8,12-Trioxa-4,8,12,12c-tetrahydrodibenzo[cd,mn]pyrenylium carbocation tetrafluoroborate (TOTA⁺). (D) 2,6-diamidoanthraquinone. (E) 3,3'-diethyloxycarbocyanine (DODC). (F) N,N'-bis[2-(1-piperidino)-ethyl]-(3,4,9,10-perylenetetracarboxylic acid diimides) (PIPER)

7.5.1. Telomestatin

Telomestatin (Figure 7.14A) is a natural product isolated from *Streptomyces anulatus* 3533-SV4 that is a very potent telomerase inhibitor (143). This compound also displays over 70 fold selectivity for quadruplex structures in comparison to duplex or single-stranded DNA (144-146). Cell assays have shown that treatment with Telomestatin is concomitant with quadruplex formation at the telomeric overhangs; the size of the overhangs is reduced in long term

treatments, leading to delayed loss of cell viability (147). Telomestatin appears to cause telomere dysfunction in various tumor cell lines and to selectively target cancer over normal cells (148, 149).

7.5.2. Porphyrins

Porphyrins have been extensively studied as anticancer drugs mainly because they appear to accumulate preferentially in tumor tissues compared to normal ones (150). Perhaps the most widely studied G-quadruplex binding porphyrin is the compound [tetra-(N-methyl-4-pyridyl)-porphine], or TmPyP4 (Figure 7.14B). Various groups have shown that this molecule is able to bind and stabilize G4, G4' and G'2 quadruplex structures (146, 151, 152). TmPyP4 is also able to inhibit the activity of the enzyme telomerase, suppress c-MYC transcriptional activation, reduce the activity of the mouse KRAS promoter, and inhibit the G-quadruplex unwinding activity of several RecQ helicases (84, 91, 120, 122-124).

There is some controversy concerning the binding mode of porphyrins to quadruplex structures. Some research suggests that porphyrin molecules stack externally to the outer tetrads of the quadruplexes, while other studies suggest they can also intercalate in between the tetrads (153, 154). It has also been recently proposed that some porphyrins can bind to the loops of quadruplexes through external groove binding (155). Structure–activity relationship studies of hundreds of porphyrins showed that charge number, hydrogen-bonds, and side-chain length are crucial to their interaction with G-quadruplexes (156-158). Selectivity for quadruplexes over double or single-stranded DNA is also dependent on the porphyrin structure; TmPyP4 is not particularly selective as it can also bind to duplex and single-stranded DNA (159-164). On the other hand, the anionic porphyrin N-methyl mesoporphyrin, or NMM, is highly specific for quadruplex structures (161, 162, 165).

7.5.3. TOTA⁺

The trioxatriangulenium ion (TOTA⁺, Figure 7.14C) is a stable cation that can bind and photooxidize duplex DNA, leading to cleavage chiefly at G residues (166, 167). X-ray crystallography diffraction of TOTA⁺ in the presence of a duplex oligonucleotide showed that it behaved as an intercalator and that it strongly polarized the binding site (167).

Prior work investigated the interactions of this cation with duplex and quadruplex oligonucleotides through gel electrophoresis, ESI mass spectrometry and NMR spectroscopy (168). At lower concentrations this compound appears to interact with quadruplex structures by end-stacking at the outer tetrads, but presents additional binding modes at higher ratios. Oligonucleotides containing either the human telomeric repeats or the Tetrahymena telomeric repeats are readily photooxidized by TOTA⁺ on the central guanine residues in each telomeric repeat when they are in a duplex form. However, there was significantly less photocleavage of these residues when the sequences formed quadruplex structures.

7.5.4. Disubstituted Anthraquinone Derivatives

Anthraquinone derivatives were originally studied as double stranded DNA intercalative agents. Fox *et al.* noted that various 1,4- and 2,6- substituted diamidoanthraquinones could selectively bind to triplex DNA structures compared to double stranded DNA (169). This led the authors to speculate about their possible interaction with G-quadruplex DNA. Computer modeling predicted that these compounds could be potential G-quadruplex interactive agents. Indeed, NMR and UV-Vis spectroscopy studies showed that 2,6-diamidoanthraquinone (Figure 7.14D) could bind and stabilize quadruplex structures. Since then, this compound and several other anthraquinone

derivatives have proven to be effective telomerase inhibitors (170, 171). The anthraquinone system has also been replaced with an acridine core, generating higher quadruplex specific ligands with lower dissociation rates (172, 173).

7.5.5. Carbocyanine dyes

Using DOCK computer modeling to predict compounds that could have preferential interactions with the grooves of G'-DNA compared to the minor groove of duplex DNA, Chen and co-authors identified the carbocyanine dye N,N'-diethyloxatricarbocyanine (DOTC) as a potential G'-DNA selective ligand (174). However, this compound has poor aqueous solubility so the more soluble analog, N,N'-diethyloxadicarbocyanine (DODC, Figure 7.14E) was used in *in vitro* studies (175). This compound exhibited unique spectroscopic changes in the presence of dimeric G-quadruplex structures, but not in the presence of single-stranded, duplex or parallel G-quadruplex DNA. However, there is also evidence that DODC can bind to triplex DNA structures with a higher affinity than quadruplex structures (176). Since then, Kerwin *et al.* have identified other carbocyanine dyes such as DTC (N,N'-diethylthiacarbocyanine iodide) which can bind to G4'-DNA (177). This family of compounds presents an alternative approach to study quadruplex structures, because unlike the majority of quadruplex ligands they appear to interact with the grooves of the quadruplexes rather than with the end tetrads (173).

7.5.6. Perylene Diimides

Previous studies identified through DOCK computer modeling that the 3,4,9,10-perylenetetra-carboxylic acid diimides (PTCDIs), with their planar, heterocyclic aromatic core could be potential G-quadruplex interactive molecular scaffolds. The compound N,N'-bis[2-(1-piperidino)-ethyl]-(3,4,9,10-perylene

tetracarboxylic acid diimide) (Figure 7.14F) was designed and synthesized by Fedoroff *et al.* to investigate its interactions with quadruplex structures (178). NMR spectroscopy revealed that this ligand could be sandwiched in between the terminal planes of two quadruplexes in a 2:1 tail-to-tail complex with a 5'-TTAGGG sequence. It could also end stack to form 1:1 complexes with longer telomeric sequences, such as TTAGGGTT, TTAGGGTTA, and TAGGGTTA.

PIPER displayed polymerase and telomerase inhibition the *in vitro* telomerase stop assay. It was also observed that this compound could significantly aid in the formation of quadruplex structures; the initial rate of formation of G₂ DNA was increased approximately 100 fold in the presence of 10 mM PIPER (179). PIPER also facilitates the formation of G-quadruplex DNA from the G-rich duplex DNA sequence found in the nuclease hypersensitive site that controls the c-myc proto-oncogene (86).

The interactions between PIPER and quadruplex structures have served as the impetus to research other analogs of this compound. Because the majority of quadruplex DNA binders can also interact with other nucleic acid structures, it is important to investigate the factors that determine selectivity. This body of work seeks to accomplish two major goals: 1) To investigate the structural elements in the perylene diimide core that are important for G-quadruplex binding and 2) To examine the factors that influence the selectivity of perylene diimides for G-quadruplex over double or single stranded DNA.

CHAPTER 8. PERYLENE DIIMIDES LIGAND AGGREGATION AND G-QUADRUPLEX DNA SELECTIVITY UNDER LOW SALT CONDITIONS

8.1. Properties of Perylene Diimides

As mentioned in section 7.5.6, computer modeling identified the 3,4,9,10-perylenetetracarboxylic acid diimides (PTCDIs) as potential G-quadruplex interactive moieties. NMR studies of a representative member of this family, the compound N,N'-bis(2-(1-piperidino)ethyl)-3,4,9,10-perylene tetracarboxylic acid diimide (PIPER) confirmed that the ligand could interact with the 3' or 5' end G-tetrad faces of various quadruplexes (178). A schematic representation of PIPER end-stacking to a tetrad is shown in Figure 8.1. Federoff *et al.* suggested that this binding mode would be preferred over conventional intercalation due to the high energy cost of disrupting the stable tetrad planes within the quadruplex structure (178). Since then it has been observed that a vast number of quadruplex-ligand interactions occur through this binding mode.

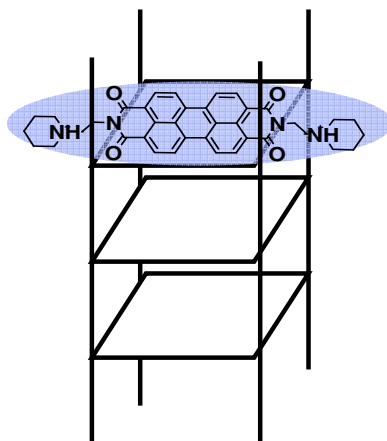


Figure 8.1. *End-stacking ligand interactions.* Schematic of PIPER forming end-stacking interactions with G4 DNA.

Structure-activity relationship studies carried out by Kerwin and co-workers investigated the effects of pH on G-quadruplex DNA binding by PIPER and N,N'-bis-(3-(4-morpholino)-propyl)-3,4,9,10-perylenetetracarboxylic acid diimide (Tel01, Figure 8.2) (180). The authors noted a high dependency on pH with respect to G-quadruplex binding selectivity: Tel01 was more selective than PIPER at pH values close to 7, but at higher pHs both compounds behaved similarly. Additionally, Kern *et al.* compared the NMR spectra of PIPER and Tel01 bound to quadruplex DNA and found no structural basis for differential G-quadruplex selectivity between the two, finding instead that the aggregation state of these molecules was a primary determinant of their G-quadruplex selectivity (181). The ligands formed aggregates under pH conditions where they displayed preferential G-quadruplex binding over duplex sequences, whereas in non-aggregating conditions the binding affinities for both DNA species were similar (180, 181). The pK_a s of the side chains play an important role in the pH at which the compounds begin to aggregate; PIPER with its more basic piperidino groups aggregates at pH values higher than 7, while Tel01 with the morpholino substituents starts forming aggregates at pH 7 (Figure 8.2). In addition to G-quadruplex selectivity, conditions that favored ligand aggregation also promoted ligand mediated G-quadruplex formation from double-stranded DNA (181).

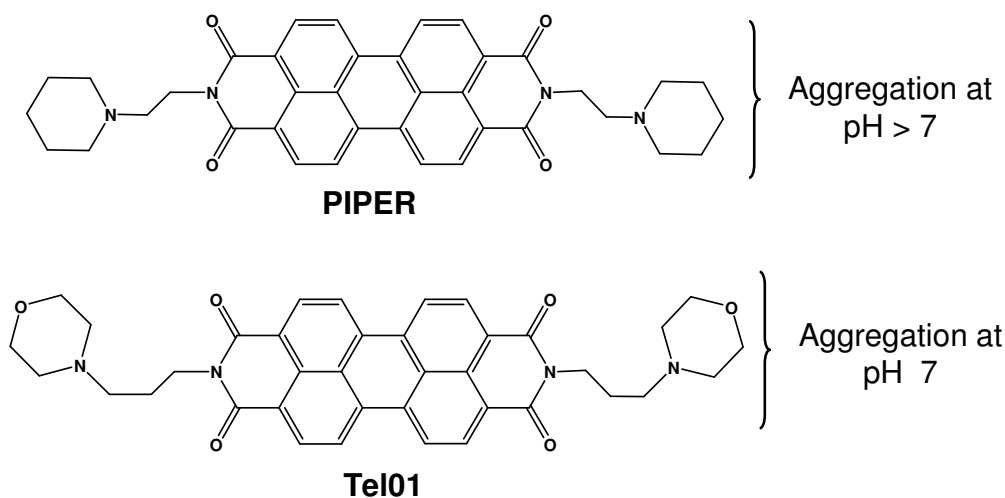


Figure 8.2. Structures of PIPER and Tel01 and their pH-dependant aggregation. PIPER has more basic side chains than Tel01 and aggregates and forms aggregates at higher pH values.

Since the original studies with PIPER and Tel01, other research groups have recently synthesized perylene diimides with modifications in the perylene aromatic core, bay-area or side chains (Figure 8.3) and found similar results. For instance, Rossetti and co workers studied PTCDis with different side chains and noticed that G-quadruplex formation appeared to be related to drugs' self-association, which in turn was influenced by the side chains' basicity (182, 183). Tuntiwechapikul *et al.* reached similar conclusions by studying PTCDis with positively, negatively or neutral side chains whose charge and self-association was as influenced by pH, determining the type of G-quadruplex that could be formed as well as binding selectivity (159). Tri-, tetra- and heptacyclic perylene analogs prepared by Sissi and co-authors also displayed quadruplex selectivity in relationship to their degree of self-aggregation (184).

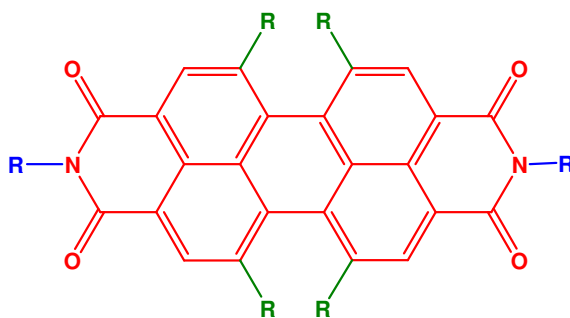


Figure 8.3. *Modifications in the PTCDI structure.* Modifications to the perylene structure include changes in the number of aromatic rings of the core (red), modifications of the side chains (blue) or modifications to the bay-area (green).

Ligand aggregation has generally been regarded as problematic in medicinal chemistry since the discovery by Shoichet and co-workers that aggregating molecules could lead to non-specific inhibition of a wide range of enzymes (185). However, this is not necessarily the case for G-quadruplex interactive molecules. There is evidence that PTCDIs under aggregating conditions can selectively inhibit the SV-40 Large T-antigen helicase unwinding of quadruplex sequences and not double stranded-DNA (117). If these molecules were inhibiting the enzyme through non-specific aggregation interactions they would be equally effective in preventing the unwinding of both substrates. Therefore, it is likely that the observed discriminating enzymatic inhibition is due to the selective G-quadruplex binding of aggregating PTCDIs.

Likewise, Sissi *et al.* also observed selective inhibition of the enzyme telomerase compared to other polymerases by perylene derivatives that paralleled their extent of self-aggregation (184). However, the increase in selectivity *via* aggregation was accompanied by an overall decrease in telomerase inhibition and interactions with G-quadruplex structures. This suggested that ligand aggregation could increase G-quadruplex selectivity by reducing the affinity towards other nucleic acid conformations and not necessarily by enhancing affinity towards G-quadruplexes.

Because of their planar, heterocyclic aromatic nature, PTCDIs can easily self-assemble through stacking interactions. It is not currently known how their aggregates interact with DNA; aggregate formation could occur upon DNA binding, or aggregates in solution could be capable of binding to DNA. There is clearly much needed research in this field to understand the mechanism of action and selectivity of these compounds. In any case, the findings so far point out the importance of monitoring self-assembly of G-quadruplex ligands as a means to control their affinity for quadruplex-forming sequences. It is important to understand the structural features and factors that regulate their aggregation to design selective and efficient G-quadruplex interactive agents. The following work investigates structural and physical properties that affect PTCDI aggregation and G-Quadruplex selectivity as an extension of the work performed by Jonathan Kern (*186*).

8.2. Modified Perylene Diimide Analogs

Analogs were previously synthesized by Jonathan Kern that contain representative structural modifications of the PTCDI core (*186, 187*). The charged perylenes Tel11 and Tel12 bear cationic and anionic sidearms respectively (Figure 8.4A and B); Tel18 is an analog of Tel01 with chlorine substituents in the bay-area (Figure 8.4C); Tel32 and Tel34 have an extended benzannulated aromatic core (Figure 8.4D and E).

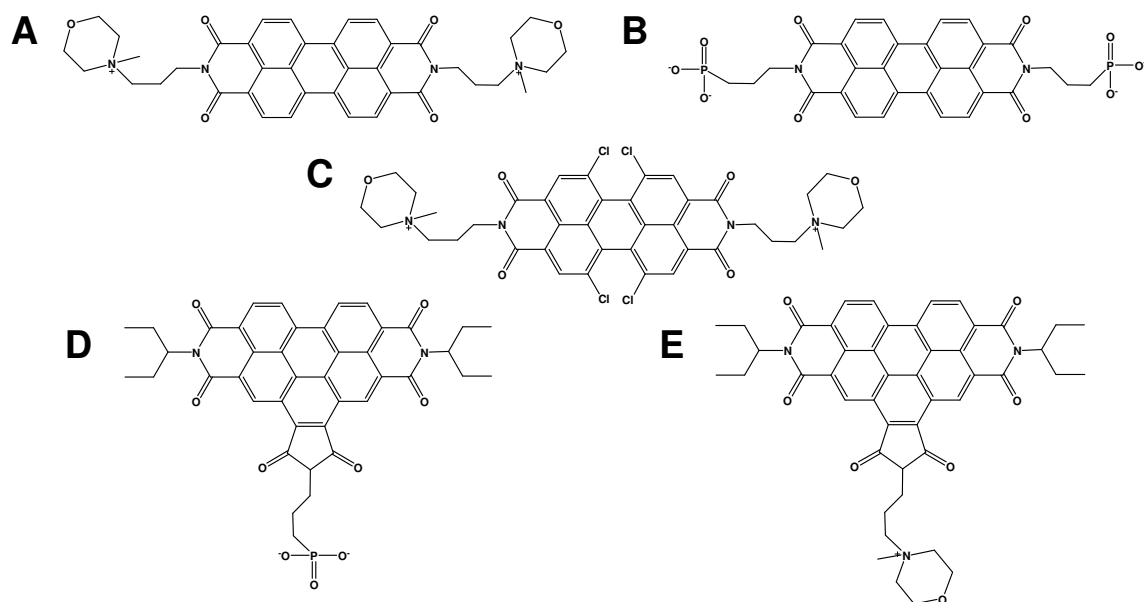


Figure 8.4. Structures of perylene diimides analogs. (A) The positively charged analog Tel11. (B) The negatively charged perylene Tel12. (C) The polychlorinated analog Tel18. (D and E) The benzannulated analogs Tel 32 and Tel34 respectively.

Previous studies of the aggregation state and G-quadruplex DNA binding selectivity of these analogs were carried out under relatively high-salt conditions, in 170 mM KCl phosphate buffer (180, 181, 186, 187). As discussed in the previous section, the selectivity of PTCDI towards G-quadruplex DNA depends on the aggregation state of these ligands, which, in addition to pH, may also be affected by ligand concentration, buffer ionic strength, and the presence of non-aqueous co-solvents. It is therefore important to investigate the aggregation behavior and G-quadruplex ligands under different solvent conditions. A lower salt buffer was selected (3:1 25 mM ammonium acetate/methanol) that could also be easily used in high-throughput techniques such as ESI-MS analysis to monitor the perylene-quadruplex interactions. As discussed in the introductory chapter, G-quadruplex stability and topology is also highly dependent on ionic strength and could also affect the ligand-DNA interactions. The following sections detail the experiments used to monitor the G-quadruplex selectivity and aggregation state of these compounds.

8.3. Results and Discussion

8.3.1. Visible Absorbance Spectroscopy experiments

Visible absorbance spectroscopy is useful to investigate the aggregation state of perylene diimides as there is characteristic spectral changes dependant on the type of aggregate formed (188-190). A well-resolved vibrational structure with maxims close to 490 and 525 nm and a shoulder at 460 nm is typical of a monomeric species, while a red-shifted, lower intensity absorption maximums close to 500 nm and 540 nm, with a shoulder around 480 nm are representative of dimeric or lower aggregate species. Higher aggregated species display a blue shift in the maximum absorption peak toward lower wavelengths (close to 475 nm, with a shoulder around 545 nm) with an overall hypochromism.

UV-Vis spectroscopy was used to identify changes in the spectra of the previously mentioned perylene diimide and benzannulated perylene diimide compounds in the methanolic buffer in the presence of different DNA structures. An intermolecular G4 quadruplex was used for this studies, $[d(T_2G_5T)]_4$, denominated here on as G5-DNA. This particular G-quadruplex is preferred over intramolecular G-quadruplexes because it can be easily distinguished from single-stranded DNA in the ESI-MS spectra. To verify that this sequence was in fact forming the expected parallel-oriented quadruplex in the 3:1 25 mM ammonium acetate/methanol buffer, its structure was monitored by CD spectroscopy. The CD spectra, Figure 8.5, presented a maximum at 263 and a minimum at 243 nm which is typical for parallel G-quadruplex structures, confirming an adequately folded structure (191, 192).

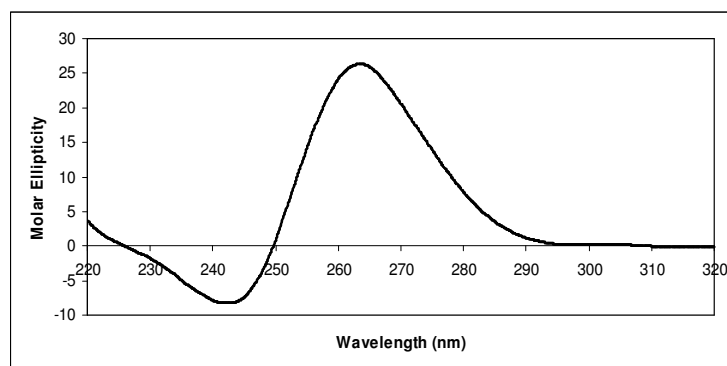


Figure 8.5. CD spectra of G5-DNA. 100 μ M of $[d(T_2G_5T)]_4$ in 3:1 water/methanol 25mM ammonium acetate buffer, pH 7

The absorption spectra of PIPER and Tel01 are highly dependent on the pH conditions of the buffer; there is a blue-shift from 500 nm to a broader peak at 470 nm with an overall hypochromism at higher pH values, which is indicative of aggregation (Figure 8.6). This shift occurs at pH 8 in the case of PIPER, and at pH 7 for Tel01, which is in agreement with the spectral changes observed in the higher salt phosphate buffer (180, 181)

At pH 7, the maximum absorbance peak for Tel01 is at 470 nm. Similar absorbance spectra are recorded for solutions of Tel01 in the presence of equimolar duplex or single-stranded DNA. However, in the presence of equimolar G-quadruplex DNA, the absorbance spectrum of Tel01 is significantly different, consisting of two large peaks at 550 and 510 nm. In contrast, the UV-Vis spectrum of PIPER at this pH displays an absorbance peak at 500 nm, which shifts to 510 nm in the presence of equimolar single-stranded, double-stranded, or G5 DNA. Additionally, in the presence of each of these DNA structures, there is a new absorbance from the PIPER chromophore at 550 nm. The intensity of this long-wavelength band increases in the order single-stranded DNA > double-stranded DNA > G-quadruplex DNA. As the pH increases to 8, the spectra of PIPER is similar to that of Tel01 at pH 7, and its affinity for double or single stranded-DNA is greatly diminished, evidenced by the lesser spectral shifts

observed upon addition of these structures. However, the spectrum has a significant shift to 510 nm in the presence of G5 DNA.

The UV-Vis spectral changes at different pH values for Tel01 and PIPER indicate a divergence in the G-quadruplex DNA binding selectivity of these two ligands that is dependant on their aggregation state. At neutral pH Tel01, whose absorbance spectrum in the absence of DNA is blue-shifted due to ligand aggregation, forms a complex with G-quadruplex DNA that absorbs in the 550 nm region. PIPER, whose spectrum in the absence of DNA at this pH does not indicate ligand aggregation, forms similar long-wavelength absorbing complexes with G-quadruplex, duplex, and even single-stranded DNA. When both ligands are aggregated (pH >8) their affinities for double stranded DNA are similar, displaying a marked preference for the quadruplex structures.

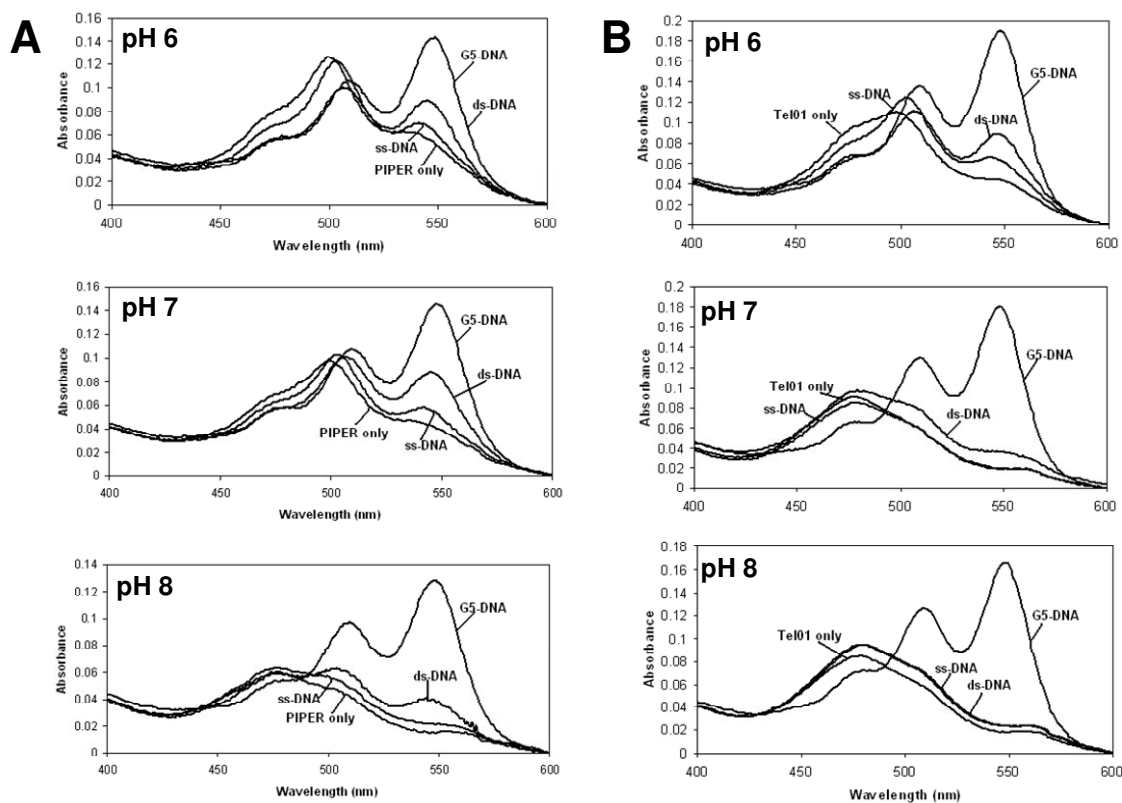


Figure 8.6. Absorption spectra of PIPER and Tel01 with different DNA structures. Absorption spectra of 10 μ M PIPER (A) or TEL01 (B) in 3:1 water/methanol 25mM ammonium acetate buffer pH 7, alone or in the presence of 1 equivalent G5-DNA [d(T₂G₅T)]₄, ds-DNA [d(GCAAATTTTCG)]₂, or ss-DNA [d(T₈)] at the indicated pH values.

The charged perylene diimides Tel11 and Tel12, whose absorbance spectra in the absence of DNA is similar to that of PIPER, display only modest changes as a function of pH. Their spectra are indicative of a dimeric or lower aggregated species. Both compounds also form complexes with G-quadruplex DNA characterized by absorbance peaks at 550, but only Tel11 gives rise to a peak at 550 nm in the presence of double-stranded DNA, as seen in Figure 8.7. The spectra of Tel 12, which appears slightly more aggregated at lower pH values, shows a clear shift in the presence of G5 DNA from 500 to 545 at the lower pH 6, which is less marked at pH 8.

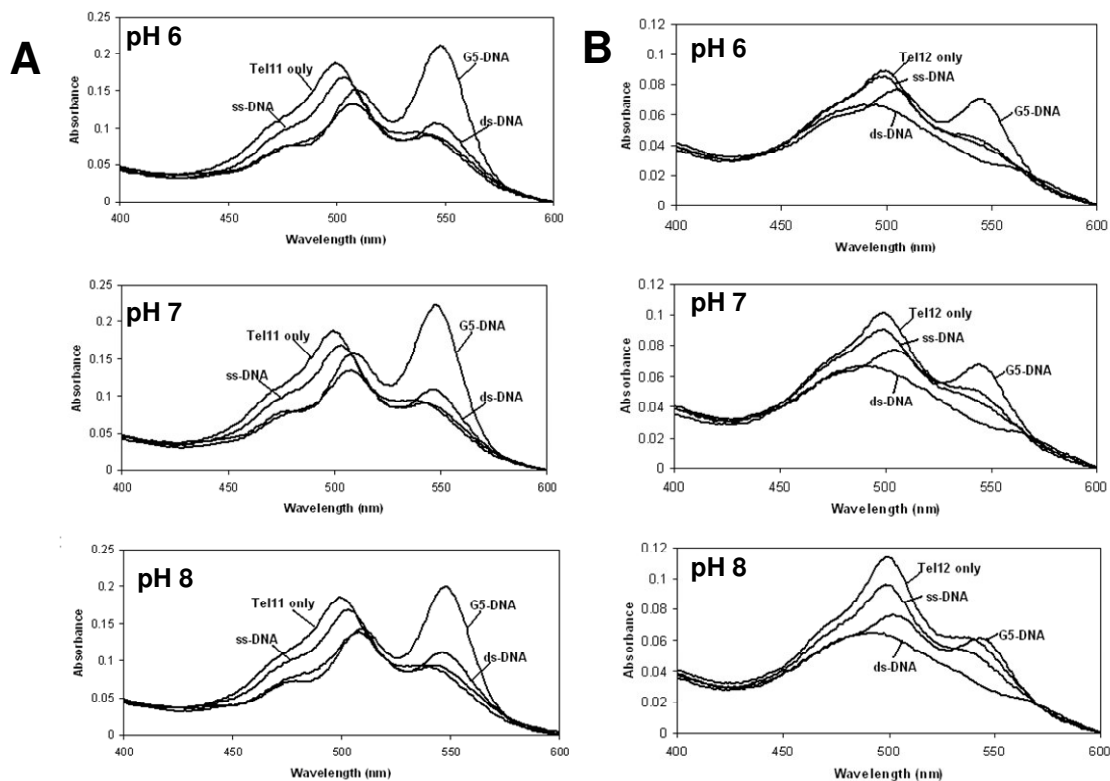


Figure 8.7. Absorption spectra of charged perylenes with different DNA structures. Absorption spectra of 10 μ M Tel11 (A) or Tel12 (B) in 3:1 water/methanol 25mM ammonium acetate buffer pH 7, alone or in the presence of 1 equivalent G5-DNA [d(T₂G₅T)]₄, ds-DNA [d(GCAAATTTTCG)]₂, or ss-DNA [d(T₈)] at the indicated pH values.

Introduction of chemical groups onto the bay region of the perylene core generally results in a non-planar, twisted aromatic chromophore with increased solubility (193). This is demonstrated in the spectra of Tel18, Figure 8.8A, which presents characteristic spectra of monomeric perylene species with a maximums at 525 nm and 492 nm. This compound is largely unaffected by pH changes in the range studied and presents hypochromic and bathochromic shifts to 532 nm in the presence of G-quadruplex DNA. Similar changes are also observed in the presence of duplex DNA, and to a lesser extent, single-stranded DNA.

The absorbance spectrum of Tel34 (Figure 8.8B) includes a long wavelength peak at 450 nm with a shoulder at 490 nm. In the presence of G-quadruplex DNA, there is a shift of the 490 nm absorbance to 480 nm, accompanied by slight hyperchromism. Immediately after the addition of double-stranded or single-stranded DNA, there is a slight hypochromism in the Tel34 absorbance spectrum, but no appreciable changes in the position of the absorbance peak. Over a period of an hour, solutions of Tel34 containing duplex or single-stranded DNA exhibit a pronounced decrease in UV-Vis absorbance that is accompanied by the formation of insoluble material. This behavior is not observed in the presence of G5 DNA, presumably because the complex formed between this benzannulated PDI and the G-quadruplex DNA is more soluble in the buffer than the ligand itself. The benzannulated and uncharged PDI Tel32 is also relatively insoluble, and at the concentration employed for these absorbance studies (10 μ M), the ligand precipitated from solution over the course of a few minutes and could not be recorded.

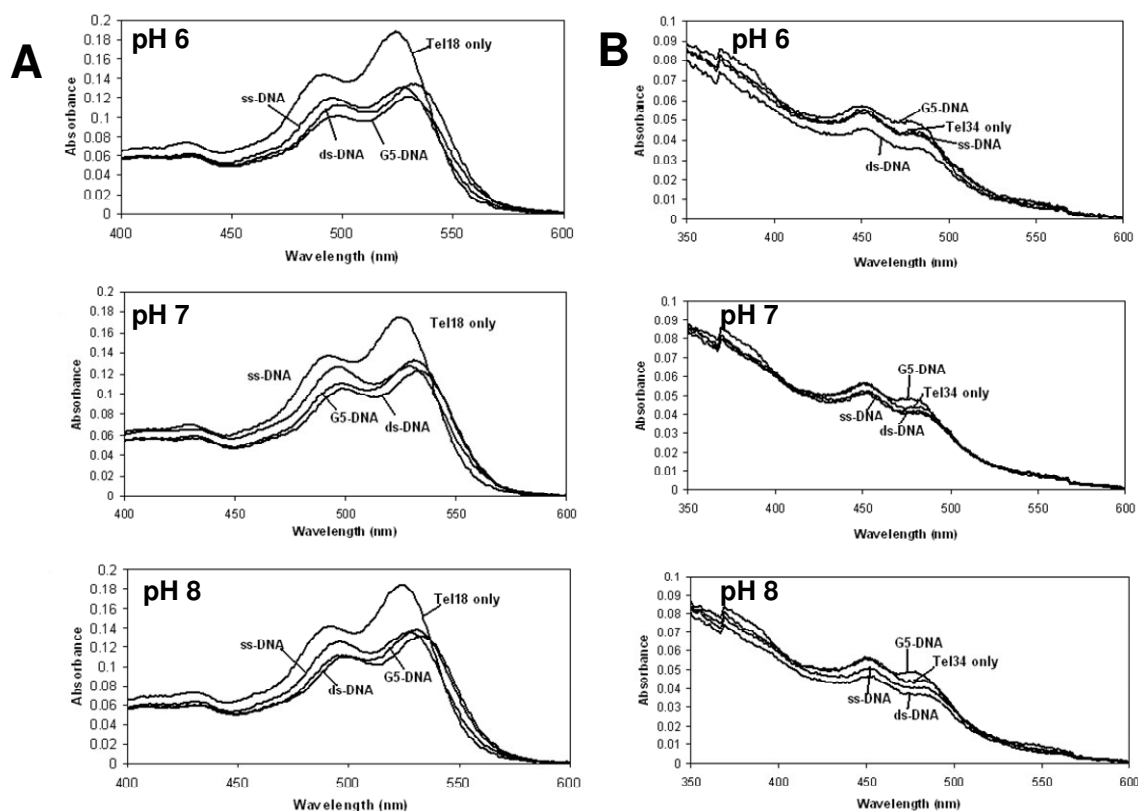


Figure 8.8. Absorption spectra of bay-substituted and benzannulated perylenes with different DNA structures. Absorption spectra of 10 μ M Tel18 (A) or Tel34 (B) in 3:1 water/methanol 25mM ammonium acetate buffer pH 7, alone or in the presence of 1 equivalent G5-DNA [d(T₂G₅T)]₄, ds-DNA [d(GCAAATTCG)]₂, or ss-DNA [d(T₈)] at the indicated pH values; spectra shown were recorded after 1 hr addition of DNA.

8.3.2. Fluorescence and Resonance Light Scattering experiments

Fluorescence and Resonance light scattering (RLS) signal have been previously used as a qualitative measure of the aggregation state of PTCDI in solution (180, 181). Fluorescence is a useful technique to monitor these compound's aggregation state, as non-aggregated perylene diimides tend to be highly fluorescent in solution (194, 195). RLS is also a sensitive and selective method for studying electronically coupled chromophore arrays, since aggregated species can display enhancement in light scattering of several orders of magnitude compared to their monomeric counterparts (196).

Solutions of Tel01 display very low fluorescence and correspondingly large RLS signal (Figure 8.9). In contrast, the RLS signal for PIPER is absent and the compound displays a relatively high fluorescence signal. These data present further evidence that under these buffer conditions Tel01 displays extensive aggregation while PIPER does not. Similar observations were made for solutions of Tel01 and PIPER in high-salt buffer conditions, indicating that the aggregation state of these two PTCDis is largely unaffected by the methanolic buffer conditions employed here (180, 181).

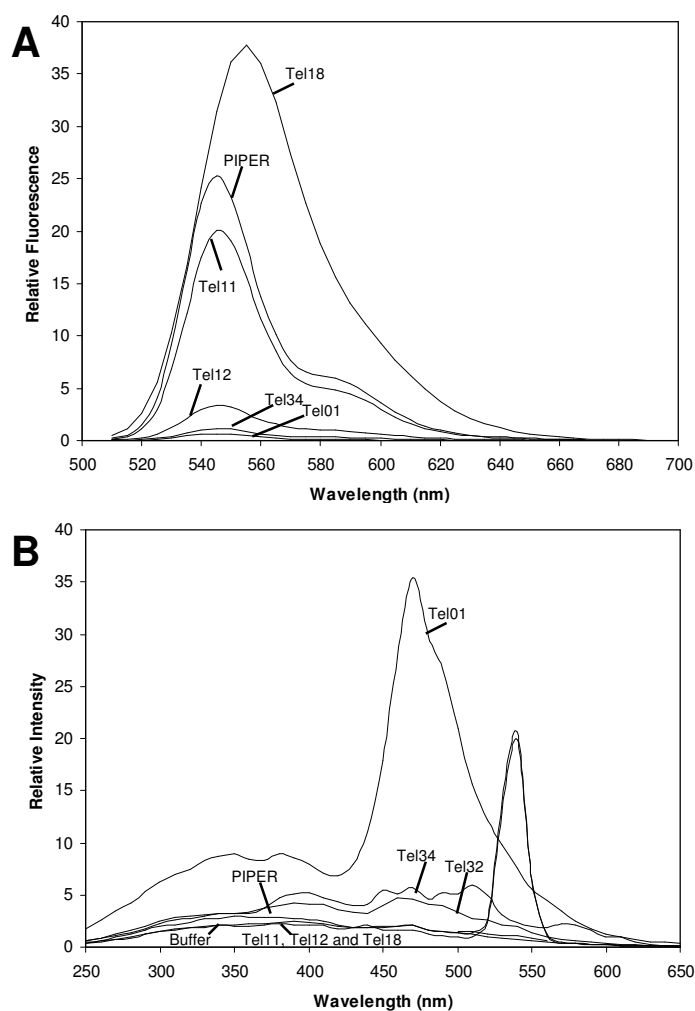


Figure 8.9. Relative fluorescence and RLS signal of PTCDis. Relative fluorescence (A) or RLS signal (B) of 1 μ M ligand in 3:1 water/methanol 25mM ammonium acetate buffer, pH 7. Excitation was at 495 nm for all ligands except Tel34, which was excited at 469 nm.

The fluorescence and RLS spectra of the other PTCDI s were also examined under the methanolic buffer conditions. As shown in Figure 8.9, PIPER, Tel11, and Tel18 are not aggregated in solution, judged by the strong fluorescence and lack of RLS signals of these solutions. Peaks close to 585 nm are contamination from the fluorescence of the compounds; compounds that had higher fluorescence values were the ones to present this contamination pattern in the RLS spectra. Tel12 displays only weak fluorescence and no significant RLS spectra. The weak fluorescence of Tel12 may be due to ligand dimerization, or lower aggregate formation, as has been noted for this compound in 150 mM KCl phosphate buffer (187). However, the fluorescence intensity of Tel12 in methanolic buffer is higher than that in the high-salt buffer (data not shown), indicating that aggregation is likely less extensive in the methanolic buffer. Like Tel01, solutions of the benzannulated perylene Tel34 in methanolic buffer do not have significant fluorescence; however, unlike Tel01, Tel34 solutions do not display a strong RLS signal, indicating that if Tel34 is aggregated in solution, the aggregates are RLS-silent. Attempts to compare the aggregation state of Tel34 in methanolic ammonium acetate and 150 mM KCl phosphate buffer were unsuccessful due to the very low solubility of this analog in the high-salt buffer. Similarly, the low solubility of Tel32, even in methanolic ammonium acetate, made characterization of this PTCDI difficult. Immediately prepared solutions of Tel32 showed very low fluorescence and RLS signals. However, over a period of minutes the ligand began to precipitate from these solutions.

8.3.3. Fluorescence quenching experiments

DNA-drug complexation leads to optical changes that can provide useful information about the nature and strength of their binding interaction (197). Monitoring such changes using fluorescence spectroscopy relies on the fact that

the spectra are altered upon binding. Fluorescence emission of the DNA-bound drugs can be enhanced, as the case with the well-known intercalator ethidium bromide, or efficiently quenched, as with the majority of the perylene diimides compounds (180, 181, 187).

Fluorescence-quenching experiments of the analogs with quadruplex, duplex, and single-stranded DNA allow better quantification and insight into the affinity and selectivity differences of these ligands for G-quadruplex DNA. Solutions of 1 μ M perylene compound in 3:1 25 mM ammonium acetate/methanol buffer, pH 7 were titrated with concentrated stock solutions of each DNA structure in the same buffer. Fluorescence spectra were recorded at appropriate emission and excitation wavelengths for each class of chromophore: unmodified PTCDIs Tel01, Tel11, Tel12, Tel34, and PIPER (emission at 545 nm, excitation at 495 nm); chlorinated analog Tel18 (emission at 555 nm, excitation at 495 nm); and benzannulated compound Tel32 (emission at 565 nm, excitation at 469 nm). Examples of the fluorescence titration curves obtained with quadruplex G5-DNA [d(TTGGGGGT)]₄ duplex [d(GCAAATTTTCG)]₂, and single-stranded [d(T₈)] are shown in Figure 8.10.

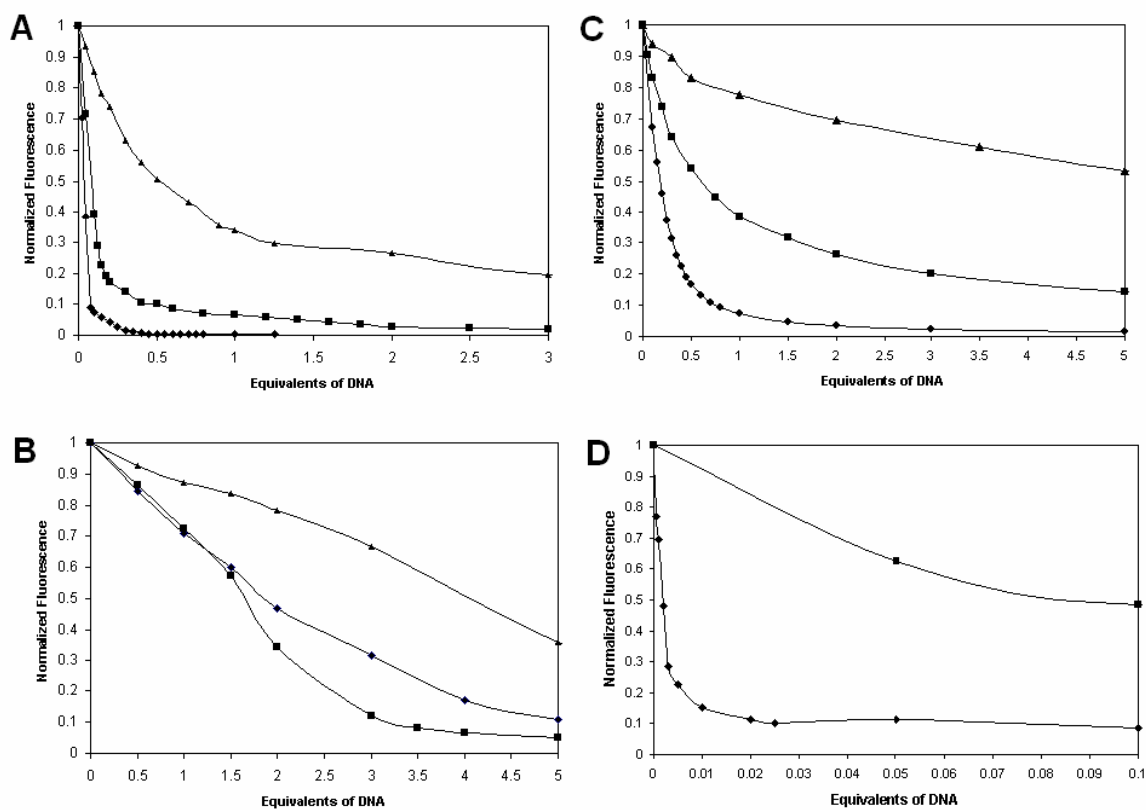


Figure 8.10. Normalized fluorescence titration data for different perylene diimides at $1\mu\text{M}$ concentration in the presence of G5-DNA $[\text{d}(\text{T}_2\text{G}_5\text{T})_4$ (diamonds), ds-DNA $[\text{d}(\text{GCAAATTCG})_2$ (squares), or ss-DNA $[\text{d}(\text{T}_8)]$ (triangles) in 3:1 water/methanol 25mM ammonium acetate buffer, pH 7. Fluorescence emission ($\text{ex}=495\text{nm}$, $\text{em}=555$) was determined at each DNA concentration. (A) TEL11. (B) TEL12. (C) TEL18. (D) TEL34

It can be observed from the titration curves that Tel11 has similar affinity to G5 DNA as it does to double stranded DNA, and that its fluorescence gets quenched at very small ratios of DNA to ligand; it needs less than 0.2 equivalents of G5 DNA to quench half of its total fluorescence (Figure 8.10A). On the other hand, Tel12 needs several equivalents of G5 DNA to achieve the quenching of half the total fluorescence. At low DNA ratios there is higher preference for G5 DNA, but at higher equivalents of DNA, there seems to be a greater affinity for the double stranded DNA in this buffer (Figure 8.10B). However, titration of the same DNA sequences in high salt buffer shows no significant binding to double stranded DNA up to 5 equivalents excess of the structure (Figure 8.11). It must

be noted that the overall fluorescence is lower at the higher salt buffer, indicating a higher degree of aggregation that could be aiding in this analogs' selectivity in this buffer.

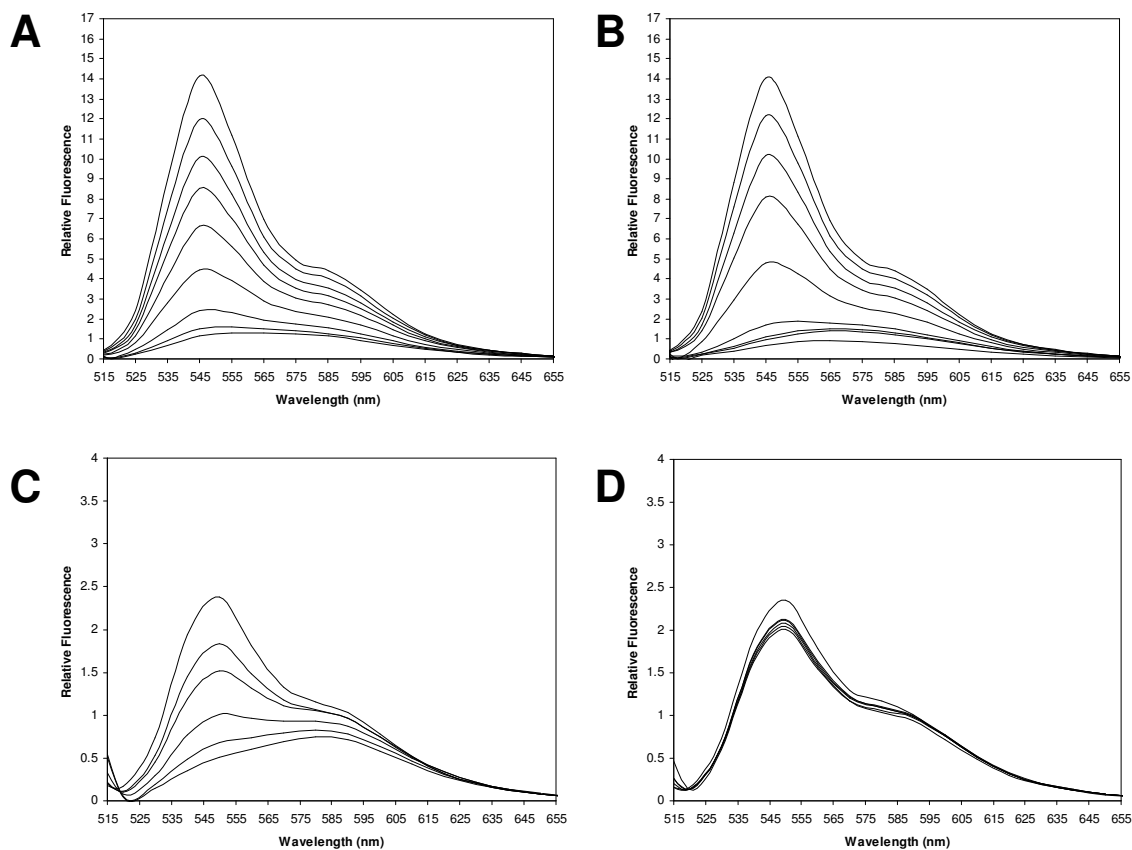


Figure 8.11. Fluorescence quenching of Tel12 in low and high salt buffers. Fluorescence titrations of $1\mu\text{M}$ Tel12 in 3:1 water/methanol 25 mM ammonium acetate buffer, pH 7 in the presence of increasing ratios of G5-DNA $[\text{d}(\text{T}_2\text{G}_5\text{T})_4]_4$, (A) or ds-DNA $[\text{d}(\text{GCAAATTTTCG})_2]_2$ (B). Titrations were repeated in 170 mM K Phosphate Buffer, pH 7 with G5-DNA (C) or ds-DNA (D); $\text{ex}=495\text{nm}$

While all three DNA samples quench the fluorescence of Tel18 there is clearly a difference between the efficiency of fluorescence-quenching, with G5-DNA causing the most extensive quenching at low concentrations, single-stranded DNA producing the least quenching, and duplex DNA leading to intermediate quenching (Figure 8.10C). In the case of G-quadruplex DNA, there is nearly 80% fluorescence quenching after the addition of just one-half

equivalent of DNA, indicating that multiple Tel18 ligands are binding to the DNA. Tel34 appears to be selective for G5 structures when compared to double stranded DNA, and it seems to bind at very low DNA concentrations (Figure 8.10D). It takes less than 0.01 equivalents of G5 to quench half the total fluorescence intensity of Tel34. It must be noted however, that the fluorescence of Tel34 by itself decreases rapidly with time since the compound comes out of solution, which makes its characterization difficult. Fluorescence titrations were not performed on Tel01 or Tel32 because the compounds did not have considerable readings at pH 7 in the conditions the study was carried out.

The results of the fluorescence-quenching studies of the perylene compounds are summarized in Table 8.1, which shows the percent PTCDI fluorescence-quenching after the addition of one equivalent of the different DNA structures. In accord with the UV-Vis absorbance studies (Figure 8.6) Tel01 displays a high degree of selectivity for G-quadruplex DNA binding, as shown by the minimal fluorescence quenching in the presence of either duplex or single-stranded DNA compared to G-quadruplex DNA. Other analogs such as PIPER and Tel11, appear to interact more strongly with G-quadruplex DNA when compared to Tel01, but show very little selectivity for G-quadruplex DNA versus duplex DNA. Both PIPER and Tel18 also show significant interactions with single-stranded DNA; the addition of one equivalent of single-stranded DNA to these PTCDI quenchers their fluorescence by more than 50%. Tel18 and Tel34 appear to be of intermediate selectivity for G-quadruplex DNA versus duplex DNA and have moderate affinity for single-stranded DNA. Tel12 does not interact strongly with G-quadruplex DNA in the methanolic buffer, as evidenced by only 29% fluorescence quenching in the presence of one equivalent of G5-DNA; however, this PTCDI is relatively selective for G-quadruplex DNA at 1:1 ratios and does not bind to single-stranded DNA. Tel12 binds double stranded with greater affinity than quadruplexes at higher duplex/ligand ratios in the methanolic buffer, but not in the high salt 170 mM potassium phosphate buffer. There was insignificant fluorescence quenching of Tel32, indicating that this compound does

not interact with any of these DNA structures, perhaps because it does not remain in solution after a few minutes.

Table 8.1. Fluorescence quenching of PTCIDs by quadruplex, duplex, and single-stranded DNA. Percent fluorescence quenching in the presence of 1 μ M ligand and 1 μ M DNA in 3:1 water/methanol 25 mM ammonium acetate buffer, pH 7.

Ligand	%Fluorescence Quenching in the presence of 1eq DNA		
	G5-DNA ^a	ds-DNA ^b	ss-DNA ^c
TEL01 ^d	64 \pm 4	6 \pm 2	2 \pm 1
PIPER ^d	100 \pm 1	94 \pm 2	57 \pm 4
TEL11 ^d	99.8 \pm 0.1	96 \pm 1	67 \pm 5
TEL12 ^d	29 \pm 6	16 \pm 8	13 \pm 6
TEL18 ^e	92.9 \pm 0.1	66 \pm 3	12 \pm 9
TEL32 ^d	4 \pm 2	1 \pm 2	7 \pm 2
TEL34 ^f	90 \pm 2	62 \pm 4	40 \pm 6

^a[d(T₂G₅T)]₄.
^b[d(GCAAATTCG)]₂.
^c[d(T₈)].
^dEx=495nm, em=545.
^eEx=495nm, em=555.
^fEx=469nm, em=565.

8.4. Conclusions

There is good agreement between spectroscopic binding studies performed in the low and high salt buffer conditions. Similar binding behavior was observed in both cases and the quadruplex structure used in the study is also folded correctly under the experimental conditions. The buffer and quadruplex sequence used in this study can be easily employed in high throughput screening techniques such as ESI-MS analysis to quickly identify selective G-quadruplex DNA binding agents.

The results of this work indicate that ligand aggregation is correlated with G-quadruplex selectivity within the compounds studied. The selectivity of PIPER and Tel01 for G-quadruplex DNA is directly related to the pH conditions where the compounds are aggregated; under physiological conditions (pH7) Tel01 is aggregated and binds G-quadruplex selectively while PIPER is not and binds

similarly to all DNA structures. The bay substituted analog Tel18 does not have a planar chromophore, which makes it monomeric under the conditions studied and binds to double stranded and single-stranded DNA with high affinity. Similar behavior is observed with the compound Tel11, which is dimeric in solution under experimental conditions and binds all DNA structures even at very low ratios of ligand. The benzannulated analog Tel34 has an extended aromatic ring system was originally designed to increase the interactions with G-tetrads (186). This compound does indeed appear promising in terms of selectivity, but the hydrophobic nature of both Tel32 and Tel34 and their poor solubility makes it difficult to accurately determine their interactions with DNA in aqueous solutions. Novel analogs with an extended aromatic system but with hydrophilic groups that increase their solubility could potentially overcome this problem and be selective G-quadruplex interactive agents.

Perhaps the most intriguing analog is Tel12, which presents marked G-quadruplex selective binding in high salt conditions but not in the methanolic buffer. Fluorescence spectra of Tel12 indicate that the compound is less aggregated in the methanolic buffer which could explain the observed divergence in selectivity. Salt and buffer conditions are more important in determination of the aggregation state of Tel12 than changes in pH (as is the case for Tel01 and PIPER). It is therefore important to further study the factors that affect this compound's aggregation state and G-quadruplex selectivity. These parameters will be further investigated in the following chapter.

In conclusion, compound aggregation does appear to influence G-quadruplex selectivity of the PTCDis studied here. It is known that perylene diimides can interact with G-quadruplexes by end-stacking (178). Since this type of interaction requires only one free face from the ligand, it is possible that binding to G-tetrads occurs with both aggregated and monomeric species. On the other hand, binding to double stranded DNA through intercalation likely requires the ligand to be monomeric or dimeric, which is why affinity for these structures are diminished when the ligands are aggregated.

CHAPTER 9. PERYLENE DIIMIDES METAL AND THERMAL MEDIATED AGGREGATION AND G-QUADRUPLEX SELECTIVITY

9.1. Temperature and metal ion dependant-aggregation of perylene diimide compounds in the presence of metal ions and temperature changes

Because of their intense color hues, perylene diimides were originally studied as industrial dyes, but their high electron affinity and prominent fluorescence quantum yields has led to their use in electronic materials and fluorescence applications (198). Much interest has also been devoted to supramolecular perylene diimides assemblies because of their ease to form aggregate species through π - π stacking interactions and their potential use in optical devices, photosensitizers, and fluorescence probes (198, 199). Supramolecular structures such as those formed by perylene compounds are held together by non-covalent interactions, and have received great attention in materials science because their associations are reversible and can therefore be controlled by experimental conditions (200).

There are many factors that affect the aggregation of perylene diimides and thus their supramolecular assemblies, such as charge, substituents, concentration and pH. Recently, metal-coordination-directed self-assembly of certain perylene diimides has been achieved in the presence of metal ions; amongst the metals studied that can promote aggregation for some of PTCDIs are Cu^{2+} , Ni^{2+} , Zn^{2+} , Fe^{2+} , Ru^{2+} , Pt^{2+} , Ca^{2+} , Li^+ , Ba^{2+} , Pb^{2+} , Mn^{2+} , Cd^{2+} (190, 201-206). As mentioned in the previous chapter, the aggregation state of perylene compounds has been correlated to their preferential G-quadruplex binding (159, 180, 181). However, metal-mediated aggregation of perylene compounds has

never been studied in relationship to G-Quadruplex selectivity, and could present a promising avenue for regulation of PTCDI-quadruplex interactions; metallo-supramolecular assemblies could be obtained by addition of metal salts, affecting their interactions with varying DNA structures. The following work examines the metal ion coordination and aggregation state of a series of perylene diimide compounds in aqueous buffers, their binding to duplex and quadruplex DNA, and their biological properties.

9.1.1. Absorbance Spectroscopy

It is important to note that the majority of current studies that encompass metal-ion induced PTCDI aggregation are involved in material science applications and have been carried out in organic solvents, where perylene diimides are very soluble (201, 204, 206, 207). An example is the bis-2,2':6',2''-terpyridine functionalized perylene diimide synthesized by Dobrawa *et al.*, which can coordinate metal cations through the nitrogen atoms of the terpyridine group in chloroform:acetonitrile mixtures forming higher order structures upon zinc complexation, as shown in Figure 9.1A (201, 204). One of the few perylene derivatives that has been studied in the presence of metal ions in aqueous environments is Perylene-EDTA, which was synthesized by Tuntiwechapikul and co-workers and is a PIPER derivative modified with EDTA side chains (Figure 9.1B). This compound was able to chelate Fe^{2+} and Ni^{2+} cations and bind with greater selectivity toward quadruplex structures when metal coordinated, but its aggregation state did not appear to be affected by metal chelation (205, 208). For this study, the metal ion induced aggregation was investigated for the compounds PIPER and TEL01 (Figure 8.2) as well as the water soluble derivatives Tel11, Tel12 and Tel18 (Figure 8.4). The UV-Vis spectra was recorded in 8 mM sodium phosphate, 185 mM NaCl, pH 7.0 (BPS buffer) in the presence and absence of Mg^{2+} , Ca^{2+} , Zn^{2+} , Ni^{2+} , and Cu^{2+} nitrate salts.

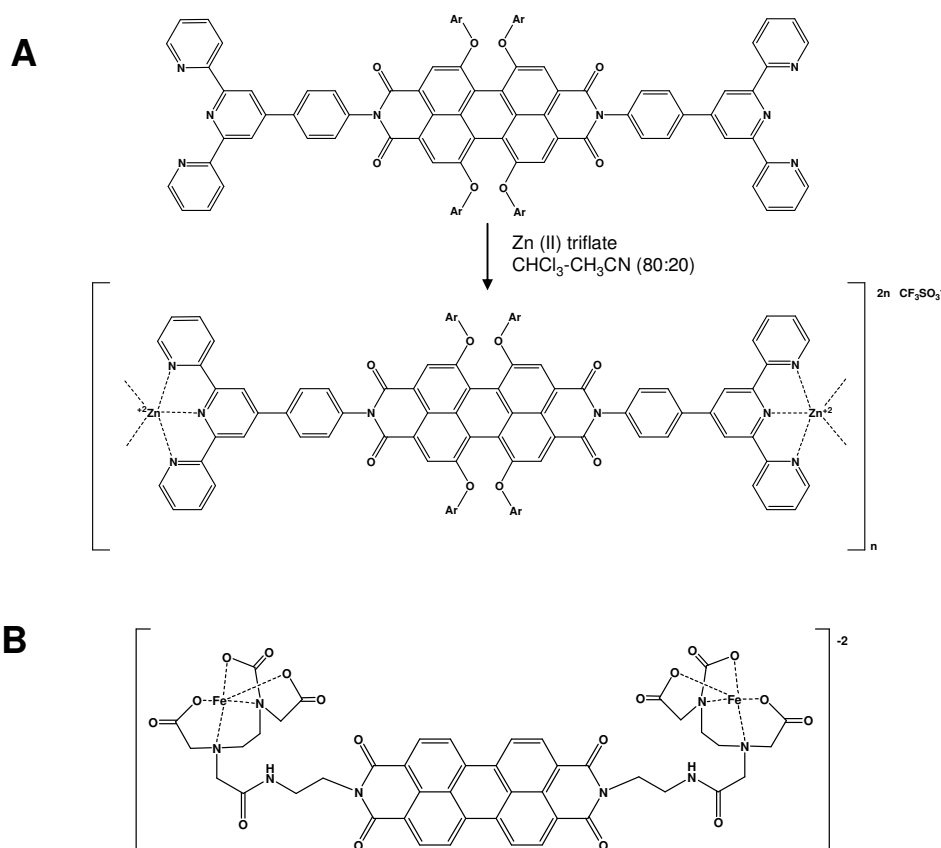


Figure 9.1. Terpyridine and EDTA functionalized perylene derivatives. (A) Complexation of zinc bis-2,2':6',2''-terpyridine perylene diimides with zinc (II) triflate in chloroform:acetonitrile (80:20) (201, 204). (B) Perylene-EDTA coordinated with Fe²⁺ (205, 208)

Under these buffer conditions Tel01 was already aggregated and addition of metal ions did not cause changes in the absorbance spectra. Addition of 1:1 or 2:1 metal:perylene resulted in no significant spectral changes in the case of PIPER, Tel18 and Tel11 (Figure 9.2A-C). In contrast, Tel12 displayed slight hypochromicity at 500 nm upon addition of 1 equivalent Cu²⁺ and Ni²⁺ ions (Figure 9.2D). There was also a major shift upon addition of Zn²⁺ ions, where the peak at 500 nm blue-shifted to a broader peak at 470 nm with an overall hypochromism, indicating the formation of higher aggregated species. To further test the metal-mediated aggregation of Tel12, the compound was examined in the presence of Fe²⁺, Fe³⁺, and Co²⁺ ions. However, no spectral changes were observed with these metal cations.

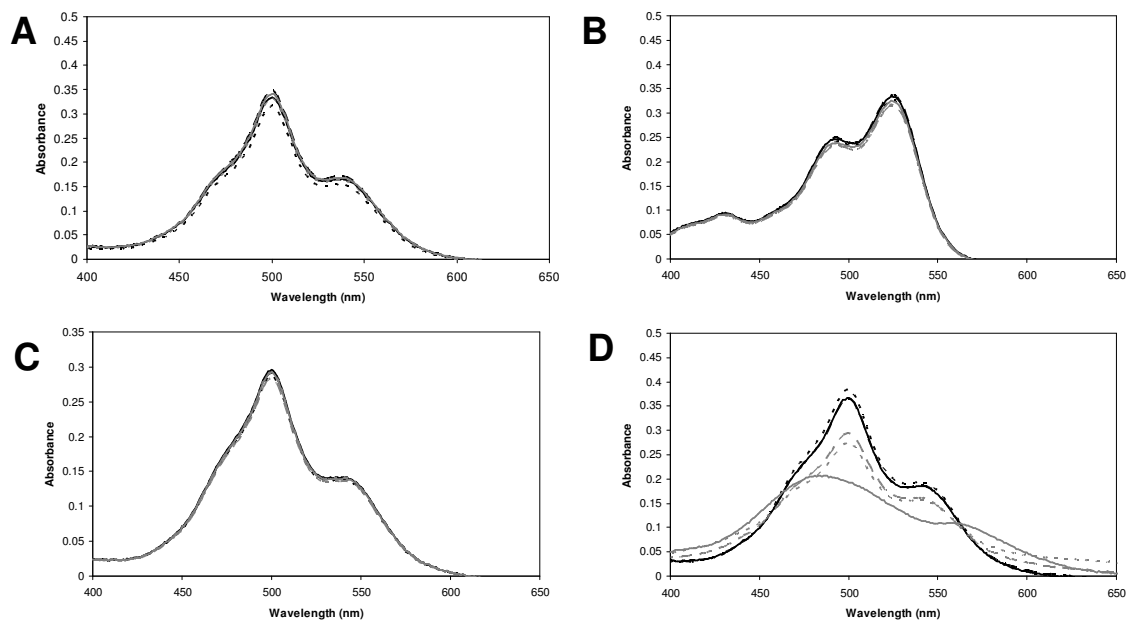


Figure 9.2. Absorbance spectra of perylene diimides in the presence of metal cations. Spectra were recorded with 10 μM PIPER (A), Tel18 (B), Tel11 (C), or Tel12 (D) in 8 mM Na Phosphate, 185 mM NaCl, pH 7, alone (solid black line) or in the presence of 10 μM $\text{Mg}(\text{NO}_3)_2$ (dashed black line), $\text{Ca}(\text{NO}_3)_2$ (dotted black line), $\text{Zn}(\text{NO}_3)_2$ (solid gray line), $\text{Cu}(\text{NO}_3)_2$ (dashed grey line), or $\text{Ni}(\text{NO}_3)_2$ (dotted grey line)

Within this series, the only analog that appeared to form aggregated species in the presence of metal cations is the negatively charged Tel12. However, there are examples of neutral PTCDIs with penta-oxa-heptadecane chains which have been reported to display metal-ion-induced aggregation in organic solvents (206). Taking this into consideration, a new neutral analog was devised with potential metal ion coordination sites; the tetra-MEM-serinol PTCDI, Tel45 (Figure 9.3), was synthesized by Sean Kerwin by introducing methoxyethoxymethyl (MEM) groups to the PTCDI core (unpublished results). In addition to metal-coordination, the MEM groups in Tel45 should increase solubility in aqueous buffers.

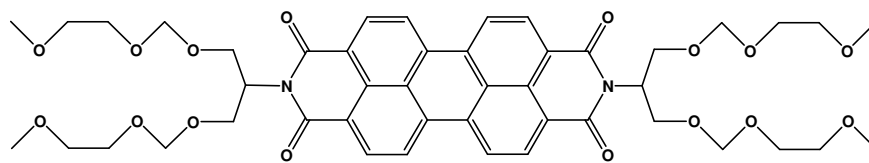


Figure 9.3. Structure of Tel45.

The new perylene compound was in fact soluble in water and aqueous buffers, exhibiting brightly red colored solutions. To test for metal mediated aggregation, the UV-Vis spectra of Tel45 was recorded in BPS buffer, corresponding to a dimeric species; the spectral changes were monitored upon addition of equimolar amounts of Mg^{2+} , Ca^{2+} , Zn^{2+} , Co^{2+} , Cu^{2+} , Ni^{2+} , Fe^{2+} , or Fe^{3+} (Figure 9.4A). Unexpectedly, none of the metal salts produced any significant spectral shifts. Further additions of metal cations (> 5 eq.) resulted in slight hyperchromicity, indicating a less aggregated species. To investigate if this analog could form aggregates in organic solvents, measurements were also carried out in DCM/MeOH, observing a spectra corresponding to monomeric Tel45. Spectral changes of the analog in DCM/MeOH were monitored in the presence of $(\text{CF}_3\text{SO}_3)_2\text{Zn}$, $\text{CF}_3\text{SO}_3\text{Ag}$, and $\text{Cu}(\text{ClO}_4)_2$, but no significant spectral shifts were observed (Figure 9.4B). The data suggest that under the conditions used for this study Tel45 does not form higher aggregated species by addition of metal cations.

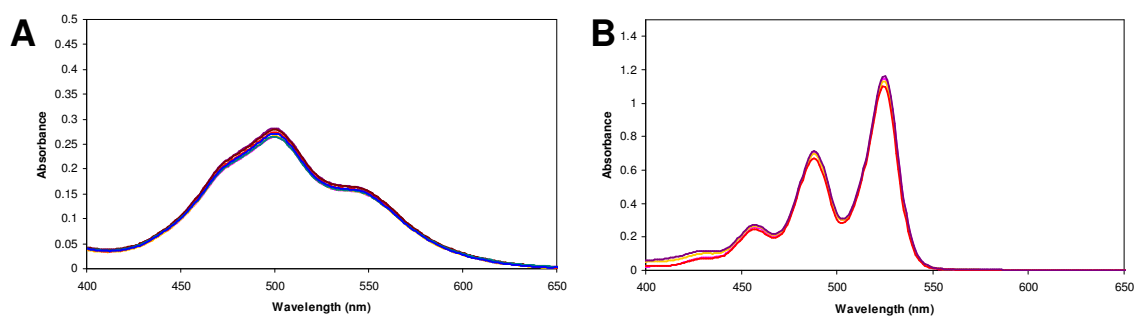


Figure 9.4. Absorbance spectra of Tel45 with metal cations in aqueous and organic solvents. (A) Spectra of 10 μM Tel45 in BPS buffer in the presence of 10 μM $\text{Mg}(\text{NO}_3)_2$, $\text{Ca}(\text{NO}_3)_2$, $\text{Zn}(\text{NO}_3)_2$, $\text{Cu}(\text{NO}_3)_2$, $\text{Ni}(\text{NO}_3)_2$, $\text{Co}(\text{NO}_3)_2$, or $\text{Fe}(\text{NO}_3)_2$. (B) Spectra of 10 μM Tel45 in DCM/MeOH 1:1 in the presence of 10 μM $(\text{CF}_3\text{SO}_3)_2\text{Zn}$, $\text{CF}_3\text{SO}_3\text{Ag}$, and $\text{Cu}(\text{ClO}_4)_2$.

Although Tel45 did not appear to form supramolecular assemblies in the presence of metal ions it did present an unanticipated thermal-mediated aggregation. As seen in Figure 9.5A, upon heating Tel 45 between 10-50 °C the peak at 500 nm is red-shifted to approximately 520 nm with an overall hypochromicity, concomitant with an increase in absorbance intensity in the 565-700 region. This bathochromic shift (red shift towards longer wavelengths) is different than the hypsochromic (blue-shifted towards shorter wavelengths) from 500 to 470 nm, generally observed when most perylenes (such as PIPER, Tel01, or Tel12, recall Figure 8.6 and Figure 9.2D) display aggregation.

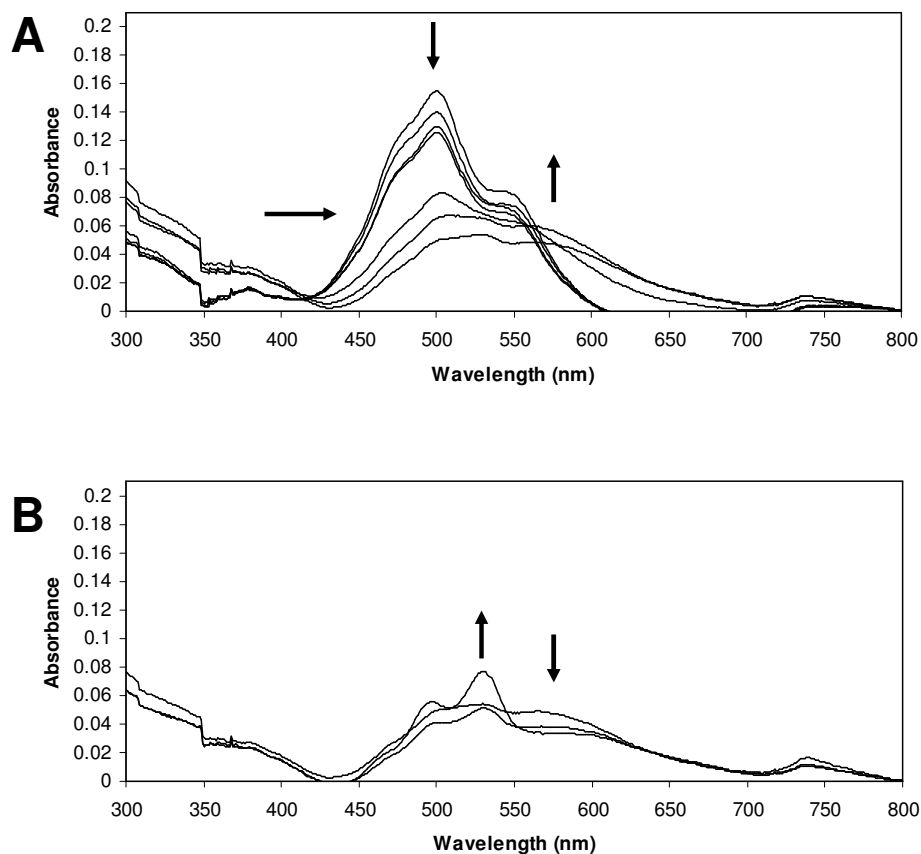


Figure 9.5. Absorbance Spectra of Tel45 with increasing temperature. UV-Vis spectral changes of 10 μ M Tel45 in 170 mM potassium phosphate buffer at 5, 10, 15, 20, 25, 30, 40 and 50 °C (A) or 50, 70 and 90 °C (B). Arrows indicate direction of changes with increasing temperature.

There are two main types of aggregates described in the literature: J- and H-aggregates (209). H-aggregates present blue-shifts with respect to the monomeric chromophore as well as a decrease in fluorescence upon aggregation, while J-aggregates display red-shifts in their absorption and emission maxima and no fluorescence quenching upon aggregation. H-aggregates lose their fluorescence because they are stacked one on top of the other, while J-aggregates are slipped with respect to each other (Figure 9.6). The observed spectral changes are in agreement with those corresponding to H-type aggregation for Tel01, PIPER and Tel12, while Tel45 shares some of the characteristics of J-type aggregation. This finding is surprising in the case of Tel45 because most perylene diimides that form J-aggregates have substituents in the bay which enforce core twisting and facilitate slipped arrangements (210, 211). However, the observed Tel45 aggregates are broader than those reported for other PTCDI J-aggregates held together through hydrogen bonding networks (211). It is possible that the Tel45 aggregates are formed by stacking of the perylene core, but the MEM groups on the side chains force the aggregated species to have a slipped configuration and thus cause the aggregates to exhibit similar properties to those of J-aggregates. To further investigate the unusual Tel45 aggregates, the fluorescence of this PTCDI will also be examined in the next section with increasing temperature; bathochromically shifted fluorescence is characteristic for J-type aggregates and could aid in the investigation of the temperature-dependant Tel45 aggregates.

Although the formation of higher aggregate species upon heating is very atypical it has been reported by Wang and co-workers for hybrid structures consisting of alternating hydrophobic perylene diimides and hydrophilic single-stranded DNA sequences connected by tetraethylene glycol groups (212). Their study showed that the strength of hydrophobic forces holding the chromophores together in their molecular assembly was more pronounced at higher temperatures. In the case of Tel45, there is a balance where the aggregated species appear when the temperature is raised from 10 to 50 °C (Figure 9.5A). At

higher temperatures (heating from 50 °C to 90 °C, Figure 9.5B), the peaks corresponding to the aggregates decrease and those corresponding to the monomeric species (530 nm) increase.

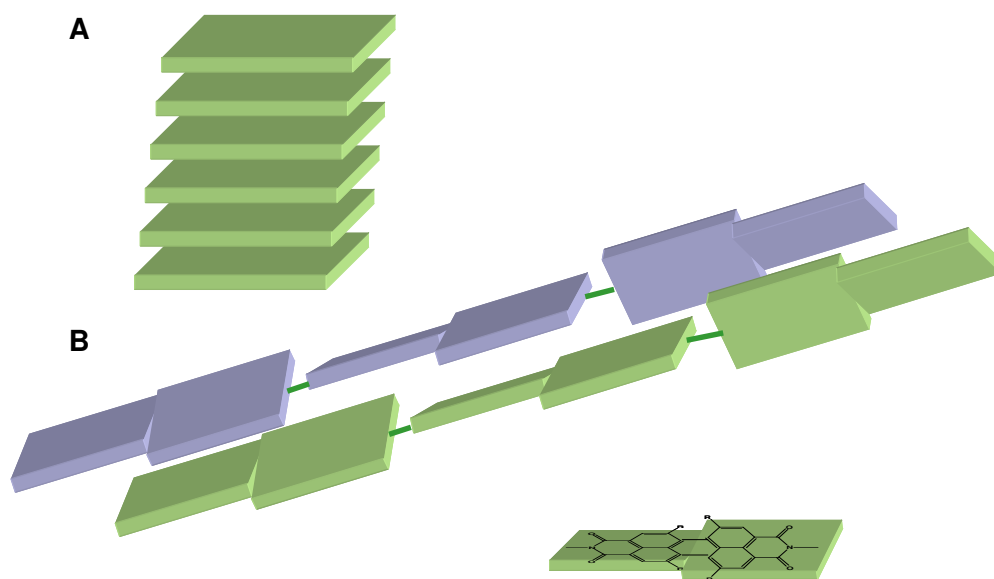


Figure 9.6. *H- and J-aggregates.* (A) In H-aggregates molecules are stacked on top of each other in a “deck of cards” fashion, quenching fluorescence properties. (B) J-aggregates the molecule have slipped more with respect to each other; this aggregates are usually facilitated when substituents in the bay area (such as shown in the lower right corner) cause chromophore twisting and loss of planarity

9.1.2. Resonance Light Scattering and fluorescence spectroscopy

To further confirm that Tel12 and Tel45 were forming aggregates in a metal ion and thermal dependent fashion respectively, fluorescence and Resonance Light Scattering (RLS) experiments were conducted. As discussed in the previous section, decreases in fluorescence concomitant with increases in RLS signal are indicative of aggregation in the case of H-type aggregates. As seen in Figure 9.7, Tel 12 displayed close to 4-fold decrease in fluorescence signal at 550 nm along with an over a 10-fold increase in RLS signal upon

addition of 1 equivalent Zn^{2+} ions; this corresponds well with H-aggregate formation.

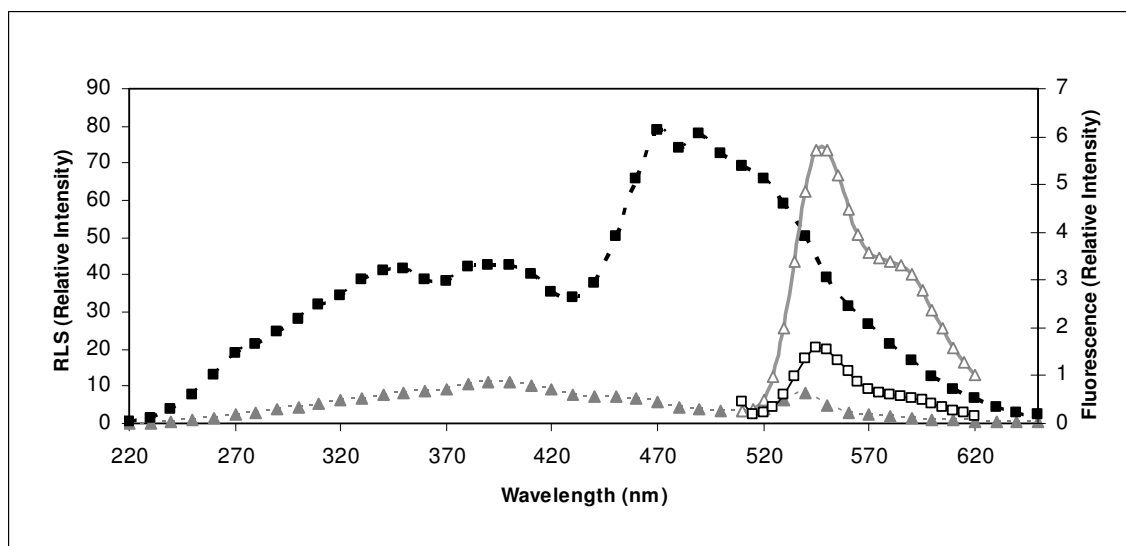


Figure 9.7. Fluorescence and Resonance Light scattering of Tel12 in the presence of Zn^{2+} ions. Fluorescence (empty marks) and RLS (filled marks) spectra of 10 μM Tel12 in BPS buffer alone (triangles) or in the presence of 10 μM Zn^{2+} ions (squares).

The fluorescence and RLS of Tel45 was monitored at 10 and 100 μM at temperatures ranging from 5-100 $^{\circ}C$. As seen in Figure 9.8A, upon increasing the temperature to 50 $^{\circ}C$ there was an increase in the peak at 550 nm, but there was also the appearance of a red-shifted peak at 655 nm, which is more evident at higher concentrations (Figure 9.8B). Similar bathochromic shifts have been reported in J-type PTCDI aggregates but have narrower peaks and higher quantum yields than those formed by Tel45 (209-211). The data suggest that under these conditions there may be equilibrium between monomeric and aggregated species; it is likely that the increase in fluorescence at 550 nm corresponds to formation of monomeric species while the appearance of the peak at 655 nm is related to formation of the aggregates. This idea is supported by the larger ratio of the peak at 655 nm to the peak at 550 nm observed at higher concentrations of Tel45.

Furthermore, at both concentrations there is a very sharp increase in RLS signal when the temperature reaches 30 °C for 10 μ M Tel45 (Figure 9.8C) or 25 °C for 100 μ M Tel45 (Figure 9.8D). The RLS peaks also occur in the region where the aggregate was observed in the UV-Vis spectra (compare to Figure 9.5) and have a maximum at 600 and 640 nm for 10 and 100 μ M solutions of Tel45 respectively. The formation of these RLS peaks occurs concurrently with the appearance of a fluorescence peak at 655 nm, which indicates that this bathochromically shifted fluorescence peak is related to the compound's aggregation. When temperatures are increased from 50 - 100 °C there is an overall increase in the fluorescence signal and a slight decrease in RLS signal, indicating at least partial de-stabilization of the aggregated species. The observed aggregate formation is reversible upon decreasing the temperature below 25 °C.

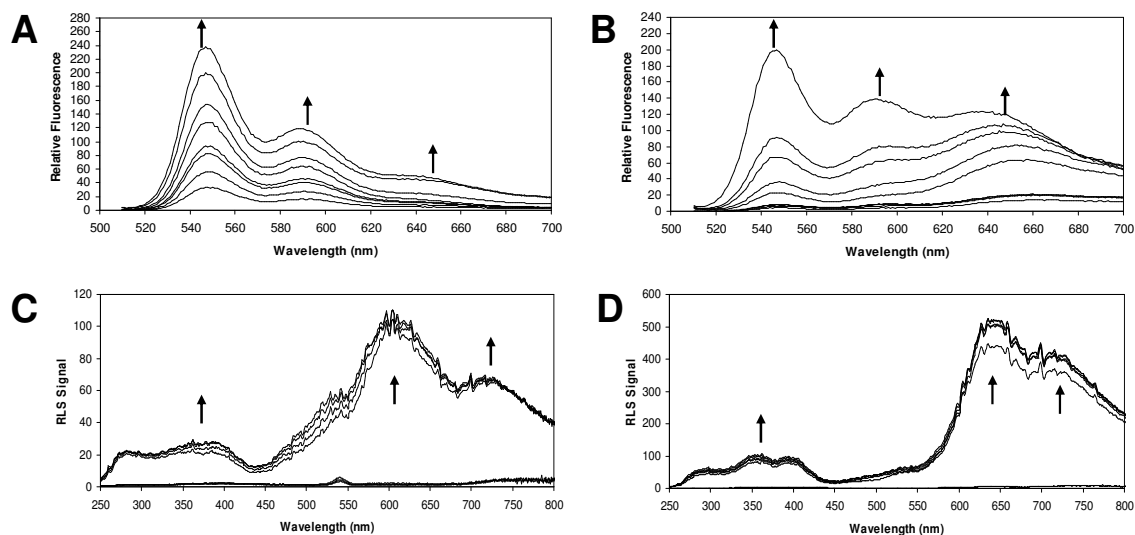


Figure 9.8. Fluorescence and Resonance light scattering of Tel45 with increasing temperature. Fluorescence of 10 μ M (A), or 100 μ M (B) Tel 45 at 5, 10, 15, 20, 25, 30, 40 and 50 °C (arrows indicate fluorescence changes observed as temperature increases). Resonance Light Scattering of 10 μ M (C), or 100 μ M (D) Tel 45 at temperatures ranging from 5 to 100 °C; a large increase in RLS signal was observed upon heating to 30 °C and 25 °C for 10 and 100 μ M Tel45 respectively.

These results agree with the observed UV-Vis spectral changes and indicate that Tel45 is capable of forming fluorescent J-like aggregates by increasing temperature and Tel12 can form H-aggregates upon Zn^{2+} binding. It also appears that the aggregates formed by Tel45 are stable between 30-50 °C, after which further temperature increments start favoring the monomeric species. Therefore at physiological temperature (37 °C) Tel45 should be significantly aggregated and display preferential binding to G-quadruplexes. The two types of aggregation can be used to broaden the understanding as to how PTCDI aggregation is related to G-quadruplex selectivity.

9.2. G-Quadruplex DNA Selectivity

9.2.1. Visible Absorbance Spectroscopy Experiment

9.2.1.1. DNA binding in the presence of Zn^{2+} -mediated aggregation

As discussed in section 8.3.1, visible absorbance spectroscopy is a useful tool to investigate the interactions between perylene diimides and DNA structures. Spectral changes upon addition of DNA are indicative of formation of DNA-drug complexes (197). Experiments were carried out in BPS buffer in the presence and absence of 1 or 10 equivalents zinc ions, using Tel12 and Tel11 as a negative control because they are both are charged PTCDI, negatively and positively charged respectively. The absorbance spectra of 10 μ M solutions of the perylene analogs with and without zinc were monitored after addition of 1 equivalent G4'-DNA, G4-DNA or DS-DNA. As seen in Figure 9.9A, in the absence of zinc, addition of the DNA structures cause an increase in the absorbance at 510 and 550 nm for both compounds, denoting complex formation. The spectral changes of Tel12 indicate a higher preference for G4'-

DNA followed by G4-DNA, and to a lesser extent, DS-DNA. Conversely, Tel11 displays similar spectral shifts in the presence of both quadruplex and duplex DNA, indicating lower G-quadruplex binding selectivity than that observed for Tel12.

Addition of 10 μM Zn^{2+} (Figure 9.9B) results in aggregation of Tel12 but not Tel11. However, addition of the DNA structures at this Zn^{2+} concentration do not show significant spectral differences than those observed when no zinc is present. It is possible that the nucleic acids sequester available zinc, resulting in a non-aggregated Tel12 species. To test this idea, higher concentrations of zinc were employed (100 μM , Figure 9.9C); the control compound Tel11 did not experience any changes in DNA binding in the presence of Zn^{2+} under these conditions. In contrast, addition of 100 μM $\text{Zn}(\text{NO}_3)_2$ caused diminished binding of Tel12 to double stranded-DNA as judged by the minor differences between the spectra of the aggregated PTCDI and that in the presence of ds-DNA. Contrary to the behavior observed after addition of duplex DNA, the spectra of Tel12 in the presence of G4' and G4-DNA at 100 μM Zn^{2+} result in the formation of marked peaks at 550 nm, which indicate binding to these structures and thus a higher preference for quadruplex DNA under aggregating conditions. However, there is a slight decrease in the intensity of these peaks compared to those observed in the absence of Zn^{2+} , suggesting that the preference for quadruplex over duplex structures is accompanied by an overall decrease in DNA binding.

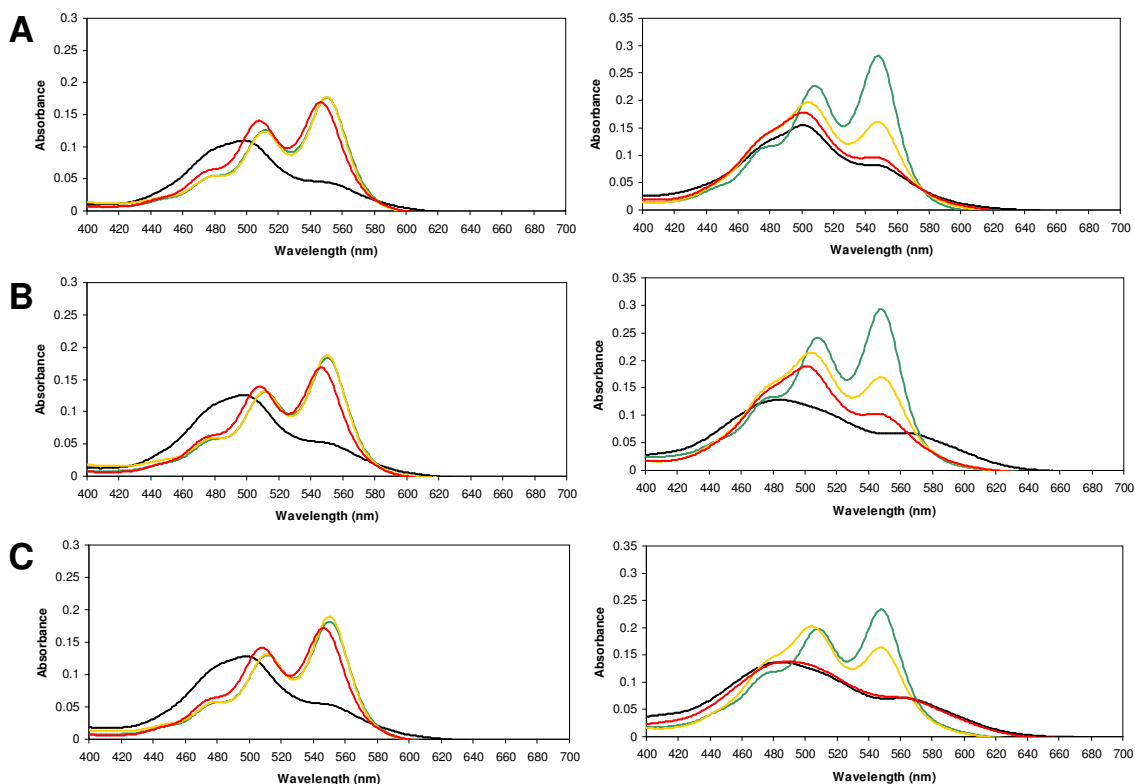


Figure 9.9. UV-Vis Spectra of Tel11 and Tel12 in the presence of Zn^{2+} with quadruplex and duplex DNA. Spectra of 10 μM Tel11 (left panels) and Tel12 (right panels) alone (black line) or in the presence of 10 μM G4-DNA, [d(TAGGGTTA)]₄ (yellow line), G4'-DNA, [d(TTAGGG)]₄ (green line) or DS-DNA, [d(CGCGCGATATCGCGCG)]₂ (red line) at (A) 0 (B) 10 or (C) 100 μM $Zn(NO_3)_2$.

An estimate of the effect of metal-mediated aggregation on G-quadruplex DNA binding selectivity can be obtained by comparing the changes in absorbance at 550 nm for both PTCIDIs under different Zn^{2+} concentrations after addition of G4'-DNA, G4-DNA, and ds-DNA. When the ligands exhibit a larger change in the absorbance at 550 nm in the presence of G-quadruplex DNA when compared to the absorbance change upon addition of duplex DNA they are considered more selective than when spectral changes at 550 nm are similar in the presence of both DNA structures. Table 9.1 summarizes the observed quadruplex-binding selectivity under the different Zn^{2+} concentrations employed. As the zinc concentration increases from 0 μM to 10 μM and then to 100 μM

there is a large increase in the selectivity for both G4' and G4-DNA compared to DS-DNA for Tel12; there is over a 6-fold increase in quadruplex selectivity at 100 μM Zn^{2+} . In contrast, the binding ratios for the control compound Tel11 are largely unaffected by addition of Zn^{2+} . The data indicates that the Tel12 metal-mediated aggregation is correlated with an increase in quadruplex binding selectivity, particularly for G4' structures.

Table 9.1. Relationship between metal-mediated PTCDI aggregation and G-Quadruplex Selectivity

Zn^{2+} Conc. (μM)	PTDCI	$\Delta A_{550\text{nm}}$ ^a in the presence of			Relative G4' Selectivity ^b	Relative G4 Selectivity ^c
		G4'- DNA	G4- DNA	DS- DNA		
0	Tel11	0.132	0.132	0.117	1.12	1.13
	Tel12	0.221	0.101	0.033	6.62	3.01
10	Tel11	0.131	0.135	0.112	1.17	1.21
	Tel12	0.196	0.078	0.014	14.31	5.70
100	Tel11	0.128	0.136	0.111	1.15	1.22
	Tel12	0.160	0.092	0.004	43.65	25.01

^a Difference between the $A_{550\text{nm}}$ of a 10 μM solution of the PTCDI in BPS buffer, pH 7, in the presence of the DNA sample (10 μM structure) and in the absence of the DNA; DNA structures used were G4'-DNA, [d(TTAGGG)₄], G4-DNA, [d(TAGGGTTA)₄], and DS-DNA, [d(CGCGCGATATCGCGCG)₂]

^b Ratio of $\Delta A_{550\text{nm}}$ in the presence of G4'-DNA to $\Delta A_{550\text{nm}}$ in the presence of ds-DNA

^c Ratio of $\Delta A_{550\text{nm}}$ in the presence of G4-DNA to $\Delta A_{550\text{nm}}$ in the presence of ds-DNA

9.2.1.2. DNA binding in the presence of temperature-dependant aggregation.

Spectral changes of Tel45 in 170 mM potassium phosphate buffer, pH 7 were monitored in the presence of G4'-DNA, G4-DNA or DS DNA with increasing temperature; the PTCDI Tel11 was used as negative control because it does not exhibit temperature-dependant aggregation. As seen in figure Figure 9.10A, at 20 °C, where Tel45 does not form aggregates, the spectra of this ligand indicates binding to G4'-DNA, followed by G4-DNA and to a lesser extent, DS-DNA. As the temperature increases to 40 and 50 °C, there is evidence of aggregate formation concomitant with an overall decrease in DNA binding, especially for the duplex sequence (Figure 9.10 B and C). In contrast, Tel11 binding to all the DNA structures remained relatively unaffected by these temperature changes. Figure 9.10B shows that at 40 °C, which is a temperature below the melting point of all of the DNA structures, there are only modest spectral differences between the spectra of Tel45 in the presence and absence of double-stranded DNA. On the other hand, there are significant spectral shifts in the presence of G4'-DNA. Similar to the results obtained from Zn²⁺-mediated Tel12 aggregation, the data implies that the temperature dependant aggregation of Tel45 results in a reduction of double-stranded-DNA binding and therefore a preference for quadruplex structures when the PTCDis are aggregated. An estimate of the quadruplex-binding selectivity was done by comparing the absorbance changes at 550 nm of both PTCDis in the presence of G4', G4 and DS-DNA at temperatures ranging from 20 to 90°C; the results are summarized in Table 9.2.

There is almost a 3 and 1.5-fold increase in G4' and G4-DNA binding respectively when the temperature increases from 20 °C to 40 °C. In contrast, Tel11 quadruplex selectivity is slightly diminished after the same temperature raise. At 70 °C (Figure 9.10D) there is less Tel45 binding observed to any of the DNA structures which could be related to a combination of factors including a lower amount of Tel45 aggregates present in solution, melting of the DNA

structures, and an overall diminished affinity for nucleic acids with aggregation. This is reflected on the lack of quadruplex selectivity observed for Tel45 at temperatures above 70 °C (Table 9.2). The quadruplex selectivity index of Tel11 is also diminished at higher temperatures. These results suggest that Tel45 temperature mediated aggregation increases G-quadruplex binding selectivity for a temperature window between 30 and 50 °C.

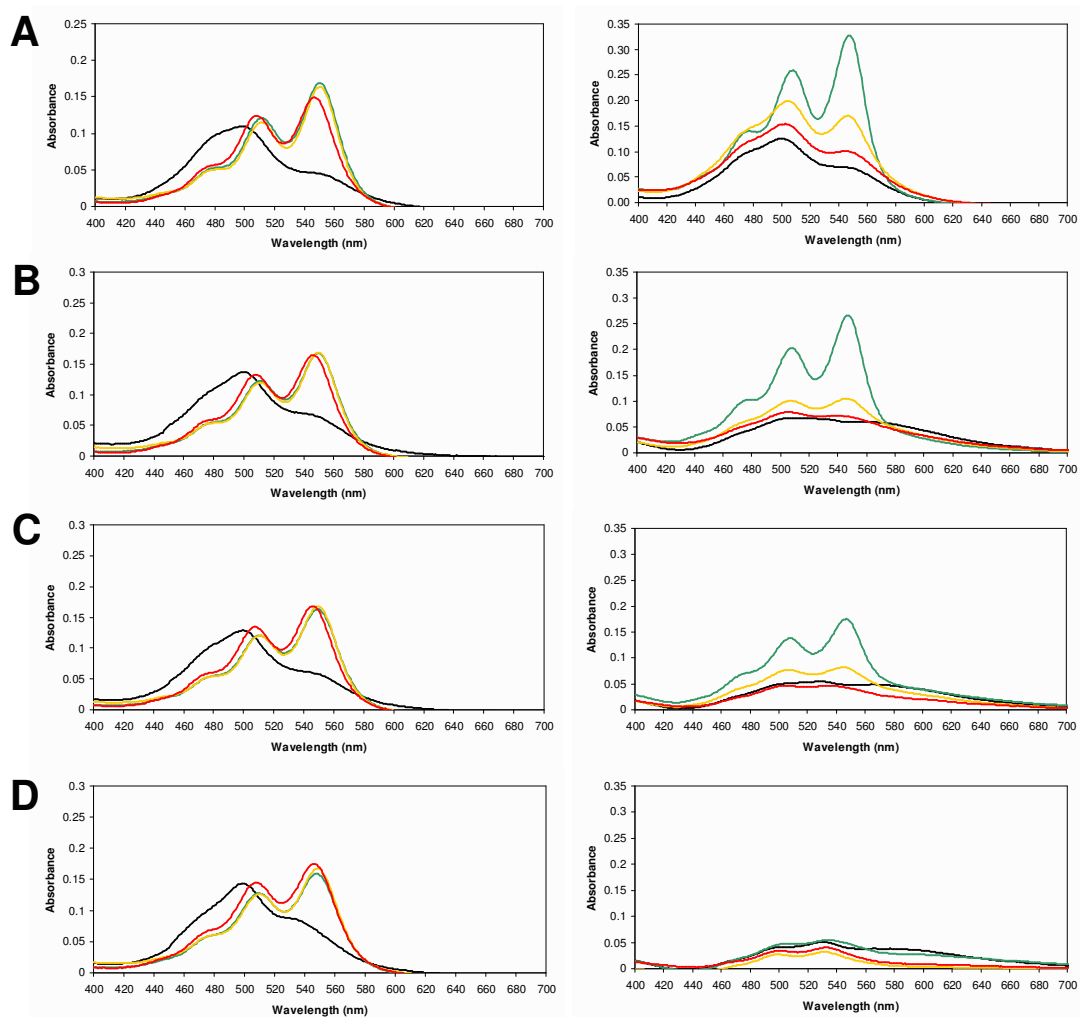


Figure 9.10. UV-Vis Spectra of Tel11 and Tel45 at different temperatures in the presence of quadruplex and duplex DNA. Spectra of 10 μ M Tel11 (left panels) or Tel45 (right panels) alone (black line) or in the presence of 10 μ M G4-DNA, [d(TAGGGTTA)]₄ (yellow line), G4'-DNA, [d(TTAGGG)₄] (green line) or DS-DNA, [d(CGCGCATATCGCGG)]₂ (red line) at (A) 20 °C (B) 40 °C (C) 50 °C, or (D) 70 °C

Table 9.2. Relationship between temperature dependant PTCDI aggregation and G-Quadruplex Selectivity

Temp. (°C)	PTCDI	ΔA_{550nm}^a in the presence of			Relative G4' Selectivity ^b	Relative G4 Selectivity ^c
		G4'- DNA	G4- DNA	DS- DNA		
20	Tel11	0.124	0.119	0.099	1.25	1.20
	Tel45	0.253	0.098	0.031	8.14	3.15
30	Tel11	0.114	0.116	0.100	1.14	1.16
	Tel45	0.240	0.069	0.022	10.85	3.11
40	Tel11	0.104	0.106	0.094	1.10	1.12
	Tel45	0.197	0.043	0.009	21.61	4.67
50	Tel11	0.105	0.111	0.103	1.03	1.08
	Tel45	0.121	0.031	0.006	18.75	4.74
70	Tel11	0.093	0.102	0.104	0.89	0.98
	Tel45	0.008	0.021	0.012	0.63	1.65
90	Tel11	0.018	0.051	0.068	0.26	0.75
	Tel45	0.015	0.022	0.015	0.98	1.42

^a Difference between the A_{550nm} of a 10 μ M solution of the PTCDI in the presence of the DNA sample (10 μ M structure) and in the absence of the DNA; DNA structures used were G4'-DNA, [d(TTAGGG)₄], G4-DNA, [d(TAGGGTTA)₄], and DS-DNA, [d(CGCGCGATATCGCGCG)₂]

^b Ratio of ΔA_{550nm} in the presence of G4'-DNA to ΔA_{550nm} in the presence of ds-DNA

^c Ratio of ΔA_{550nm} in the presence of G4-DNA to ΔA_{550nm} in the presence of ds-DNA

9.2.2. Surface Plasmon Resonance Experiments

To further understand how perylene diimides ligands interact with G-quadruplex structures, Surface Plasmon Resonance (SPR) analysis were carried out in conjunction with Bodin Tuesuwan and Dr. Wendi David at Texas State University. Tel11 was chosen as a representative candidate of the PTCDI family and the well characterized G-Quadruplex interactive agent, TmPyP₄ (Figure 7.14B) was used as a control to investigate their differences in binding affinity and kinetics. PTCDI aggregation was not investigated using this technique due to potential clogging of the instrument's fluidics system. A biotinylated intramolecular human telomeric sequence, 5' biotinylated- (TTAGGG)₄TT was immobilized on a streptavidin coated chip, and the binding of the two ligands was monitored by injecting solutions of varying ligand concentrations in running buffer. The sensograms obtained are shown in Figure 9.11.

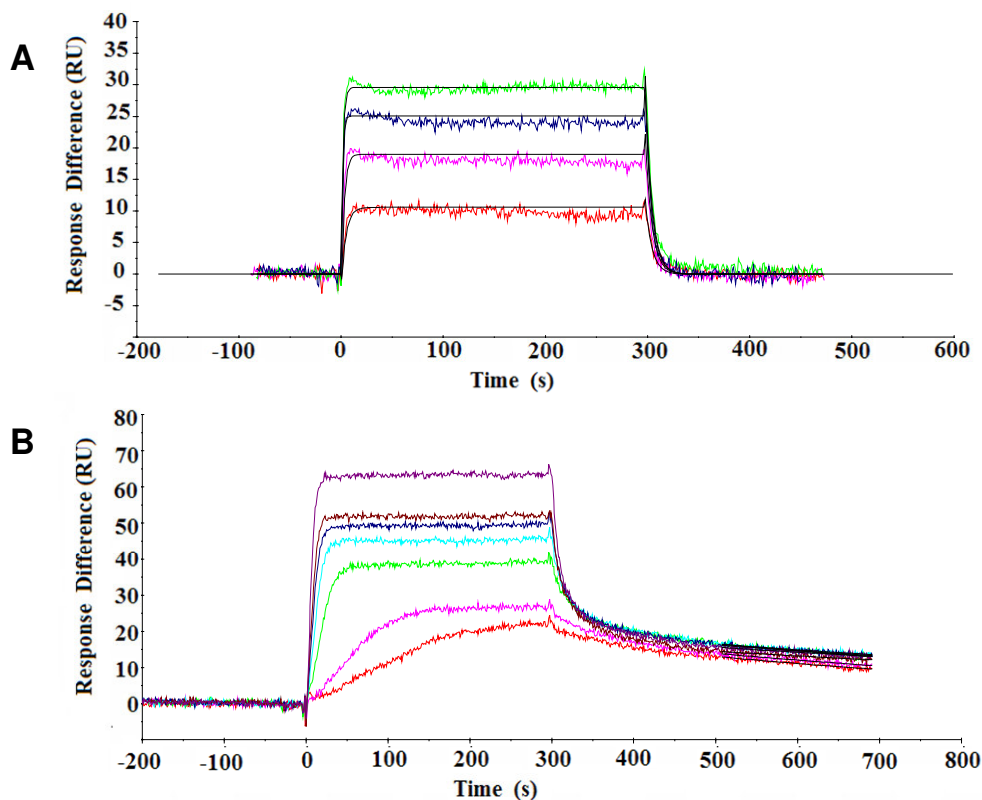


Figure 9.11. SPR sensograms TMPyP₄ and Tel11 binding to G4' human telomeric DNA. The interaction of 5' biotinylated- (TTAGGG)₄TT in HBS-EP buffer supplemented with 200 mM K⁺ quadruplex was monitored with increasing ligand concentrations; 50 μ l were injected at a flow rate of 10 μ L/min. (A) Injections of TMPyP₄ at 50, 150, 300, and 450 nM concentration. (B) Tel11 injections solutions were 5, 10, 50, 100, 150, 200, and 350 nM.

The two molecules exhibited very different binding behaviors. TmPyP₄ displayed a fast k_{on} and k_{off} rates at all the concentrations studied (Figure 9.11A). This compound also reached steady-state equilibrium almost immediately after the start of the injections and dissociated rapidly from the quadruplex substrate directly after the injection end. The observed RU (response units) in the steady-state region were plotted against the concentration of TMPyP₄ to calculate its binding constant ($K_A = 6.04 \cdot 10^6 \text{ M}^{-1}$, $K_D = 16.6 \text{ }\mu\text{M}$). The kinetic k_{on} and k_{off} values were also determined using the 1:1 Langmuir binding model using the BIAevaluation software ($8.05 \cdot 10^5 \text{ M}^{-1}$ and 0.133 s^{-1}).

On the other hand, as seen in Figure 9.11B, Tel11 presented a much slower dissociation rate; in fact, consecutive regeneration buffer injections were

required to return to the original baseline levels (buffer flow was sufficient to regenerate the surface in the case of TMPyP₄). Closer inspection revealed that there is an initial fast dissociation at higher Tel11 concentrations, but after approximately 80 seconds the dissociation phase is similar at all the concentrations studied. Plotting the differential RU units in the steady state regions of the sensograms did not fit well to a 1:1 binding model. In addition, the differential behavior observed at higher compound concentrations complicated the calculations for kinetic constants. Fitting of k_{off} separately from k_{on} in BIAevaluation software beginning 80 seconds after the injection end gave a value of $1.4 \pm 0.1 \cdot 10^{-3} \text{ s}^{-1}$ for all the Tel11 concentrations studied, which is two orders of magnitude slower than the rate observed for TMPyP₄. Furthermore, in contrast to the porphyrin compound, Tel11 does not reach steady state equilibrium rapidly at the lower concentrations tested. Overall, the observed kinetic behavior suggests that Tel11 possesses two different binding modes; at low compound concentrations there is tighter, more specific binding with a slow dissociation while at higher concentrations there is a less specific binding mode. These results are in agreement with the observed fluorescence quenching and circular dichroism experiments that indicate that multiple ligands are able to associate with a quadruplex structure. It is likely that the higher specificity binding mode corresponds to the initial G-tetrad end-stacking interactions while the non-specific interactions involve chromophore aggregation onto the DNA substrate.

9.3. Cell entry and cytotoxicity

A549 (human lung cancer) and MCF-7 (human breast cancer) cells were treated with 20 μM Tel11, Tel12 or Tel45 for 24 h after which their morphology was analyzed by microscopic analysis. Cellular entry varied considerably

depending on the PTCDI used. Tel 11–treated cells (Figure 9.12A) exhibited overall red staining which was most intense in the nucleus, suggesting nuclear localization. The observed staining is not uniform within the nucleus, which could indicate binding to specific Treatment with Tel12 resulted in large aggregates, both in the media and surrounding the cells (Figure 9.12B), while incubation with Tel45 also formed aggregated species of smaller size (Figure 9.12C). However, although aggregate formation has promising potential in G-quadruplex selectivity, neither Tel12 nor Tel45 stained the cells red which could be interpreted as no cellular uptake.

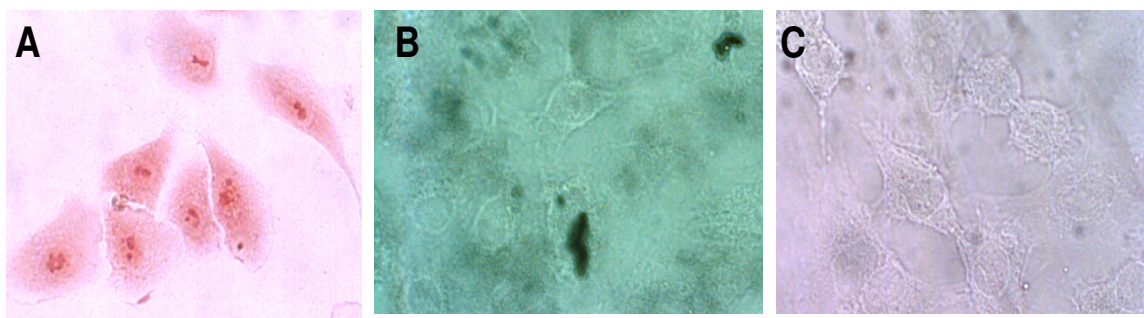


Figure 9.12. Cellular localization of A549 cells treated with Tel11, Tel12 and Tel45. A549 cells grown on chamber slides were treated with 20 μ M Tel11 (A), Tel12 (B), or Tel18 (C) for 24 h before microscopic analysis.

To further verify if any of the aggregated species were entering the cells they were visualized using fluorescence microscopy. Cells were fixed and propidium iodide (PI) was used to stain the nucleus. PI displays fluorescence when bound to nucleic acids, the absorption maximum for PI is 535 nm and the fluorescence emission maximum is 617 nm). Cells were also examined under the FITC filter which is in the fluorescence range of perylene diimides (FITC excitation maxima is 494nm, and emission is 518nm). Figure 9.13 shows the results obtained in MCF-7 cells in the absence (panels A and B) and presence of 20 μ M Tel12 (panels C and D) or Tel45 (panels E and F). Treatment with Tel12 appears to surround the cells, making it difficult to discern if there is cellular entry on cells treated with this compound.

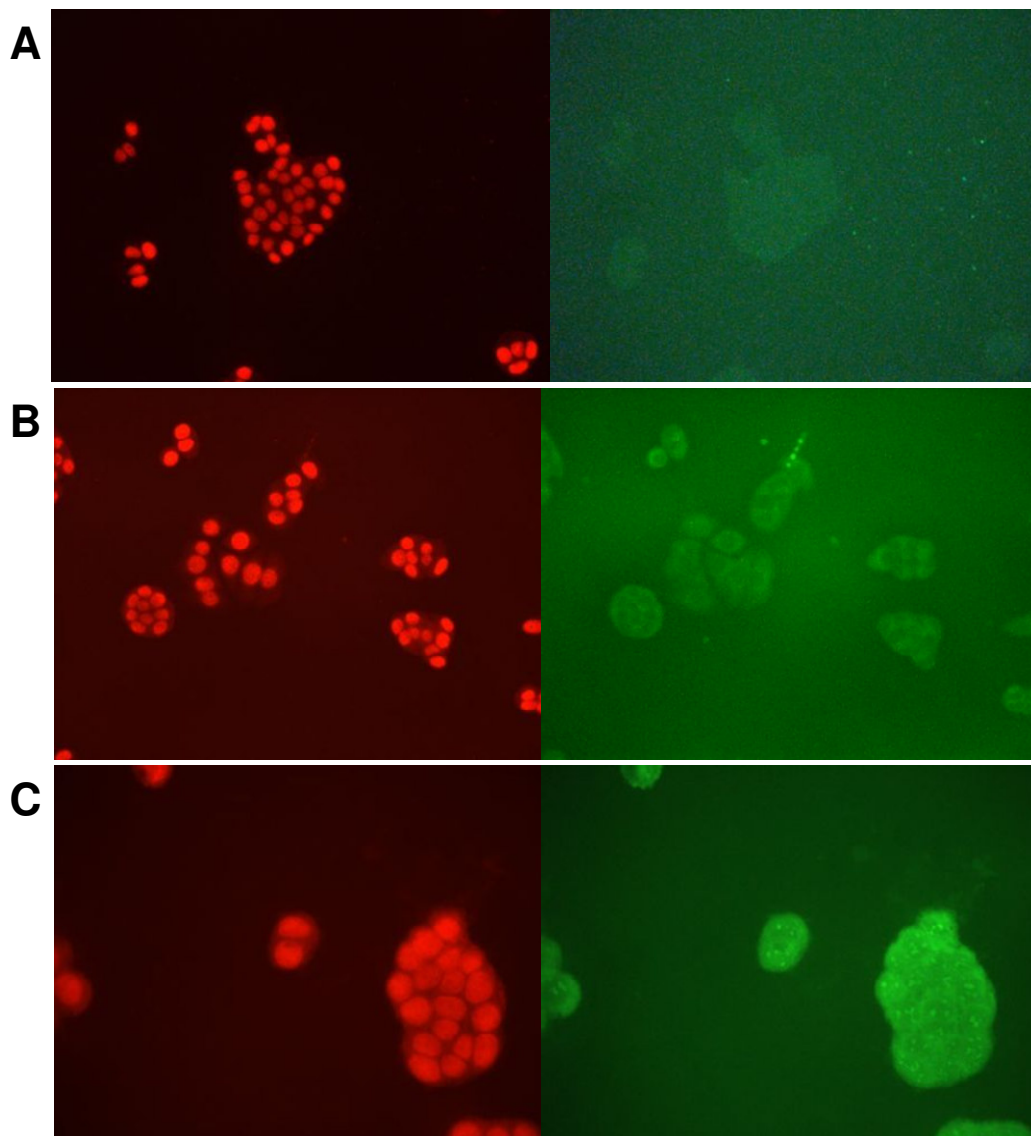


Figure 9.13. *Fluorescence micrographs of MCF-7 cells.* MCF-7 cells were fixed with mounting media containing PI and visualized under a PI filter (left panels) or a FITC filter (right panels). Cells were left untreated (A), or incubated for 24 h with 20 μ M Tel12 (B) or Tel 45 (C) prior to visualization.

In contrast, treatment with Tel45 show fluorescence in the cytoplasmic region of treated cells, which indicates that although this analog forms aggregates in the media, it is able to enter the cells. This is particularly clear from

micrographs of Tel45 in A549 cells that display bright fluorescence in the cytoplasm when stained with this PTCDI (Figure 9.14).

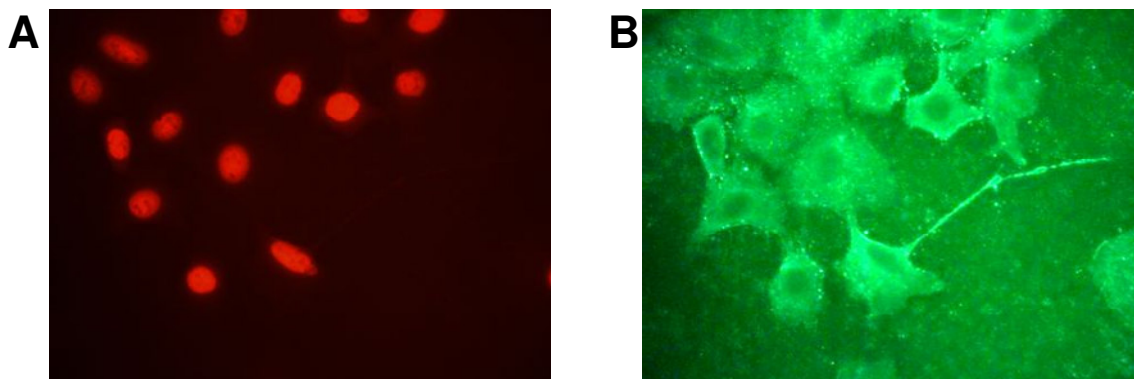


Figure 9.14. *Fluorescence micrographs of A549 cells.* A549 cells were treated for 24 h with 20 μ M Tel45 and subsequently fixed with mounting media which contains PI and visualized under a PI filter (left panels) or a FITC filter (right panels).

It is evident that charge plays an important role in the cellular entry of the PTCDI ligands. The positively charged Tel11 is able to enter the cells and can bind to the nucleus. In contrast, the negatively charged Tel12 appears to aggregate on the media and cellular surface. Although the neutral compound Tel45 also aggregates in the media it does appear to enter the cells from its fluorescence properties. The aggregation of Tel45 was confirmed by fluorescence and RLS at the concentrations employed for this study; the ligand displays fluorescence at 655 nm and RLS signal in both A549 and MCF-7 cell media at 37 $^{\circ}$ C but not at 20 $^{\circ}$ C (Figure 9.15).

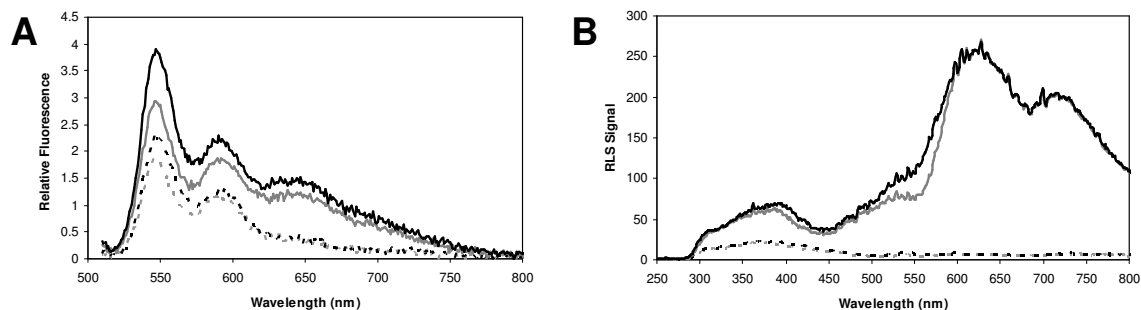


Figure 9.15. Fluorescence and RLS of Tel45 in cell culture media. Fluorescence emission (ex = 500 nm) spectra (A) and RLS signal (B) of 20 μM Tel45 in A549 (black lines) or MCF-7 (gray lines) cell culture media at 20 $^{\circ}\text{C}$ (dashed lines) or 37.5 $^{\circ}\text{C}$ (solid lines)

Cellular cytotoxicity was also evaluated in MCF-7 and A549 cells using the AlamarBlue assay after treating the cells with varying concentrations of Tel11, Tel12, and Tel45 for 72 h. Because these ligands have a high intrinsic fluorescence, the fluorescence response at each ligand concentration tested was subtracted from the values calculated using the assay. The cytotoxicity values obtained are shown in Table 9.3. Tel11 displayed activity in both cells lines with IC_{50} values of 4 and 18 μM for MCF-7 and A549 cells respectively. Tel45 displayed similar levels in MCF-7 cells ($\text{IC}_{50} = 2 \mu\text{M}$) but exhibited less than 50% cell death at the highest concentration studied (100 μM). Tel12 was the least cytotoxic analog, with no apparent inhibition of cellular growth in the concentration range studied. It is possible that the extensive aggregation or negative charge of Tel12 prohibits its cellular entry and therefore no cellular death is observed. This makes sense in regards to the positively charged Tel11 which experienced an overall lower cytotoxicity; it is possible that the positive charge in Tel11 facilitates its interactions with DNA. The neutral Tel45 is only partially successful in killing the cancer cells, but it still has a larger effect than compound Tel12. Furthermore, the observation that Tel45 can form aggregates at physiological conditions could indicate that this compound is binding preferentially at the nucleus (where the fluorescence is quenched in the micrographs).

Table 9.3 Cytotoxicity of MCF-7 or A549 cells treated with PTCDI analogs during 72h. Cellular proliferation was assayed using the AlamarBlue assay. IC₅₀ values represent 50% growth inhibition relative to cell treated with vehicle alone

Compound	IC ₅₀ for MCF7 (μM)	IC ₅₀ for A549 (μM)
Tel11	4.3 ± 1.3	18 ± 4
Tel12	>100	>100
Tel45	1.7±0.6	>100
MMC	0.59 ± 0.08	0.39 ± 0.09

9.4. Conclusions

This study has illustrated several of the mechanisms that affect perylene diimide aggregation and their biological properties. Tel12, with its negatively charged phosphate groups, can aggregate in the presence of metal cations, particularly in the presence of Zn²⁺ ions. Tel45 was designed with MEM groups to facilitate metal-mediated aggregation. In spite of this, no aggregation was observed with any of the metal cations used in this study even in organic solutions. However, this analog unexpectedly displayed aggregation at higher temperatures. This unusual behavior has been reported for perylene diimides synthesized by Wang *et al.* which contain alternating single-stranded DNA and planar PTCDI chromophores (212).

The metal- and thermal-mediated aggregation of Tel12 and Tel45 respectively allowed for evaluation of their G-quadruplex selectivity. Both compounds displayed enhancement in selectivity upon aggregation, particularly for G4' structures. In contrast, the positively charged compound Tel11 does not aggregate in any of the pH ranges studied, nor is influenced by temperature changes or metal coordination; it displays similar affinities for duplex and both

inter and intra-molecular quadruplexes under the conditions studied. Nevertheless, ligand-DNA ratios determined by fluorescence quenching and SPR experiments indicate that Tel11 may aggregate upon binding to DNA structures. In addition, its positive charge may aid in its interactions with DNA and cell death observed in cultured cells.

Cells treated Tel11 show that this compound is capable of entering cells and is preferentially located in specific portions of the nucleus. Tel12 and Tel45 form aggregate structures in the media and on the cellular surface. In spite of the lack of visible red staining, fluorescence microscopy showed that both compounds fluoresce within the cells, suggesting that these ligands are at least partially capable of cell entry. Cytotoxicity studies showed that Tel11 was highly cytotoxic, while Tel12 and Tel45 only displayed moderate cytotoxicity. The observed behavior for Tel12 and Tel45 can be related to their lower cellular incorporation compared to Tel11.

In general, the water soluble perylene diimides present different but interesting interactions with DNA. The positively charged Tel11 can translocate into the nucleus and induce cytotoxicity in cells perhaps aided by its charge. Tel12 displays aggregation upon metal coordination and a higher preference for G-quadruplex in *in vitro* studies, but its negative charge could present problems for cellular entry. The neutral compound Tel45 is particularly important because its aggregation occurs at physiologically relevant temperatures and appears to be capable of entering cells with specificity for the nucleus.

CHAPTER 10. SUMMARY AND FUTURE DIRECTIONS

10.1. Summary

G-Quadruplexes are four stranded nucleic acid structures which can form in G-rich sequences such as telomeric regions. There is continuously increasing evidence that these unique four-stranded structures not only occur in vitro but also have biological significance. Furthermore, computational studies have shown that there is at least one putative quadruplex sequence (PQS) in over 40% of all human promoter sequences. G-Quadruplexes have thus emerged as an important target for drug design both to inhibit enzymes that interact at G-rich regions of the genome, such as telomerase, and to control the transcriptional regulation of genes with PQS. Moreover, G-quadruplex interactive molecules may not only be used as therapeutic agents but can also be used as biophysical probes to investigate the biological role of quadruplexes in cells. It is therefore vital to understand the mechanisms that regulate drug-DNA interactions in order to design compounds that specifically target quadruplexes.

One group of compounds that is capable of binding G-quadruplexes are the perylene diimides tetracarboxylic acid diimides (PTCDIs). Original studies observed a correlation between the aggregation state of PTCDI ligands at varying pH values and their selectivity for G-quadruplex DNA versus duplex DNA. This work expanded on the initial studies by investigating a series of PTCDIs with different structural features under high and low salt buffers, changes in pH, metal binding and temperature changes. Studies performed at low and high salt buffers at pH values ranging from 6 to 8 indicated that compounds whose side chain basicity was dependant on pH, such as PIPER and Tel01, displayed pH-dependent aggregation concomitant with G-quadruplex selectivity. The charged perylenes Tel11 and Tel12, and the bay-substituted compound Tel18 were not significantly affected by pH changes. It was also observed that

analogs with extended benz-annulated ring systems in the perylene core displayed promising G-quadruplex selectivity but also exhibited decreased solubility, impeding accurate characterization of their DNA interactions.

Tel12, with its negatively charged phosphate side chains was able to form abundant H-aggregates in the presence of Zn^{2+} ions, and was the only PTCDI studied that displayed metal-mediated aggregation in aqueous buffers. Under conditions where the ligand was aggregated, less pronounced binding to duplex DNA was observed by UV-Vis. On the other hand, the positively charged analog Tel11 was not able to form aggregates under any of the conditions used, and did not present marked structural selectivity. Nonetheless, Tel11 was able to enter the nuclei of cultured cells and displayed cellular toxicity. The aggregation state of a new PTCDI with hydrophilic methoxyethoxymethyl groups, Tel45, was also examined. It was observed that this compound could form unusual fluorescent aggregates similar to reported PTCDI J-aggregates in a novel- thermal dependant fashion. This compound was the most selective for quadruplex structures at temperatures where it displayed aggregation. In addition, it was observed that Tel45 was able to enter the cells and exhibit cellular cytotoxicity under aggregating conditions. Overall, this work supports the idea that ligand aggregation increases quadruplex selectivity by decreasing double-stranded DNA binding. These findings can be used to design more G-quadruplex selective ligands with increased solubility and cellular/nuclear entry.

10.2. Future Directions

New PTCDI analogs are currently being designed to have improved physical properties and potential interaction with the tetrads of G-quadruplexes. Benz-annulated analogs of Tel45 (such as in Figure 10.1A) could display increased π - π stacking interactions with G-tetrads and retain solubility by having hydrophilic side chains. Ansa-bridged PTCDIs (Figure 10.1B) could also display

decreased interactions with double stranded DNA analogous to PTCDI aggregation.

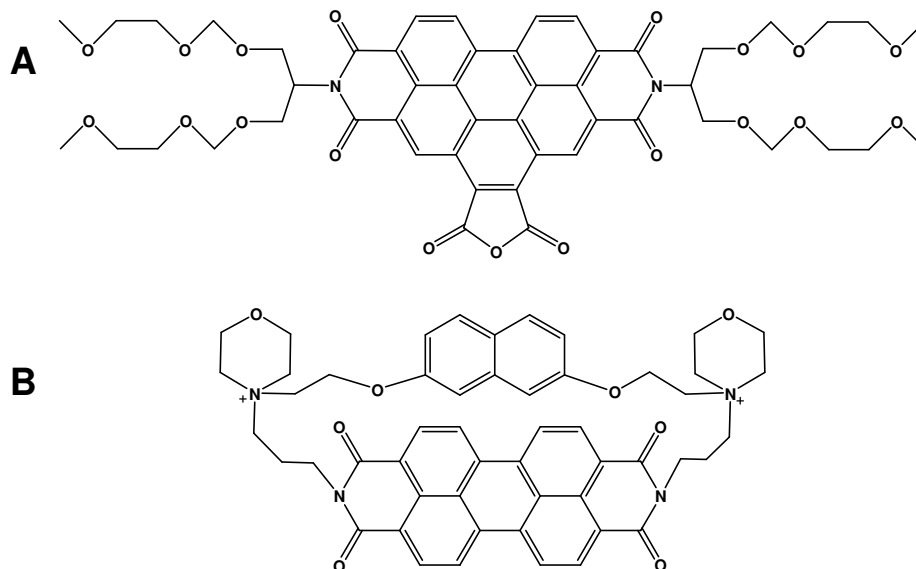


Figure 10.1. Future PTCDI analogs. (A) Benz-annulated analog of Tel45. (B) Ansa-bridged analog of Tel01

In addition to synthesizing new analogs, the effects of PTCDI ligands are currently being studied with G-quadruplex-processing enzymes. The results from this work can be adapted to study enzyme inhibition with quadruplex and duplex substrates under experimental conditions that affect ligand aggregation. Aside from G-quadruplex interactions, this work also has implications in cell imaging and supramolecular chemistry. Supramolecular polymers formed by PTCDIs have potential applications in optical devices, photosensitizers, and as fluorescent probes. The ease of formation of aggregates in conjunction with their fluorescence properties make the perylene diimides studied here valuable polymer building blocks. In particular, the unusual thermophilic J- like aggregates formed by Tel45 display increased fluorescence upon ligand aggregation, properties that should be exploited and require further investigation. It is also important to investigate whether having a positive charge within aggregated species could facilitate cellular entry and retain G-quadruplex specificity.

CHAPTER 11. EXPERIMENTALS FOR PART II

11.1. General Information

Unless otherwise noted, all materials were obtained from commercial suppliers and used without further purification. PTCDI analogs PIPER, Tel01, Tel11, Tel12, Tel18, Tel32 and Tel34 were synthesized by Jonathan Kern (181, 186, 187). The new analog Tel45 was synthesized by Dr. Sean Kerwin (unpublished results). Stock solutions of Tel01 and PIPER were prepared in 0.1% trifluoroacetic acid; Tel11, Tel12, Tel18, and Tel45 in deionized water, Tel32 and Tel34 in dimethylsulfoxide and stored at room temperature.

11.2. DNA Synthesis

Oligonucleotides were synthesized on a 10 or 1 μ M scale in columns from Glen Research (Sterling, VA) using a Perceptive Biosystems Expedite 8909 automatic DNA synthesizer using a DMT-on or DMT-off procedure. Quadruplex forming sequences included G5-DNA, [d(T₂G₅T)₄]; G4-DNA, [d(TAGGGTTA)₄]; and G4'-DNA, [d(TTAGGG)₄]. The self-complimentary duplex-forming sequences used were oligos [d(CGCGCGATATCGCGCG)₂] and [d(GCAAATTTTCG)₂] and the single-stranded sequence employed was d(T)₈.

The oligos were cleaved from the column and purified with Poly-Pak (II) Cartridges (Glen Research, Sterling, VA) when synthesized with DMT-on strategy, or by RP-HPLC when synthesized with a DMT group off. HPLC collected fractions were dialyzed against deionized water and completely

lyophilized. The oligos were then annealed by preparing a 2mM stock solution in buffer (3:1 25 mM ammonium acetate/methanol buffer (pH 7), 70 mM potassium phosphate, 100 mM potassium chloride, 1 mM EDTA buffer (pH 7), or BPS buffer consisting of 8 mM sodium phosphate, 185 mM NaCl (pH 7) as indicated in the text) by heating to 90 °C for five minutes, and slowly letting them cool down to room temperature. Quadruplex forming sequences were also submitted to two successive freeze-thaw cycles. Select structures were confirmed by CD spectroscopy and are included in Appendix D.

11.3. Fluorescence and RLS Spectroscopy

Spectra were recorded on a Hitachi model F-2000 spectrofluorometer or a Cary-Varian Fluorescence spectrophotometer. Quartz and glass cuvettes were treated with SigmaCote (Cat. No. SI2, Sigma Aldrich, St. Louis, MO) for 1 h followed by extensive washing with water to minimize nonspecific binding of the ligands to the surface of the cuvette. Fluorescence and resonance light scattering (RLS) measurements were carried out on the ligands under both high- and low-salt conditions. The high-salt conditions employed solutions of compound in 70 mM potassium phosphate, 100 mM potassium chloride, 1 mM EDTA buffer at the indicated pH. Low-salt conditions employed solutions of compound in 3:1 25 mM ammonium acetate/methanol at the indicated pH. Solutions were allowed to equilibrate for the specified time before scans were performed at 25 °C using the noted excitation and emission wavelengths.

Tel12 Zn⁺²-mediated aggregation were carried in BPS buffer consisting of 8 mM sodium phosphate, 185 mM NaCl, pH 7.0, at 1 and 10 μM ligand and the indicated metal cation concentrations. Thermal studies were performed using a Varian Peltier temperature controller, varying the temperature from 5 to 100 °C.

11.4. Visible and absorbance Spectroscopy

Spectra were recorded on Varian Cary Spectrophotometer. Experiments were carried out in polystyrene cuvettes or quartz cuvettes treated with SigmaCote to minimize nonspecific binding of the ligands to the surface of the cuvettes. For DNA binding experiments, the absorption spectra were obtained under high and low salt conditions. For the high salt conditions, the compound (20 μM) in 70 mM potassium phosphate, 100 mM potassium chloride, 1 mM EDTA buffer (pH 7) was analyzed alone or in the presence 20 μM structure of G4-DNA [d(TAGGGTTA)]₄, G4'-DNA [d(TTAGGG)]₄ double-stranded DNA [d(CGCGCGATATCGCGCG)]₂, or single-stranded DNA d(TTTTTTTT). For the low salt conditions, the compound (10 μM) in 3:1 25 mM ammonium acetate/methanol was analyzed alone or in the presence of 10 μM structure of G4-DNA [d(TTGGGGGT)]₄, double-stranded DNA [d(GCAAATTTTCG)]₂ or single-stranded DNA d(TTTTTTTT). Samples were monitored until equilibrium was achieved, as evidenced by constant absorbance readings.

For metal-mediated aggregation studies the utilized aqueous buffers were 50 mM potassium Cacodylate (pH =7.4), or BPS buffer consisting of 8 mM sodium phosphate, 185 mM NaCl (pH 7.0). Spectra were recorded in the presence and absence of the following salts: Mg(NO₃)₂, Ca(NO₃)₂, Zn(NO₃)₂, Ni(NO₃)₂, Cu(NO₃)₂, Co(NO₃)₂, Fe(NO₃)₂, and Fe(NO₃)₃. Tel45 studies were also carried out in dichloromethane/methanol in the presence of (CF₃SO₃)₂Zn, CF₃SO₃Ag, and Cu(ClO₄)₂.

11.5. Circular Dichroism

Determination of CD spectrum was carried out on a JASCO-J815 CD spectropolarimeter. The instrument conditions were as follows: scan range, 320

200 nm; scan speed, 100 nm/min; quartz cell length, 1 mm; accumulation times, 2; temperature, 25 °C. Samples containing the only the buffer of interest were used for reference subtraction.

11.6. Surface Plasmon Resonance Experiments

The SPR experiments were performed using a Biacore X instrument on streptavidin-coated SA5 sensor chips (part no. BR-1000-32, from BIAcore, Piscataway, NJ) with HBS-EP buffer (10 mM HEPES, 150 mM NaCl, 3 mM EDTA, 0.005% v/v polysorbate 20, pH 7.4). Sensor chips were prepared and derivatized as described in section 6.3. Flow cell 1 was used as a reference cell, and flow cell 2 was immobilized with 243 RU units of 5'-Bio-TEG-(TTAGGG)₄TT-3' oligonucleotide (Integrated DNA Technologies, Coralville, IA). Intramolecular G-quadruplex formation was facilitated by addition of KCl (200 mM) to the running and storage buffers.

Samples of TMPyP₄ and Tel11 were prepared in running buffer and injected manually (50 µL) at different concentrations using a flow rate of 10 µL/min, with delayed wash of 420 s. The surface was regenerated by injection of running buffer in the case of TMPyP₄, but required alternating injections of running buffer, 5% DMSO, and 1% P20 for injections of Tel11. All binding responses were determined by subtraction of the reference flow cell 1. Fitting of steady-state equilibrium binding constants and kinetic association and dissociation curves was performed using BIAevaluation software supplied with the Biacore X instrument.

11.7. Cytotoxicity Assays

Cell viability was determined using the AlamarBlue assay as described in section 6.5. MCF-7 and A549 cells were treated with 2 μ l of compound in DMSO at different concentrations and incubated during 72 h at 37 °C prior to data evaluation. There was no effect on the growth of cells compared to that of cells in culture media alone at this DMSO concentration. Tel11, Tel12, and Tel45, along with Mitomycin-C (part no. 100498, from MP Biomedicals, Solon, OH) as a positive control were evaluated at final concentrations ranging from 0.005 to 100 μ M. IC₅₀ values were determined as described in section 6.5.

11.8. Fluorescence detection of PTCDI cellular entry

A549 and MCF-7 cells were grown at 37 °C, trypsinized, and inoculated into four chambered slide plates (Lab Tek II part no. 125652, Nalgene Nunc International, Rochester, NY) at approximately 1.0×10^5 cells per well. Cells were grown at 24 h at 37 °C before treatment with PTCDI analogs at 20 μ M or vehicle for an additional 24 h. Both sets of cells were collected after 24 following treatment. Cells were then fixed in ice-cold 1:1 methanol/acetone for 10 minutes and air-dried. Following three washes with PBS, the slides were then mounted using VectorShield mount (VectorLabs, part no. H-1300, Burlingame, CA) containing PI to stain the nucleus. Evaluation of fluorescence cell morphology was performed using a Nikon TMS-100 phase contrast microscope and images were captured using a Nikon CoolSnap digital camera and images were processed using MetaMorph imaging software.

REFERENCES FOR PART II

1. Watson, J. D., and Crick, F. H. (1953) Molecular structure of nucleic acids; a structure for deoxyribose nucleic acid, *Nature* 171, 737-738.
2. Wang, J. C. (1979) Helical repeat of DNA in solution, *Proc Natl Acad Sci U S A* 76, 200-203.
3. Mandelkern, M., Elias, J. G., Eden, D., and Crothers, D. M. (1981) The dimensions of DNA in solution, *J Mol Biol* 152, 153-161.
4. Ghosh, A., and Bansal, M. (2003) A glossary of DNA structures from A to Z, *Acta Crystallogr D Biol Crystallogr* 59, 620-626.
5. Bates, A. D., and Maxwell, A. (2005) *DNA topology*, 2nd ed., Oxford University Press, Oxford ; New York.
6. Wahl, M. C., and Sundaralingam, M. (1997) Crystal structures of A-DNA duplexes, *Biopolymers* 44, 45-63.
7. Blackburn, G. M., and Royal Society of Chemistry (Great Britain) (2006) *Nucleic acids in chemistry and biology*, 3rd ed., RSC Pub., Cambridge.
8. Wang, G., and Vasquez, K. M. (2007) Z-DNA, an active element in the genome, *Front Biosci* 12, 4424-4438.
9. Herbert, A., and Rich, A. (1996) The biology of left-handed Z-DNA, *J Biol Chem* 271, 11595-11598.
10. Phan, A. T., Kuryavyi, V., and Patel, D. J. (2006) DNA architecture: from G to Z, *Curr Opin Struct Biol* 16, 288-298.
11. Wadkins, R. M. (2000) Targeting DNA secondary structures, *Curr Med Chem* 7, 1-15.
12. Bukowiecka-Matusiak, M., and Wozniak, L. A. (2006) [DNA structure from A to Z--biological implications of structural diversity of DNA], *Postepy Biochem* 52, 229-238.
13. Courey, A. J. (1999) Analysis of altered DNA structures: cruciform DNA, *Methods Mol Biol* 94, 29-40.
14. Timsit, Y., and Moras, D. (1996) Cruciform structures and functions, *Q Rev Biophys* 29, 279-307.
15. Liu, Y., and West, S. C. (2004) Happy Hollidays: 40th anniversary of the Holliday junction, *Nat Rev Mol Cell Biol* 5, 937-944.
16. Holliday, R. A. (1964) A mechanism for gene conversion in fungi., *Genet Res Camb* 5, 282-304.
17. Chan, P. P., and Glazer, P. M. (1997) Triplex DNA: fundamentals, advances, and potential applications for gene therapy, *J Mol Med* 75, 267-282.
18. Frank-Kamenetskii, M. D., and Mirkin, S. M. (1995) Triplex DNA structures, *Annu Rev Biochem* 64, 65-95.
19. Gilbert, D. E., and Feigon, J. (1999) Multistranded DNA structures, *Curr Opin Struct Biol* 9, 305-314.

20. Gellert, M., Lipsett, M. N., and Davies, D. R. (1962) Helix formation by guanylic acid, *Proc Natl Acad Sci U S A* 48, 2013-2018.
21. Sen, D., and Gilbert, W. (1990) A sodium-potassium switch in the formation of four-stranded G4-DNA, *Nature* 344, 410-414.
22. Sen, D., and Gilbert, W. (1988) Formation of parallel four-stranded complexes by guanine-rich motifs in DNA and its implications for meiosis, *Nature* 334, 364-366.
23. Guschlbauer, W., Chantot, J. F., and Thiele, D. (1990) Four-stranded nucleic acid structures 25 years later: from guanosine gels to telomer DNA, *J Biomol Struct Dyn* 8, 491-511.
24. Wang, Y., and Patel, D. J. (1992) Guanine residues in d(T2AG3) and d(T2G4) form parallel-stranded potassium cation stabilized G-quadruplexes with anti glycosidic torsion angles in solution, *Biochemistry* 31, 8112-8119.
25. Hardin, C. C., Henderson, E., Watson, T., and Prosser, J. K. (1991) Monovalent cation induced structural transitions in telomeric DNAs: G-DNA folding intermediates, *Biochemistry* 30, 4460-4472.
26. Kerwin, S. M. (2000) G-Quadruplex DNA as a target for drug design, *Curr Pharm Des* 6, 441-478.
27. Sa-Carvalho, D., and Traub-Cseko, Y. M. (1995) Sequences with high propensity to form G-quartet structures in kinetoplast DNA from *Phytomonas serpens*, *Mol Biochem Parasitol* 72, 103-109.
28. Simonsson, T. (2001) G-quadruplex DNA structures--variations on a theme, *Biol Chem* 382, 621-628.
29. Gehring, K., Leroy, J. L., and Gueron, M. (1993) A tetrameric DNA structure with protonated cytosine-cytosine base pairs, *Nature* 363, 561-565.
30. Gueron, M., and Leroy, J. L. (2000) The i-motif in nucleic acids, *Curr Opin Struct Biol* 10, 326-331.
31. Phan, A. T., and Mergny, J. L. (2002) Human telomeric DNA: G-quadruplex, i-motif and Watson-Crick double helix, *Nucleic Acids Res* 30, 4618-4625.
32. Lee, J. Y., Okumus, B., Kim, D. S., and Ha, T. (2005) Extreme conformational diversity in human telomeric DNA, *Proc Natl Acad Sci U S A* 102, 18938-18943.
33. Krafft, C., Benevides, J. M., and Thomas, G. J., Jr. (2002) Secondary structure polymorphism in *Oxytricha nova* telomeric DNA, *Nucleic Acids Res* 30, 3981-3991.
34. Li, J., Correia, J. J., Wang, L., Trent, J. O., and Chaires, J. B. (2005) Not so crystal clear: the structure of the human telomere G-quadruplex in solution differs from that present in a crystal, *Nucleic Acids Res* 33, 4649-4659.

35. Mills, M., Lacroix, L., Arimondo, P. B., Leroy, J. L., Francois, J. C., Klump, H., and Mergny, J. L. (2002) Unusual DNA conformations: implications for telomeres, *Curr Med Chem Anticancer Agents* 2, 627-644.
36. Wang, Y., and Patel, D. J. (1993) Solution structure of the human telomeric repeat d[AG₃(T₂AG₃)₃] G-tetraplex, *Structure* 1, 263-282.
37. Parkinson, G. N., Lee, M. P., and Neidle, S. (2002) Crystal structure of parallel quadruplexes from human telomeric DNA, *Nature* 417, 876-880.
38. Zhang, X. Y., Cao, E. H., Zhang, Y., Chou, C., and Bai, C. (2003) K⁺ and Na⁺-induced self-assembly of telomeric oligonucleotide d(TTAGGG)_n, *J Biomol Struct Dyn* 20, 693-702.
39. Ying, L., Green, J. J., Li, H., Klenerman, D., and Balasubramanian, S. (2003) Studies on the structure and dynamics of the human telomeric G quadruplex by single-molecule fluorescence resonance energy transfer, *Proc Natl Acad Sci U S A* 100, 14629-14634.
40. Phan, A. T., Luu, K. N., and Patel, D. J. (2006) Different loop arrangements of intramolecular human telomeric (3+1) G-quadruplexes in K⁺ solution, *Nucleic Acids Res* 34, 5715-5719.
41. Luu, K. N., Phan, A. T., Kuryavyi, V., Lacroix, L., and Patel, D. J. (2006) Structure of the human telomere in K⁺ solution: an intramolecular (3 + 1) G-quadruplex scaffold, *J Am Chem Soc* 128, 9963-9970.
42. Petraccone, L., Erra, E., Esposito, V., Randazzo, A., Mayol, L., Nasti, L., Barone, G., and Giancola, C. (2004) Stability and structure of telomeric DNA sequences forming quadruplexes containing four G-tetrads with different topological arrangements, *Biochemistry* 43, 4877-4884.
43. Gros, J., Rosu, F., Amrane, S., De Cian, A., Gabelica, V., Lacroix, L., and Mergny, J. L. (2007) Guanines are a quartet's best friend: impact of base substitutions on the kinetics and stability of tetramolecular quadruplexes, *Nucleic Acids Res* 35, 3064-3075.
44. Risitano, A., and Fox, K. R. (2003) Stability of intramolecular DNA quadruplexes: comparison with DNA duplexes, *Biochemistry* 42, 6507-6513.
45. Xue, Y., Kan, Z. Y., Wang, Q., Yao, Y., Liu, J., Hao, Y. H., and Tan, Z. (2007) Human Telomeric DNA Forms Parallel-Stranded Intramolecular G-Quadruplex in K(+) Solution under Molecular Crowding Condition, *J Am Chem Soc*.
46. Miyoshi, D., Karimata, H., and Sugimoto, N. (2006) Hydration regulates thermodynamics of G-quadruplex formation under molecular crowding conditions, *J Am Chem Soc* 128, 7957-7963.
47. Kan, Z. Y., Yao, Y., Wang, P., Li, X. H., Hao, Y. H., and Tan, Z. (2006) Molecular crowding induces telomere G-quadruplex formation under salt-deficient conditions and enhances its competition with duplex formation, *Angew Chem Int Ed Engl* 45, 1629-1632.

48. Miyoshi, D., Nakao, A., and Sugimoto, N. (2002) Molecular crowding regulates the structural switch of the DNA G-quadruplex, *Biochemistry* 41, 15017-15024.
49. Yu, H. Q., Miyoshi, D., and Sugimoto, N. (2006) Characterization of structure and stability of long telomeric DNA G-quadruplexes, *J Am Chem Soc* 128, 15461-15468.
50. Kang, C., Zhang, X., Ratliff, R., Moyzis, R., and Rich, A. (1992) Crystal structure of four-stranded Oxytricha telomeric DNA, *Nature* 356, 126-131.
51. Chen, F. M. (1992) Sr²⁺ facilitates intermolecular G-quadruplex formation of telomeric sequences, *Biochemistry* 31, 3769-3776.
52. Williamson, J. R., Raghuraman, M. K., and Cech, T. R. (1989) Monovalent cation-induced structure of telomeric DNA: the G-quartet model, *Cell* 59, 871-880.
53. Inoue, M., Miyoshi, D., and Sugimoto, N. (2005) Structural switch of telomere DNA by pH and monovalent cation, *Nucleic Acids Symp Ser (Oxf)*, 243-244.
54. Marathias, V. M., and Bolton, P. H. (1999) Determinants of DNA quadruplex structural type: sequence and potassium binding, *Biochemistry* 38, 4355-4364.
55. Lu, M., Guo, Q., and Kallenbach, N. R. (1992) Structure and stability of sodium and potassium complexes of dT4G4 and dT4G4T, *Biochemistry* 31, 2455-2459.
56. Miura, T., Benevides, J. M., and Thomas, G. J., Jr. (1995) A phase diagram for sodium and potassium ion control of polymorphism in telomeric DNA, *J Mol Biol* 248, 233-238.
57. Schultze, P., Hud, N. V., Smith, F. W., and Feigon, J. (1999) The effect of sodium, potassium and ammonium ions on the conformation of the dimeric quadruplex formed by the Oxytricha nova telomere repeat oligonucleotide d(G(4)T(4)G(4)), *Nucleic Acids Res* 27, 3018-3028.
58. Zakian, V. A. (1995) Telomeres: beginning to understand the end, *Science* 270, 1601-1607.
59. Makarov, V. L., Hirose, Y., and Langmore, J. P. (1997) Long G tails at both ends of human chromosomes suggest a C strand degradation mechanism for telomere shortening, *Cell* 88, 657-666.
60. Wright, W. E., Tesmer, V. M., Huffman, K. E., Levene, S. D., and Shay, J. W. (1997) Normal human chromosomes have long G-rich telomeric overhangs at one end, *Genes Dev* 11, 2801-2809.
61. Griffith, J. D., Comeau, L., Rosenfield, S., Stansel, R. M., Bianchi, A., Moss, H., and de Lange, T. (1999) Mammalian telomeres end in a large duplex loop, *Cell* 97, 503-514.
62. Olovnikov, A. M. (1973) A theory of marginotomy. The incomplete copying of template margin in enzymic synthesis of polynucleotides and biological significance of the phenomenon, *J Theor Biol* 41, 181-190.

63. Bryan, T. M., and Cech, T. R. (1999) Telomerase and the maintenance of chromosome ends, *Curr Opin Cell Biol* 11, 318-324.
64. Allsopp, R. C., Chang, E., Kashefi-Azham, M., Rogaev, E. I., Piatyszek, M. A., Shay, J. W., and Harley, C. B. (1995) Telomere shortening is associated with cell division in vitro and in vivo, *Exp Cell Res* 220, 194-200.
65. Harley, C. B., Futcher, A. B., and Greider, C. W. (1990) Telomeres shorten during ageing of human fibroblasts, *Nature* 345, 458-460.
66. Levy, M. Z., Allsopp, R. C., Futcher, A. B., Greider, C. W., and Harley, C. B. (1992) Telomere end-replication problem and cell aging, *J Mol Biol* 225, 951-960.
67. Counter, C. M. (1996) The roles of telomeres and telomerase in cell life span, *Mutat Res* 366, 45-63.
68. Linskens, M. H., Harley, C. B., West, M. D., Campisi, J., and Hayflick, L. (1995) Replicative senescence and cell death, *Science* 267, 17.
69. Shay, J. W., and Wright, W. E. (2000) Hayflick, his limit, and cellular ageing, *Nat Rev Mol Cell Biol* 1, 72-76.
70. Bryan, T. M., Englezou, A., Dunham, M. A., and Reddel, R. R. (1998) Telomere length dynamics in telomerase-positive immortal human cell populations, *Exp Cell Res* 239, 370-378.
71. Hertzog, R. G. (2006) Ancestral telomere shortening: a countdown that will increase mean life span?, *Med Hypotheses* 67, 157-160.
72. Kyo, S., and Inoue, M. (2002) Complex regulatory mechanisms of telomerase activity in normal and cancer cells: how can we apply them for cancer therapy?, *Oncogene* 21, 688-697.
73. Greider, C. W., and Blackburn, E. H. (1985) Identification of a specific telomere terminal transferase activity in Tetrahymena extracts, *Cell* 43, 405-413.
74. Shippen-Lentz, D., and Blackburn, E. H. (1990) Functional evidence for an RNA template in telomerase, *Science* 247, 546-552.
75. Shida, T. (1995) [Structure of four-stranded telomeric DNA], *Tanpakushitsu Kakusan Koso* 40, 1578-1582.
76. Smith, F. W., and Feigon, J. (1992) Quadruplex structure of Oxytricha telomeric DNA oligonucleotides, *Nature* 356, 164-168.
77. Oganessian, L., and Bryan, T. M. (2007) Physiological relevance of telomeric G-quadruplex formation: a potential drug target, *Bioessays* 29, 155-165.
78. Han, H., and Hurley, L. H. (2000) G-quadruplex DNA: a potential target for anti-cancer drug design, *Trends Pharmacol Sci* 21, 136-142.
79. Tsai, Y. C., Qi, H., and Liu, L. F. (2007) Protection of DNA ends by telomeric 3' G-tail sequences, *J Biol Chem* 282, 18786-18792.
80. Paeschke, K., Simonsson, T., Postberg, J., Rhodes, D., and Lipps, H. J. (2005) Telomere end-binding proteins control the formation of G-quadruplex DNA structures in vivo, *Nat Struct Mol Biol* 12, 847-854.

81. Zahler, A. M., Williamson, J. R., Cech, T. R., and Prescott, D. M. (1991) Inhibition of telomerase by G-quartet DNA structures, *Nature* **350**, 718-720.
82. Kim, N. W., Piatyszek, M. A., Prowse, K. R., Harley, C. B., West, M. D., Ho, P. L., Coviello, G. M., Wright, W. E., Weinrich, S. L., and Shay, J. W. (1994) Specific association of human telomerase activity with immortal cells and cancer, *Science* **266**, 2011-2015.
83. Shay, J. W., and Bacchetti, S. (1997) A survey of telomerase activity in human cancer, *Eur J Cancer* **33**, 787-791.
84. Siddiqui-Jain, A., Grand, C. L., Bearss, D. J., and Hurley, L. H. (2002) Direct evidence for a G-quadruplex in a promoter region and its targeting with a small molecule to repress c-MYC transcription, *Proc Natl Acad Sci U S A* **99**, 11593-11598.
85. Yang, D., and Hurley, L. H. (2006) Structure of the biologically relevant G-quadruplex in the c-MYC promoter, *Nucleosides Nucleotides Nucleic Acids* **25**, 951-968.
86. Rangan, A., Fedoroff, O. Y., and Hurley, L. H. (2001) Induction of duplex to G-quadruplex transition in the c-myc promoter region by a small molecule, *J Biol Chem* **276**, 4640-4646.
87. Guo, K., Pourpak, A., Beetz-Rogers, K., Gokhale, V., Sun, D., and Hurley, L. H. (2007) Formation of Pseudosymmetrical G-Quadruplex and i-Motif Structures in the Proximal Promoter Region of the RET Oncogene, *J Am Chem Soc* **129**, 10220-10228.
88. Phan, A. T., Kuryavyi, V., Burge, S., Neidle, S., and Patel, D. J. (2007) Structure of an unprecedented G-quadruplex scaffold in the human c-kit promoter, *J Am Chem Soc* **129**, 4386-4392.
89. Kumari, S., Bugaut, A., Huppert, J. L., and Balasubramanian, S. (2007) An RNA G-quadruplex in the 5' UTR of the NRAS proto-oncogene modulates translation, *Nat Chem Biol* **3**, 218-221.
90. Dai, J., Chen, D., Jones, R. A., Hurley, L. H., and Yang, D. (2006) NMR solution structure of the major G-quadruplex structure formed in the human BCL2 promoter region, *Nucleic Acids Res* **34**, 5133-5144.
91. Cogoi, S., and Xodo, L. E. (2006) G-quadruplex formation within the promoter of the KRAS proto-oncogene and its effect on transcription, *Nucleic Acids Res* **34**, 2536-2549.
92. Dexheimer, T. S., Sun, D., and Hurley, L. H. (2006) Deconvoluting the structural and drug-recognition complexity of the G-quadruplex-forming region upstream of the bcl-2 P1 promoter, *J Am Chem Soc* **128**, 5404-5415.
93. Skoblov, M., Shakhbazov, K., Oshchepkov, D., Ivanov, D., Guskova, A., Rubtsov, P., Prasolov, V., Yankovsky, N., and Baranova, A. (2006) Human RFP2 gene promoter: unique structure and unusual strength, *Biochem Biophys Res Commun* **342**, 859-866.

94. Dai, J., Dexheimer, T. S., Chen, D., Carver, M., Ambrus, A., Jones, R. A., and Yang, D. (2006) An intramolecular G-quadruplex structure with mixed parallel/antiparallel G-strands formed in the human BCL-2 promoter region in solution, *J Am Chem Soc* *128*, 1096-1098.
95. Sun, D., Guo, K., Rusche, J. J., and Hurley, L. H. (2005) Facilitation of a structural transition in the polypurine/polypyrimidine tract within the proximal promoter region of the human VEGF gene by the presence of potassium and G-quadruplex-interactive agents, *Nucleic Acids Res* *33*, 6070-6080.
96. Rankin, S., Reszka, A. P., Huppert, J., Zloh, M., Parkinson, G. N., Todd, A. K., Ladame, S., Balasubramanian, S., and Neidle, S. (2005) Putative DNA quadruplex formation within the human c-kit oncogene, *J Am Chem Soc* *127*, 10584-10589.
97. Cogoi, S., Quadrioglio, F., and Xodo, L. E. (2004) G-rich oligonucleotide inhibits the binding of a nuclear protein to the Ki-ras promoter and strongly reduces cell growth in human carcinoma pancreatic cells, *Biochemistry* *43*, 2512-2523.
98. Jansson, B. (1996) Potassium, sodium, and cancer: a review, *J Environ Pathol Toxicol Oncol* *15*, 65-73.
99. Nagy, I., Lustyik, G., Lukacs, G., Nagy, V., and Balazs, G. (1983) Correlation of malignancy with the intracellular Na⁺:K⁺ ratio in human thyroid tumors, *Cancer Res* *43*, 5395-5402.
100. Bortner, C. D., and Cidlowski, J. A. (1998) A necessary role for cell shrinkage in apoptosis, *Biochem Pharmacol* *56*, 1549-1559.
101. Roomans, G. M., and Von Euler, A. (1996) X-ray microanalysis in cell biology and cell pathology, *Cell Biol Int* *20*, 103-109.
102. Scaria, V., Hariharan, M., Arora, A., and Maiti, S. (2006) Quadfinder: server for identification and analysis of quadruplex-forming motifs in nucleotide sequences, *Nucleic Acids Res* *34*, W683-685.
103. Huppert, J. L., and Balasubramanian, S. (2007) G-quadruplexes in promoters throughout the human genome, *Nucleic Acids Res* *35*, 406-413.
104. Kikin, O., D'Antonio, L., and Bagga, P. S. (2006) QGRS Mapper: a web-based server for predicting G-quadruplexes in nucleotide sequences, *Nucleic Acids Res* *34*, W676-682.
105. Huppert, J. L., and Balasubramanian, S. (2005) Prevalence of quadruplexes in the human genome, *Nucleic Acids Res* *33*, 2908-2916.
106. Todd, A. K., Johnston, M., and Neidle, S. (2005) Highly prevalent putative quadruplex sequence motifs in human DNA, *Nucleic Acids Res* *33*, 2901-2907.
107. Gross, D. S., and Garrard, W. T. (1988) Nuclease hypersensitive sites in chromatin, *Annu Rev Biochem* *57*, 159-197.
108. Riou, J. F., Gomez, D., Lemarteleur, T., and Trentesaux, C. (2003) [G-quadruplex DNA: myth or reality?], *Bull Cancer* *90*, 305-313.

109. Schaffitzel, C., Berger, I., Postberg, J., Hanes, J., Lipps, H. J., and Pluckthun, A. (2001) In vitro generated antibodies specific for telomeric guanine-quadruplex DNA react with *Stylonychia lemnae* macronuclei, *Proc Natl Acad Sci U S A* 98, 8572-8577.
110. Dong, Q. (2006) [Generation and characterization of the monoclonal antibody and scFv against yeast telomeric guanine-quadruplex DNA], *Fen Zi Xi Bao Sheng Wu Xue Bao* 39, 482-488.
111. Brown, J. C., Brown, B. A., 2nd, Li, Y., and Hardin, C. C. (1998) Construction and characterization of a quadruplex DNA selective single-chain autoantibody from a viable moth-eaten mouse hybridoma with homology to telomeric DNA binding proteins, *Biochemistry* 37, 16338-16348.
112. Fry, M. (2007) Tetraplex DNA and its interacting proteins, *Front Biosci* 12, 4336-4351.
113. Mohaghegh, P., Karow, J. K., Brosh Jr, R. M., Jr., Bohr, V. A., and Hickson, I. D. (2001) The Bloom's and Werner's syndrome proteins are DNA structure-specific helicases, *Nucleic Acids Res* 29, 2843-2849.
114. Huber, M. D., Duquette, M. L., Shiels, J. C., and Maizels, N. (2006) A conserved G4 DNA binding domain in RecQ family helicases, *J Mol Biol* 358, 1071-1080.
115. Fry, M., and Loeb, L. A. (1999) Human werner syndrome DNA helicase unwinds tetrahelical structures of the fragile X syndrome repeat sequence d(CGG)n, *J Biol Chem* 274, 12797-12802.
116. Sun, H., Karow, J. K., Hickson, I. D., and Maizels, N. (1998) The Bloom's syndrome helicase unwinds G4 DNA, *J Biol Chem* 273, 27587-27592.
117. Tuesuwan, B., Kern, J. T., Thomas, P. W., Rodriguez, M., David, W. M., Li, J., and Kerwin, S. (2007) Simian Virus 40 Large T-antigen G-Quadruplex DNA Helicase Inhibition by G-Quadruplex DNA-Interactive Agents., *Biochem*, submitted.
118. Vaughn, J. P., Creacy, S. D., Routh, E. D., Joyner-Butt, C., Jenkins, G. S., Pauli, S., Nagamine, Y., and Akman, S. A. (2005) The DEXH protein product of the DHX36 gene is the major source of tetramolecular quadruplex G4-DNA resolving activity in HeLa cell lysates, *J Biol Chem* 280, 38117-38120.
119. Baran, N., Pucshansky, L., Marco, Y., Benjamin, S., and Manor, H. (1997) The SV40 large T-antigen helicase can unwind four stranded DNA structures linked by G-quartets, *Nucleic Acids Res* 25, 297-303.
120. Li, J. L., Harrison, R. J., Reszka, A. P., Brosh, R. M., Jr., Bohr, V. A., Neidle, S., and Hickson, I. D. (2001) Inhibition of the Bloom's and Werner's syndrome helicases by G-quadruplex interacting ligands, *Biochemistry* 40, 15194-15202.
121. Han, H., Bennett, R. J., and Hurley, L. H. (2000) Inhibition of unwinding of G-quadruplex structures by Sgs1 helicase in the presence of N,N'-bis[2-(1-

- piperidino)ethyl]-3,4,9,10-perylenetetracarboxylic diimide, a G-quadruplex-interactive ligand, *Biochemistry* 39, 9311-9316.
122. Huber, M. D., Lee, D. C., and Maizels, N. (2002) G4 DNA unwinding by BLM and Sgs1p: substrate specificity and substrate-specific inhibition, *Nucleic Acids Res* 30, 3954-3961.
 123. Wu, X., and Maizels, N. (2001) Substrate-specific inhibition of RecQ helicase, *Nucleic Acids Res* 29, 1765-1771.
 124. Han, H., Langley, D. R., Rangan, A., and Hurley, L. H. (2001) Selective interactions of cationic porphyrins with G-quadruplex structures, *J Am Chem Soc* 123, 8902-8913.
 125. Giraldo, R., Suzuki, M., Chapman, L., and Rhodes, D. (1994) Promotion of parallel DNA quadruplexes by a yeast telomere binding protein: a circular dichroism study, *Proc Natl Acad Sci U S A* 91, 7658-7662.
 126. Giraldo, R., and Rhodes, D. (1994) The yeast telomere-binding protein RAP1 binds to and promotes the formation of DNA quadruplexes in telomeric DNA, *EMBO J* 13, 2411-2420.
 127. Lu, Q., Schierer, T., Kang, S. G., and Henderson, E. (1998) Purification, characterization and molecular cloning of TGP1, a novel G-DNA binding protein from *Tetrahymena thermophila*, *Nucleic Acids Res* 26, 1613-1620.
 128. Lu, Q., and Henderson, E. (2000) Two *Tetrahymena* G-DNA-binding proteins, TGP1 and TGP3, share novel motifs and may play a role in micronuclear division, *Nucleic Acids Res* 28, 2993-3001.
 129. Hanakahi, L. A., Sun, H., and Maizels, N. (1999) High affinity interactions of nucleolin with G-G-paired rDNA, *J Biol Chem* 274, 15908-15912.
 130. Arimondo, P. B., Riou, J. F., Mergny, J. L., Tazi, J., Sun, J. S., Garestier, T., and Helene, C. (2000) Interaction of human DNA topoisomerase I with G-quartet structures, *Nucleic Acids Res* 28, 4832-4838.
 131. Anuradha, S., and Muniyappa, K. (2004) Meiosis-specific yeast Hop1 protein promotes synapsis of double-stranded DNA helices via the formation of guanine quartets, *Nucleic Acids Res* 32, 2378-2385.
 132. Liu, Z., and Gilbert, W. (1994) The yeast KEM1 gene encodes a nuclease specific for G4 tetraplex DNA: implication of in vivo functions for this novel DNA structure, *Cell* 77, 1083-1092.
 133. Sun, H., Yabuki, A., and Maizels, N. (2001) A human nuclease specific for G4 DNA, *Proc Natl Acad Sci U S A* 98, 12444-12449.
 134. Duquette, M. L., Handa, P., Vincent, J. A., Taylor, A. F., and Maizels, N. (2004) Intracellular transcription of G-rich DNAs induces formation of G-loops, novel structures containing G4 DNA, *Genes Dev* 18, 1618-1629.
 135. Hanahan, D., and Weinberg, R. A. (2000) The hallmarks of cancer, *Cell* 100, 57-70.
 136. Blagosklonny, M. V. (2003) Cell immortality and hallmarks of cancer, *Cell Cycle* 2, 296-299.
 137. Kim Sh, S. H., Kaminker, P., and Campisi, J. (2002) Telomeres, aging and cancer: in search of a happy ending, *Oncogene* 21, 503-511.

138. Simonsson, T., Pecinka, P., and Kubista, M. (1998) DNA tetraplex formation in the control region of c-myc, *Nucleic Acids Res* 26, 1167-1172.
139. Alberti, P., Lacroix, L., Guittat, L., Helene, C., and Mergny, J. L. (2003) Nucleic acids as targets for antitelomerase agents, *Mini Rev Med Chem* 3, 23-36.
140. Hurley, L. H., Wheelhouse, R. T., Sun, D., Kerwin, S. M., Salazar, M., Fedoroff, O. Y., Han, F. X., Han, H., Izbicka, E., and Von Hoff, D. D. (2000) G-quadruplexes as targets for drug design, *Pharmacol Ther* 85, 141-158.
141. Mergny, J. L., and Helene, C. (1998) G-quadruplex DNA: a target for drug design, *Nat Med* 4, 1366-1367.
142. Riou, J. F. (2004) G-quadruplex interacting agents targeting the telomeric G-overhang are more than simple telomerase inhibitors, *Curr Med Chem Anticancer Agents* 4, 439-443.
143. Shin-ya, K., Wierzba, K., Matsuo, K., Ohtani, T., Yamada, Y., Furihata, K., Hayakawa, Y., and Seto, H. (2001) Telomestatin, a novel telomerase inhibitor from *Streptomyces anulatus*, *J Am Chem Soc* 123, 1262-1263.
144. Rosu, F., Gabelica, V., Shin-ya, K., and De Pauw, E. (2003) Telomestatin-induced stabilization of the human telomeric DNA quadruplex monitored by electrospray mass spectrometry, *Chem Commun (Camb)*, 2702-2703.
145. Kim, M. Y., Gleason-Guzman, M., Izbicka, E., Nishioka, D., and Hurley, L. H. (2003) The different biological effects of telomestatin and TMPyP4 can be attributed to their selectivity for interaction with intramolecular or intermolecular G-quadruplex structures, *Cancer Res* 63, 3247-3256.
146. De Cian, A., Guittat, L., Shin-ya, K., Riou, J. F., and Mergny, J. L. (2005) Affinity and selectivity of G4 ligands measured by FRET, *Nucleic Acids Symp Ser (Oxf)*, 235-236.
147. Gomez, D., Paterski, R., Lemarteleur, T., Shin-Ya, K., Mergny, J. L., and Riou, J. F. (2004) Interaction of telomestatin with the telomeric single-strand overhang, *J Biol Chem* 279, 41487-41494.
148. Tauchi, T., Shin-ya, K., Sashida, G., Sumi, M., and Okabe, S. (2006) Telomerase inhibition with a novel G-quadruplex interactive agent, telomestatin: in vitro and in vivo studies in acute leukemia, *Oncogene* 25, 5719-5725.
149. Tahara, H., Shin-ya, K., Seimiya, H., Yamada, H., and Tsuruo, T. (2006) G-Quadruplex stabilization by telomestatin induces TRF2 protein dissociation from telomeres and anaphase bridge formation accompanied by loss of the 3' telomeric overhang in cancer cells, *Oncogene* 25, 1955-1966.
150. Schuitmaker, J. J., Baas, P., van Leengoed, H. L., van der Meulen, F. W., Star, W. M., and van Zandwijk, N. (1996) Photodynamic therapy: a promising new modality for the treatment of cancer, *J Photochem Photobiol B* 34, 3-12.

151. Anantha, N. V., Azam, M., and Sheardy, R. D. (1998) Porphyrin binding to quadrupled T4G4, *Biochemistry* 37, 2709-2714.
152. Wheelhouse, R. T., Sun, D., Han, H., Han, F. X., and Hurley, L. H. (1998) Cationic Porphyrins as Telomerase Inhibitors: the Interaction of Tetra-(N-methyl-4-pyridyl)porphine with Quadruplex DNA *J Am Chem Soc* 120, 3261-3262.
153. Han, F. X., Wheelhouse, R. T., and Hurley, L. H. (1999) Interactions of TMPyP4 and TMPyP2 with Quadruplex DNA. Structural Basis for the Differential Effects on Telomerase Inhibition, *J Am Chem Soc* 121, 3561-3570.
154. Haq, I., Trent, J. O., Chowdhry, B. Z., and Jenkins, T. C. (1999) Intercalative G-Tetraplex Stabilization of Telomeric DNA by a Cationic Porphyrin, *J Am Chem Soc* 121, 1768-1779.
155. Yamashita, T., Uno, T., and Ishikawa, Y. (2005) Stabilization of guanine quadruplex DNA by the binding of porphyrins with cationic side arms, *Bioorg Med Chem* 13, 2423-2430.
156. Han, H., Hurley, L. H., and Salazar, M. (1999) A DNA polymerase stop assay for G-quadruplex-interactive compounds, *Nucleic Acids Res* 27, 537-542.
157. Shi, D. F., Wheelhouse, R. T., Sun, D., and Hurley, L. H. (2001) Quadruplex-interactive agents as telomerase inhibitors: synthesis of porphyrins and structure-activity relationship for the inhibition of telomerase, *J Med Chem* 44, 4509-4523.
158. Goncalves, D. P., Ladame, S., Balasubramanian, S., and Sanders, J. K. (2006) Synthesis and G-quadruplex binding studies of new 4-N-methylpyridinium porphyrins, *Org Biomol Chem* 4, 3337-3342.
159. Tuntiwechapikul, W., Taka, T., Bethencourt, M., Makonkawkeyoon, L., and Randall Lee, T. (2006) The influence of pH on the G-quadruplex binding selectivity of perylene derivatives, *Bioorg Med Chem Lett* 16, 4120-4126.
160. Dixon, I. M., Lopez, F., Esteve, J. P., Tejera, A. M., Blasco, M. A., Pratviel, G., and Meunier, B. (2005) Porphyrin derivatives for telomere binding and telomerase inhibition, *ChemBiochem* 6, 123-132.
161. Arthanari, H., Basu, S., Kawano, T. L., and Bolton, P. H. (1998) Fluorescent dyes specific for quadruplex DNA, *Nucleic Acids Res* 26, 3724-3728.
162. Ren, J., and Chaires, J. B. (1999) Sequence and structural selectivity of nucleic acid binding ligands, *Biochemistry* 38, 16067-16075.
163. Pasternack, R. F., Brigandi, R. A., Abrams, M. J., Williams, A. P., and Gibbs, E. J. (1990) Interactions of porphyrins and metalloporphyrins with single-stranded poly(dA) *Inorg Chem* 29, 4483-4486.
164. Pasternack, R. F., Gurrieri, S., Lauceri, R., and Purrello, R. (1996) Single-stranded nucleic acids as templates for porphyrin assembly formation, *Inorg Chim Acta* 246, 7-12.

165. Li, Y., Geyer, C. R., and Sen, D. (1996) Recognition of anionic porphyrins by DNA aptamers, *Biochemistry* 35, 6911-6922.
166. Pothukuchy, A., Ellapan, S., Gopidas, K. R., and Salazar, M. (2003) Photo-oxidation of duplex DNA with the stable trioxatriangulenium ion, *Bioorg Med Chem Lett* 13, 1491-1494.
167. Reynisson, J., Schuster, G. B., Howerton, S. B., Williams, L. D., Barnett, R. N., Cleveland, C. L., Landman, U., Harrit, N., and Chaires, J. B. (2003) Intercalation of trioxatriangulenium ion in DNA: binding, electron transfer, x-ray crystallography, and electronic structure, *J Am Chem Soc* 125, 2072-2083.
168. Pothukuchy, A., Mazzitelli, C. L., Rodriguez, M. L., Tuesuwan, B., Salazar, M., Brodbelt, J. S., and Kerwin, S. M. (2005) Duplex and quadruplex DNA binding and photocleavage by trioxatriangulenium ion, *Biochemistry* 44, 2163-2172.
169. Fox, K. R., Polucci, P., Jenkins, T. C., and Neidle, S. (1995) A molecular anchor for stabilizing triple-helical DNA, *Proc Natl Acad Sci U S A* 92, 7887-7891.
170. Read, M. A., Wood, A. A., Harrison, J. R., Gowan, S. M., Kelland, L. R., Dosanjh, H. S., and Neidle, S. (1999) Molecular modeling studies on G-quadruplex complexes of telomerase inhibitors: structure-activity relationships, *J Med Chem* 42, 4538-4546.
171. Sun, D., Thompson, B., Cathers, B. E., Salazar, M., Kerwin, S. M., Trent, J. O., Jenkins, T. C., Neidle, S., and Hurley, L. H. (1997) Inhibition of human telomerase by a G-quadruplex-interactive compound, *J Med Chem* 40, 2113-2116.
172. Harrison, R. J., Gowan, S. M., Kelland, L. R., and Neidle, S. (1999) Human telomerase inhibition by substituted acridine derivatives, *Bioorg Med Chem Lett* 9, 2463-2468.
173. White, E. W., Tanious, F., Ismail, M. A., Reszka, A. P., Neidle, S., Boykin, D. W., and Wilson, W. D. (2007) Structure-specific recognition of quadruplex DNA by organic cations: influence of shape, substituents and charge, *Biophys Chem* 126, 140-153.
174. Chen, Q., Kuntz, I. D., and Shafer, R. H. (1996) Spectroscopic recognition of guanine dimeric hairpin quadruplexes by a carbocyanine dye, *Proc Natl Acad Sci U S A* 93, 2635-2639.
175. Shafer, R. H. (1998) Stability and structure of model DNA triplexes and quadruplexes and their interactions with small ligands, *Prog Nucleic Acid Res Mol Biol* 59, 55-94.
176. Ren, J., and Chaires, J. B. (2000) Preferential Binding of 3,3'-Diethyloxadicarbocyanine to Triplex DNA, *J Am Chem Soc* 122, 424-425.
177. Kerwin, S. M., Sun, D., Kern, J. T., Rangan, A., and Thomas, P. W. (2001) G-quadruplex DNA binding by a series of carbocyanine dyes, *Bioorg Med Chem Lett* 11, 2411-2414.

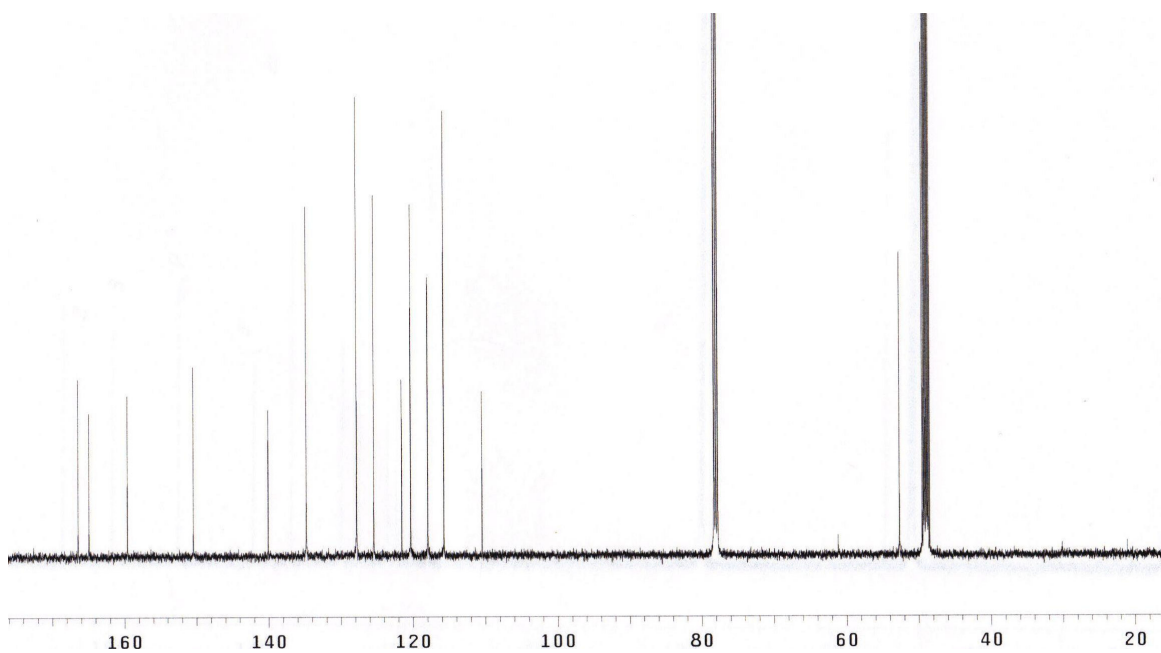
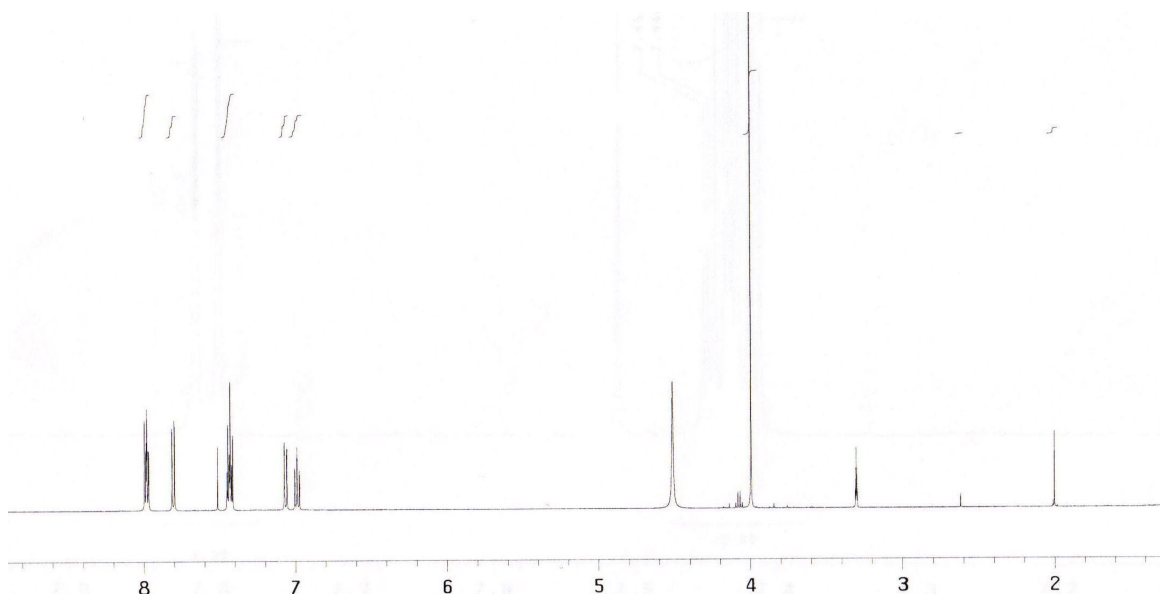
178. Fedoroff, O. Y., Salazar, M., Han, H., Chemeris, V. V., Kerwin, S. M., and Hurley, L. H. (1998) NMR-Based model of a telomerase-inhibiting compound bound to G-quadruplex DNA, *Biochemistry* **37**, 12367-12374.
179. Han, H., Cliff, C. L., and Hurley, L. H. (1999) Accelerated assembly of G-quadruplex structures by a small molecule, *Biochemistry* **38**, 6981-6986.
180. Kerwin, S. M., Chen, G., Kern, J. T., and Thomas, P. W. (2002) Perylene diimide G-quadruplex DNA binding selectivity is mediated by ligand aggregation, *Bioorg Med Chem Lett* **12**, 447-450.
181. Kern, J. T., Thomas, P. W., and Kerwin, S. M. (2002) The relationship between ligand aggregation and G-quadruplex DNA selectivity in a series of 3,4,9,10-perylenetetra-carboxylic acid diimides, *Biochemistry* **41**, 11379-11389.
182. Rossetti, L., Franceschin, M., Bianco, A., Ortaggi, G., and Savino, M. (2002) Perylene diimides with different side chains are selective in inducing different G-quadruplex DNA structures and in inhibiting telomerase, *Bioorg Med Chem Lett* **12**, 2527-2533.
183. Rossetti, L., Franceschin, M., Schirripa, S., Bianco, A., Ortaggi, G., and Savino, M. (2005) Selective interactions of perylene derivatives having different side chains with inter- and intramolecular G-quadruplex DNA structures. A correlation with telomerase inhibition, *Bioorg Med Chem Lett* **15**, 413-420.
184. Sissi, C., Lucatello, L., Paul Krapcho, A., Maloney, D. J., Boxer, M. B., Camarasa, M. V., Pezzoni, G., Menta, E., and Palumbo, M. (2007) Tri-, tetra- and heptacyclic perylene analogues as new potential antineoplastic agents based on DNA telomerase inhibition, *Bioorg Med Chem* **15**, 555-562.
185. McGovern, S. L., Caselli, E., Grigorieff, N., and Shoichet, B. K. (2002) A common mechanism underlying promiscuous inhibitors from virtual and high-throughput screening, *J Med Chem* **45**, 1712-1722.
186. Kern, J. T. (2002) *Studies on 3,4,9,10-perylenetetra-carboxylic acid diimide based ligands as G-quadruplex DNA interactive agents*, The University of Texas Libraries, Austin, TX.
187. Kern, J. T., and Kerwin, S. M. (2002) The aggregation and G-quadruplex DNA selectivity of charged 3,4,9,10-perylenetetra-carboxylic acid diimides, *Bioorg Med Chem Lett* **12**, 3395-3398.
188. Ford, W. E. (1987) Photochemistry of 3,4,9,10-perylenetetra-carboxylic dianhydride dyes: visible absorption and fluorescence of the di(glycyl)imide derivative monomer and dimer in basic aqueous solutions, *J Photochem* **37**, 189-204.
189. Karolin, J., Johansson, L. B.-A., Ring, U., and Langhals, H. (1996) Aggregation of perylene dyes in lipid vesicles: the effect of optically active substituents, *Spectrochim Acta, Part A* **52**, 747-753.
190. Marcon, R. O., dos Santos, J. G., Figueiredo, K. M., and Brochsztain, S. (2006) Characterization of a novel water-soluble 3,4,9,10-

- perylene-tetracarboxylic diimide in solution and in self-assembled zirconium phosphonate thin films, *Langmuir* **22**, 1680-1687.
191. Gray, D. M., Wen, J. D., Gray, C. W., Regges, R., Regges, C., Raabe, G., and Fleischhauer, J. (2007) Measured and calculated CD spectra of G-quartets stacked with the same or opposite polarities, *Chirality*.
 192. Sun, X. G., Cao, E. H., He, Y. J., and Qin, J. F. (1999) Spectroscopic comparison of different DNA structures formed by oligonucleotides, *J Biomol Struct Dyn* **16**, 863-872.
 193. Kohl, C., Weil, T., Qu, J., and Mullen, K. (2004) Towards highly fluorescent and water-soluble perylene dyes, *Chemistry* **10**, 5297-5310.
 194. Johansson, L. B.-A., and Langhals, H. (1991) Spectroscopic studies of fluorescent perylene dyes *Spectrochim Acta A Mol Biomol Spectrosc* **47**, 857-861.
 195. Langhals, H., Jona, W., Einsiedl, F., and Wohnlich, S. (1998) Self-Dispersion: Spontaneous Formation of Colloidal Dyes in Water, *Adv. Mater.* **10**, 1022-1024.
 196. Pasternack, R. F., and Collings, P. J. (1995) Resonance light scattering: a new technique for studying chromophore aggregation, *Science* **269**, 935-939.
 197. Fox, K. R. (1997) *Drug-DNA interaction protocols*, Humana Press, Totowa, NJ.
 198. Wurthner, F. (2004) Perylene bisimide dyes as versatile building blocks for functional supramolecular architectures, *Chem Commun (Camb)*, 1564-1579.
 199. Chen, Z., Stepanenko, V., Dehm, V., Prins, P., Siebbeles, L. D., Seibt, J., Marquetand, P., Engel, V., and Wurthner, F. (2007) Photoluminescence and conductivity of self-assembled pi-pi stacks of perylene bisimide dyes, *Chemistry* **13**, 436-449.
 200. Albrecht, M. (2007) Supramolecular chemistry-general principles and selected examples from anion recognition and metallosupramolecular chemistry, *Naturwissenschaften*.
 201. Dobrawa, R., and Wurthner, F. (2002) Photoluminescent supramolecular polymers: metal-ion directed polymerization of terpyridine-functionalized perylene bisimide dyes, *Chem Commun (Camb)*, 1878-1879.
 202. Wu, Y., Li, B., Wang, W., Bai, F., and Liu, M. (2003) Coordination assisted molecular assemblies of perylene-3,4,9,10-tetracarboxylic acid with copper (II) ion at the air/water interface *Mater Sci Eng C* **23**, 605-609.
 203. Li, Y., Wang, N., Gan, H., Liu, H., Li, H., He, X., Huang, C., Cui, S., Wang, S., and Zhu, D. (2005) Synthesis and characterization of 3,5-bis(2-hydroxyphenyl)-1,2,4-triazole functionalized tetraaryloxy perylene bisimide and metal-directed self-assembly, *J Org Chem* **70**, 9686-9692.
 204. Dobrawa, R., Kurth, D. G., and Würthner, F. (2004) Electrostatic Self-Assembly Of Fluorescent Perylene Bisimide Coordination Polymers, *Polym Prepr* **45**, 378-379.

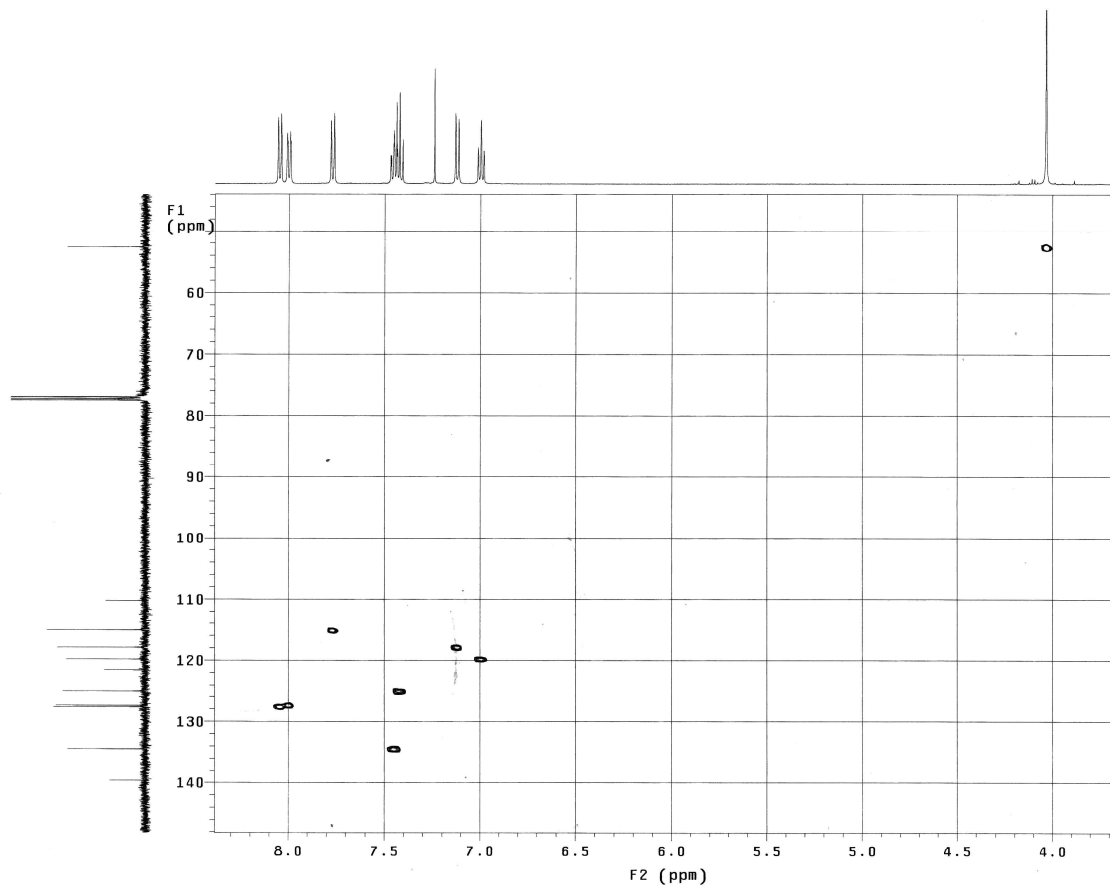
205. Tuntiwechapikul, W., and Salazar, M. (2001) Cleavage of telomeric G-quadruplex DNA with perylene-EDTA*Fe(II), *Biochemistry* 40, 13652-13658.
206. Zheng, X., Zhang, D., and Zhu, D. (2006) A new tetrathiafulvalene–perylene diimide dyad with a penta-oxa-heptadecane chain as the spacer: metal-ions-induced aggregation, *Tetrahedron Lett* 47, 9083–9087.
207. Wurthner, F., Sautter, A., Schmid, D., and Weber, P. J. (2001) Fluorescent and electroactive cyclic assemblies from perylene tetracarboxylic acid bisimide ligands and metal phosphane triflates, *Chemistry* 7, 894-902.
208. Tuntiwechapikul, W., Lee, J. T., and Salazar, M. (2001) Design and synthesis of the G-quadruplex-specific cleaving reagent perylene-EDTA.iron(II), *J Am Chem Soc* 123, 5606-5607.
209. Bohn, P. W. (1993) Aspects of Structure and Energy Transport in Artificial Molecular Assemblies, *Annu Rev Phys Chem* 44, 37-60.
210. Wurthner, F., Thalacker, C., Diele, S., and Tschierske, C. (2001) Fluorescent J-type aggregates and thermotropic columnar mesophases of perylene bisimide dyes, *Chemistry* 7, 2245-2253.
211. Kaiser, T. E., Wang, H., Stepanenko, V., and Wurthner, F. (2007) Supramolecular construction of fluorescent J-aggregates based on hydrogen-bonded perylene dyes, *Angew Chem Int Ed Engl* 46, 5541-5544.
212. Wang, W., Wan, W., Zhou, H. H., Niu, S., and Li, A. D. (2003) Alternating DNA and pi-conjugated sequences. Thermophilic foldable polymers, *J Am Chem Soc* 125, 5248-5249.

APENDIX A. SELECTED SPECTRA FOR UK-1 ANALOGS

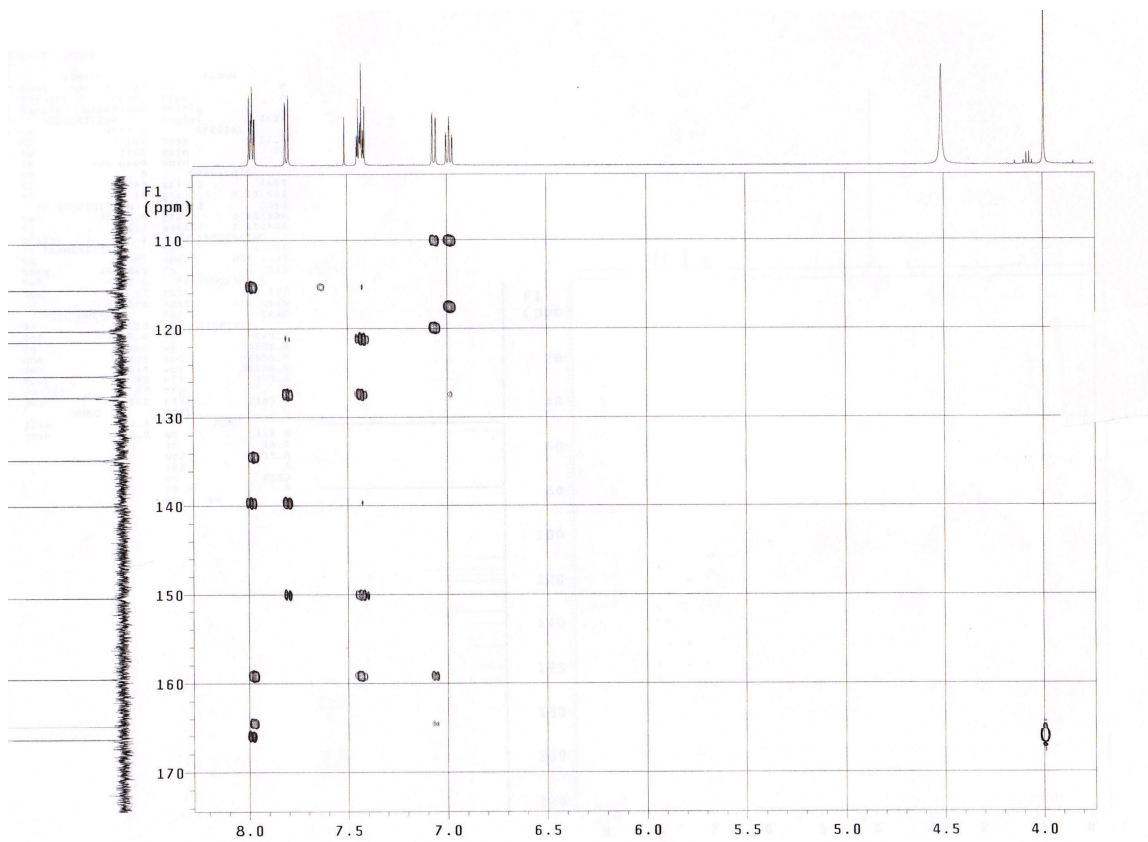
A.1. ^1H and ^{13}C NMR of compound **8** in $\text{CDCl}_3/\text{MeOD}$ 1:1



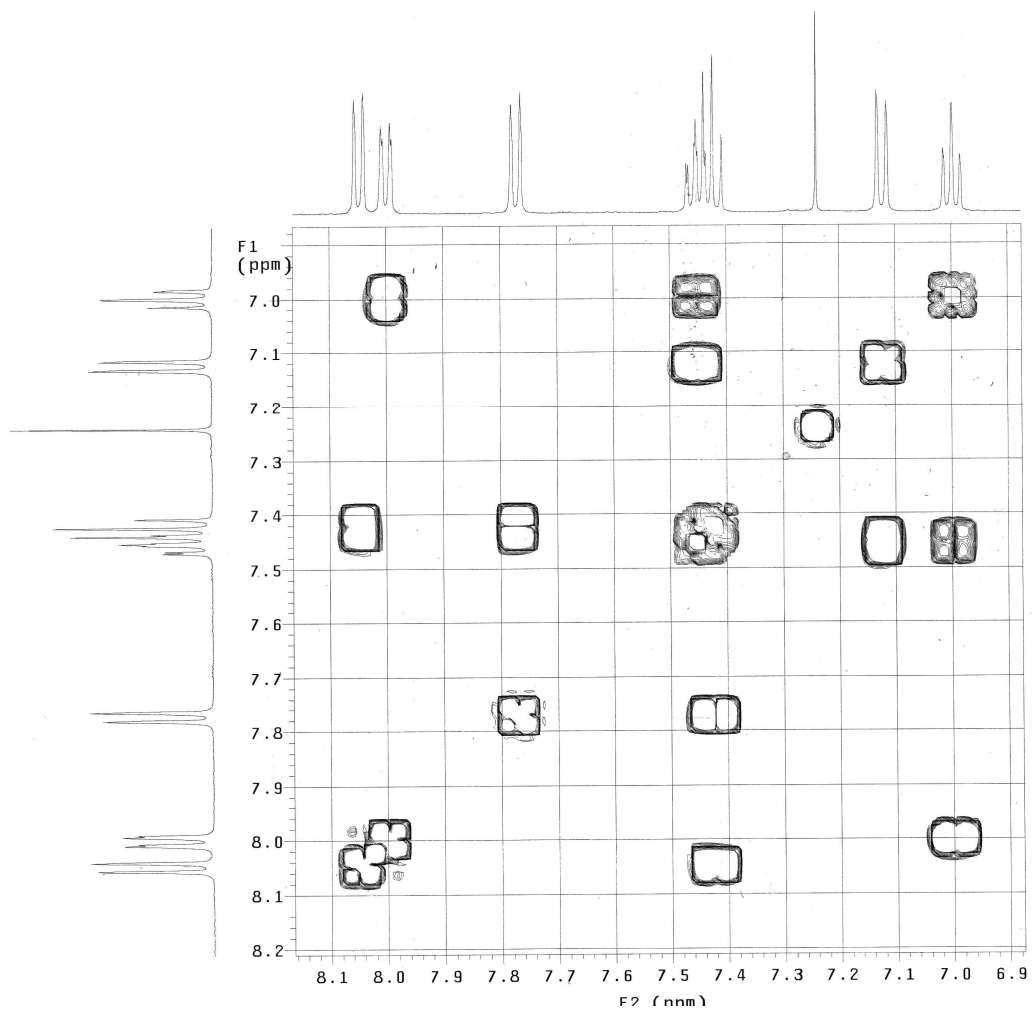
A.2. gHSQC of compound **8** in CDCl₃



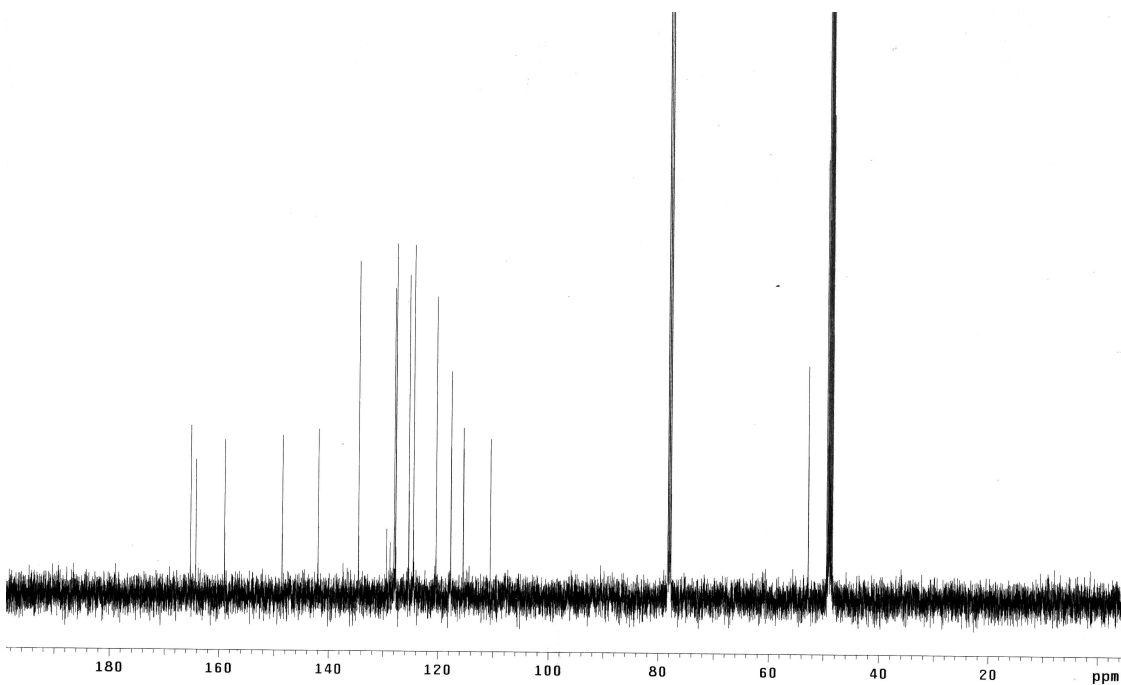
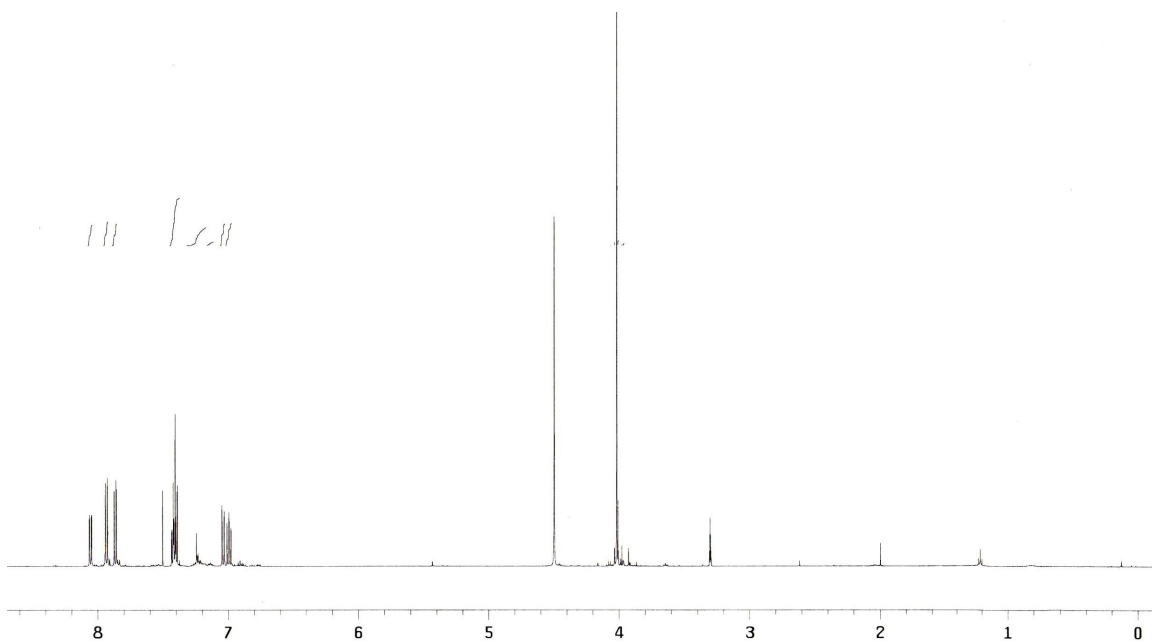
A.3. gHMBC Compound 8 in CDCl₃/MeOD 1:1



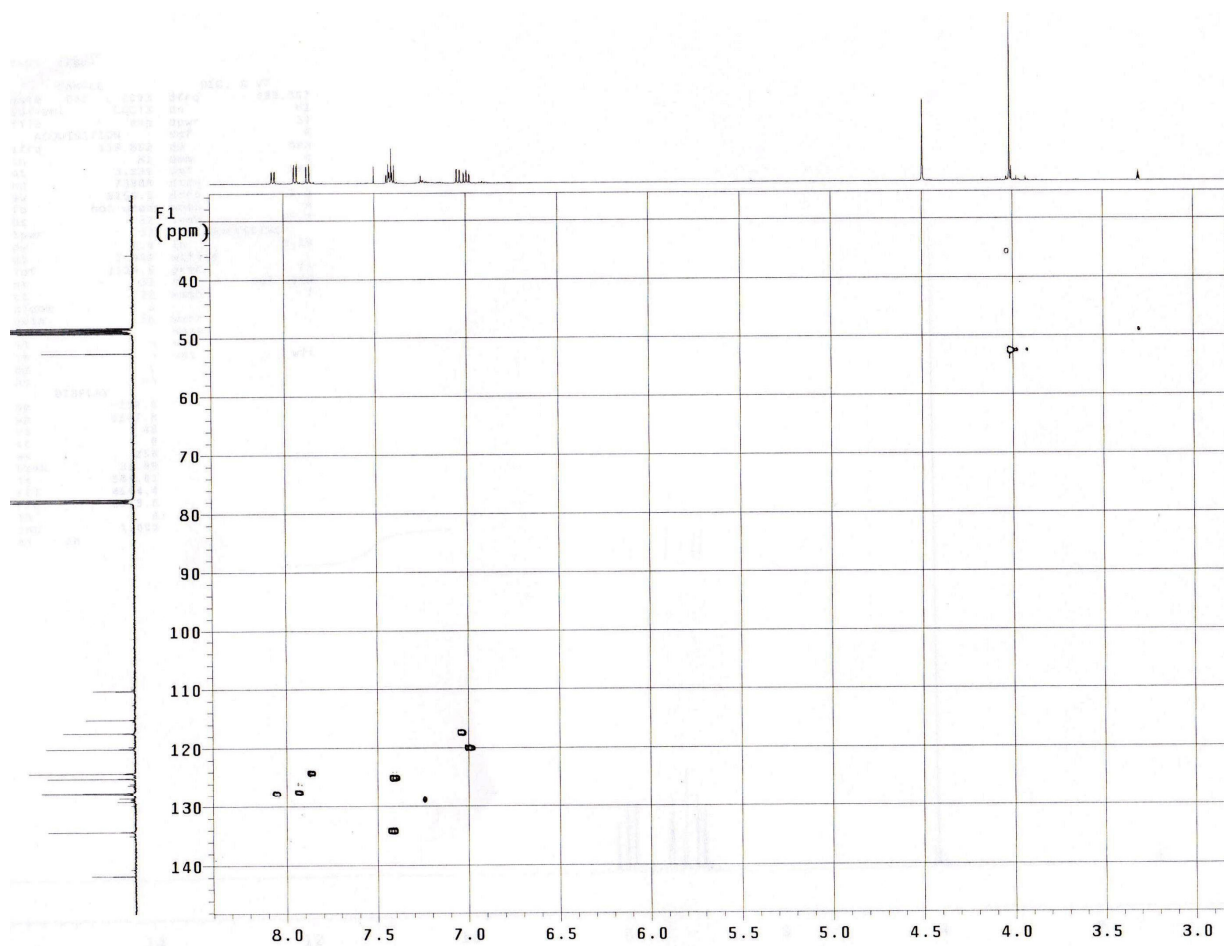
A.4. Compound **8** COSY in CDCl₃



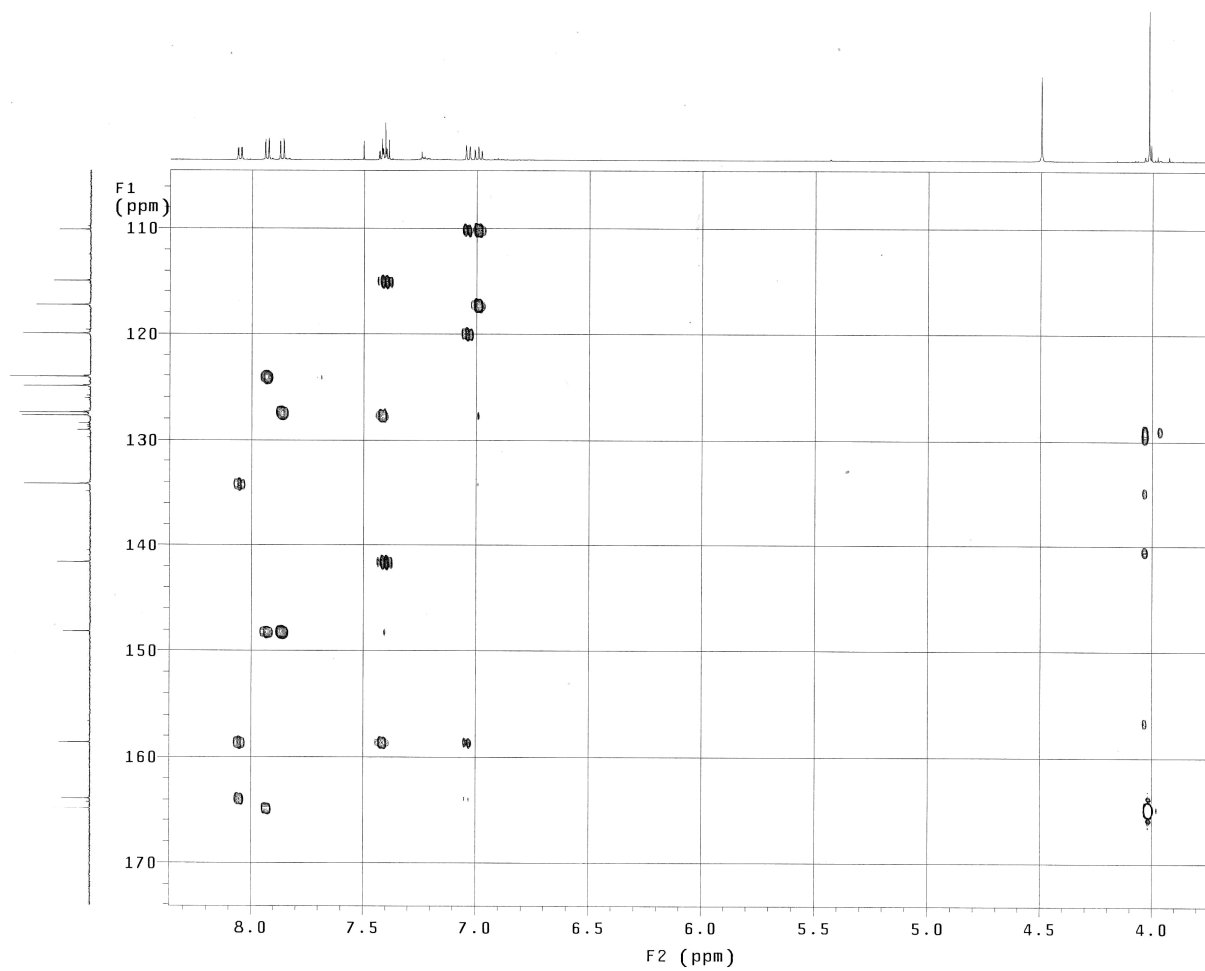
A.5. ^1H and ^{13}C NMR of Compound **9** ($\text{CDCl}_3/\text{MeOD}$ 1:1)



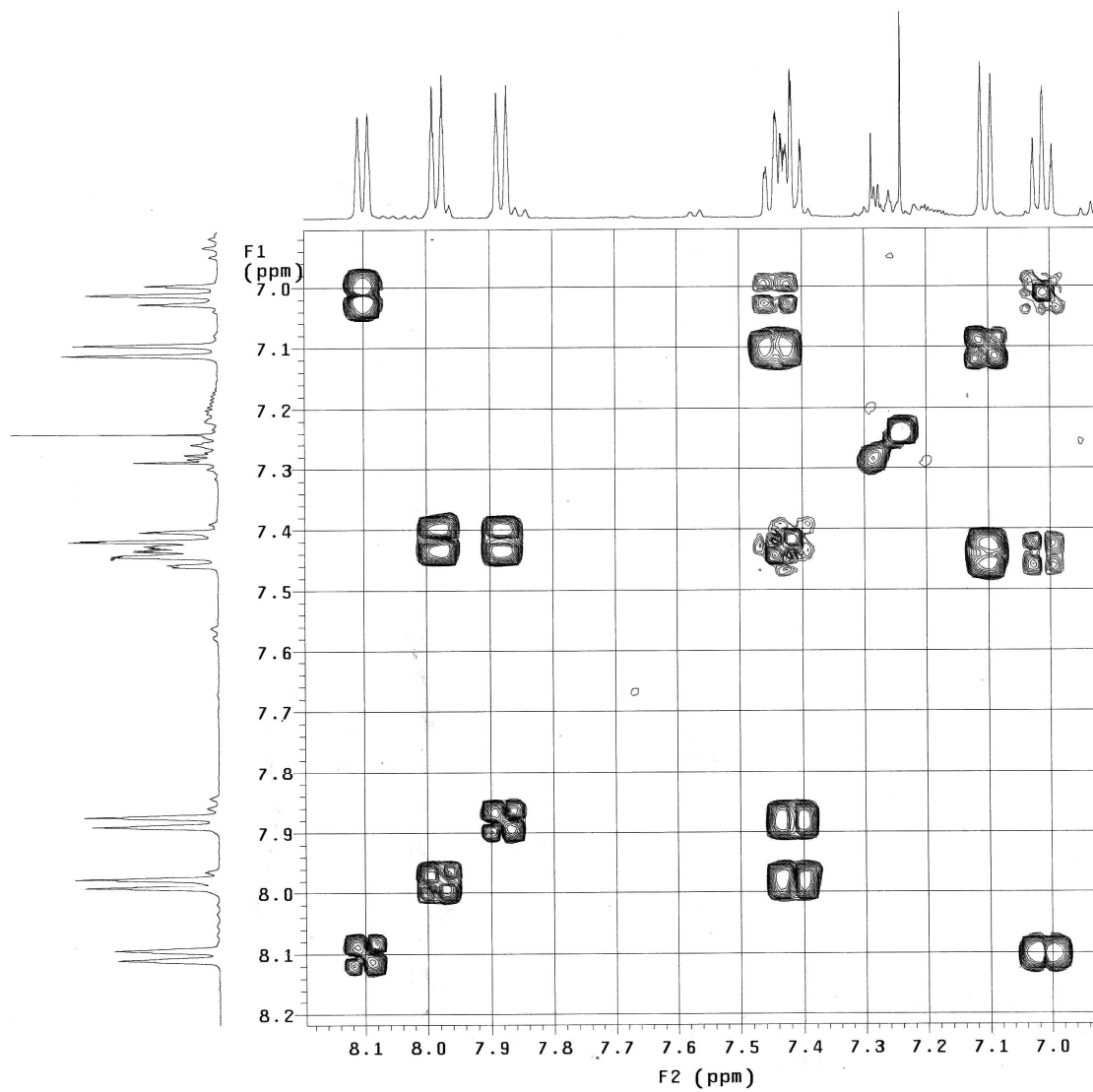
A.6. gHSQC compound **9** in CDCl₃/MeOD 1:1



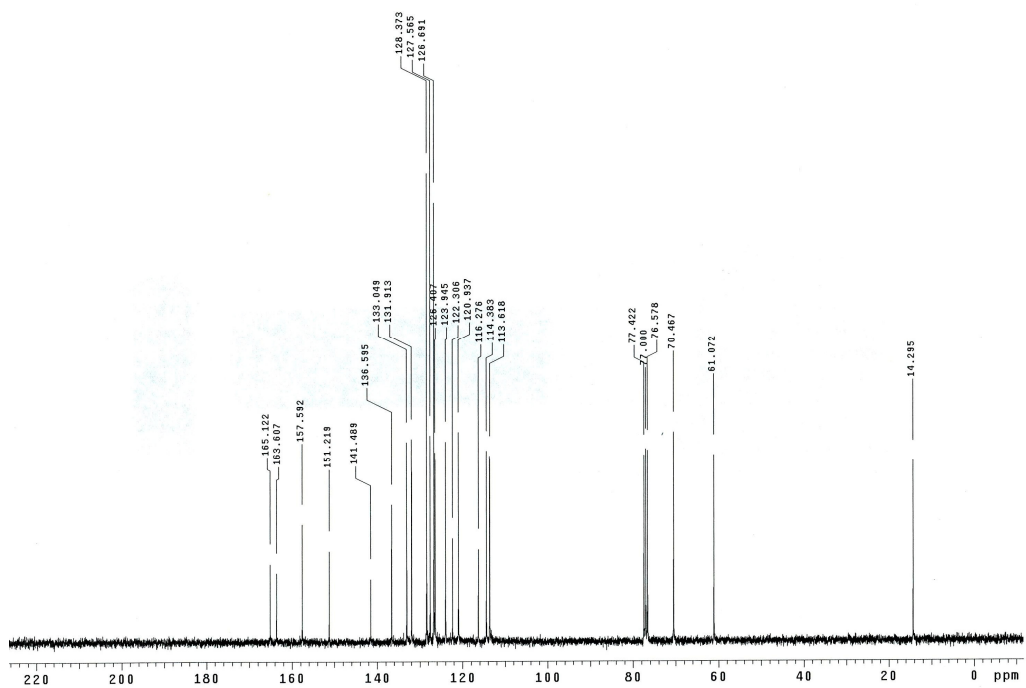
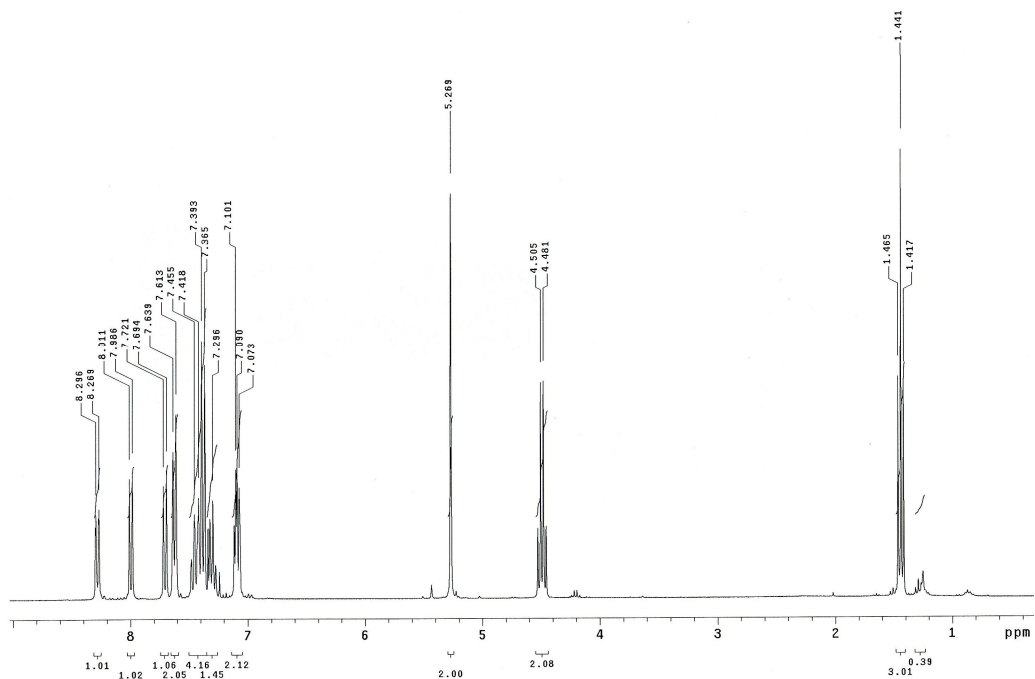
A.7. gHMBC of compound **9** in CDCl₃/MeOD 1:1



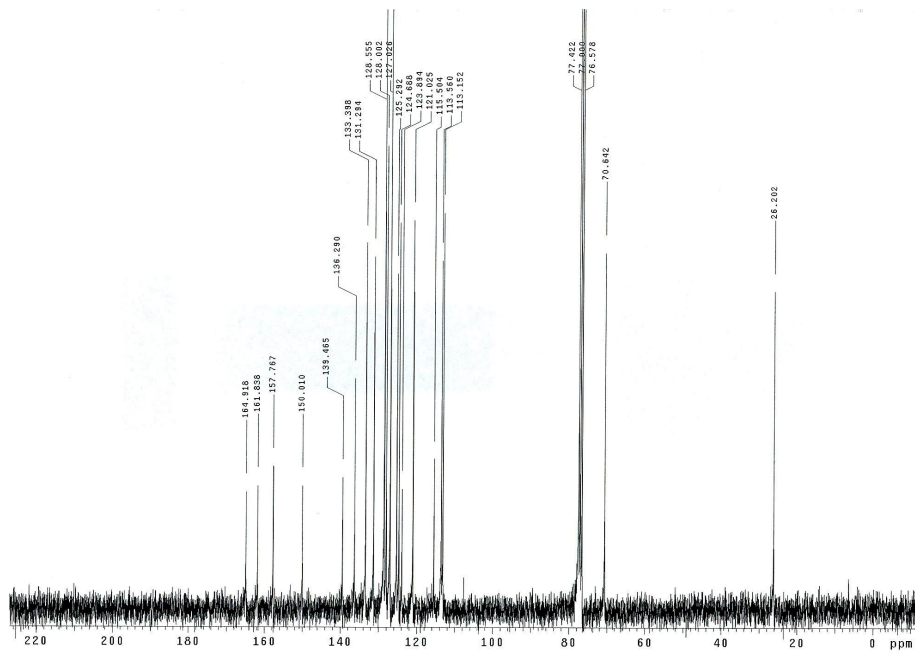
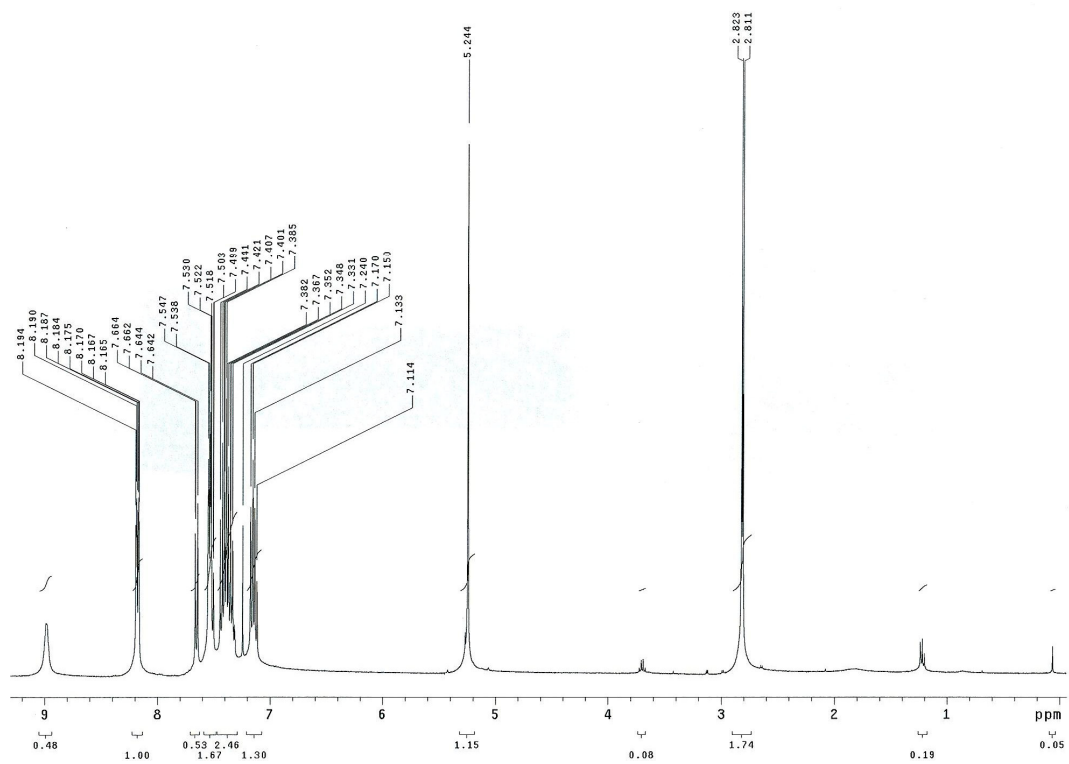
A.8. Compound **9** COSY in CDCl₃



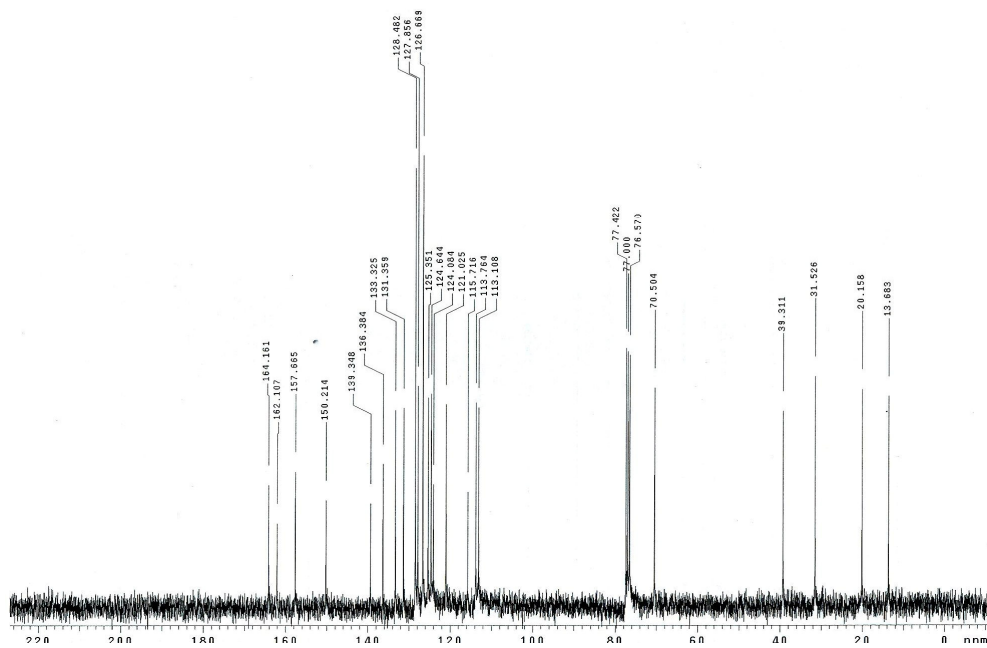
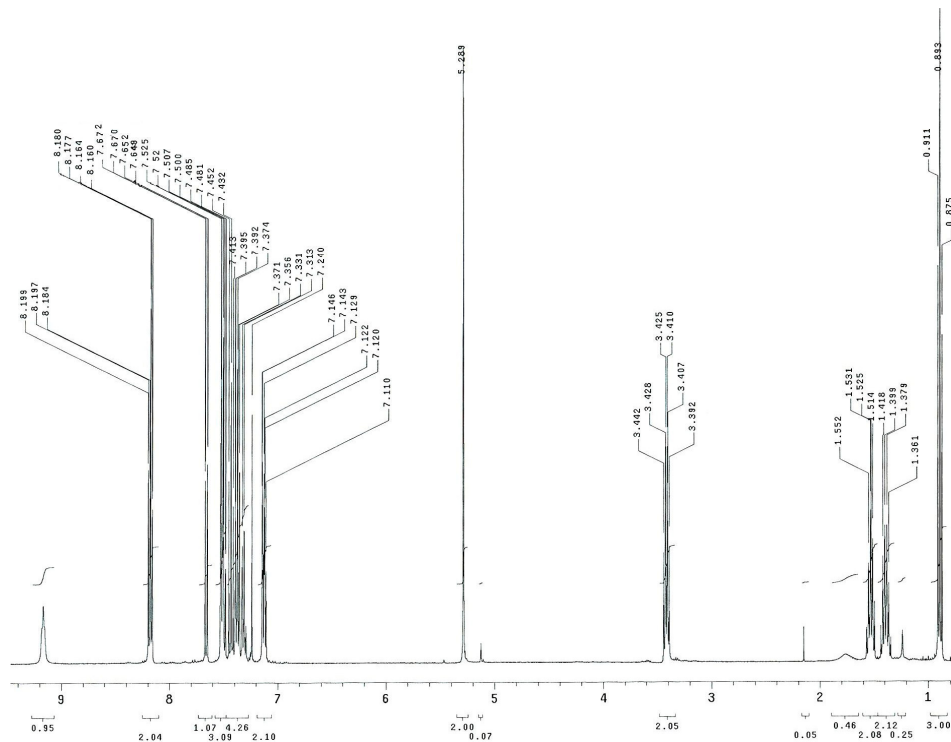
A.9. ^1H and ^{13}C NMR of compound **10**



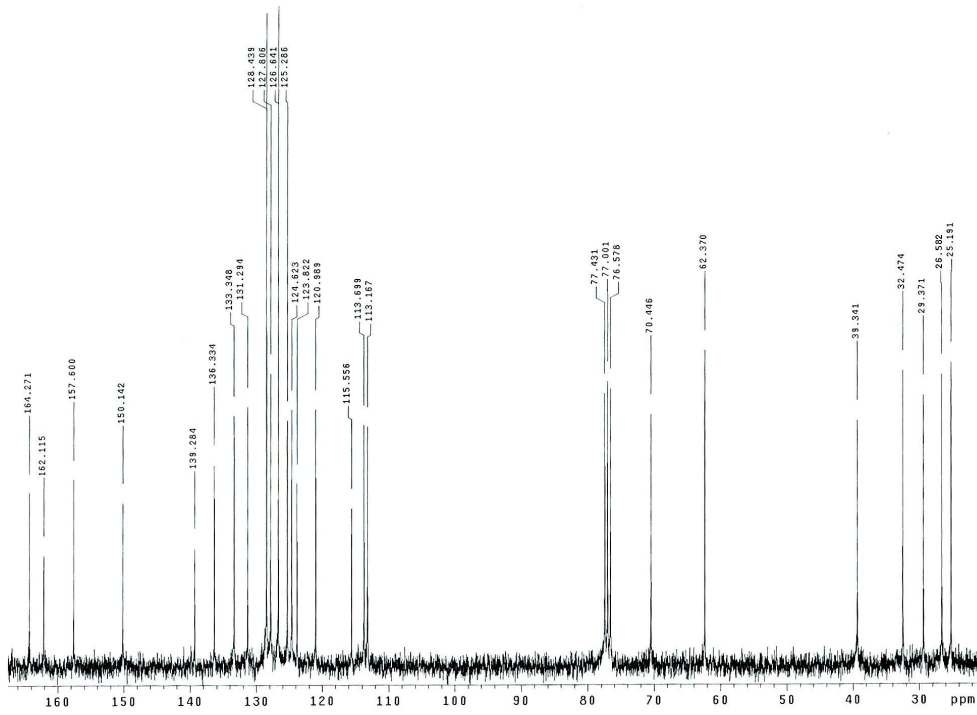
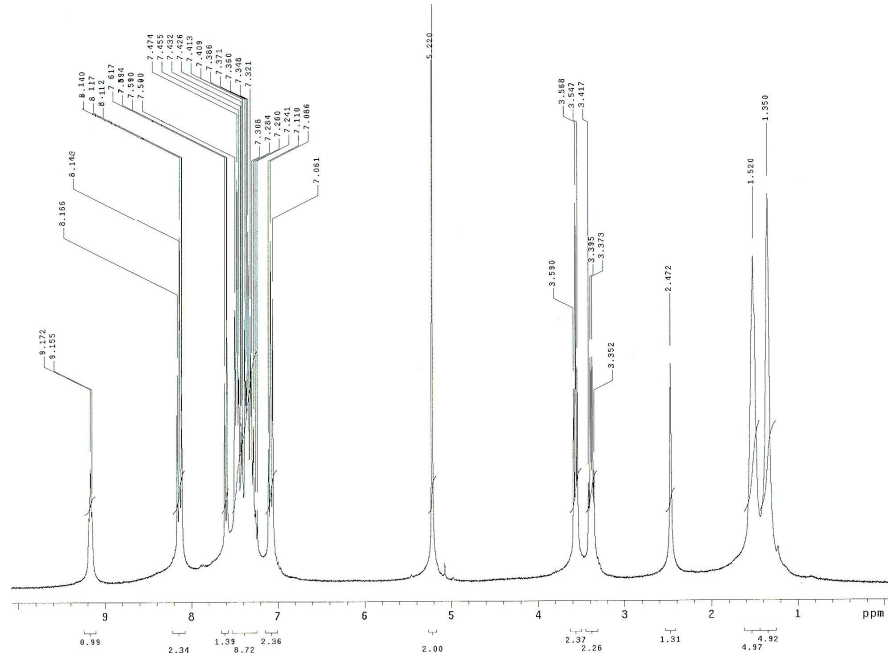
A.10. ^1H and ^{13}C NMR of compound 11



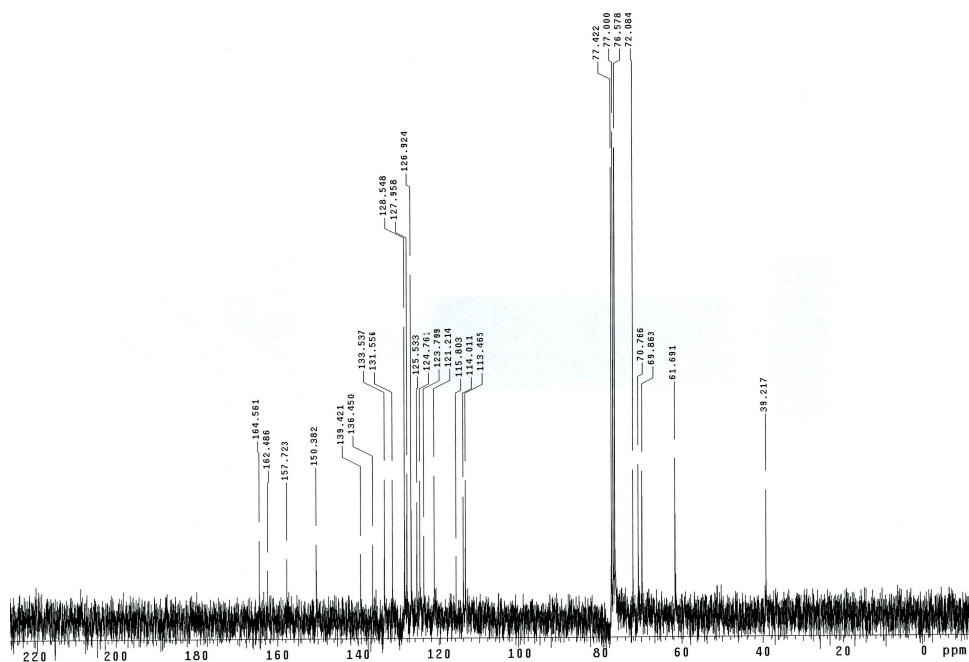
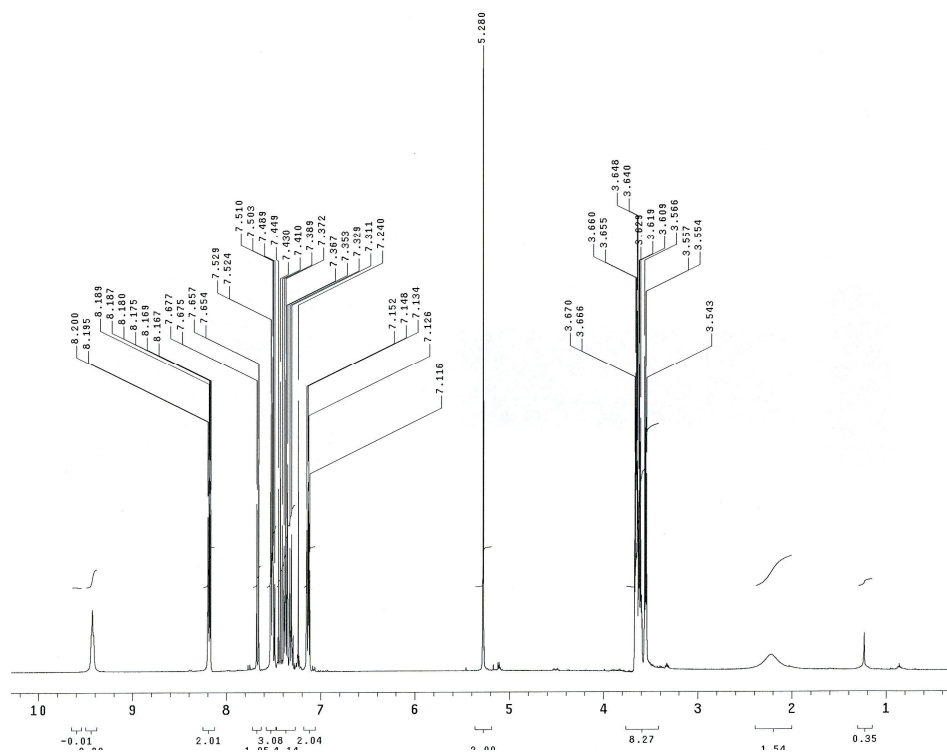
A.11. ^1H and ^{13}C NMR of compound **12**



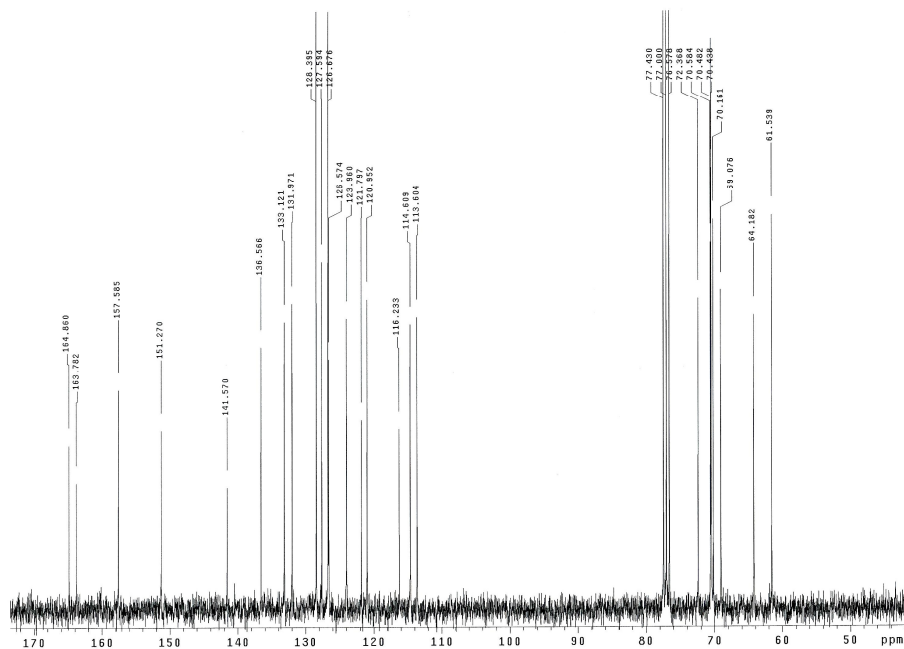
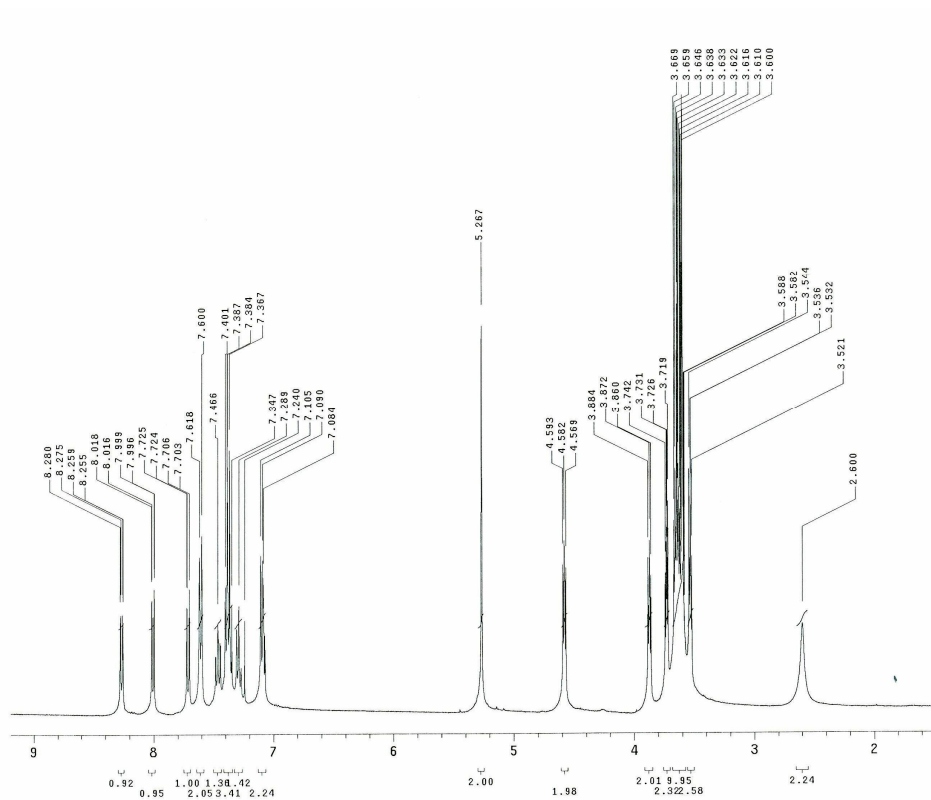
A.12. ^1H and ^{13}C NMR of compound **13**



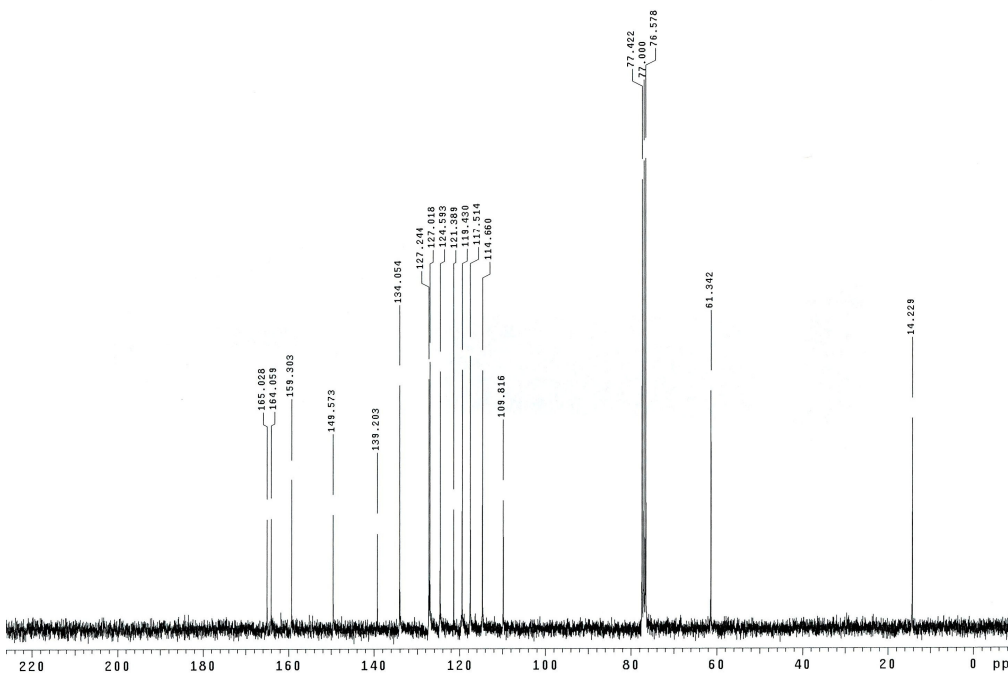
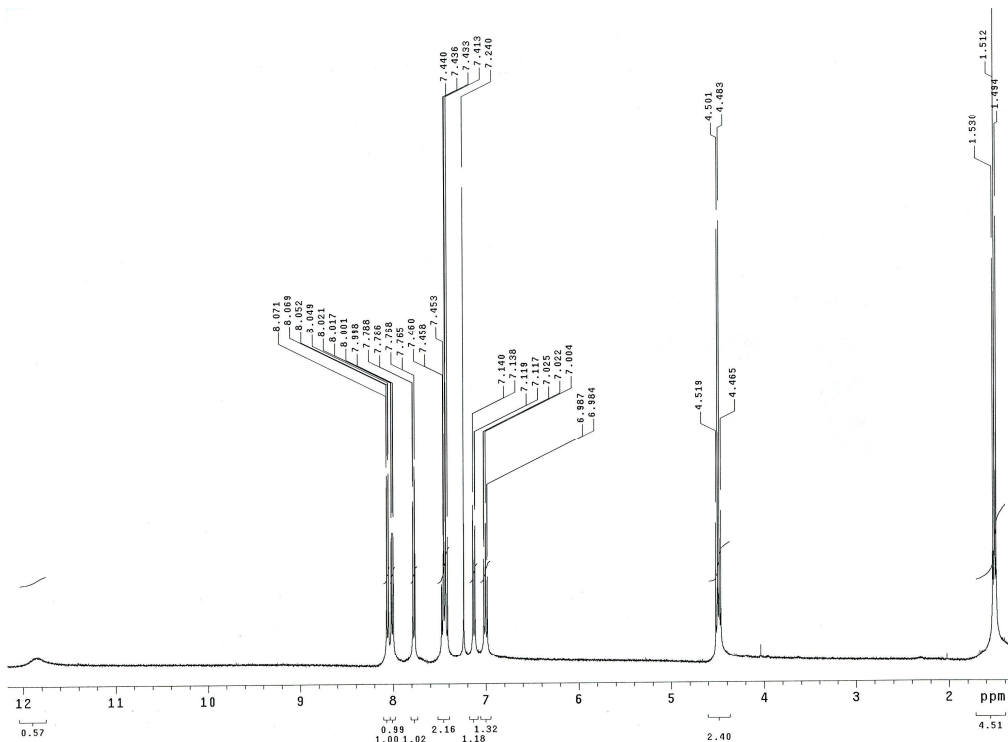
A.13. ^1H and ^{13}C NMR of compound **14**



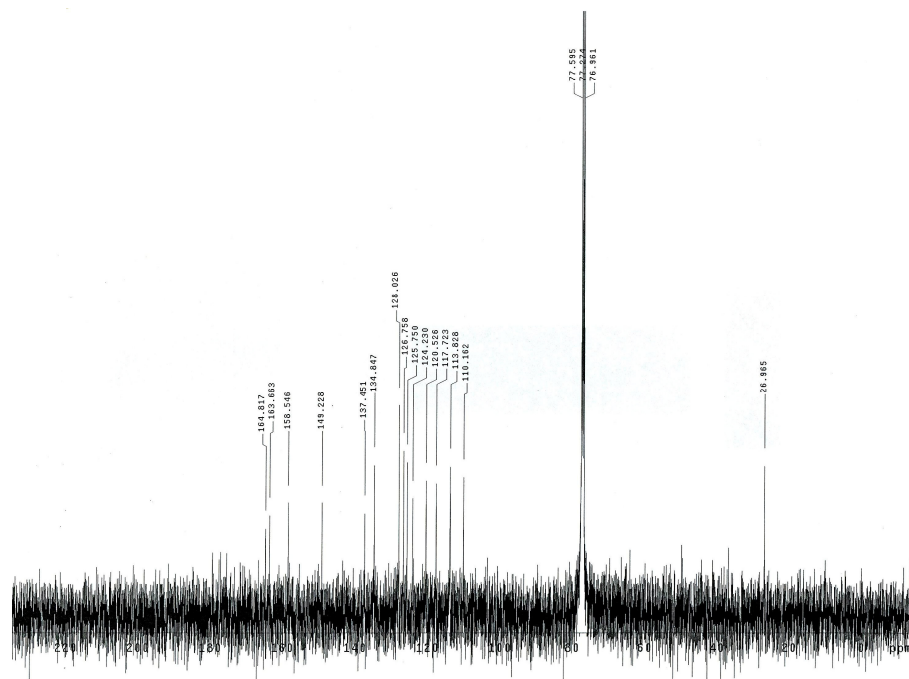
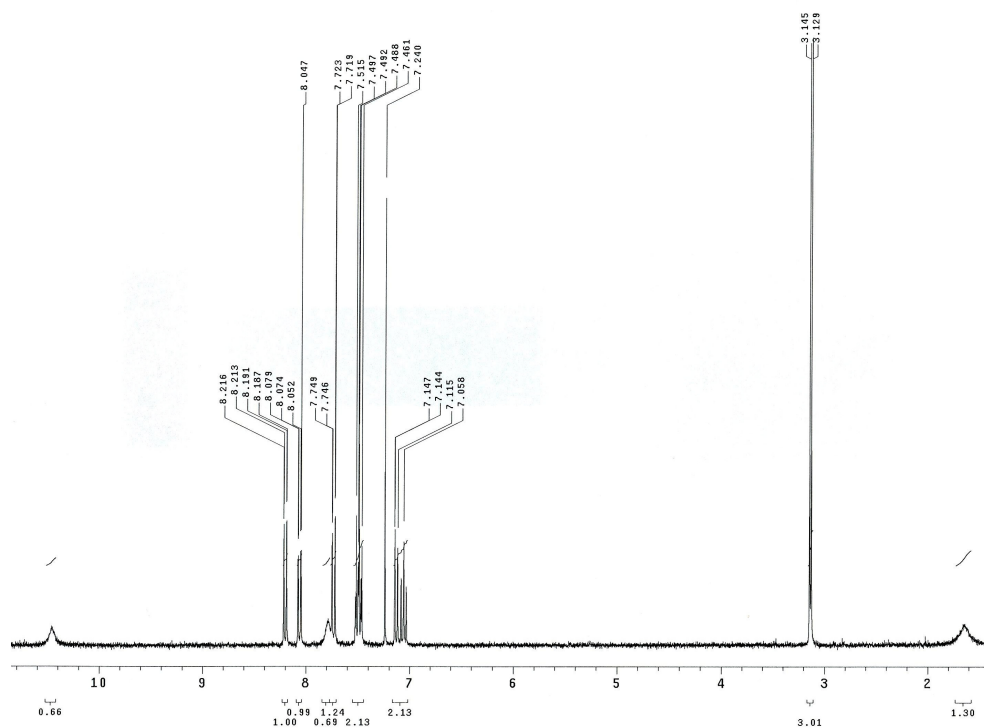
A.14. ¹H and ¹³C NMR of compound 15



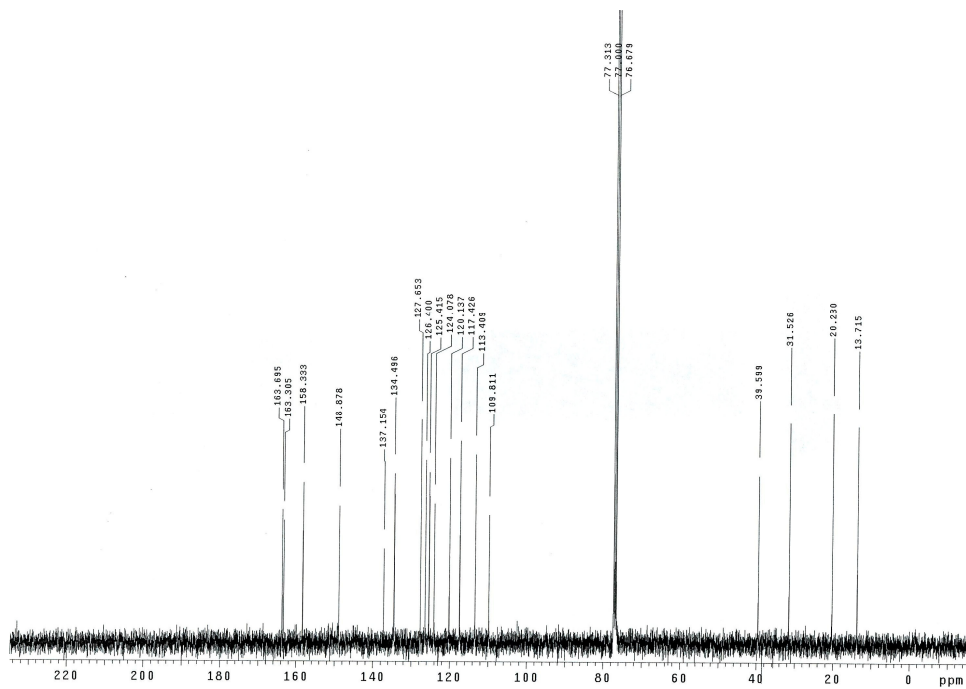
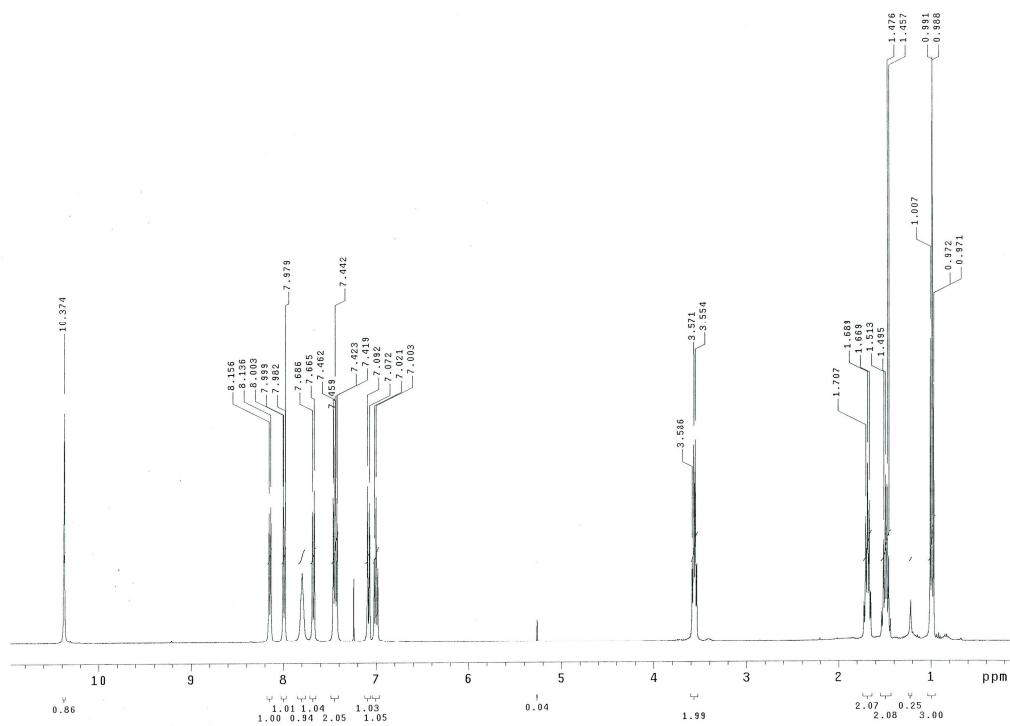
A.15. ^1H and ^{13}C NMR of compound **16**



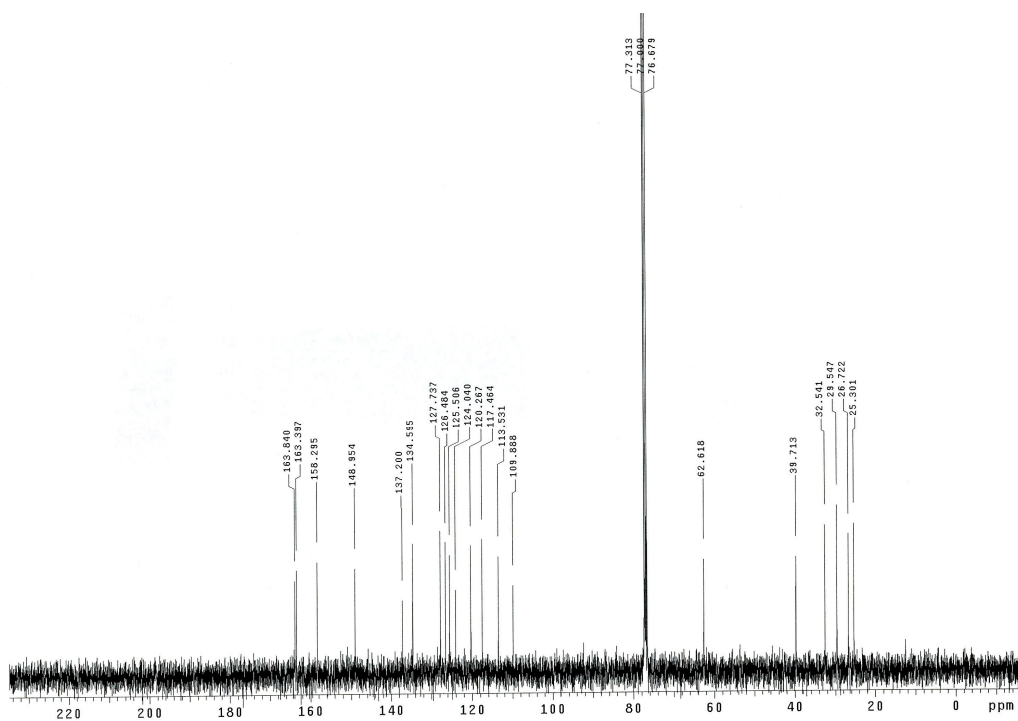
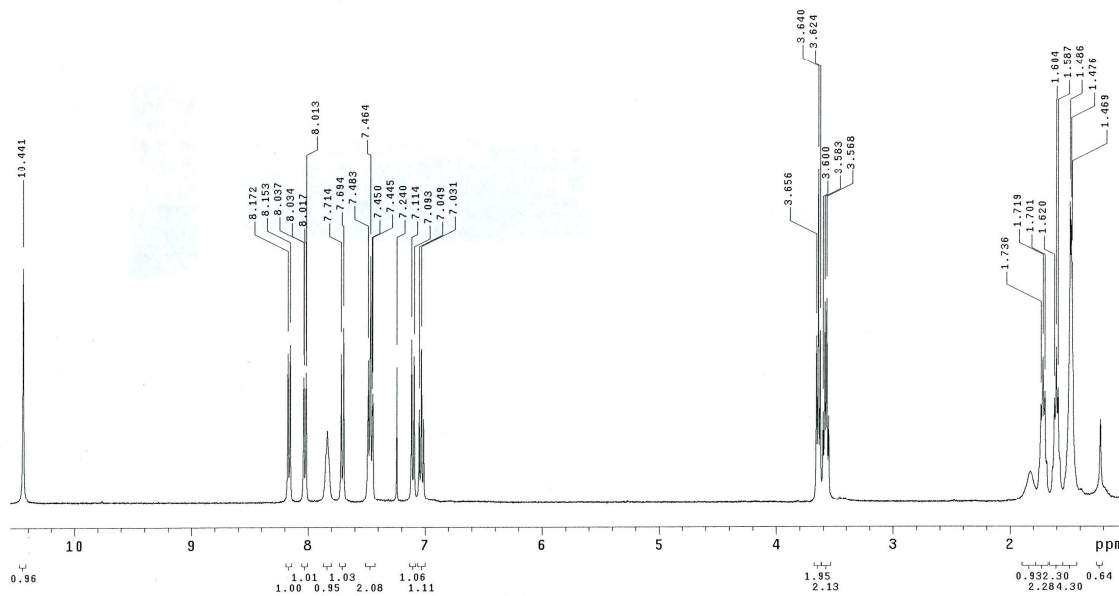
A.16. ^1H and ^{13}C NMR of compound 17



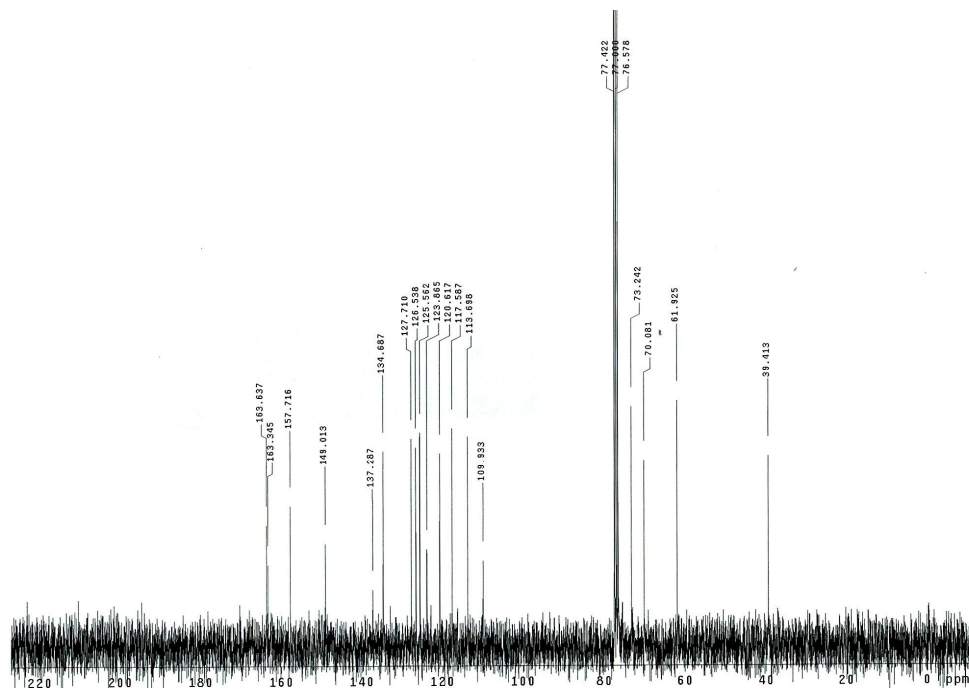
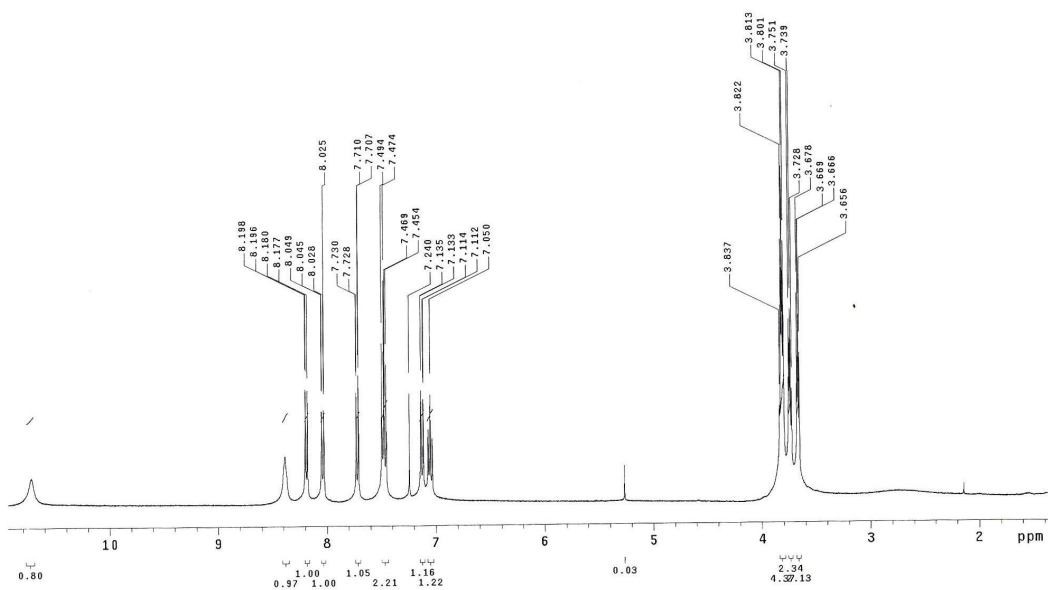
A.17. ^1H and ^{13}C NMR of compound **18**



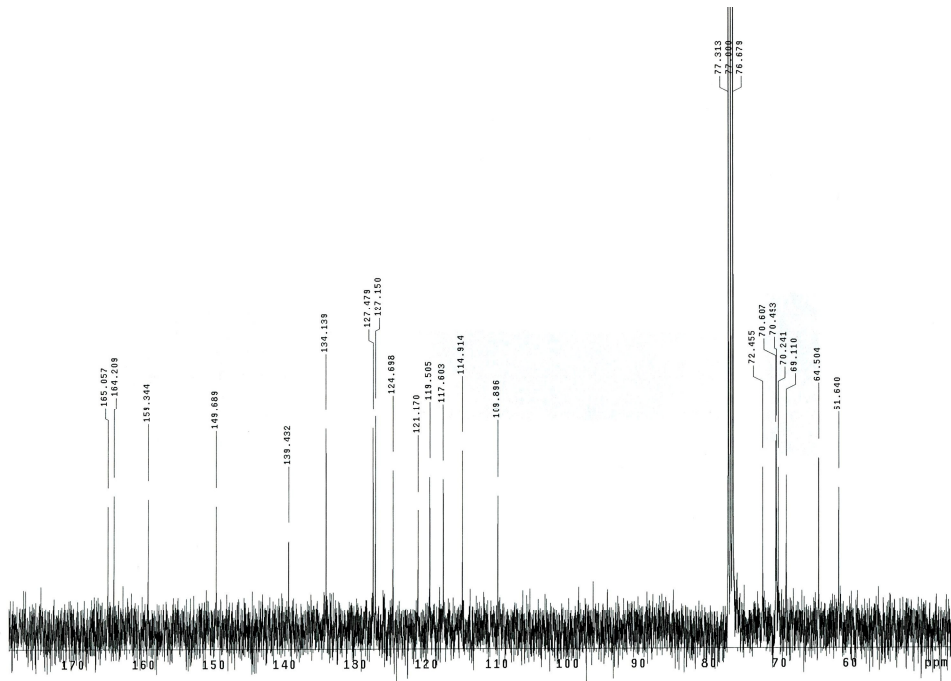
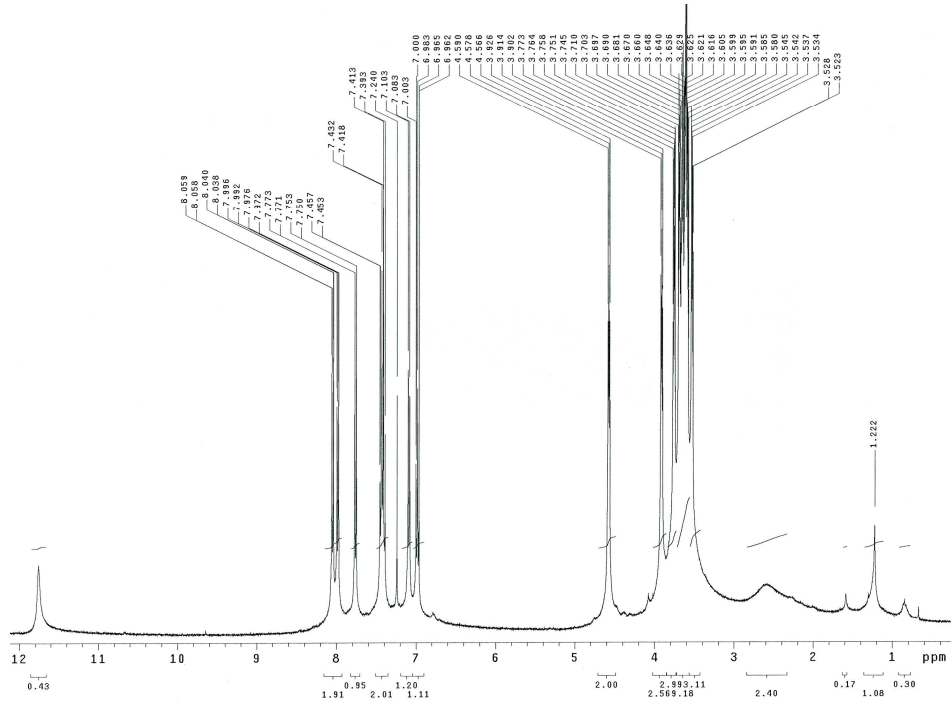
A.18. ^1H and ^{13}C NMR of compound **19**



A.19. ^1H and ^{13}C NMR of compound **20**



A.20. ¹H and ¹³C NMR of compound 21



APENDIX B. NMR CHEMICAL SHIFTS OF COMPOUNDS 8 AND 9 IN THE PRESENCE OF $\text{Mg}(\text{NO}_3)_2$

B.1. ^1H NMR shifts of compound **8** in $\text{CDCl}_3/\text{MeOD}$ 1:1 in the absence or presence of 0.25, 0.50, 0.75, or 1.00 eq. $\text{Mg}(\text{NO}_3)_2$.

Table B.1. ^1H NMR shifts upon addition of Mg^{2+} to compound **8**. Chemical shifts referenced to CDCl_3

	NO ADDI- TIONS (ppm)	0.25eq MgNO_3 (Δ ppm)	0.50eq MgNO_3 (Δ ppm)	0.75eq MgNO_3 (Δ ppm)	1.00eq MgNO_3 (Δ ppm)
C₅-H	7.987	0.006	-0.002	-0.011	-0.018
C₆'-H	7.972	0.006	-0.002	-0.012	-0.018
C₇-H	7.803	0.012	0.008	0.002	-0.001
C₄'-H, C₆-H	7.439	0.000	-0.006	-0.012	-0.020
C₃'-H	7.062	-0.005	-0.015	-0.026	-0.032
C₅'-H	6.987	-0.003	-0.010	-0.017	-0.023
MeOD	4.511	0.026	0.068	0.112	0.140
CH₃	3.993	-0.006	-0.014	-0.023	-0.028

B.2. ^{13}C NMR shifts of compound **8** in $\text{CDCl}_3/\text{MeOD}$ 1:1 in the absence or presence of 0.25, 0.50, 0.75, or 1.00 eq. $\text{Mg}(\text{NO}_3)_2$.

Table B.2. ^{13}C NMR shifts upon addition of Mg^{2+} to compound **8**. Chemical shifts referenced to CDCl_3

	NO ADDI- TIONS (ppm)	0.25eq MgNO₃ (Δ ppm)	0.50eq MgNO₃ (Δ ppm)	0.75eq MgNO₃ (Δ ppm)	1.00eq MgNO₃ (Δ ppm)
CO_2	166.389	0.007			-0.067
C_1	164.899	0.024			-0.023
C_2	159.558	-0.004		-0.079	-0.060
C_{7a}	150.417	0.019	-0.009		-0.045
C_{3a}	140.041	0.008			-0.048
$\text{C}_{5'}$	134.780	-0.004	-0.012	-0.020	-0.032
$\text{C}_{6'}$	127.804	-0.012	-0.028	-0.052	-0.068
C_5	127.788				
C_6	125.408	0.012	0.004	-0.008	-0.011
C_4	121.499				
$\text{C}_{4'}$	120.277		-0.008		-0.040
$\text{C}_{3'}$	117.922	-0.020	-0.049	-0.064	-0.093
C_7	115.692	0.016	0.012	0.021	0.013
$\text{C}_{2'}$	110.420	0.003	-0.025	-0.049	-0.061
CH_3	52.662	-0.028	-0.040	-0.072	-0.088
MeOD	48.994	-0.057	-0.077	-0.101	-0.117

B.3. ^1H NMR shifts of compound **9** in $\text{CDCl}_3/\text{MeOD}$ 1:1 in the absence or presence of 0.25, 0.50, 0.75, 1.00, or 2.00 eq. $\text{Mg}(\text{NO}_3)_2$.

Table B.3. ^1H NMR shifts upon addition of Mg^{2+} to compound **9**. Chemical shifts referenced to CDCl_3

	NO ADDI- TIONS (ppm)	0.25eq MgNO₃ (Δ ppm)	0.50eq MgNO₃ (Δ ppm)	0.75eq MgNO₃ (Δ ppm)	1.00eq MgNO₃ (Δ ppm)	2.00eq MgNO₃ (Δ ppm)
C₆-H	8.054	-0.019	-0.024	-0.035	-0.046	-0.063
C₆-H	7.933	-0.017	-0.022	-0.031	-0.040	-0.058
C₄-H	7.865	-0.017	-0.021	-0.031	-0.039	-0.056
C₄-H, C₅-H	7.421	-0.015	-0.018	-0.026	-0.033	-0.046
C₃-H	7.038	-0.017	-0.021	-0.030	-0.038	-0.055
C₅-H	6.992	-0.015	-0.019	-0.027	-0.034	-0.048
MeOD	4.495	0.036	0.070	0.106	0.142	0.233
CH₃	4.172	-0.015	-0.018	-0.027	-0.034	-0.049

B.4. ^{13}C NMR shifts of compound **9** in $\text{CDCl}_3/\text{MeOD}$ 1:1 in the absence or presence of 0.25, 0.50, 0.75, 1.00, or 2.00 eq. $\text{Mg}(\text{NO}_3)_2$.

Table B.4. ^{13}C NMR shifts upon addition of Mg^{2+} to compound **9**. Chemical shifts referenced to CDCl_3

	NO ADDI- TIONS (ppm)	0.25eq MgNO₃ (Δ ppm)	0.50eq MgNO₃ (Δ ppm)	0.75eq MgNO₃ (Δ ppm)	1.00eq MgNO₃ (Δ ppm)	2.00eq MgNO₃ (Δ ppm)
CO_2	165.227	-0.028	-0.040	-0.052	-0.065	-0.101
C_2	164.272	-0.028	-0.048	-0.068	-0.089	-0.145
C_{3a}	159.008	-0.028	-0.048	-0.073	-0.094	-0.154
C_{7a}	148.612	-0.032	-0.052	-0.072	-0.097	-0.154
C_{3a}	141.996	-0.028	-0.048	-0.069	-0.090	-0.150
$\text{C}_{4'}$	134.554	-0.024	-0.032	-0.048	-0.061	-0.089
$\text{C}_{6'}$	128.075	-0.028	-0.040	-0.056	-0.073	-0.121
C_6	127.804	-0.024	-0.036	-0.052	-0.065	-0.101
C_5	125.340	-0.020	-0.028	-0.040	-0.049	-0.073
C_4	124.486	-0.028	-0.040	-0.056	-0.073	-0.109
$\text{C}_{5'}$	120.354	-0.024	-0.032	-0.044	-0.056	-0.084
$\text{C}_{3'}$	117.667	-0.032	-0.048	-0.068	-0.085	-0.133
C_7	115.413	-0.028	-0.044	-0.064	-0.085	-0.141
$\text{C}_{1'}$	110.521	-0.028	-0.044	-0.063	-0.081	-0.129
CH_3	52.824	-0.032	-0.040	-0.052	-0.069	-0.097
MeOD	48.994	-0.036	-0.048	-0.064	-0.085	-0.121

APENDIX C. METAL-MEDIATED DNA BINDING OBSERVED BY ESI-MS

C.1. Fraction of HPB bound to DNA in the presence of metal ions

The changes in the degree of ligand binding upon addition of the metal salt were determined by Carolyn Mazzitelli using ESI-MS; the fraction of bound DNA values were calculated by expressing the sum of the abundances of all ions attributed to DNA/ligand complexes as a fraction of the total abundances of all DNA containing ions (both free DNA and DNA/ligand complexes). The fraction of bound DNA values is summarized in Table C.1.

Table C.1. Fraction of bound DNA values^a for the benzoxazole ligands and d(GCGGGAATTGGGCG/CGCCAATTCCCGC) with Ni²⁺, Cu²⁺, or Zn²⁺ and in the absence of metals. Solutions contained equimolar (10 μ M) concentration of ligand, DNA, and, where appropriate, metal ion^b.

HPB analog	No Metal	Ni ²⁺	Cu ²⁺	Zn ²⁺
8	0	0.18	0.17	0
16	0	0	0.14	0
17	0	0.14	0.27	0
18	0	0	0.40	0
19	0.20	0.13	0.32	0.17
20	0.09	0.08	0.15	0.17
21	0.17	0.34	0.27	0.27

^a All values ± 0.05 . This error represents the largest standard deviation for experiments that were repeated on three separate days.

^b All solutions were prepared in a solvent composed of 50 mM ammonium acetate with 50% methanol (vol/vol).

APENDIX D. CD SPECTRA OF DNA SEQUENCES USED IN PTCDI STUDIES

D.1. DNA sequences in 70 mM potassium phosphate, 100 mM potassium chloride, 1 mM EDTA buffer, pH 7

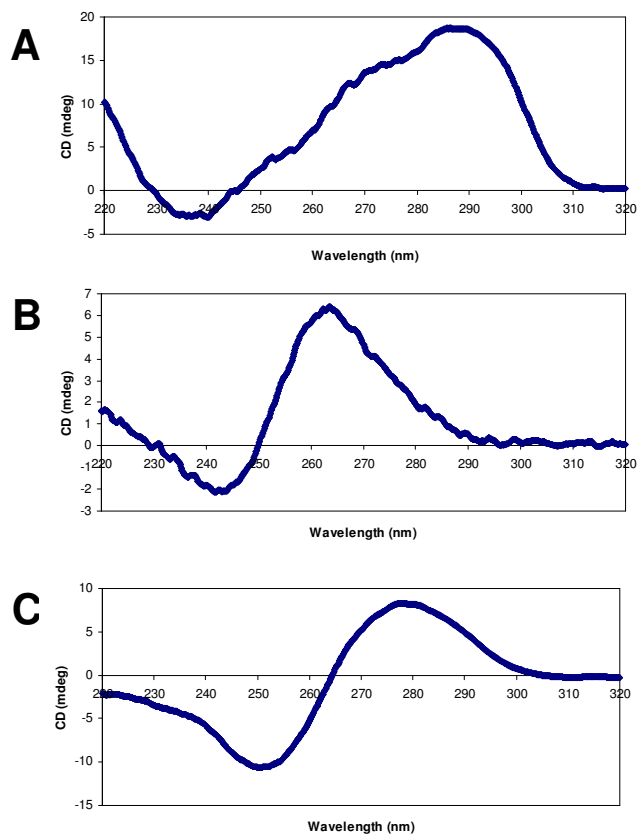


Figure D.1. CD spectra of G4'-DNA, [d(TTAGGG)₄] (A), G4-DNA, [d(TAGGGTTA)₄] (B), DS-DNA, [d(CGCGCATATCGCGCG)₂] in 170 mM K phosphate buffer, pH 7

D.2. DNA sequences in 8 mM sodium phosphate, 185 mM NaCl, pH 7 (BPS buffer)

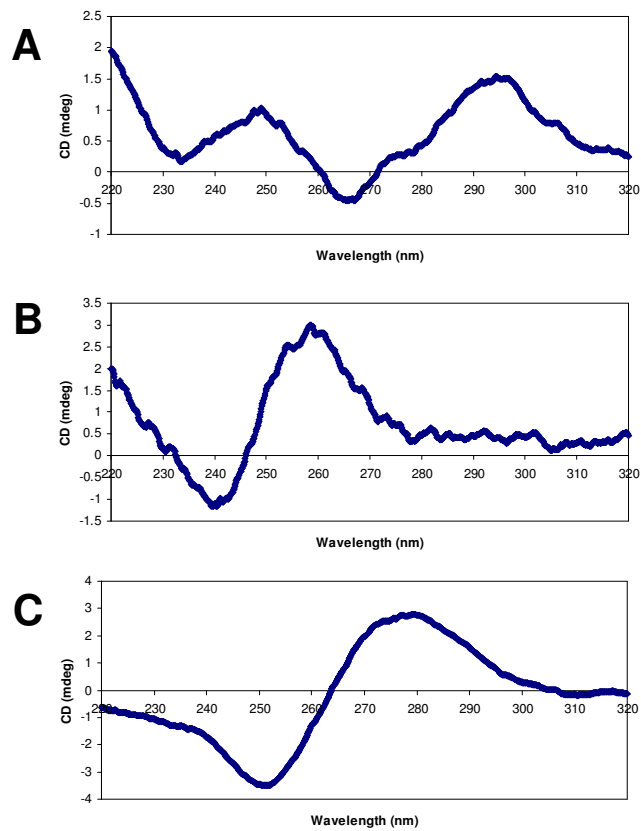


Figure D.2. CD spectra of G4'-DNA, [d(TTAGGG)₄] (A), G4-DNA, [d(TAGGGTTA)₄] (B), DS-DNA, [d(CGCGCATATCGCGCG)₂] in BPS buffer

D.3. CD Spectra of DNA sequences in 8 mM sodium phosphate, 185 mM NaCl, pH 7 (BPS buffer), supplemented with 25 μM $\text{Zn}(\text{NO}_3)_2$.

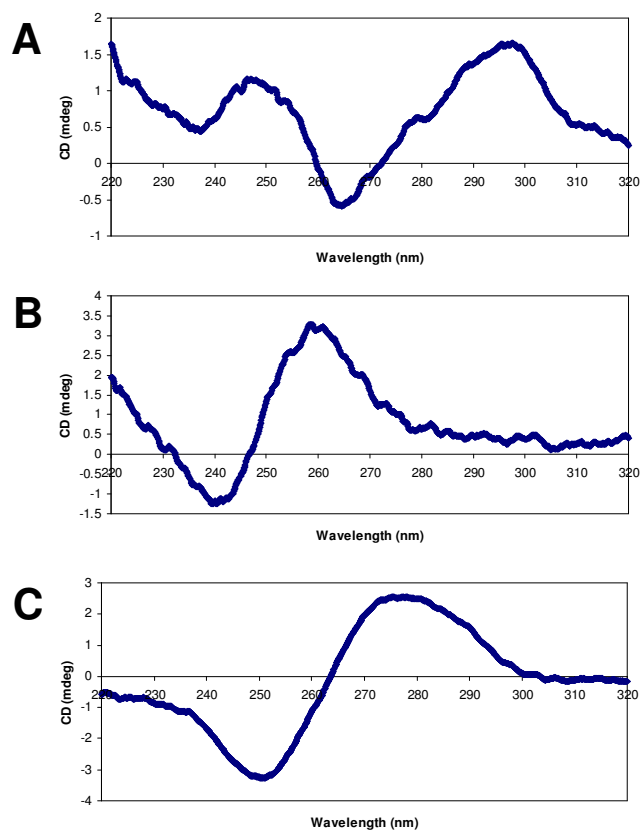


Figure D.3. CD spectra of G4'-DNA, [d(TTAGGG)₄] (A), G4-DNA, [d(TAGGGTTA)₄] (B), DS-DNA, [d(CGCGCGATATCGCGCG)₂] in BPS buffer supplemented with 25 μM $\text{Zn}(\text{NO}_3)_2$

VITA

Mireya Loreley McKee was born the daughter of Enrique Rodriguez and Mireya Loreley Gonzalez on January 19, 1978. She grew up in Tampico, Mexico where she attended the American School of Tampico throughout elementary and junior high school, obtaining a full scholarship for her high school studies at the Instituto Tecnologico y de Estudios Superiores de Monterrey (ITESM), Tampico Campus, where she graduated with an Excellence Merit Award. She then moved to Monterrey, Mexico to pursue a B. S. degree in Chemistry at ITESM, Monterrey Campus. She participated in extra-curricular activities at the university and was named president of the Chemical Society, Student Chapter in 2000. During her presidency she organized several events including the Symposium "Alchemy in the XXI Century". During her last year at the university Mireya had the opportunity to perform an internship at Texas A&M Citrus Center-Kingsville in Weslaco, TX. There she worked under the tutelage of Dr. Bhimu Patil, isolating limonoids from citrus seeds for anticancer studies. She graduated with honors from ITESM in December 2001, and continued to pursue a higher education at the University of Texas at Austin. Mireya studied a Ph. D. in Biochemistry under the mentorship of Dr. S. Kerwin and obtained a CONACyT scholarship and a Lewis award in Biochemistry during her studies.

Permanent address: Paraguay #106, Col. Las Americas. Cd. Madero, Tams Mexico

This dissertation was typed by the author